SEPARATION OF A PHOTOPLETHYSMOGRAPHIC SIGNAL AND A MOTION ARTIFACT SIGNAL BY FREQUENCY TRANSLATION

ANANTA SINCHAI

A THESIS SUBMITTED IN PARTIAL FULFILLMENT

OF THE REQUIREMENT FOR THE DEGREE OF

DOCTOR OF ENGINEERING IN ELECTRICAL ENGINEERING

FACULTY OF ENGINEERING

KING MONGKUT'S INSTITUTE OF TECHNOLOGY LADKRABANG

2020

KMITL-2020-EN-D-018-023

SEPARATION OF A PHOTOPLETHYSMOGRAPHIC SIGNAL AND A MOTION ARTIFACT SIGNAL BY FREQUENCY TRANSLATION

ANANTA SINCHAI

A THESIS SUBMITTED IN PARTIAL FULFILLMENT

OF THE REQUIREMENT FOR THE DEGREE OF

DOCTOR OF ENGINEERING IN ELECTRICAL ENGINEERING

FACULTY OF ENGINEERING

KING MONGKUT'S INSTITUTE OF TECHNOLOGY LADKRABANG

2020

KMITL-2020-EN-D-018-023

หัวข้อวิทยานิพนธ์	การแยกสัญญาณการไหลเวียนโลหิตและสัญญาณรบกวนที่เกิดจากการเคลื่อนไหวโดยการย้ายความถี่
นักศึกษา	นาย อนันตา สินไชย
รหัสนักศึกษา	58601019
ปริญญา	วิศวกรรมศาสตรดุษฎีบัณฑิต
สาขาวิชา	วิศวกรรมไฟฟ้า
พ.ศ.	2563
อาจารย์ที่ปรึกษาวิทยานิพนธ์	รศ.ดร. จีรสุดา โกษียาภรณ์
อาจารย์ที่ปรึกษาวิทยานิพนธ์ร่วม	รศ.ดร. ปราโมทย์ วาดเขียน

บทคัดย่อ

เปอร์เซ็นต์ความอิ่มตัวของออกซิเจนหรือที่เรียกว่าค่า SpO2 ที่ได้รับจากเครื่องวัดความอิ่มตัวของออกซิเจนขึ้นอยู่กับคู่สัญญาณการไหลเวียนโลหิต (Photoplethysmographic (PPG) signal) ที่เหมาะสมที่ได้จากแสงสีแดงและแสงอินฟาเรด ในทางปฏิบัติ สัญญาณ PPG ที่ได้จากแสงสีแดงและแสงอินฟาเรดมักถูกทำให้เสียรูปร่างโดยสัญญาณรบกวนที่เกิดจากการเคลื่อนไหว (Motion artifact (MA) signal) อยู่เสมอๆ ด้วยการมีอิทธิผลของสัญญาณ MA ในสัญญาณ PPG ที่ได้จากแสงสีแดงและแสงอินฟาเรด ทำให้ค่า SpO2 ไม่น่าเชื่อถือ เพื่อจัดการกับประเด็นสัญญาณ MA จึงได้ทำการศึกษาการกระจายทางความถี่ของสัญญาณ MA จากท่าทางที่เป็นไปได้ที่คนไข้มักทำ ผลจากการศึกษาเผยให้เห็นว่าองค์ประกอบทางความถี่ของสัญญาณ MA จากท่าทางที่เป็นไปได้กระจายอยู่ในช่วงเดียวกันกับองค์ประกอบทางความถี่ของสัญญาณ PPG เทคนิคการย้ายความถี่อยู่บนพื้นฐานของการมอดูเลตทางขนาดหรือเอเอ็ม (Amplitude modulation (AM)) ถูกนำมาประยุกต์ใช้เพื่อแก้ปัญหาการเหลื่อมกันทางองค์ประกอบทางความถี่ของทั้งสัญญาณ PPG และสัญญาณ MA ซึ่งเทคนิคที่นำเสนอได้เปลี่ยนระบบการขับแสงหลอดแอลอีดี (LED) จากแบบเดิมที่ใช้อยู่ในเครื่องวัดความอิ่มตัวของออกซิเจน วิธีการแก้ปัญหาที่นำเสนอจะขับหลอดแอลอีดีแสงสีแดงและแสงอินฟาเรดไปพร้อมๆ กัน แต่ละหลอดถูกขับด้วยสัญญาณคลื่นรูปไซน์ที่ความถี่แตกต่างกัน โดยสัญญาณคลื่นรูปไซน์ถูกสร้างจากแหล่งกำเนิดกระแสสลับ (AC) สำหรับระบบการขับหลอดแอลอีดีแบบเดิมนั้นหลอดแอลอีดีแสงสีแดงและแสงอินฟาเรดถูกขับด้วยแหล่งกำเนิดกระแสตรง (DC) สลับกัน นอกจากนี้แล้วยังได้ทำการศึกษาการเปลี่ยนแปลงความเข้มแสงที่ใช้ขับหลอดแอลอีดีแต่ละหลอด อีกทั้งยังได้ทำการศึกษาเชิงเปรียบเทียบในเชิงประสิทธิภาพของเทคนิคที่นำเสนอกับ วิธีการแบบเดิม, วิธีการแปลงความอิ่มตัวแบบแยกกัน (DST), วิธีการวิเคราะห์องค์ประกอบแบบอิสระ (ICA) และวิธีการบีบอัดค่าสัมประสิทธิ์ฟูริเยร์ (CFC) กลยุทธ์ที่นำเสนอแสดงให้เห็นว่าองค์ประกอบทางความถี่ของสัญญาณ PPG ถูกยกไปยังตำแหน่งความถี่ที่ต้องการและยังคงรักษาลักษณะรูปพรรณของสัญญาณ PPG ไว้ได้ดี ค่า SpO2 ถูกคำนวณเพื่อยืนยันความถูกต้อง ในขณะที่มีการเคลื่อนไหวพบว่าค่า SpO2 ที่คำนวณมานั้นไม่เสียหายและปรากฏออกมาว่าการเปลี่ยนแปลงความเข้มแสงไม่ได้ทำให้ค่า SpO2 ดีขึ้นหรือแย่ลง นอกจากนี้ค่า SpO2 ที่คำนวณมาได้แสดงให้เห็นว่าประสิทธิภาพของวิธีการที่นำเสนอเหนือกว่าวิธีการอื่นๆ ที่กล่าวไว้ข้างต้น ค่าเฉลี่ยของค่าสัมบูรณ์ของเปอร์เซ็นต์ของค่าความคลาดเคลื่อน (Mean absolute percentage error (MAPE)) ของเทคนิคที่นำเสนอสูงสุด 1.35% เท่านั้น สำหรับวิธีการแบบเดิม, DST, ICA และ CFC ให้ค่า MAPE สูงสุดถึง 12.77%, 2.27%, 75.85% และ 11.89% ตามลำดับ

Thesis Title	Separation of a Photoplethysmographic Signal and a Motion Artifact Signal by Frequency Translation
Student	Mr. Ananta Sinchai
Student ID.	58601019
Degree	Doctor of Engineering
Program	Electrical Engineering
Year	2020
Thesis Advisor	Assoc. Prof. Dr. Jeerasuda Koseeyaporn
Thesis Co-Advisor	Assoc. Prof. Dr. Paramote Wardkein

ABSTRACT

A percentage of oxygen saturation, known as a SpO2 value, obtained by a pulse oximeter relies on a pair of proper red and infrared (IR) photoplethysmographic (PPG) signals. In practice, both red and IR PPG signals are frequently distorted by a motion artifact (MA) signal. By having the MA influence on the red and IR PPG signals makes the SpO2 value unreliable. To handle the MA issue, the MA frequency distributions of likely regular postures induced by a patient are studied. The study reveals that the MA frequency components of possible usual poses distribute in the identical range of the PPG frequency components. To solve the overlapping frequency components of both PPG and MA signals, a technique of frequency translation based on an amplitude modulation (AM) is thus applied. The proposed technique remodels a traditional LEDs-driving system in the pulse oximeter. The presented solution emits both red and IR LEDs simultaneously. Each LED is driven by a sinusoidal signal having a distinct frequency generated by an alternating current (AC) source. For the conventional LEDs-shining system, red and IR LEDs are driven by a direct current (DC) source alternately. Besides, change of light intensity emitted by each LED is studied. Also, a comparative study regarding the performances of the proposed technique, the conventional scheme, discrete saturation transform (DST), independent component analysis (ICA) and compression of Fourier coefficients (CFC) is performed. The proposed strategy manifests that the PPG frequency components are shifted to the desirable frequency location and all PPG morphologies are well maintained. To verify the correctness, the SpO2 value is calculated. While motions, the computed SpO2 values are found to be intact and emerge that the change of light intensity neither improves nor deteriorates the SpO2 values. Moreover, the calculated SpO2 values show that the performance of the present approach is superior to the performances of the given methods. The mean absolute percentage error (MAPE) of the proposed technique is up to only 1.35%. By contrast, the MAPE values of the methods of conventional scheme, DST, ICA and CFC are up to 12.77%, 2.27%, 75.85% and 11.89%, respectively.

Acknowledgements

This thesis is fully complete due to the encouragement and heed given by my parents. Nonetheless, this thesis would have not ever happened if there were no good academic suggestions provided by both of my thesis advisors.

First of all, I would like to thank Assoc. Prof. Dr. Paramote Wardkein, who is my thesis co-advisor, for giving me the doctoral topic and financial supports in order to fulfill my doctoral degree.

Secondly, I also would like to thank Assoc. Prof. Dr. Jeerasuda Koseeyaporn, who is my major thesis advisor, for providing me academic knowledge and constantly urging me to finish this thesis. Importantly, she carefully peruses all of my academic documents.

Thirdly, I feel appreciative of Assoc. Prof. Dr. Panwit Tuwanut for his academic guidance when I face any difficulties during doing my doctoral degree.

Fourthly, I am thankful for Mr. Pattana Kainan who well assists me in constructing and designing various circuits in this thesis.

Next, I feel thankful to Miss Vireeya Chaidon who at all times boosts me some morale.

Also, I thank to everyone who either directly or indirectly helps me but is not mentioned in this acknowledgements.

Last but not least, I would like to thank all participating personnel at the Territorial Defense Command (TDC) who voluntarily perform all experiments conducted in this thesis. Most importantly, I would like to thank Commanding General of TDC very much for granting me to conduct the experiments regarding this thesis.

Finally, I am cordially grateful with all my heart to all members of my family for their advocating, urging, and encouraging. However, I would like to highlight the wholehearted cares nurtured by my mother and father. They are highly influential to my life in pursuing my doctoral degree.

Ananta Sinchai

Table of Contents

Table of Contents (continued)

List of Figures

List of Figures (continued)

List of Tables

List of Tables (continued)

List of Tables (continued)

List of Tables (continued)

List of Tables (continued)

List of Tables (continued)

List of Tables (continued)

List of Tables (continued)

List of Tables (continued)

CHAPTER 1
Introduction

A photoplethysmographic (PPG) signal known as a PPG signal is a biological signal that exhibits a characteristic of blood volume change in human's blood vessel. The characteristic of the blood volume change behaves in line with contraction and expansion of a human's heart. With this reason, the PPG signal somewhat exhibits a beat interval equal to an electrocardiographic (ECG) signal or an ECG signal [1][2], as depicted in Figure 1.1 [2]. Figure 1.1(a) is the natural PPG waveform and Figure 1.1(b) is the habitual ECG waveform. Some vital signs of a human such as heart rate (HR) [3][4], heart rate variability (HRV) [5] can be extracted from the PPG signal rather than occupying the ECG signal. For a convenient cause of measurement, the PPG signal becomes an effective alternative utilized to analyze some human's vital signs in lieu of the ECG signal. Nonetheless, the main objective of the PPG signal usage purposely quantifies oxygen saturation (SpO2) in human blood by employing a pulse oximeter instead of blood analyzing by an invasive method. The pulse oximeter is an optical bio-sensing device having two light sources and a photo-detector. To measure an amount of oxygen saturation (SpO2) in human blood, two major components of the PPG signal are used to compute. These two components consist of an alternating current (AC) component and a direct current (DC) component, as marked in Figure 1.1(a).

To obtain a PPG signal, a light source emits light onto a human absorbing medium of interest. By traveling through the human absorbing medium of interest, the light intensity is absorbed and the leftover light intensity after being absorbed falling upon a photo-detector is the PPG signal. Acquiring the PPG signal is drawn in Figure 1.2 which demonstrates a cross-sectioned fingertip as the absorbing medium of interest [6][7]. In this human contextual, the absorbing medium of interest comprises of various absorbing sub-media such as pulsating arterial blood, non-pulsating arterial blood, venous blood, skin, bone and tissue. The sub-media, arterial blood, non-pulsating arterial blood, refer to the arterial capillary and the sub-medium, venous blood, is the vein capillary. The skin medium consists of epidermis and dermis, and the bone medium contains nail plate, nail bed and phalanx. For the tissue medium composes of fibrous septa and nerves. In spite of having various absorbing sub-media, the given sub-media can be classified into two principal groups which are dynamic and static media as illustrated in Figure 1.3 [8]. The dynamic medium represents the light intensity absorption of the pulsating arterial blood which is contemplated as the AC component. For the static medium refers the rest mentioned sub-media because the light intensity

penetrating these sub-media is absorbed at a constant rate over time. With unchanged absorption, the static medium is considered as the DC component.

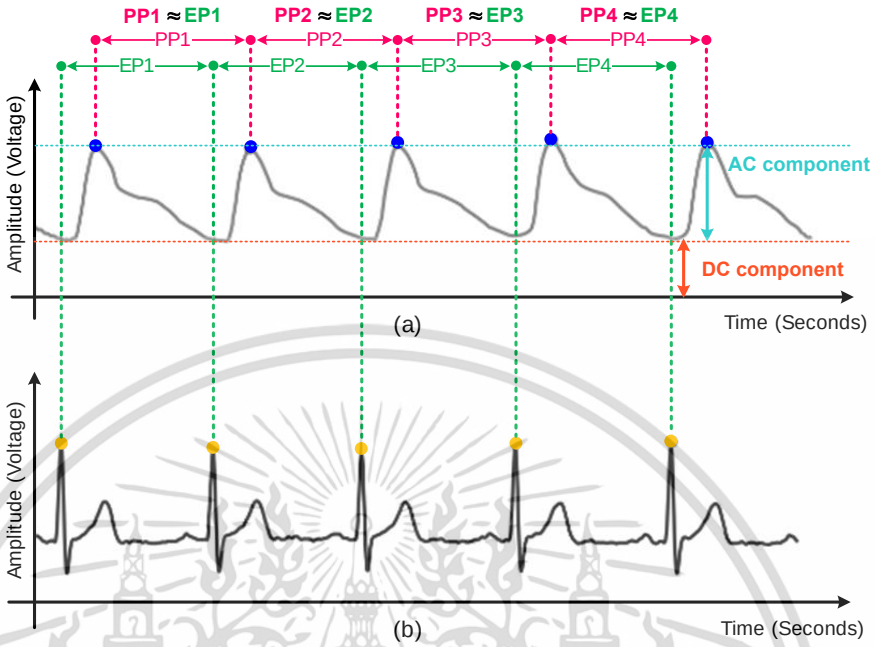

Figure 1.1 Beat interval comparison between PPG and ECG signals. (a) PPG waveform and (b) ECG waveform.

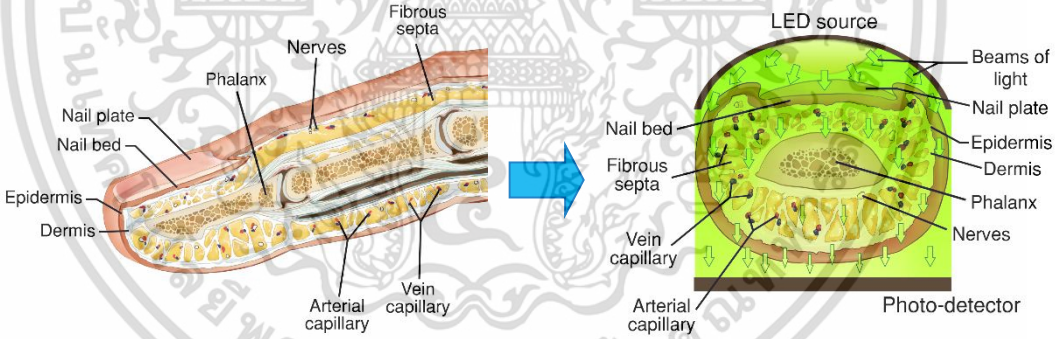

Figure 1.2 A cross-sectioned fingertip.

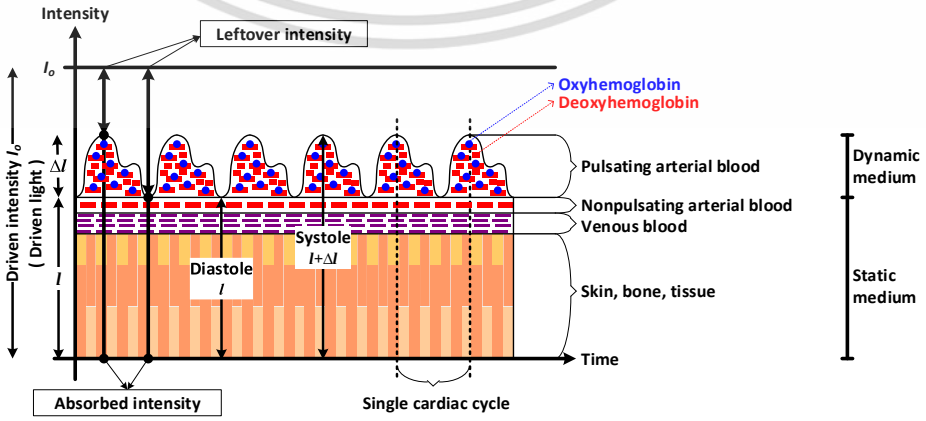

Figure 1.3 Media grouping.

In a pulse oximeter, a SpO2 value is calculated from the ratio of deoxyhemoglobin (Hb) to oxyhemoglobin (HbO2) in a human. To acquire the amounts of deoxyhemoglobin (Hb) and oxyhemoglobin (HbO2), two light sources which are red and infrared (IR) lights are implemented in the pulse oximeter. The red light is best absorbed by the deoxyhemoglobin (Hb). On the contrary, the IR light is well digested by the oxyhemoglobin (HbO2). In order to acquire red and IR PPG signals by mounting only one photo-detector in the pulse oximeter, both lights are driven alternately in a time division multiplexing (TDM) manner. By illuminating both lights alternately at high frequency [9], the red and IR PPG signals are generated almost at the same time. However, the phase difference of the red and IR PPG signals as a result of the TDM manner is fairly low as well as insignificant, and does not show any impact on the SpO2 value. Both red and IR PPG signals are thus considered to be produced simultaneously. Ordinarily, the pulse oximeter is worn at a fingertip, an earlobe and a forehead to measure the SpO2 value.

A SpO2 value has not only a merit of assessing hypoxemia [10] but also other merits of pre-screening some symptoms for instance, pulmonary embolism disease [11], lower extremity arterial disease [12], congenital heart disease [13], acute heart failure [14], and chronic obstructive pulmonary disease [15]. Aside from the mentioned symptoms, the SpO2 value is also practical in evaluating testicular torsion [16] and pulp vitality [17].

All in all, to perform any good merit of a SpO2 value obtained from a pulse oximeter, the SpO2 value is suggested to measure while a subject is at rest. In other words, the pulse oximeter should be worn at the subject's organ (fingertip, earlobe and forehead) fitly and the subject should move his/her organ as little as possible. Otherwise, the measured SpO2 value is distorted and worthless.

1.1 Problem statement

In practice, a subject does not stay still while measuring is taken place. With organ moving, a pulse oximeter also moves and causes both red and IR PPG signals to deform. Since SpO2 computation relies on the proper red and IR PPG signals, hence, the disfigured red and IR PPG signals lead to the unacceptable SpO2 value. The proper red and IR PPG signals as well as the disfigured red and IR PPG signals are illustrated in Figure 1.4. By diagnosing any symptom based on the unreliable SpO2 value, the subject may not be taken care by a proper manner and in a suitable time. In the event of motion involvement, an unwanted signal called a motion artifact signal or an MA signal appears to make the clean red and IR PPG signals misshape. This is owing to the MA signal contains some frequency components overlapping with the significant frequency components of the red and IR PPG signals.

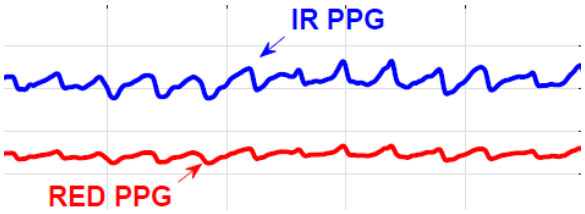

(a) Proper red and IR PPG signals.

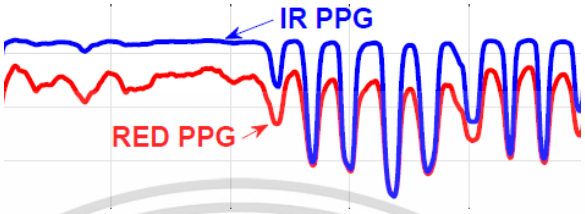

(b) Disfigured red and IR PPG signals.

Figure 1.4 Suitable and corrupted PPG signals.

1.2 Literature review

According to the problem statement, numerous pieces of research have dedicated to alleviate an MA impact to gain a better quality of a corrupted PPG signal. Among solutions toward the MA problem, the reported MA resolutions are categorized into two chief groups. The first kind uses a reference signal to cancel an MA signal [18]-[30] and the second kind applies sundry techniques of signal processing to improve the polluted PPG signal [31]-[44].

The former group mainly concentrates on an adaptive filtering method. The adaptive filtering method is the most common implementation due to its simple structure. Although the adaptive filtering structure is plain, a reference signal fed to the adaptive filtering method is the knotty part to synthesize since the MA signal is not deterministic. With the MA indeterminism makes synthesizing the reference signal thus involve applying different convoluted signal processing techniques to capture the MA characteristics. Keeping in mind, the artificial reference signal is significant because feeding the poor synthetic reference signal to the adaptive filter results the resultant recovered PPG signal even more aggravated. Typically, the reference signal is extracted from either motion relating sensors [18]-[23] or human vital signs [24]-[29]. Aside from focusing on motion relating sensors or human vital signs, the reference signal is also applicably generated from multiple sinusoidal frequency components to alleviate the MA signal [30]. For those methods depending on the motion relating sensors like an accelerometer [18,21,22], an optoelectronic sensor [19], an optical sensor [20] and a piezoelectric sensor [23] seems to acquire the reference signal simply. Nonetheless, the raw sensed signals provided by any kinds of sensors need be fine extracted by sophisticated algorithms [20]-[23] to highly correlate to the MA signal or the PPG signal.

In this viewpoint, for those approaches [24]-[30] synthesizing the reference signal relying on the human vital signs looks like to have the advantage over the methods employing the additional sensors. Fundamentally, the human vital sign signal has some common components which the PPG signal also has. With this reason, synthesizing the human vital signs furnishes the reference signal more correlated to the PPG signal or the MA signal than using the auxiliary sensors. Even though synthesizing the human vital signs produces a high correlated reference signal but the synthesizing approaches are also complicated not lesser than those methods applying the supplementary sensors. In extracting or synthesizing the reference signal, diverse schemes of signal processing have been implemented. Those prominent schemes are developed by an approach of frequency-locked loop (FLL) [22], a linear subspace [24][28], a technique of discrete saturation transformation (DST) [25] and a method of independent component analysis (ICA) [26,27,29].

The latter group involves different signal processing techniques [31]-[44] striving to overcome the MA problem. Essentially, the MA signal is induced either intentionally or unintentionally. The MA signal has some frequency components which overlap with the frequency components of the PPG signal. To eliminate the overlapped frequencies, a multi-rate filter bank is designed [31]. Due to both PPG and MA signals contain some mutual frequencies, thus, attenuating the MA signal also worsen the PPG signal at the same time. Instead of applying the multi-rate filter bank, the PPG signal is analyzed by a cycle-by-cycle basis of Fourier series analysis [32]. In each analyzed cycle, only fundamental Fourier coefficients of the PPG signal are kept and the rest coefficients are truncated. By truncating those unnecessary Fourier coefficients, the MA effect being beyond the fundamental coefficients is lessened but those MA frequencies residing in the fundamental coefficients still exist. Analyzing cycle-by-cycle influences only the cycle which is being focused. Unlike the multi-rate filter bank affects the overall PPG signal. Evidently, the MA-dominated PPG signal may not exhibit each cycle therefore severing each cycle to analyze is fairly difficult to do so. The Fourier series analysis performs well with the stationary signal but the MA signal is a non-stationary signal. With the non-stationary issue, a wavelet analysis [33] is brought to detect the MA signal in both time and frequency domains at the same time. Still, the wavelet analysis may detect the location of MA occurring in the time domain well. Nevertheless, the wavelet analysis has to combine with additional algorithms to remove the MA signal. To avoid the difficult implementation of the wavelet analysis, a simple statistical approach is utilized to detect the location of MA occurring [34]. Basically, the PPG and MA signals are considered independent of each other. Taking into account, a linear summation of PPG and MA signals are constituted to discriminate the components of the PPG and MA signals. This linear summation is known as the independent component analysis

(ICA) [35]-[38]. The technique of ICA is vastly used but occasionally faces the problem of falling into the pitfall of a local optimum. Converging to the local optimum makes some of the MA components remain in the PPG component. As the PPG and MA components are unrelated to each other, both components are distinguished using a minimum correlation discrete saturation transform (MCDST) approach [39]. For MCDST, the distinguishing process depends on an optimal search manner which may lead to a chance of returning a false component. In a similar manner, a method of singular value decomposition (SVD) [40] is brought to decompose the PPG signal from the MA signal. The singular value decomposition may yield the appropriate PPG signal, but requires a substantial amount of computations in turn. In [41], an estimation of signal parameters via rotational invariance techniques (ESPRIT) solves the considerable computational costs of the SVD so that a real-time processing manner is applicable. Among the state-of-the-art strategies, a simple model of 3rd-order polynomial [42] is designed to fit the MA signal in order to subtract from the contaminated PPG signal. The desirable MA signal fit by the 3rd-order polynomial model only disposes of the baseline of MA though the existence of other MA frequency components is yet present. Another uncomplicated concept corrects the polluted PPG signal by employing a set of thresholding criteria relying on an untainted PPG morphological waveform [43]. Upon simplicity, the defined thresholding criteria may not match all MA patterns resulting some MA patterns may be corrected. Not only the signal processing techniques are implemented but circuit design such as a differential amplifier with common-mode rejection [44] is also performed to cancel the MA signal. The main drawback of using a circuit is the inconvenience in making a circuit adjustment. From the given research study, four criteria of each method for comparison which are domain involvement, purpose of signal processing, computational cost and implementation are summarized in Table 1.1.

Grounded on the literature review, in view of those cited techniques aim to retrieve intact PPG signals sustaining all significant morphological shapes from the MA-intertwined PPG signals. As a matter of fact, retrieving the accurate PPG signal is laborious. In addition, some approaches may work perfectly only under a particular constraint.

Table 1.1 Summary of literature research.

Techniques	Domain involvement	Purpose of signal processing	Computational cost	Implementation
1. Adaptive filter	Time	Correction	Moderate to High	Simple to complex
2. Frequency locked loop (FLL)	Frequency	Detection	Moderate	Moderately complex
3. Multi-rate filter bank	Frequency	Correction	Moderate	Moderately complex
4. CFC[1]	Frequency	Correction	Quite high	Moderately complex
5. Wavelet transform	Time and Frequency	Detection	High	Complex
6. ICA[2]	Time	Correction	Very High	Highly complex
7. MCDST[3]	Time	Correction	High	Complex
8. SVD[4]	Time	Correction	Very high	Highly complex
9. ESPRIT[5]	Time	Correction	High	Highly complex
10. Polynomial regression	Time	Correction	Moderate	Simple
11. Thresholding of morphological waveform mapping	Time	Correction	Moderate to high	Simple to moderately complex
12. Differential amplifier in common mode rejection	Time	Correction	Not available	Moderately complex

1 – CFC stands for Compression of Fourier coefficient series

2 – ICA stands for Independent component analysis

3 – MCDST stands for Minimum correlation discrete saturation transform

4 – SVD stands for Singular value decomposition

5 – ESPRIT stands for Estimation of signal parameters via rotational invariance techniques

1.3 Objective propositions

All optical bio-sensing instruments are highly susceptible to motions. When any kinds of motions take place, the performance of the optical bio-sensing equipment is inevitably depreciated because an MA signal exacerbates a biological signal. Under motion circumstances, the MA signal is induced by the assumption as follows.

Any human body movements that are not human body exercises would partially cause the PPG signal to misshape in line with the human body movements. Some misshapen portions in the PPG signal are distorted as though the human body movements generate the MA signal which is superimposed on the PPG signal. With the superimposition of the MA signal on the PPG signal suggests that the MA signal behaves like an additive kind of interference. Due to partial misshapenness of the PPG signal during any human motions indicates that the MA signal contains some frequency components overlapping with some frequency components of the PPG signal. Besides, during any human motions, external light sources penetrating through the optical bio-sensing equipment would also be considered to have the effect on the PPG signal. Since the undesirable light produced by those external light sources appears while any human motions take place, the influence of that light bears the constructive superposition in the MA signal. The effect of those external light sources can thus be inferred to be the additive kind of interference implicitly.

For this thesis, the optical bio-sensing instrument of interest is a pulse oximeter. To cope with the MA problem, the given assumption is successfully proved and the frequency components of the MA signal are unveiled as a part of the assumption proof. Once the MA frequency components are realized, a preventive strategy developed from an amplitude modulation (AM) is proposed to isolate the biological signal from the MA signal successfully. In this context, the PPG signal is the biological signal.

1.4 Contributions

To accomplish the objective propositions, a framework is designed as follows. Initially, the behavior of the MA signal produced by any motions is studied and analyzed. Secondarily, a preventive solution is implemented on a pulse oximeter to circumvent the PPG signal from mingling with the MA signal in lieu of correcting the MA-corrupted PPG signal. The proposed preventive approach is based on a method of an amplitude modulation (AM). Next, this presented approach is experimented to confirm that the PPG frequency components are shifted away from the MA frequency components. Later, the influence of amplitude modulation sensitivity is examined whether the AM sensitivity has the impact that raises the performance of the introduced approach. Lastly, the proposed technique is compared to other contemporary sophisticated methods to strengthen its reliability.

1.5 Structure of substantive chapters

The remainder of this thesis is organized as follows. Chapter 2 describes the concepts of pulse oximetry such as PPG acquiring, SpO2 calculation etc., and the general principles of amplitude modulation (AM) as well as amplitude demodulation. Also in the same chapter, the related theories of the contemporary methods are provided for the purpose of comparative study. The contemporary approaches are discrete saturation transformation (DST) [25], independent component analysis (ICA) [26][35] and compression of Fourier series coefficients (CFC) [32]. In Chapter 3, the relevant principles of implementing the proposed technique are explained and the design and implementation of the presented approach on a commercial pulse oximeter are given. Subsequent, Chapter 4 initially studies the characteristics of the MA signals. Next, various experiments pertaining to the performance of the proposed strategy are rendered. Later in the same chapter, influence of light intensity on the performance of the proposed method is illustrated while motions are induced. Lastly, the performances of the proposed approach and the contemporary methods are compared in this chapter. Finally, the conclusions are drawn in Chapter 5.

CHAPTER 2
Associated Fundamental Principles

This chapter begins with deriving an absorbing model of light intensity used in a pulse oximeter. This derived absorbing model is utilized to represent a photoplethysmographic (PPG) signal. Next, the same absorbing model is explained how to estimate an amount of oxygen saturation (SpO2) which is expressed in terms of percentage. Later, a foundation principle of a proposed solution is delineated. The amplitude modulation and demodulation which are involved with the presented strategy will be briefly reviewed. Lastly, a brief summary to selected contemporary approaches is described.

2.1 Photoplethysmographic (PPG) mathematical expression

Detecting change in blood volume of a human circulatory system through light absorption gives rise to a photoplethysmographic (PPG) signal. In order to handle the PPG signal, a mathematical model is necessary. The PPG signal is normally expressed in forms of the mathematical model by applying the light absorbing law of Beer-Lambert [8]. The Beer-Lambert's law plainly states that any light infiltrating into an absorbing medium is absorbed [8]. The absorbing medium is sometimes called as an absorber. In Beer-Lambert's absorption, the light absorbed refers to its intensity. The light intensity absorption of the given law abides by the function of exponential decay written in Eq. (2.1) where the i variable is the leftover intensity after being absorbed. The leftover light intensity, i, is the product of the incident light intensity falling upon medium surface, i_o, and the exponential decaying function, $e^{-\varepsilon(\lambda)cd}$. The exponent of the exponential decaying function consists of three parameters that multiply to each other. The first parameter is the molar absorptivity, $\varepsilon(\lambda)$, of a specific wavelength λ. This molar absorptivity, $\varepsilon(\lambda)$, is the ability of medium absorption at a specific wavelength λ. Next, the second factor is the medium concentration c and the last one is the optical path length, d. The medium concentration refers to the amount of absorbing substance residing the medium and the optical path length d is the distance that the light passes through the medium. The light intensity absorption of Beer-Lambert expressed in Eq. (2.1) is simply explained by a simple diagram shown in Figure 2.1.

$$i = i_o e^{-\varepsilon(\lambda)cd} \tag{2.1}$$

In case of various media stacking or one medium stuffed inside one another, the Beer-Lambert's absorbing law is still usable. For this case, the remaining light intensity from the previous medium is the beginning light intensity to the next medium. This absorbing process absorbs iteratively and finishes when the remnant light intensity penetrates the last medium and falls onto a photo-detector. By having media stacking or one medium packed within another medium, Eq. (2.1) is slightly adjusted to Eq. (2.2) by the aforementioned iterative absorption. The given absorbing process stated by Eq. (2.2) for a perplexed medium is simply portrayed by Figure 2.2.

$$i = i_o e^{-\sum_{k=1}^{N} \varepsilon_k(\lambda) c_k d_k} \tag{2.2}$$

In Eq. (2.2), the N variable refers to the total media through which the light seeps and the k variable is the medium order. Moreover, $\varepsilon_k(\lambda)$, c_k, and d_k are the absorbing parameters of the medium number k and the other two variables, i and i_o, have the same senses as mentioned in Eq. (2.1).

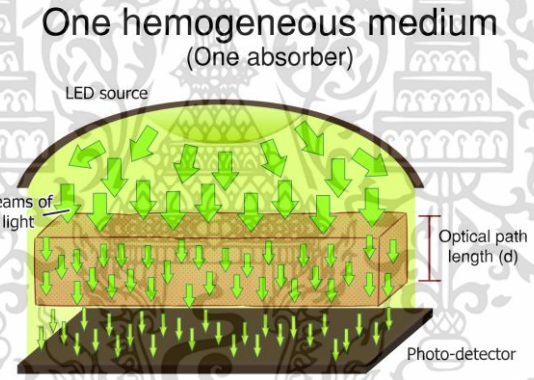

Figure 2.1 A homogeneous medium.

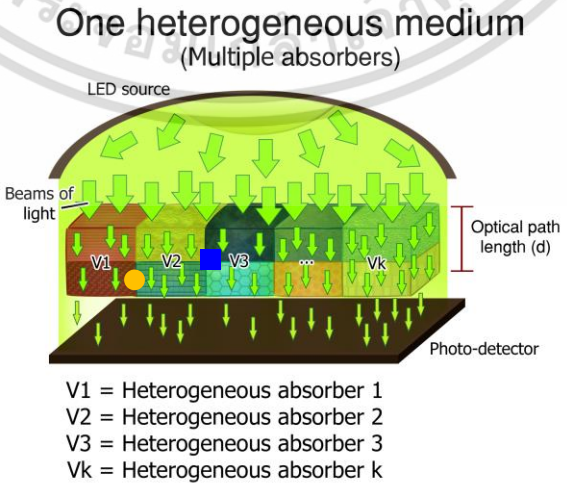

Figure 2.2 A heterogeneous medium.

For a human perspective, a human body is considered as one whole medium. This whole medium of the human body is complex, and consists of diverse media intertwining as illustrated in Figure 1.2. Figure 1.2 shows a cross-sectioned fingertip as an example. As can be noticed in Figure 1.2, those different media are not just rectangular shape media but most of those media are capillaceous-like. Nonetheless, the derivative of Beer-Lambert in Eq. (2.2) is yet valid with the human medium. By emitting light onto the human medium, light absorption is split into two aspects. The first aspect is the light absorption taking place in the arterial blood vessel under the expansion and contraction of the human circulatory system. With the human nature of the expansion and contraction, the light absorption in the arterial blood vessel changes over time and creates a pulsating waveform as exhibited in Figure 1.3. The first aspect is considered as a dynamic medium. Next, the other one is the light absorption arising in the rest media in the human body as displayed in Figure 1.3. In contrast to the first aspect, the light absorption in the second aspect does not vary over time and gives a constant amount of the light absorption. The second aspect is contemplated as a static medium. In the event of no blood flow in the human body, the dynamic medium no longer has the influence in the light absorption [**45**]. The impact of the light absorption thus only occurs in the static medium. With this reason, a mathematical model for the human absorption is concluded to be the summation of both light absorbing aspects as drawn in Eq. (2.3).

$$i = i_o[Static\,Medium + Dynamic\,Medium] \tag{2.3}$$

The expression in Eq. (2.3) is based on Eq. (2.2). To rephrase the human condition having no blood flow by Eq. (2.3), the $Dynamic\,Medium$ term has no effect and vanishes and the light absorption depends solely on the $Static\,Medium$ term.

Naturally, change in blood volume occurring in the pulsating arterial blood vessel brings about the optical path length value of this pulsating arterial blood vessel to change over time. This explains why the pulsating arterial blood vessel is represented by the dynamic medium. This changing manner in blood volume leads to the light intensity absorption to be formed as a pulsating waveform component for the PPG signal. Mainly, the light intensity passing through the dynamic medium is absorbed by two chief absorbing substances called oxyhemoglobin (HbO2) and deoxyhemoglobin (Hb). For the non-waveform component of the PPG signal is produced by the light intensity absorption of the media such as skin, bone, tissue, venous blood and nonpulsating arterial blood. The mentioned media show little change of their optical path length values, and thus results the non-waveform component of the PPG signal. The given media are garnered as one static medium due

to their common ground in little change of their optical path length values. This static medium is then stood for the uttered media.

With a summary description of how the PPG signal is constituted, Eq. (2.3) is readjusted and rewritten in Eq. (2.4) to state the mathematical PPG signal expression.

$$i_{PPG}(t) = i_o[\underbrace{e^{-\varepsilon_{sm}(\lambda)c_{sm}d_{sm}}}_{Static\ Medium} + \underbrace{e^{-[\varepsilon_{HbO2}(\lambda)c_{HbO2}+\varepsilon_{Hb}(\lambda)c_{Hb}]d_{dm}(t)}}_{Dynamic\ Medium}] \quad (2.4)$$

In Eq. (2.4), the exponential decay function of the $Static\ Medium$ term comprises of the product of three absorbing parameters, $\varepsilon_{sm}(\lambda)$, c_{sm}, and d_{sm} at the exponent. These three absorbing parameters are made of the unchanged optical path length absorbing media grouped as one whole static medium. Due to little variation of the static medium's optical path length, the d_{sm} term is not drawn as a function of time. For the $Dynamic\ Medium$ term, the exponential decay function expresses the absorbing parameters of interests. These the absorbing parameters of interests located at the exponent are the absorbing properties ($\varepsilon_{HbO2}(\lambda)$, c_{HbO2}, $\varepsilon_{Hb}(\lambda)$ and c_{Hb}) of the oxyhemoglobin (HbO2) and the deoxyhemoglobin (Hb). Because of change in blood volume, the dynamic medium's optical path length, $d_{dm}(t)$, is therefore manifested as a function of time. Besides, the mathematical model of the PPG signal, $i_{PPG}(t)$, developed in Eq. (2.4) is the expression of the clean PPG signal having no the MA signal involved. The clean PPG signal and the PPG signal are same.

In a context of the pulse oximeter, the red and infrared (IR) lights are utilized. The red light is highly absorbed by the deoxyhemoglobin (Hb) as well as the oxyhemoglobin (HbO2) best absorbs the IR light according to [8] (see Figure 2.3). This gives the explanation why the absorbing parameters of the dynamic medium are exhibited by the absorbing properties, $\varepsilon_{HbO2}(\lambda)$, c_{HbO2}, $\varepsilon_{Hb}(\lambda)$ and c_{Hb} in Eq. (2.4).

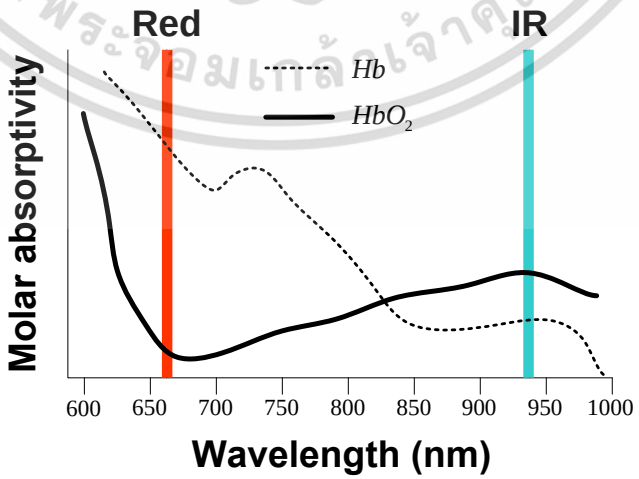

Figure 2.3 Absorbing curve of red and IR lights.

2.2 Calculation of oxygen saturation percentage (SpO2)

An amount of oxygen saturation in a human body is gauged from the oxygen concentration ridden on hemoglobin or oxyhemoglobin (HbO2). Usually, the amount of oxygen saturation is computed from the percentage of the oxyhemoglobin concentration (c_{HbO2}) over the summation of the oxyhemoglobin concentration and the deoxyhemoglobin concentration (c_{Hb}). The percentage of oxygen saturation (SpO2) is simply stated by Eq. (2.5) [8]. However, the given relation in Eq. (2.5) can be directly used to calculate the percentage of oxygen saturation with real blood analysis through a blood puncturing invasive method.

$$SpO2 = \frac{c_{HbO2}}{c_{HbO2} + c_{Hb}} \times 100 \tag{2.5}$$

For the pulse oximetry which is a noninvasive method, Eq. (2.5) is renewed in accordance with the PPG mathematical model (see Eq. (2.4)). Obtaining the oxyhemoglobin and deoxyhemoglobins concentrations (c_{HbO2}, c_{Hb}) from Eq. (2.4) is carried out as follows. At first, both sides of Eq. (2.4) are divided by the incident light intensity, i_o. Next, on the right side of Eq. (2.4) is factorized by the $Static\,Medium$ term, $e^{-\varepsilon_{sm}(\lambda)c_{sm}d_{sm}}$ and both sides of Eq. (2.4) are again divided by the $Static\,Medium$ term. With this given reorganization, Eq. (2.4) is given rise to Eq. (2.6). Later, the value of one is subtracted on both sides of Eq. (2.6) yielding Eq. (2.7).

$$\frac{i_{PPG}(t)}{i_o e^{-\varepsilon_{sm}(\lambda)c_{sm}d_{sm}}} = \left[1 + \frac{e^{-[\varepsilon_{HbO2}(\lambda)c_{HbO2} + \varepsilon_{Hb}(\lambda)c_{Hb}]d_{dm}(t)}}{e^{-\varepsilon_{sm}(\lambda)c_{sm}d_{sm}}}\right] \tag{2.6}$$

$$\frac{i_{PPG}(t)}{i_o e^{-\varepsilon_{sm}(\lambda)c_{sm}d_{sm}}} - 1 = \frac{e^{-[\varepsilon_{HbO2}(\lambda)c_{HbO2} + \varepsilon_{Hb}(\lambda)c_{Hb}]d_{dm}(t)}}{e^{-\varepsilon_{sm}(\lambda)c_{sm}d_{sm}}} \tag{2.7}$$

After that, Eq. (2.7) is recast under the optical path length varying conditions of diastole and systole periods (see Figure 1.3). During the diastole period at time t, a human heart is relaxed and this condition results the optical path length term, $d_{dm}(t)$, in Eq. (2.7) to be l. Eq. (2.7) is updated to Eq. (2.8). For the systole period at time $t + \Delta t$, the human heart pushes blood throughout the human body making the optical path length term, $d_{dm}(t)$, in Eq. (2.7) expanding by Δl. Eq. (2.7) is therefore amended to Eq. (2.9).

$$\frac{i_{PPG}(t)}{i_o e^{-\varepsilon_{sm}(\lambda)c_{sm}d_{sm}}} - 1 = \frac{e^{-[\varepsilon_{HbO2}(\lambda)c_{HbO2} + \varepsilon_{Hb}(\lambda)c_{Hb}](l)}}{e^{-\varepsilon_{sm}(\lambda)c_{sm}d_{sm}}} \tag{2.8}$$

$$\frac{i_{PPG}(t+\Delta t)}{i_o e^{-\varepsilon_{sm}(\lambda)c_{sm}d_{sm}}} - 1 = \frac{e^{-[\varepsilon_{HbO2}(\lambda)c_{HbO2} + \varepsilon_{Hb}(\lambda)c_{Hb}](l+\Delta l)}}{e^{-\varepsilon_{sm}(\lambda)c_{sm}d_{sm}}} \tag{2.9}$$

To extract the oxyhemoglobin and deoxyhemoglobins concentrations (c_{HbO2} , c_{Hb}), Eq. (2.9) is divided by Eq. (2.8). As a result, two terms, $e^{-\varepsilon_{sm}(\lambda)c_{sm}d_{sm}}$ as well as $e^{-[\varepsilon_{HbO2}(\lambda)c_{HbO2}+\varepsilon_{Hb}(\lambda)c_{Hb}](l)}$ are cancelled out and the resulting division produces Eq. (2.10). After dividing, a negative natural logarithm is taken on both sides of Eq. (2.10) generating Eq. (2.11). On the left side of Eq. (2.11) is the absorbance value, A, of the oxyhemoglobin and deoxyhemoglobin concentrations and is thus reduced to be A.

$$\frac{\dfrac{i_{PPG}(t+\Delta t)}{i_o e^{-\varepsilon_{sm}(\lambda)c_{sm}d_{sm}}}-1}{\dfrac{i_{PPG}(t)}{i_o e^{-\varepsilon_{sm}(\lambda)c_{sm}d_{sm}}}-1} = e^{-[\varepsilon_{HbO2}(\lambda)c_{HbO2}+\varepsilon_{Hb}(\lambda)c_{Hb}](\Delta l)} \tag{2.10}$$

$$\overbrace{-\ln\left[\frac{\dfrac{i_{PPG}(t+\Delta t)}{i_o e^{-\varepsilon_{sm}(\lambda)c_{sm}d_{sm}}}-1}{\dfrac{i_{PPG}(t)}{i_o e^{-\varepsilon_{sm}(\lambda)c_{sm}d_{sm}}}-1}\right]}^{A} = [\varepsilon_{HbO2}(\lambda)c_{HbO2}+\varepsilon_{Hb}(\lambda)c_{Hb}](\Delta l) \tag{2.11}$$

The term, Δl , is subject to be eliminated. To do so, two lights which are red and IR lights are employed in the pulse oximeter [8]. Hence, Eq. (2.11) is developed to be the absorbance values of red and IR lights as written in Eq. (2.12) and Eq. (2.13), respectively.

$$A_{RED} = [\varepsilon_{HbO2}(\lambda_{RED})c_{HbO2}+\varepsilon_{Hb}(\lambda_{RED})c_{Hb}](\Delta l) \tag{2.12}$$

$$A_{IR} = [\varepsilon_{HbO2}(\lambda_{IR})c_{HbO2}+\varepsilon_{Hb}(\lambda_{IR})c_{Hb}](\Delta l) \tag{2.13}$$

By dividing Eq. (2.12) by Eq. (2.13), the term, Δl , is removed and the resulting relation is stated in Eq. (2.14). The ratio of A_{RED} to A_{IR} in Eq. (2.14) is denoted as R.

$$R = \frac{[\varepsilon_{HbO2}(\lambda_{RED})c_{HbO2}+\varepsilon_{Hb}(\lambda_{RED})c_{Hb}]}{[\varepsilon_{HbO2}(\lambda_{IR})c_{HbO2}+\varepsilon_{Hb}(\lambda_{IR})c_{Hb}]}, \quad where\ R = \frac{A_{RED}}{A_{IR}} \tag{2.14}$$

At last, Eq. (2.14) is combined and rearranged with Eq. (2.5) and the new expression of the percentage of oxygen saturation (SpO2) is expressed by Eq. (2.15).

$$SpO2 = \frac{\varepsilon_{Hb}(\lambda_{RED})-\varepsilon_{Hb}(\lambda_{IR})R}{\varepsilon_{Hb}(\lambda_{RED})-\varepsilon_{HbO2}(\lambda_{RED})+[\varepsilon_{HbO2}(\lambda_{IR})-\varepsilon_{Hb}(\lambda_{IR})]R}\times 100 \tag{2.15}$$

In practice, the $Dynamic\,Medium$ term in Eq. (2.4) is the treated like an alternating current (AC) component in the electrical aspect because this term is a pulsating part. Likewise, the $Static\,Medium$ term in Eq. (2.4) is considered to be a direct

current (DC) component because of a non-waveform characteristic. Dividing Eq. (2.9) by Eq. (2.8) seemingly is the ratio of the AC component of the PPG signal to the DC component of the PPG signal. Usually, the AC part refers to the peak-to-peak value of the PPG signal and the DC part indicates the lower peak value of the PPG signal. Hence, for simplicity, the absorbance value, A, is calculated through the ratio of the AC part of the PPG signal to the DC part of the PPG signal. In addition, in a real implementation, the PPG signal is converted from the electrical current form to the electrical voltage form. For this reason, Eq. (2.12) and Eq. (2.13) are written by the other statements in Eq. (2.16) and Eq. (2.17), respectively. To distinguish the PPG signals obtained from different color light sources, the color light is placed in front of the PPG signal as a prefix. In Eq. (2.16), the value of V_{AC_RED} is the peak-to-peak value of the red PPG signal and the value of V_{DC_RED} is the lower peak value of the red PPG signal. For Eq. (2.17), the values of V_{AC_IR} and V_{DC_IR} are the peak-to-peak value of the IR PPG signal and the lower peak value of the IR PPG signal, respectively.

$$A_{RED} = \frac{V_{AC\_\mathrm{RED}}}{V_{DC\_RED}} \tag{2.16}$$

$$A_{IR} = \frac{V_{AC\_IR}}{V_{DC\_\mathrm{IR}}} \tag{2.17}$$

By revising Eq. (2.12) and Eq. (2.13) to be Eq. (2.16) and Eq. (2.17), the R ratio in Eq. (2.14) is also changed to Eq. (2.18).

$$R = \frac{A_{\mathrm{RED}}}{A_{IR}} = \frac{\dfrac{V_{AC\_\mathrm{RED}}}{V_{DC\_RED}}}{\dfrac{V_{AC\_IR}}{V_{DC\_IR}}} \tag{2.18}$$

Due to the dissimilarity of each human body and the different manufacturing material of each pulse oximeter brand, the R ratio needs to be normalized. As a result of normalizing the R ratio, the factors of human and instrumental diversities can be considered in the same norm. In fact, the R ratio has already normalized implicitly. This is because the A_{RED} absorbance value and the A_{IR} absorbance values are beforehand normalized by the process of dividing Eq. (2.9) by Eq. (2.8). Under the similar norm of the R ratio, the calculation of SpO2 value in Eq. (2.15) is improved to Eq. (2.19).

$$SpO2 = 110 - 25 \times R \tag{2.19}$$

The computation of SpO2 value in Eq. (2.19) is brought to use by empirical experiments through various human subjects and brands of pulse oximeters according to [8].

2.3 Analysis of SpO2 error

As can be observed in the section 2.2, the SpO2 value depends on the AC and DC components of the red and IR PPG signals. Hence, any undesirable factors applied on the red and IR PPG signals lead to the SpO2 error. Such unpleasant factors disfeature the waveforms of the red and IR PPG signals. Among all unwelcome factors, the factor of motion activities is the most concerned. Under motion condition, the multiplicative and additive interferences are involved in the given PPG model (see Eq. (2.4)). In this section, the interfering influences of the multiplicative and additive manner are therefore analyzed to realize how the affected PPG model throws the error to the SpO2 value.

Using both red and IR PPG signals having relative low effect of motion entailed would give a normal SpO2 value. On the other hand, utilizing both red and IR PPG signals having relative high proportion of motion intertwined would result a defective SpO2 value. This is because any human organ movement affects the optical path length values of the concerned media to either expand or shrink. During any somatic motions, the optical path length value of the dynamic medium is mostly distorted from the typical optical path length values of the processes of systole and diastole. To illustrate the moving effect, an error optical path length variable l_{e1} is added to the regular optical path length term of the diastole period in Eq. (2.8) yielding Eq. (2.20). Likewise, another error optical path length variable l_{e2} is plus to the usual optical path length term of the systole interval in Eq. (2.9) giving Eq. (2.21).

$$\frac{i_{cPPG}(t)}{i_o e^{-\varepsilon_{sm}(\lambda)c_{sm}d_{sm}}} - 1 = \frac{e^{-[\varepsilon_{HbO2}(\lambda)c_{HbO2}+\varepsilon_{Hb}(\lambda)c_{Hb}](l+l_{e1})}}{e^{-\varepsilon_{sm}(\lambda)c_{sm}d_{sm}}} \tag{2.20}$$

$$\frac{i_{cPPG}(t+\Delta t)}{i_o e^{-\varepsilon_{sm}(\lambda)c_{sm}d_{sm}}} - 1 = \frac{e^{-[\varepsilon_{HbO2}(\lambda)c_{HbO2}+\varepsilon_{Hb}(\lambda)c_{Hb}](l+\Delta l+l_{e2})}}{e^{-\varepsilon_{sm}(\lambda)c_{sm}d_{sm}}} \tag{2.21}$$

On the contrary, the optical path length value of the static medium is barely contorted while any moving gestures take place. The static medium is therefore considered to have no influence on worsening the SpO2 value. In addition, the absorbing expression of the static medium is still $e^{-\varepsilon_{sm}(\lambda)c_{sm}d_{sm}}$ as shown in Eq. (2.20) and Eq. (2.21). Moreover, the $i_{PPG}(t)$ term becomes $i_{cPPG}(t)$ to point out that the PPG signal is now contaminated, and the $i_{cPPG}(t)$ term is referred to the corrupted PPG signal. The $i_{PPG}(t+\Delta t)$ term is also applied and changed to $i_{cPPG}(t+\Delta t)$. Later, Eq. (2.20) and

Eq. (2.21) are turned into the absorbance value having motion noises involved A_c as written in Eq. (2.22).

$$A_c = [\varepsilon_{HbO2}(\lambda)c_{HbO2} + \varepsilon_{Hb}(\lambda)c_{Hb}](\Delta l + l_{e2} - l_{e1}) \quad (2.22)$$

By applying the absorbance value having noises A_n to a pulse oximetry context, Eq. (2.22) is updated to Eq. (2.23) and Eq. (2.24) for the red and IR lights, respectively.

$$A_{cRED} = [\varepsilon_{HbO2}(\lambda_{RED})c_{HbO2} + \varepsilon_{Hb}(\lambda_{RED})c_{Hb}](\Delta l + l_{e2} - l_{e1}) \quad (2.23)$$

$$A_{cIR} = [\varepsilon_{HbO2}(\lambda_{IR})c_{HbO2} + \varepsilon_{Hb}(\lambda_{IR})c_{Hb}](\Delta l + l_{e2} - l_{e1}) \quad (2.24)$$

Subsequently, the ratio containing motion interference R_c of A_{cRED} to A_{cIR} is performed by dividing Eq. (2.23) by Eq. (2.24), and written in Eq. (2.25). As can be noticed in (2.25), both error optical path length terms in Eq. (2.23) and Eq. (2.24) are canceled out. As a result, the R_c relation in Eq. (2.25) is not different from Eq. (2.14).

$$R_c = \frac{[\varepsilon_{HbO2}(\lambda_{RED})c_{HbO2} + \varepsilon_{Hb}(\lambda_{RED})c_{Hb}]}{[\varepsilon_{HbO2}(\lambda_{IR})c_{HbO2} + \varepsilon_{Hb}(\lambda_{IR})c_{Hb}]} \quad (2.25)$$

Although the ratios in Eq. (2.25) and Eq. (2.14) look identical, in fact, the R_c statement in Eq. (2.25) has the motion error hidden in the concentration parameters of c_{HbO2} and c_{Hb}. To explain the concealed motion error in the concentration parameters, c_{HbO2} and c_{Hb}, the human blood flow is assumed to be uniform and the continuity principle of fluid mechanics is introduced. The continuity equation abides by Eq. (2.26). In Eq. (2.26), the a_s variable is the cross-sectional area of the pulsating arterial blood and the v_s variable is the arterial blood velocity during no motion involvement. Next, the a_m variable is the cross-sectional area of the pulsating arterial blood and the v_m variable is the arterial blood velocity under the involvement of motion.

$$a_s v_s = a_m v_m \quad (2.26)$$

When any moving postures compress the optical path length of the dynamic medium (the pulsating arterial blood), the cross-sectional area of the optical path length of this medium is reduced. With the cross-sectional area condensed, a_m is lesser than a_s is. As a result, v_m becomes greater than v_s does according to the continuity equation in Eq. (2.26). Intrinsically, increasing the arterial blood velocity v_m speeds up the concentrations of c_{HbO2} and c_{Hb} to pass through both red and IR lights faster. By passing through red and IR lights quicker due to any motions, the absorptions of c_{HbO2} and c_{Hb} are lesser than usual when compared with those of the absorptions without motion inducing. In contrast to the compression, the optical path length of the dynamic medium is inflated and the cross-sectional area of the optical path length of

this medium is enlarged. After the cross-sectional area is bloated, a_m is greater than a_s is and v_m becomes lesser than v_s does. In consequence of the expansion, the absorptions of c_{HbO2} and c_{Hb} are more than usual when compared with those of the absorptions without body moving. The above analysis finds that the optical path length values of red and IR PPG signals are cancelled out. However, the optical path length values still generates the error on the ratio R_c by distorting the concentrations of c_{HbO2} and c_{Hb}. The concentration variables of c_{HbO2} and c_{Hb} are then altered to c'_{HbO2} and c'_{Hb} , respectively, to indicate the distorted concentrations, and Eq. (2.25) are revised to Eq. (2.27). Eq. (2.27) reveals the multiplicative interfering manner as can be seen that the unusual concentration factors, c'_{HbO2} as well as c'_{Hb}, multiply to other absorbing variables.

$$R_c = \frac{[\varepsilon_{HbO2}(\lambda_{RED})c'_{HbO2} + \varepsilon_{Hb}(\lambda_{RED})c'_{Hb}]}{[\varepsilon_{HbO2}(\lambda_{IR})c'_{HbO2} + \varepsilon_{Hb}(\lambda_{IR})c'_{Hb}]} \tag{2.27}$$

In actuality, not only the multiplicative interference appears during organ motions but the additive interference also emerges at the same time. Both multiplicative interfering expressions of red and IR PPG signals in Eq. (2.20) and Eq. (2.21) are slightly adjusted. The additive interfering term is added to Eq. (2.20) and Eq. (2.21). Therefore, Eq. (2.20) and Eq. (2.21) are updated to Eq. (2.28) and Eq. (2.29), respectively. Since both multiplicative and additive influences occur simultaneously, both impacts are thus shown in Eq. (2.28) and Eq. (2.29) for the complete expression. Mostly, the additive interfering term during organ motions stems from some distorting absorption of human organs, and some external light sources. By nature, the additive interfering term varies over time, and is hence denoted $i_{MA}(t)$ as a function of time.

$$\frac{i_{cPPG}(t)}{i_o e^{-\varepsilon_{sm}(\lambda)c_{sm}d_{sm}}} - 1 = \frac{e^{-[\varepsilon_{HbO2}(\lambda)c'_{HbO2} + \varepsilon_{Hb}(\lambda)c'_{Hb}](l+l_{e1})}}{e^{-\varepsilon_{sm}(\lambda)c_{sm}d_{sm}}} + i_{MA}(t) \tag{2.28}$$

$$\frac{i_{cPPG}(t+\Delta t)}{i_o e^{-\varepsilon_{sm}(\lambda)c_{sm}d_{sm}}} - 1 = \frac{e^{-[\varepsilon_{HbO2}(\lambda)c'_{HbO2} + \varepsilon_{Hb}(\lambda)c'_{Hb}](l+\Delta l+l_{e2})}}{e^{-\varepsilon_{sm}(\lambda)c_{sm}d_{sm}}} + i_{MA}(t) \tag{2.29}$$

By switching the $i_{MA}(t)$ terms of Eq. (2.28) and Eq. (2.29) to the other side, Eq. (2.28) and Eq. (2.29) are rearranged to Eq. (2.30) and Eq. (2.31), in order. As can be noticed in both Eq. (2.30) and Eq. (2.31), the terms of $i_{cPPG}(t)$ and $i_{cPPG}(t+\Delta t)$ are even more aggravated by the effect of $i_{MA}(t)$ after suffering the multiplicative interfering impact.

$$\frac{i_{cPPG}(t)}{i_o e^{-\varepsilon_{sm}(\lambda)c_{sm}d_{sm}}} - 1 - i_{MA}(t) = \frac{e^{-[\varepsilon_{HbO2}(\lambda)c'_{HbO2} + \varepsilon_{Hb}(\lambda)c'_{Hb}](l+l_{e1})}}{e^{-\varepsilon_{sm}(\lambda)c_{sm}d_{sm}}} \tag{2.30}$$

$$\frac{i_{cPPG}(t+\Delta t)}{i_o e^{-\varepsilon_{sm}(\lambda)c_{sm}d_{sm}}} - 1 - i_{MA}(t) = \frac{e^{-[\varepsilon_{HbO2}(\lambda)c'_{HbO2} + \varepsilon_{Hb}(\lambda)c'_{Hb}](l+\Delta l+l_{e2})}}{e^{-\varepsilon_{sm}(\lambda)c_{sm}d_{sm}}} \tag{2.31}$$

Eq. (2.30) and Eq. (2.31) are converted to the absorbance value containing motion interference as resulted in Eq. (2.32). After that, Eq. (2.32) is developed into two absorbance statements of the red and IR lights as written in Eq. (2.33) and Eq. (2.34).

$$\begin{aligned} A_c &= -\ln\left[\frac{\frac{i_{cPPG}(t)}{i_o e^{-\varepsilon_{sm}(\lambda)c_{sm}d_{sm}}}-1-i_{MA}(t)}{\frac{i_{cPPG}(t+\Delta t)}{i_o e^{-\varepsilon_{sm}(\lambda)c_{sm}d_{sm}}}-1-i_{MA}(t)}\right] \\ &= [\varepsilon_{HbO2}(\lambda)c'_{HbO2}+\varepsilon_{Hb}(\lambda)c'_{Hb}](\Delta l + l_{e2}-l_{e1}) \end{aligned} \tag{2.32}$$

$$\begin{aligned} A_{cRED} &= -\ln\left[\frac{\frac{i_{cPPG}(t)}{i_o e^{-\varepsilon_{sm}(\lambda_{RED})c_{sm}d_{sm}}}-1-i_{MA}(t)}{\frac{i_{cPPG}(t+\Delta t)}{i_o e^{-\varepsilon_{sm}(\lambda_{RED})c_{sm}d_{sm}}}-1-i_{MA}(t)}\right] \\ &= [\varepsilon_{HbO2}(\lambda_{RED})c'_{HbO2}+\varepsilon_{Hb}(\lambda_{RED})c'_{Hb}](\Delta l + l_{e2}-l_{e1}) \end{aligned} \tag{2.33}$$

$$\begin{aligned} A_{cIR} &= -\ln\left[\frac{\frac{i_{cPPG}(t)}{i_o e^{-\varepsilon_{sm}(\lambda_{IR})c_{sm}d_{sm}}}-1-i_{MA}(t)}{\frac{i_{cPPG}(t+\Delta t)}{i_o e^{-\varepsilon_{sm}(\lambda_{IR})c_{sm}d_{sm}}}-1-i_{MA}(t)}\right] \\ &= [\varepsilon_{HbO2}(\lambda_{IR})c'_{HbO2}+\varepsilon_{Hb}(\lambda_{IR})c'_{Hb}](\Delta l + l_{e2}-l_{e1}) \end{aligned} \tag{2.34}$$

Eq. (2.33) and Eq. (2.34) are turned to the R_C ratio in Eq. (2.35). In Eq. (2.35), the right hand side appears to equal to R_c in Eq. (2.27). Nevertheless, the absorbing characteristic showing on the right hand side of Eq. (2.35) is worse than the absorbing manner expressing of Eq. (2.27) due to the $i_{MA}(t)$ outturn.

No matter the calculated R ratio is either R_C or R_c makes the obtained SpO2 value deviates from the actual SpO2 value using Eq. (2.19) in the computation.

$$\overbrace{\left(\frac{\ln\left[\frac{\frac{i_{cPPG}(t)}{i_o e^{-\varepsilon_{sm}(\lambda_{RED})c_{sm}d_{sm}}}-1-i_{MA}(t)}{\frac{i_{cPPG}(t+\Delta t)}{i_o e^{-\varepsilon_{sm}(\lambda_{RED})c_{sm}d_{sm}}}-1-i_{MA}(t)}\right]}{\ln\left[\frac{\frac{i_{cPPG}(t)}{i_o e^{-\varepsilon_{sm}(\lambda_{IR})c_{sm}d_{sm}}}-1-i_{MA}(t)}{\frac{i_{cPPG}(t+\Delta t)}{i_o e^{-\varepsilon_{sm}(\lambda_{IR})c_{sm}d_{sm}}}-1-i_{MA}(t)}\right]}\right)}^{R_C} = \frac{[\varepsilon_{HbO2}(\lambda_{RED})c'_{HbO2}+\varepsilon_{Hb}(\lambda_{RED})c'_{Hb}]}{[\varepsilon_{HbO2}(\lambda_{IR})c'_{HbO2}+\varepsilon_{Hb}(\lambda_{IR})c'_{Hb}]} \tag{2.35}$$

In the end of this analysis, one obvious fact is brought to contemplate. The pulse oximeter is normally placed at one of the following places, fingertip, earlobe or forehead during the measurement takes place. The mentioned human organs essentially do not have the arterial and vein vessels inside but contain the arterial and

vein capillaries instead. This fact suggests that the multiplicative interference may not exacerbate the SpO2 value because the optical path length values of the arterial and vein capillaries are hardly altered. The reason behind bare alteration is that the average diameters of the arterial and vein capillaries are miniscule between 6 to 8 μm [46]. Therefore, the optical path length values of the arterial and vein capillaries do not exhibit any length-change significantly while organ moving. Due to very tiny diameters, the cross-sectional area while no motion, a_s, and the cross-sectional area during moving, a_m, written in Eq. (2.26) are approximately equal, $a_s \simeq a_m$. When a_s and a_m are more or less identical, the arterial blood velocities, v_s and v_m, in the arterial capillary during no motion and motion are also approximately equal. Having the similar velocities of the blood flow while at rest and moving, the concentrations of c_{HbO2} and c_{Hb}, are still not changed so the absorptions of c_{HbO2} and c_{Hb}, are usual. The multiplicative interference may be concluded to have low impact to the PPG absorbing model. In this thesis, only the additive interference is concerned and Eq. (2.28) is rearranged to be Eq. (2.36). In addition, Eq. (2.36) is revised to manifest the general PPG form like Eq. (2.4).

$$i_{cPPG}(t) = i_o[e^{-\varepsilon_{sm}(\lambda)c_{sm}d_{sm}} + e^{-[\varepsilon_{HbO2}(\lambda)c_{HbO2}+\varepsilon_{Hb}(\lambda)c_{Hb}]d_{dm}(t)}] + Gi_{MA}(t) \quad \text{where "G" is } i_o e^{-\varepsilon_{sm}(\lambda)c_{sm}d_{sm}}. \tag{2.36}$$

In Eq. (2.36), the G variable is a constant value behaving as gain to $i_{MA}(t)$ so the $Gi_{MA}(t)$ term is simplified to $i_{MA}(t)$ as rewritten in Eq. (2.37). The $i_{MA}(t)$ term in Eq. (2.37) is commonly known as the MA signal.

$$i_{cPPG}(t) = i_o[e^{-\varepsilon_{sm}(\lambda)c_{sm}d_{sm}} + e^{-[\varepsilon_{HbO2}(\lambda)c_{HbO2}+\varepsilon_{Hb}(\lambda)c_{Hb}]d_{dm}(t)}] + i_{MA}(t) \tag{2.37}$$

Eventually, the mathematical model in Eq. (2.37) is later employed to stand for the corrupted mathematical PPG signal expression.

2.4 Frequency translation

To communicate over radio waves, an antenna is required. However, a baseband signal contains low frequency components causing the antenna size to be enormous in order to transmit the baseband signal over the radio waves at any specific velocity. Frequency translation is thus introduced to resolve the antenna issue. By applying the frequency translation, the baseband signal is ridden on a carrier signal. Typically, the carrier signal has high frequency components. With high frequency components of the carrier signal, the antenna size is smaller. Aside from the antenna issue, the frequency translation is also utilized to circumvent any noises having frequency components overlapping with the baseband signal.

For the aspect of radio communications, three well-known techniques of frequency translation are implemented. The first one is an amplitude modulation (AM) and the second is a frequency modulation (FM). The last one is a phase modulation (PM). In this thesis, the amplitude modulation (AM) is made practical use with an emitting-LED system of the pulse oximeter. Only the amplitude modulation (AM) and an amplitude demodulation are furnished.

2.4.1 Amplitude modulation (AM)

An amplitude modulation (AM) [47] can be implemented by various different ways through modifying a mathematical amplitude modulating model. The mathematical model of amplitude modulation is simply derived from a product-to-sum formula of trigonometry to generate the translation of frequency. Adjusting the trigonometric product-to-sum formula in conjunction with filtering methods can potentially give AM double side band suppressed carrier (AM-DSBSC), AM single side band (AM-SSB) and AM-DSB with carrier. Quadrature AM (QAM) and AM vestigial side band (AM-VSB) are also initially developed from the trigonometric product-to-sum formula like the others. Among the AM techniques, the AM-DSB with carrier (AM-DSBWC) is ubiquitously utilized because other methods of AM face the difficulty of demodulating. The AM-DSB with carrier recognized as the standard AM is mostly found in radio and television broadcasts. To avoid complication in demodulation, the AM-DSB with carrier is opted to put into practice on the pulse oximeter. Only the AM-DSB with carrier, which will be referred as the standard AM for short, is centered and its principle is described as follows.

For convenience in explanation, let $m(t)$ be a message signal of interest containing only one frequency component and contain no dc component, as represented by Eq. (2.38). In Eq. (2.38), the A_m and ω_m variables are the amplitude and the angular frequency of the message signal of interest, respectively.

$$m(t) = A_m \cos(\omega_m t) \tag{2.38}$$

To shift the message signal of interest to a desirable angular frequency, a carrier sinusoidal signal having the carrier angular frequency ω_c denoted $c(t)$ as written in Eq. (2.39) is introduced.

$$c(t) = \cos(\omega_c t) \tag{2.39}$$

The carrier sinusoidal signal $c(t)$ is brought to multiply with the concerned message signal $m(t)$ yielding the frequency translation of AM-DSBSC resulted in Eq. (2.40).

$$\phi_{DSBSC}(t) = \overbrace{\cos(\omega_c t)}^{c(t)}[\underbrace{A_m \cos(\omega_m t)}_{m(t)}] \tag{2.40}$$

By applying the trigonometric product of cosine and cosine to sum formula provided in Eq. (2.41) to Eq. (2.40), the AM-DSBSC expression in Eq. (2.40) becomes Eq. (2.42).

$$\cos(a)\cos(b) = \tfrac{1}{2}[\cos(a+b) + \cos(a-b)] \tag{2.41}$$

$$\phi_{DSBSC}(t) = \frac{A_m}{2}[\overbrace{\cos(\omega_c - \omega_m)t}^{Lower\ side\ band} + \overbrace{\cos(\omega_c + \omega_m)t}^{Upper\ side\ band}] \tag{2.42}$$

As can be observed in Eq. (2.42), the carrier signal $c(t)$ is absent and lower ($\omega_c - \omega_m$) and upper ($\omega_c + \omega_m$) side bands containing the message of interest signal $m(t)$ are created. For the AM-DSBSC confronts the hassle problem of $m(t)$ demodulation. To make the $m(t)$ demodulation easier, the same carrier signal $c(t)$ gained by a factor of A_c is added to Eq. (2.40). Eq. (2.40) is rearranged to Eq. (2.43) which represents the standard AM, and the system of the standard AM according to Eq. (2.43) can be diagramed in Figure 2.4. The ratio of A_m to A_c in Eq. (2.43) is called as the modulation index and assigned to μ. Eq. (2.43) is thus updated to Eq. (2.44).

$$\phi_{AM}(t) = A_c[1 + \frac{A_m}{A_c}\cos(\omega_m t)]\cos(\omega_c t) \tag{2.43}$$

$$\phi_{AM}(t) = A_c[1 + \mu\cos(\omega_m t)]\cos(\omega_c t) \tag{2.44}$$

For a complex message signal having multiple frequency components, the modulation index is calculated through dividing the minimum value of the absolute message signal by the value of A_c. The mathematical form is written in Eq. (2.45).

$$\mu = \frac{|m(t)|_{\min}}{A_c} \tag{2.45}$$

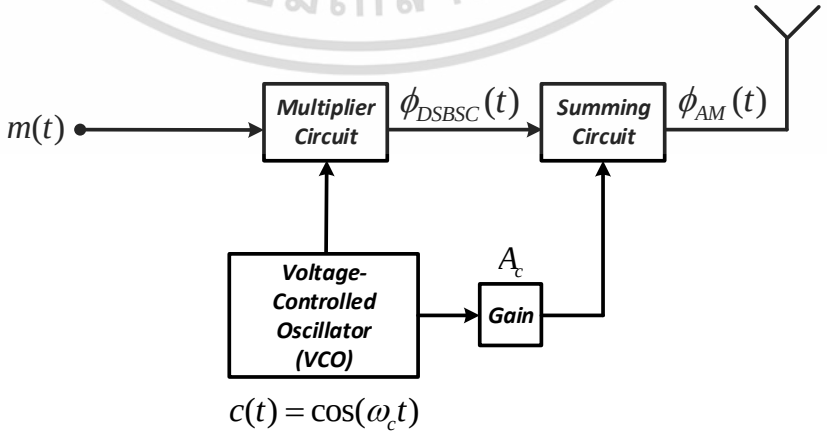

Figure 2.4 The system of the AM.

The modulation index indicates the quantity by which the message of interest signal $m(t)$ rides on the carrier signal $c(t)$. Riding on the carrier signal $c(t)$ of the concerned message signal $m(t)$ generates an envelope resembling to the message signal. The envelope does not actually form but the actuality is an imaginary line connecting the peaks of the modulated carrier signal as if the actual line of envelope is formed [47]. The envelope is relevant to the modulation index because the value of the modulation index defines the obviousness of the envelope. The blatancy of the envelope is the heart of the AM since the envelope helps the AM demodulation to be simple. Otherwise, a complicated method of AM demodulation such as coherent demodulation is implemented. The modulation index is in the range of -1 and 1 ($|\mu| \leq 1$). With the modulation index approaching to either -1 or 1, the envelope is fully present. By contrast, the modulation index pointing to 0 causes the envelope to show poorly. Normally, the modulation index is manifested in terms of percentage as written in Eq. (2.46). In Figure 2.5, three different modulation indices are illustrated.

$$Percentage\,of\ Modulation = |\mu| \times 100 \tag{2.46}$$

From Figure 2.5, the upper trace shows the 50% of modulation index and the middle row renders the 100% of modulation index. The lower subplot is the more than 100% of the modulation index. When the percentage of the modulation index is more than 100%, the phenomenon of over-modulation occurs. The over-modulation causes the phase of the carrier signal to reverse. With phase inverting of the carrier signal results in distortion of the recovered message signal because undesirable harmonic components are also demodulated along with the message signal.

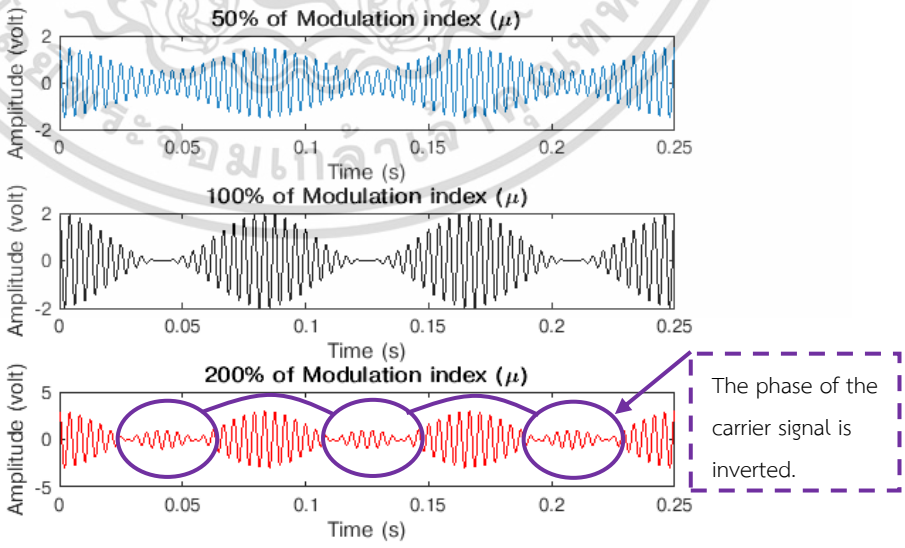

Figure 2.5 Different modulation indices.

To determine the bandwidth usage of the standard AM, Eq. (2.44) is readjusted by the trigonometric product-to-sum formula. Eq. (2.44) is turned to Eq. (2.47). The second term in Eq. (2.47) consists of the lower and upper side bands of the modulated message signal and the bandwidth usage of both bands are computed by Eq. (2.48).

$$\phi_{AM}(t) = \overbrace{A_c \cos(\omega_c t)}^{Carrier\ signal} + \underbrace{\overbrace{\frac{A_m}{2}\cos(\omega_c - \omega_m)t}^{Lower\ side\ band} + \overbrace{\frac{A_m}{2}\cos(\omega_c + \omega_m)t}^{Upper\ side\ band}}_{Modulated\ message\ signal} \tag{2.47}$$

$$\begin{aligned} Bandwidth &= (\omega_c + \omega_m) - (\omega_c - \omega_m) \\ &= 2\omega_m \end{aligned} \tag{2.48}$$

The efficiency of the AM in terms of power dissipation is considered by finding the ratio of the total power to the sum power of sidebands, as shown in Eq. (2.49).

$$Efficiency = \frac{Power_{sidebands}}{Power_{total}} \times 100\% \tag{2.49}$$

The total power is the sum of the root mean squares (RMS) power of all terms in Eq. (2.47), and can be stated by Eq. (2.50). For the sum power of sidebands is the sum of the RMS power of the last two terms of Eq. (2.47), and can be rendered by Eq. (2.51).

$$Power_{total} = \frac{A_c^2}{2} + \frac{A_m^2}{8} + \frac{A_m^2}{8} \tag{2.50}$$

$$Power_{sidebands} = \frac{A_m^2}{8} + \frac{A_m^2}{8} \tag{2.51}$$

By plugging Eq. (2.50) and Eq. (2.51) into Eq. (2.49) as well as reorganizing the edited Eq. (2.49) yields Eq. (2.52). Under the best condition in which the percentage of μ is 100% approximately gives the 33% power efficiency of the message signal at best. The other 67% power efficiency is dissipated by the carrier signal. For the circumstances of the percentage of μ below 100%, the power efficiency of the message signal will be lower than 33% definitely, as depicted in Figure 2.6. In reality, the message signal often contains several frequency components which is not as simple as the given example, $A_m \cos(\omega_m t)$. Implementing the standard AM by which the modulated message signal dissipates exact 33% of power to prevent the event of over-modulating is hardly accomplished. Hence, the modulated message signal is always controlled to consume the power lesser than 33%. Obviously, the technique of AM provides a simple demodulation but loses 67% of power to the carrier signal.

$$Efficiency = \frac{\mu^2}{2 + \mu^2} \times 100\% \tag{2.52}$$

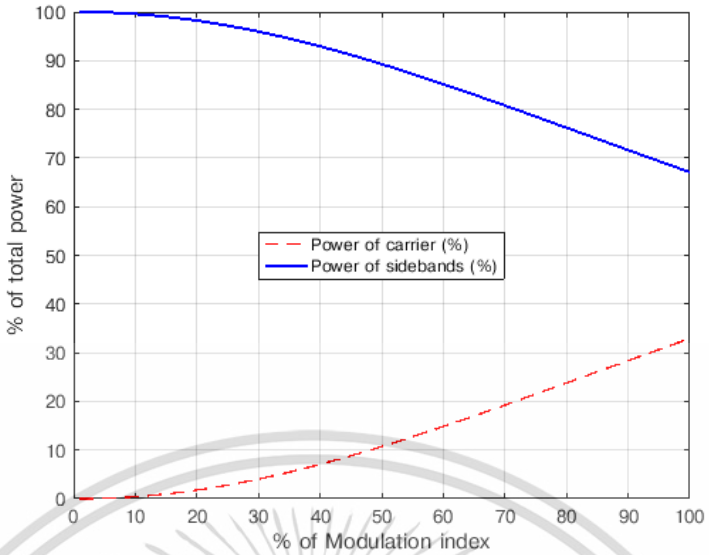

Figure 2.6 Power dissipations of sidebands and carrier.

2.4.2 Amplitude demodulation

An amplitude demodulation is the process of which a message signal is recovered back to its original waveform. Various methods are utilized. These techniques are categorized into two main methods which are asynchronous and synchronous methods. Because the system of standard AM is not necessary to synchronize the transmitted carrier signal at a receiver, mere asynchronous technique is focused.

The most ubiquitously implemented asynchronous approach of amplitude demodulation is an envelope detector. The envelope detector simply works by detecting the carrier envelope linearly varied according to the message signal through a diode associated with a combination of resistor and capacitor as illustrated in Figure. 2.7(a). In Figure 2.7(a), the received AM signal is represented by $\hat{\phi}_{AM}(t)$. Also in Figure 2.7(a), after the received AM signal passing through the envelope detector generates the recovered message signal which is symbolized as $m(t)$. To succinctly explain the amplitude demodulation, the example waveform of the received AM signal depicted in Figure 2.7(b) is considered. Initially, the diode rectifies the received AM signal to come out only the positive side of voltage, shown in Figure 2.8(a). After rectifying, the received AM signal becomes a rectified AM signal and is expressed by $\phi_{rectifiedAM}(t)$ in Figure 2.7(a). As can be observed in Figure 2.8(a), the rectified AM signal still contains the high frequency component of the carrier signal. By placing the resistor and the capacitor next to the diode as shown in Figure 2.7(a), the high frequency component of the carrier signal is filtered out. This is because the combination of resistor and capacitor is equivalent to a low pass filter. Once the carrier signal is disappeared, the message signal $m(t)$ is thus recovered and graphically drawn in Figure 2.8(b).

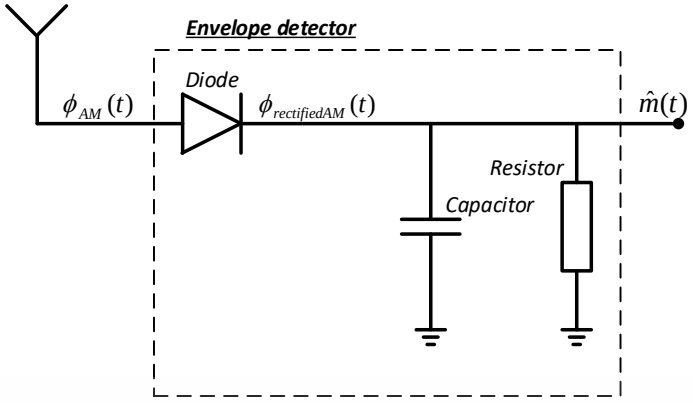

(a) A simple diode and resistor-capacitor combination circuit.

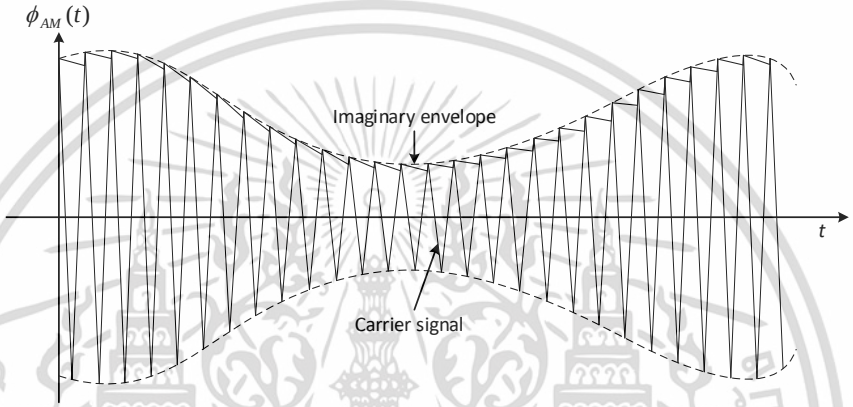

(b) Envelope detecting process.

Figure 2.7 A general envelope detector.

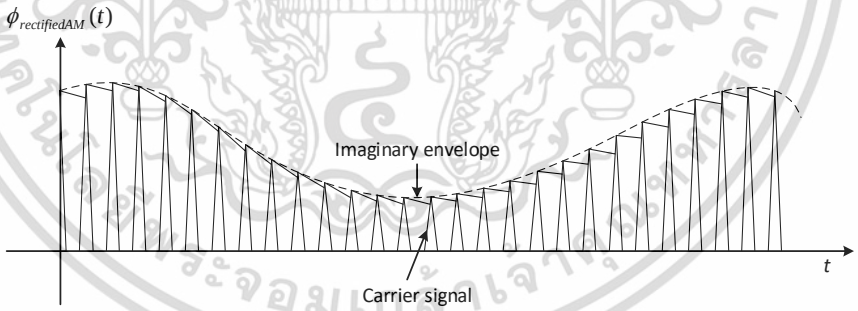

(a) A half-wave rectified signal.

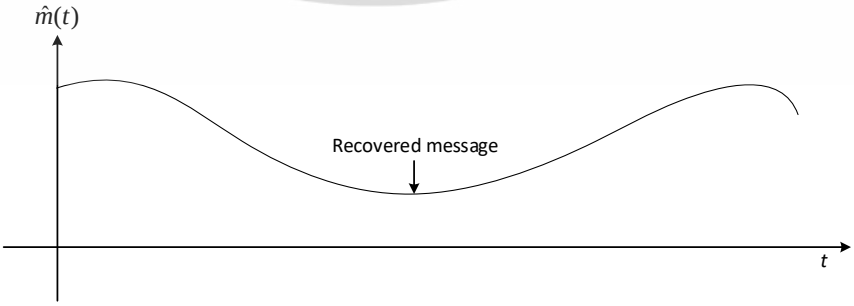

(b) A retrieved message signal.

Figure 2.8 An amplitude demodulating procedure.

2.5 Contemporary methods

In this section, three contemporary methods are briefly explained because they are brought to compare with the proposed technique of frequency translation in this thesis for a comparative study. The selected approaches are the technique of discrete saturation transform (DST), the method of independent component analysis (ICA) and the scheme of compression of Fourier series coefficients (CFC). The criteria for solution choosing are based on well performance, easiness in construction and no need of additional sensing devices.

2.5.1 Discrete saturation transformation (DST)

Discrete saturation transformation (DST) [25] is developed by utilizing an adaptive filtering algorithm and the technique of DST is simply diagrammed in Figure 2.9. The adaptive filtering algorithm used in this thesis is a least mean squares (LMS) algorithm, which is simple and powerful, for implementing the DST technique. As can be seen in the synthesizing dashed box in the Figure 2.9, synthesizing the reference signal is mathematically expressed by Eq. (2.53). The function of $i_{REF}(t)$ over time t is the synthesized reference signal. Next, the $i_{cREDPPG}(t)$ term is the corrupted red PPG signal. The last term is the product of the corrupted IR PPG signal, $i_{cIRPPG}(t)$, and the ratio R referring to the percentage of oxygen saturation (SpO2) values from 1% to 100%. The ratio R is inversely calculated from Eq. (2.19) generating Eq. (2.54).

$$i_{REF}(t) = i_{cREDPPG}(t) - R \times i_{cIRPPG}(t) \tag{2.53}$$

$$R = 4.4 - 0.04 \times SpO2 \tag{2.54}$$

With the ratio R varying from 1% to 100%, a set of the synthesized reference signals is produced. The synthesized reference signal of each ratio R is fed to the adaptive filter one by one. For the desirable signal of the adaptive filter, the pullulated red PPG signal, $i_{cREDPPG}(t)$, is employed for all ratios Rs. The adaptive filter stops when all ratios Rs are swept. The adaptive filter output of which ratio gives the maximum power is contemplated as the measured SpO2 value, as demonstrated in Figure 2.10.

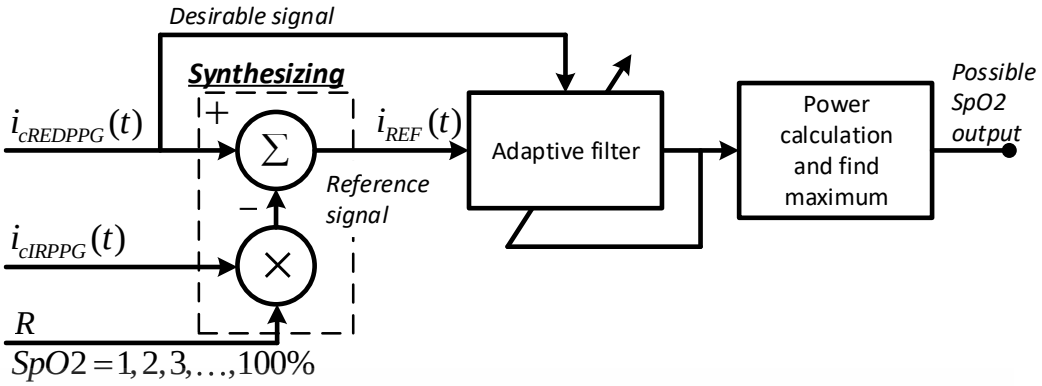

Figure 2.9 A block diagram of discrete saturation transformation (DST).

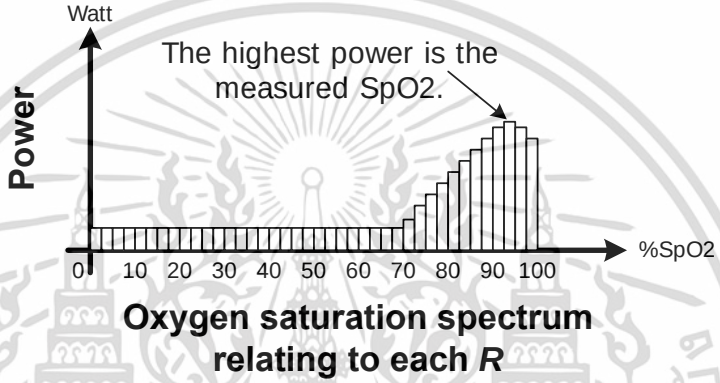

Figure 2.10 An oxygen saturation spectrum.

2.5.2 Independent component analysis (ICA)

Independent component analysis (ICA) [26][35] is a statistical method of parting linearly mingled independent signals. The ICA approach presumes that any independent signal possesses zero level of Gaussianity but when being combined with other independent signals results the mixed signal having high level of Gaussianity. To get the linearly mixed independent signals separated, in this thesis, the algorithm of fast ICA (fICA) is opted for the sake of plainness. The diagram of ICA method is plainly drawn in Figure 2.11. In this context, the linear combination of independent signals is from the clean PPG signals obtained by the red and IR lights as well as the MA signal. Each PPG signal is mixed with the same MA signal at different levels (see the dotted box in the Figure 2.11), as mathematically formed by Eq. (2.55) and Eq. (2.56). From Eq. (2.55) and Eq. (2.56), the functions of $i_{cREDPPG}(t)$ and $i_{cIRPPG}(t)$ are the MA-interfered red and IR PPG signals while $i_{REDPPG}(t)$ and $i_{IRPPG}(t)$ are the MA-free red and IR PPG signals. The MA signal is $i_{MA}(t)$ and the functions of $w_{11}(t)$, $w_{12}(t)$, $w_{21}(t)$, and $w_{22}(t)$ are the gaining coefficients fitted to the functions of $i_{REDPPG}(t)$, $i_{IRPPG}(t)$ and $i_{MA}(t)$ at time t.

$$i_{cREDPPG}(t) = w_{11}(t)i_{REDPPG}(t) + w_{12}(t)i_{MA}(t) \quad (2.55)$$

$$i_{cIRPPG}(t) = w_{21}(t)i_{IRPPG}(t) + w_{22}(t)i_{MA}(t) \quad (2.56)$$

Then, Eq. (2.55) and Eq. (2.56) are re-expressed by a matrix form of the ICA method forming Eq. (2.57) where the matrix $\mathbf{x}$ is the mixing signals referring to $i_{cREDPPG}(t)$ and $i_{cIRPPG}(t)$. The matrix $\mathbf{W}$ is the mixing coefficients of gain and the matrix $\mathbf{s}$ is the sources of signals which are $i_{REDPPG}(t)$, $i_{IRPPG}(t)$ and $i_{MA}(t)$. In ICA, $i_{REDPPG}(t)$ and $i_{IRPPG}(t)$ are just the same clean PPG signal so they are assigned to $i_{PPG}(t)$. By reiterative running the algorithm of fICA on Eq. (2.57), the matrix $\mathbf{W}$ is kept updating until the condition of non-Gaussianity is met. Once, the non-Gaussianity condition is reached. The function of $i_{PPG}(t)$ is favorably separated.

$$\mathbf{x} = \mathbf{W}\mathbf{s} \quad (2.57)$$

After the ICA solution is complete, either the extracted $i_{PPG}(t)$ or the separated $i_{MA}(t)$ is subject to further do other signal processing methods to eliminate the MA signal intertwining with $i_{cREDPPG}(t)$ and $i_{cIRPPG}(t)$. When the MA signal is removed, the repaired signals of $i_{cREDPPG}(t)$ and $i_{cIRPPG}(t)$ are used to estimate the SpO2 value according to Eq. (2.18) and Eq. (2.19).

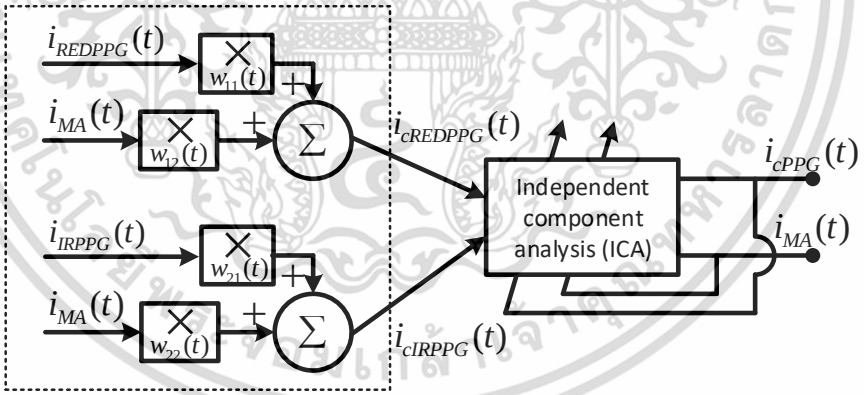

Figure 2.11 A block diagram of independent component analysis (ICA).

2.5.3 Compression of Fourier series coefficients (CFC)

Compression of Fourier series coefficients (CFC) [32] simply truncates any unwanted Fourier series coefficients which are not a member of the clean PPG signal. The processing procedures of the CFC scheme are depicted as a block diagram in Figure 2.12. Basically, Fourier series is applicable for a periodic signal. Nevertheless, the clean PPG signal is not exact the periodic signal but a quasi-periodic signal. To make use of Fourier series with the clean PPG signal, the clean PPG signal is parted cycle-by-cycle. After cycle separation, each cycle is thus analyzed. In the event of motion interference, the clean PPG signal is united with the MA signal giving the distorted PPG signal. The method of CFC is still usable however the MA-combined PPG signal must sufficiently manifest the cardiac cycle (see Figure 1.3) in order to apply the CFC technique effectively.

From Figure 2.12, both polluted red and IR PPG signals are firstly fed to the cycle split-up block to separate each cardiac cycle. After that, each parted cycle of each PPG signal is inserted to the Fourier series analysis block to extract the Fourier series coefficients. In the analysis, each split cycle of each PPG signal is expressed by a general form of Fourier series expansion in Eq. (2.58) and Eq. (2.59), respectively. In Eq. (2.58) and Eq. (2.59), $i_{cREDPPG\_cycle}(t)$ represents one cycle of the corrupted red PPG signal and $i_{cIRPPG\_cycle}(t)$ stands for single cycle of the distorted IR PPG signal. The functions of $i_{cREDPPG\_cycle}(t)$ and $i_{cIRPPG\_cycle}(t)$ are stated as the functions varied over time t. Next, the k variable is a coefficient index starting from one and the ω variable is an angular frequency. Later, ${}_{RED}a_0$, ${}_{RED}a_k$ and ${}_{RED}b_k$ are the Fourier series coefficients of $i_{cREDPPG\_cycle}(t)$ and ${}_{IR}a_0$, ${}_{IR}a_k$, and ${}_{IR}b_k$ are the Fourier series coefficients of $i_{cIRPPG\_cycle}(t)$. From there, only the first twelve significant coefficients of ${}_{RED}a_k$, ${}_{RED}b_k$, ${}_{IR}a_k$, and ${}_{IR}b_k$ are kept and the remnant coefficients are truncated. In addition, ${}_{RED}a_0$ and ${}_{IR}a_0$ are also retained. The process of keeping the desirable coefficients is accomplished in the block of truncation. Finally, all selected significant coefficients of each separated cycle of each PPG signal are reconstructed to the truncated red and IR PPG signals, $i_{trREDPPG}(t)$ and $i_{trIRPPG}(t)$ by reversing Fourier series. The truncated red and IR PPG signals are converted to the SpO2 value by Eq. (2.18) and Eq. (2.19). The truncating process runs until all split cycles created from $i_{cREDPPG}(t)$ and $i_{cIRPPG}(t)$ are analyzed. In the end, all calculated SpO2 values obtained from each cycle are averaged.

$$i_{cREDPPG\_cycle}(t) = {}_{R}a_0 + \sum_{k=1}^{\infty} {}_{R}a_k \cos(k\omega t) + {}_{R}b_k \sin(k\omega t) \quad (2.58)$$

$$i_{cIRPPG\_cycle}(t) = {}_{IR}a_0 + \sum_{k=1}^{\infty} {}_{IR}a_k \cos(k\omega t) + {}_{IR}b_k \sin(k\omega t) \quad (2.59)$$

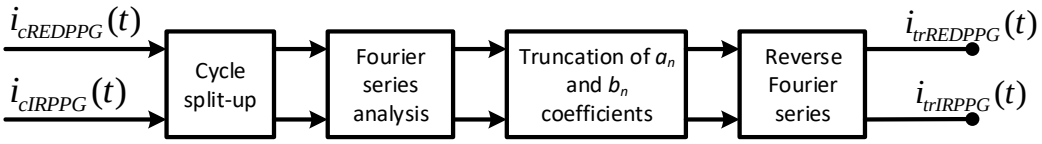

Figure 2.12 A block diagram of compression of Fourier series coefficients (CFC).

CHAPTER 3

Principles and Implementation

In this chapter, a photoplethysmographic (PPG) mathematical model is improved to satisfy a technique of frequency translation which is an approach of amplitude modulation (AM) at first. Secondly, the implementation on a practical pulse oximeter is explained. Thirdly, influence of light intensity on a PPG signal is justified. Fourthly, a few statistical indicators for signal evaluation are described. Eventually, various experiments to test the implementation are listed.

3.1 Improvement of PPG mathematical model

With being in the identical frequency band of both a PPG signal and an MA signal, the PPG signal is intertwined with the MA signal inevitably. To separate the PPG frequency components from the MA frequency components, a method of frequency translation known as an amplitude modulation (AM) is applied. By utilizing the technique of amplitude modulation (AM) effectively, the undesirable MA signal is considered to be an additive type.

In [48], an experiment pertaining to study the MA genre is conducted. The studied experiment is accomplished as follows. A stable absorbing rigid material craved like an index finger is plugged into a commercial pulse oximeter. Then, this pulse oximeter is tied to each volunteer's left index finger. Each volunteer is later asked to perform the everyday finger movements under the dark condition and the bright condition, respectively, in order to observe the output signal of each condition. The finger movements are the following postures, finger bending, horizontal finger moving, finger shivering, vertical finger moving and finger waving. Under the dark condition, the output signal of each participant comes out in the same way. The output signals for all participants do not change in line with each finger movement but their output signals are just a constant signal. For the bright condition, the output signal of each volunteer is proportional to each finger movement. Also, the output signals for all volunteers emerge in the same direction. The output signals acquired during the bright condition seem to sit over the constant output signals obtained under the dark condition. According to the superposition principle, the occurred MA signal can be inferred to be an additive kind of interference.

Since the stable absorbing rigid material is not as soft as a real finger, during finger movements unquestioningly thus makes a real finger to budge like the performed finger movements. With the actual finger plugged into a pulse oximeter during the finger movements, the appeared MA signal is considered to be generated from two sources. The first source is from the external light sources as explained in [48]. For the second source is from the distorting absorption of human organs residing inside the finger. The distorting absorption causes the effect of undesirable absorption added to the normal PPG absorption. The second source is hence contemplated to be the additive kind rather than a multiplicative kind as supported by the explanation in Chapter 2 under Section 2.3. Practically, the pulse oximeter is designed to relatively fit to the finger. The external light sources may not always penetrate through the pulse oximeter for all finger movements. Summarily, the second source is therefore more influential to the occurred MA signal than the first source.

Intrinsically, the mentioned finger movements are induced in a natural manner meaning that the given finger movements are relatively slow. As a result, the MA signals of the referred finger movements are contained with the frequency components located at lower band of frequency from 0 to 5 Hz. As the MA frequency components are at lower band similar to the PPG frequency components, this explains why the PPG signal is contaminated. However, not all frequency components of the PPG and MA signals are superimposed. Only some frequency components of both signals are overlapped and demonstrated in Figure 3.1 [48]. In Figure 3.1, the x-y axis represents the frequency components in the unit of Hertz (Hz) and the light intensity in the unit of Ampere (Amp), respectively.

As can be observed in Figure 3.1, some overlapped frequency components of the PPG and MA signals are summed. In order to resolve this overlapping issue having the additive characteristic, the usage of AM technique is fit to translate the frequency components of the PPG signal away from the frequency components of the MA signal.

By utilizing the frequency translation based on the AM technique, the desirable PPG frequency components are lifted to the desirable frequency location away from the undesirable MA frequency components. With this frequency translation, the PPG signal is mostly prevented from the MA signal in a frequency domain as graphically drawn in Figure 3.2.

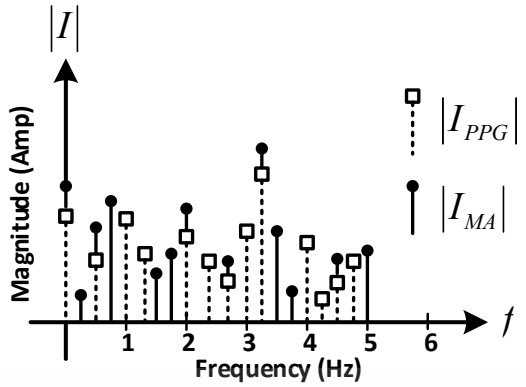

Figure 3.1 Overlapped frequency components.

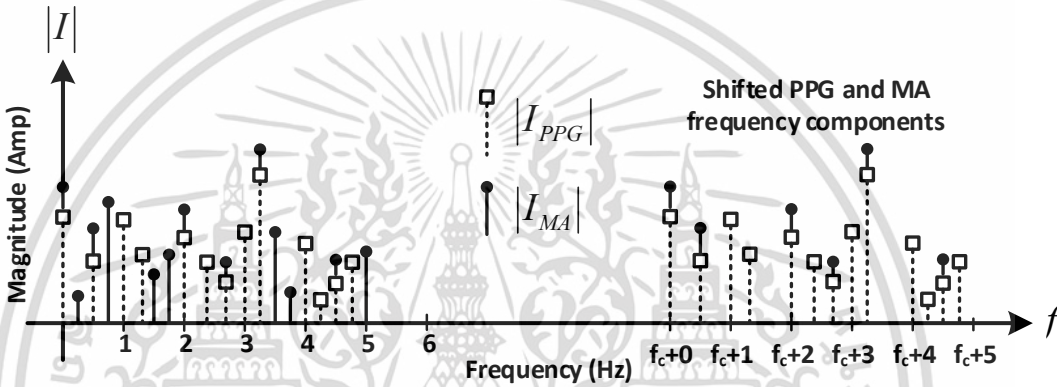

Figure 3.2 Shifted PPG and MA frequency components.

As can be noticed in Figure 3.2, the MA frequency components having the frequency components matched to the PPG frequency components are also together shifted. Nonetheless, the magnitude ratio of a pair of the shifted PPG frequency component which is superimposed to the matched shifted MA frequency component is fairly low. Having low magnitude ratio suggests that the MA signal containing only the shifted MA frequency components does not have the significant impact enough to distort the lifted PPG signal.

Before doing the development of AM strategy, the contaminated PPG mathematical expression in keeping with Eq. (2.37) is rewritten here again in Eq. (3.1).

$$i_{cPPG}(t) = i_o[e^{-\varepsilon_{sm}(\lambda)c_{sm}d_{sm}} + e^{-[\varepsilon_{HbO2}(\lambda)c_{HbO2}+\varepsilon_{Hb}(\lambda)c_{Hb}]d_{dm}(t)}] + i_{MA}(t) \qquad (3.1)$$

For simplicity, some terms are changed as follows. According to the explanation of human body absorption in Chapter 2 under Section 2.1, the $e^{-\varepsilon_{sm}(\lambda)c_{sm}d_{sm}}$ term is altered to a constant variable denoted A_s because of the reason of fairly stable absorption. Next, the term of $e^{-[\varepsilon_{HbO2}(\lambda)c_{HbO2}+\varepsilon_{Hb}(\lambda)c_{Hb}]d_{dm}(t)}$ is the concerned message which is a pulsatile signal yielding the varying absorption over time with gain A_m thus this term is converted to $A_m m(t)$. After redefining, Eq. (3.1) is updated to Eq. (3.2).

$$i_{cPPG}(t) = i_o[A_s + A_m m(t)] + i_{MA}(t) \tag{3.2}$$

To improve Eq. (3.2) to satisfy the AM technique, a direct current (DC) source employed to emit a light-emitting diode (LED) is simply changed to an alternating current (AC) source. The AC source drives the LED at the carrier angular frequency of ω_c rad/s and produces the varying incident light intensity by $i_{AC}\cos(\omega_c t)$ when touching the medium of interest. By altering the source of LED-driving, the constant incident light intensity i_o falling upon the concerned medium is transformed to $i_{AC}\cos(\omega_c t)$ abiding by the nature of the AC source. Eq. (3.2) thus becomes Eq. (3.3).

$$i_{cPPG}(t) = i_{AC}\cos(\omega_c t)[A_s + A_m m(t)] + i_{MA}(t) \tag{3.3}$$

After that, Eq. (3.3) is reorganized by pulling the A_s variable out of the square bracket and Eq. (3.3) is recast in Eq. (3.4). As can be observed in Eq. (3.4), the first combination on the right hand side satisfies the general AM form shown in Eq. (2.44).

$$i_{cPPG}(t) = \underbrace{i_{AC}A_s}_{A_c}[1 + \underbrace{(A_m/A_s)}_{\mu} m(t)]\cos(\omega_c t) + i_{MA}(t) \tag{3.4}$$

From Eq. (3.4), a few points deviate from the general AM form such as the product term $i_{AC}A_s$ and the modulation index (μ) term A_m/A_s. However, these mentioned points do not change the property of AM. The information of interest $m(t)$ is still amplitude-modulated to the desirable frequency location.

When two AC sources are implemented on the pulse oximeter, the PPG mathematical expression is actually developed to Eq. (3.5). In Eq. (3.5), $i_{rR\_IR\_AM}(t)$ represents the received signal detected by the photo-detector. Next, ϕ_{R_AM} stands for the red PPG AM signal modulated by the first AC source and ϕ_{IR_AM} acts for the IR PPG AM signal modulated by the second AC source. The first AC source produces a carrier sinusoidal signal having the carrier amplitude of i_{AC1} and the angular carrier frequency of ω_{c1} rad/s for ϕ_{R_AM}. The other AC source yields another carrier sinusoidal signal having the carrier amplitude of i_{AC2} and the angular carrier frequency of ω_{c2} rad/s for ϕ_{IR_AM}. Both ϕ_{R_AM} and ϕ_{IR_AM} are fully expanded in Eq. (3.6) and Eq. (3.7), consecutively. Eq. (3.6) and Eq. (3.7) are derived from Eq. (3.4).

$$i_{rR\_IR\_AM}(t) = \phi_{R\_AM}(t) + \phi_{IR\_AM}(t) + i_{MA}(t) \tag{3.5}$$

$$\phi_{R\_AM} = i_{AC1}A_{sR}[1 + (A_{mR}/A_{sR})m_R(t)]\cos(\omega_{c1}t) + i_{MA}(t) \tag{3.6}$$

$$\phi_{IR\_AM} = i_{AC2}A_{sIR}[1 + (A_{mIR}/A_{sIR})m_{IR}(t)]\cos(\omega_{c2}t) + i_{MA}(t) \tag{3.7}$$

In Eq. (3.6), A_{sR} is the absorbing value of red light taken place in the static medium. The A_{mR} variable is the amplitude of the concerned message $m_R(t)$ resulting from

the red light absorption in the dynamic medium. For Eq. (3.7), the variables of A_{sIR}, A_{mIR} and $m_{IR}(t)$ are also defined in the same way as A_{sR}, A_{mR} and $m_R(t)$ but expressed for the IR light absorption. In addition, keeping in mind, i_{AC1} and i_{AC2} are referred to the incident light intensities dropping upon the medium surface.

To show that the red and IR PPG signals are translated to the desirable frequencies, Eq. (3.5) including Eq. (3.6) and Eq. (3.7) is turned into a frequency domain. Eq. (3.5) in association with Eq. (3.6) and Eq. (3.7) is thus converted to the frequency domain by performing the technique of FFT, as written in Eq. (3.8).

$$\begin{aligned} I_{rR\_IR\_\mathrm{AM}}(\omega) = {} & \frac{i_{AC1}A_{sR}}{2}[\delta(\omega-\omega_{c1})+\delta(\omega+\omega_{c1})] \\ & + \frac{i_{AC1}A_{mR}}{2}[M_R(\omega-\omega_{c1})+M_R(\omega+\omega_{c1})] \\ & + \frac{i_{AC2}A_{sIR}}{2}[\delta(\omega-\omega_{c2})+\delta(\omega+\omega_{c2})] \\ & + \frac{i_{AC2}A_{mIR}}{2}[M_{IR}(\omega-\omega_{c2})+M_{IR}(\omega+\omega_{c2})] + I_{MA}(\omega) \end{aligned} \tag{3.8}$$

As can be seen in Eq. (3.8), the red PPG frequency components, M_R, are attached to the first angular carrier frequency ω_{c1}. The IR PPG frequency components, M_{IR}, are also stuck with the second angular carrier frequency ω_{c2}. By contrast, the MA frequency components, I_{MA}, is still at the near-zero frequency bands not shifted.

3.2 Practical implementation

In general, a commercial pulse oximeter employs an ordinary LEDs-drive method to emit both red and infrared (IR) LEDs as portrayed in Figure 3.3. Both LEDs are fed by a direct current (DC) source at the voltage of +5 V alternately. In other words, the red LED is on when the IR LED is off. While the red LED is off, the IR LED is on. The on-off interval is done at the frequency of 1000 Hz [9]. The reason for alternating is for separating and obtaining both red and IR PPG signals by employing only one photo-detector to calculate the SpO2 value in the pulse oximeter context.

Not alternating would result one summed PPG signal which does not meet the pulse oximeter need which requires red and IR PPG signals when only one photo-detector is applied. The resultant summed PPG signal is the aggregate of both red and IR PPG signals which are aggregated in both time and frequency domains. Due to the similarity of frequency components, the red PPG signal and the IR PPG signal are thus not able to be extracted from the resultant summed PPG signal. If the red PPG signal and the IR PPG signal are combined in the time domain but parted in the frequency domain, they can be extracted in the frequency domain.

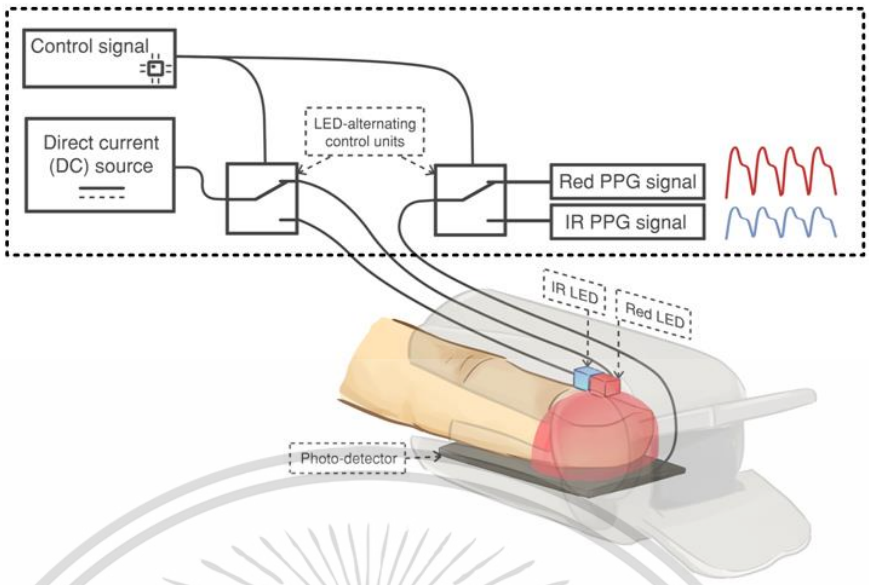

Figure 3.3 A classical LEDs-emitting method used in a pulse oximeter.

The conventional LEDs-emitting method driving both red and infrared LEDs in the manner of alternation holds the PPG frequency components in the same frequency band of a baseband signal. Aside from the PPG frequency components being in the frequency band of the baseband signal, the MA frequency components are also in the similar band. To shift the PPG frequency components away from the MA frequency, the traditional LEDs-shining approach is entirely changed to the proposed LEDs-driving technique. Instead of emitting each LED at different times, the proposed LEDs-shining technique employs two sinusoidal signals having dissimilar frequencies to concurrently emit the red and IR LEDs. One sinusoidal signal is applied to only one LED. By utilizing two sinusoidal signals containing unlike frequencies, both LEDs can be driven simultaneously and both red and IR PPG signals are not summed even one photo-detector is used. This is because both red and IR PPG signals are literally separated in a frequency domain. In order to generate two sinusoidal signals having different frequencies, two alternating current (AC) sources each having discrepant frequencies are employed. The improvement is accomplished by replacing the dotted box shown Figure 3.3 with the proposed LEDs-emitting approach drawn in Figure 3.4.

In Figure 3.4, a signal generator is brought to supplant the DC source to power red and IR LEDs. The signal generator implemented in this thesis is built from two IC AD9833 programmable waveform generators to provide two channel outputs for shining the red and IR LEDs. The IC AD9833 is manufactured to generate various common waveforms in the frequency range of 0 to 12.5 MHz, and operates at a power supply voltage of +5 V. Besides, the units of control signal and LED-alternating control are superseded by a reference voltage unit and a transimpedance amplifier (TIA).

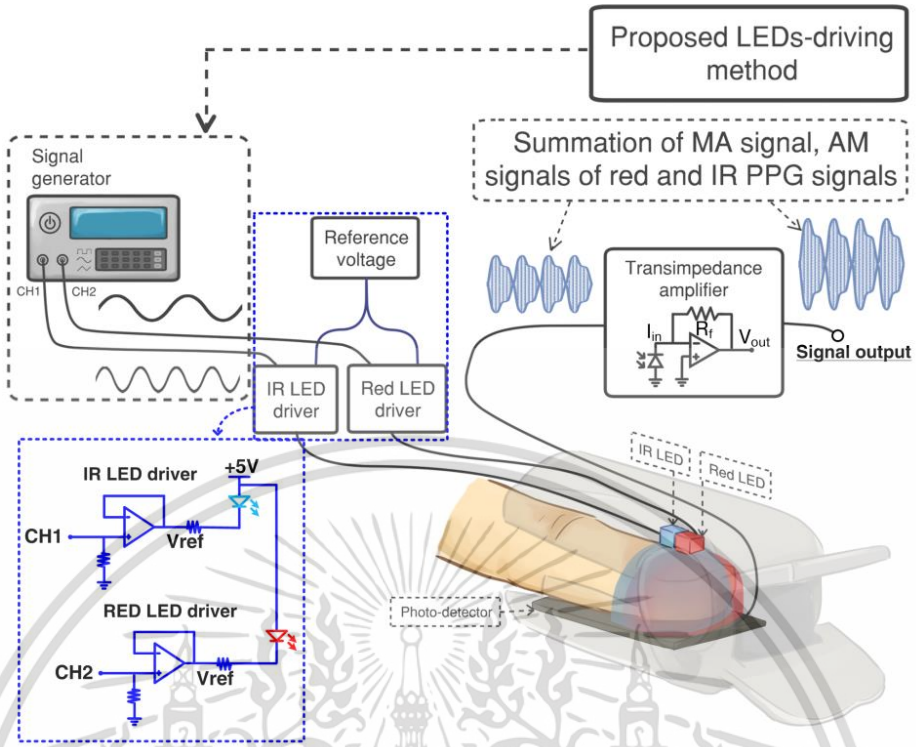

Figure 3.4 A proposed LEDs-driving technique implemented in a pulse oximeter.

The reference voltage unit is employed to function as an equivalent ground performing the reference voltage instead of connecting to the real ground for both LEDs. The reference voltage unit comprises of two buffer amplifiers. The transimpedance amplifier (TIA) is brought to augment the detected signal from the photo-detector because the strength sensed signal is fairly low. Apart from boosting the signal level, the TIA also transforms the electrical current form detected by the photo-detector to the electrical voltage form making further processing conveniently.

3.2.1 Signal generator

In this subtopic, the design of how a signal generator is built is described. The signal generator is constructed from four main components which are a controlling component, a waveform generating component, a signal offset voltage component and a signal amplifying component, respectively. These components are mingled together and graphically portrayed in Figure 3.5. The designed signal generator is powered by which a 50-watt switching power supply manufactured by MEANWELL is capable of DC supplying ±12 V and +5 V. For the DC voltage supply of +3.3 V is supplied from the microcontrollers used in the controlling component.

The controlling component consists of two microcontrollers (ATMEGA328) marked as Ctrl1 and Ctrl 2, respectively, and one 4x4 keypad signed as KP1. Ctrl1 is designed to control the waveform generators (IC AD9833) which are marked as W1 and

W2 in the waveform generating component in order to generate two different waveform signals. The communication between Ctrl1 and the waveform generators is established through the serial peripheral interface (SPI). In this thesis, two sinusoidal signals having different frequencies are required. Hence, Ctrl1 is programmed to command W1 and W2 to generate the sinusoidal signals according to the flowchart diagrammed in Figure 3.6 as follows. W1 and W2 each is designed to generate a sinusoidal signal having the frequency approaching 1000 Hz [9]. According to the flowchart exhibited in Figure 3.6, initially, an AD9833 library is included in Ctrl1 in order to make Ctrl1 recognize W1 and W2. Next, two pins are defined in Ctrl1 to identify W1 and W2. Then, two AD9833 objects related to W1 and W2 are created for calling the AD9833 methods built in the included library. After that, Ctrl1 attempts to establish connection with W1 first and W2 later. In case of failure to create the connection with either W1 or W2, an alarm event is flagged and requires manual repair until the alarm event is disappeared. After the alarm event is solved, Ctrl1 is necessary to restart itself to run from the beginning again. With this designed algorithm, W1 and W2 are surely established with Ctrl1 and generate two signal outputs to serve the signal generator purpose. When Ctrl1 is able to communicate with W1 and W2, two parameters which are a type of waveform and a desirable frequency are transmitted to W1 and W2. For W1, the sinusoidal waveform is selected and the frequency of 1070 Hz is set. For W2, the sinusoidal waveform is also chosen and the frequency of 800 Hz is set. Finally, Ctrl1 instructs W1 and W2 to enable their signal outputs (V_{sig1} and V_{sig2}). These two frequencies are opted from the available electronic devices at the time of implementation. To prevent any damages that may occur on W1 and W2, both generated sinusoidal signals are fed to two separate buffer amplifiers [49]. These two buffer amplifiers are constructed from two op-amps embedded in IC TL062 marked as OA1 in the waveform generating component. After passing through the buffer amplifiers, the output sinusoidal signals (V_{bsig1} and V_{bsig2}) are gained by which they are fed to two different instrumentation amplifiers marked as IA1 and IA2. Each instrumentation amplifier implemented in this thesis is IC AD620. The amplifying gain G_{IA} provided by each IC AD620 is calculated by Eq. (3.9) [50]. Each IC AD620 is configured to furnish the amplifying gain of 2.8 by plugging the gain resistor (R_G) of 27 $k\Omega$ into each IC AD620. The gain resistors are marked as RG1 and RG2, consecutively. After signal amplifying, the two output sinusoidal signals (V_{bsig1} and V_{bsig2}) become V_{Gsig1} and V_{Gsig2} as written in Eq. (3.10) and Eq. (3.11).

$$G_{IA} = 49.4k\Omega[R_G^{-1}] + 1 \tag{3.9}$$

$$V_{Gsig1} = G_{IA}V_{bsig1} \quad where \quad G_{IA} = 2.8 \tag{3.10}$$

$$V_{Gsig2} = G_{IA}V_{bsig2} \quad where \quad G_{IA} = 2.8 \tag{3.11}$$

For Ctrl2 is dealt with adjusting the signal offset voltage and the signal gain. Instead of using an analog potentiometer in signal gain adjustment as well as signal offset voltage alteration, a digital potentiometer (IC MCP41050) is introduced. The digital potentiometer is programmable. For MCP41050, the resistant value can be programmed to vary in the range of 0 to 50 $k\Omega$ which is divided into 256 steps starting from 0 to 255. Each step approximates 195.3 Ω. In this design, Ctrl2 is connected with four digital potentiometers marked as DP1, DP2, DP3 and DP4 in the signal offset voltage component and the signal amplifying component, respectively. Ctrl2 communicates with DP1, DP2, DP3 and DP4 via SPI. DP1 and DP2 are assigned to control the signal offset voltage as well as, DP3 and DP4 are assigned to control the signal gain. DP1 and DP2 each behaves like an analog potentiometer. Thus, the offset voltages, V_{ofst1} and V_{ofst2}, furnished by DP1 and DP2 are equivalently expressed by Eq. (3.12) and Eq. (3.13). In Eq. (3.12) and Eq. (3.13), R_{adj_DP1} and R_{adj_DP2} are the resistor values programmed by Ctrl2 of DP1 and DP2, and 3.3 is the DC voltage supplied by Ctrl2. R_{adj_DP1} and R_{adj_DP2} are functioned as varying gain from 0 to 1.

$$V_{ofst1} = 3.3R_{adj\_DP1} \tag{3.12}$$

$$V_{ofst2} = 3.3R_{adj\_DP2} \tag{3.13}$$

To sum two signals, a general non-inverting summing amplifier based on an op-amp [49] is applied. For this thesis, IC TL062 marked OA2 is brought to handle the summation of V_{ofst1} and V_{Gsig1}, and the combination of V_{ofst2} and V_{Gsig2}. When V_{ofst1} is connected to the non-inverting summing amplifier, DP1 is equivalently acted like a 3.3 V DC is connected in series with R_{adj_DP1} (see a dotted box in Figure 3.5). Due to the same structure as V_{ofst1}, V_{ofst2} is performed not different from V_{ofst1} (see a dashed box in Figure 3.5). Hence, by employing the basic non-inverting summing amplifier, the summation of V_{ofst1} and V_{Gsig1} is written in Eq. (3.14) where V_{sum1} is the summed signal of V_{ofst1} and V_{Gsig1}. Likewise, V_{ofst2} and V_{Gsig2} are combined and stated in Eq. (3.15) yielding the unified signal, V_{sum2}. In Eq. (3.14) and Eq. (3.15), the resistant values of R_{11}, Rf_{11}, Rf_{12}, R_{21}, Rf_{21}, and Rf_{22} are set to 10 $k\Omega$. By setting Rf_{12}, R_{21}, Rf_{21}, and Rf_{22} equally, the gain factor of 2 is generated and multiplied to each summed signal. Lastly, V_{sum1} and V_{sum2} are wired to DP3 and DP4, respectively, in the signal amplifying component to augment their magnitudes.

$$V_{sum1} = \left(1 + \frac{Rf_{12}}{Rf_{11}}\right)\left(V_{Gsig1} \cdot \frac{R_{adj\_DP1}}{R_{11} + R_{adj\_DP1}} + 3.3 \cdot \frac{R_{11}}{R_{11} + R_{adj\_DP1}}\right) \tag{3.14}$$

$$V_{sum2} = \left(1 + \frac{Rf_{22}}{Rf_{21}}\right)\left(V_{Gsig2} \cdot \frac{R_{adj\_DP2}}{R_{21} + R_{adj\_DP2}} + 3.3 \cdot \frac{R_{21}}{R_{21} + R_{adj\_DP2}}\right) \tag{3.15}$$

The augmented summed signals denoted V_{Gsum1} and V_{Gsum2}, in order, are expressed in Eq. (3.16) and Eq. (3.17) where R_{adj_DP3} and R_{adj_DP4} are the resistor values programmed by Ctrl2 of DP3 and DP4. From Eq. (3.16) and Eq. (3.17), R_{adj_DP3} is the gain factor of V_{sum1} and R_{adj_DP4} is likewise the gain factor of V_{sum2}. Before V_{Gsum1} and V_{Gsum2} are connected to red and IR LEDs, they are separately passed to two separate buffer amplifiers giving rise to V_{out1}(CH1) and V_{out2}(CH2). These two buffer amplifiers are implemented from two op-amps implanted in IC TL062 tagged by OA3.

$$V_{Gsum1} = V_{sum1} R_{adj\_DP3} \tag{3.16}$$

$$V_{Gsum2} = V_{sum2} R_{adj\_DP4} \tag{3.17}$$

In adjusting the signal offset voltage and the signal gain is done through KP1. Each button furnished by KP1 is set to perform a specific task according to the instruction coded in Ctrl2. In this design, eight buttons which are 1-button, 2-button, 3-button, 4-button, 5-button, 6-button, B-button and A-button are programmed as follows. The 1-button increases the signal gain by one step while the 2-button decreases the signal gain by one step. For the 3-button, the signal gain is lifted up by five steps. By contrast, the A-button moves the signal gain down by five steps. The other four buttons are for altering the signal offset voltage. The 4-button and the 6-button perform one-step increment and five-step increment, consecutively. The other way round is that the 5-button is set to one step down and the B-button is placed to five steps up. Each assigned button is programmed by the flowchart in a dashed box of Figure 3.7. The flowchart above the dashed box in Figure 3.7 is the initial controlling settings programmed like the flowchart in Figure 3.6.

In this thesis, the implementation of signal generator uses IC AD9833 to generate a desirable signal. As IC AD9833 is a low-cost product, it may thus not function as good as a commercial signal generator. IC AD9833 only operates on a +5 VDC single-supply system while the commercial signal generator operates on a ±12 VDC dual-supply system. This makes the commercial signal generator is more flexible the signal generator constructed by IC AD9833. To enhance the implemented signal generator to function as identical as the commercial signal generator, a high quality type of a signal generating IC should be brought to implement.

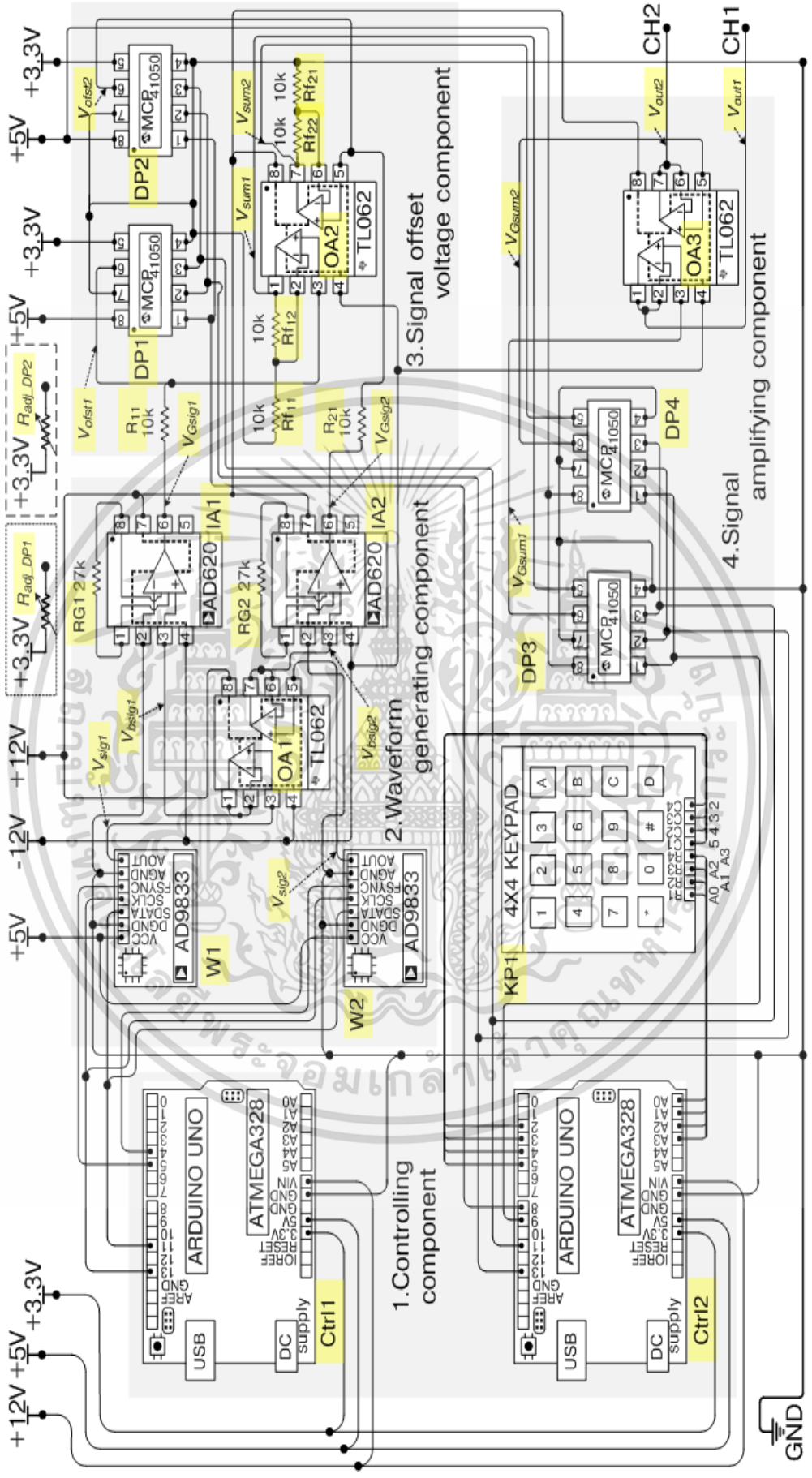

Figure 3.5 Diagram of a designed signal generator.

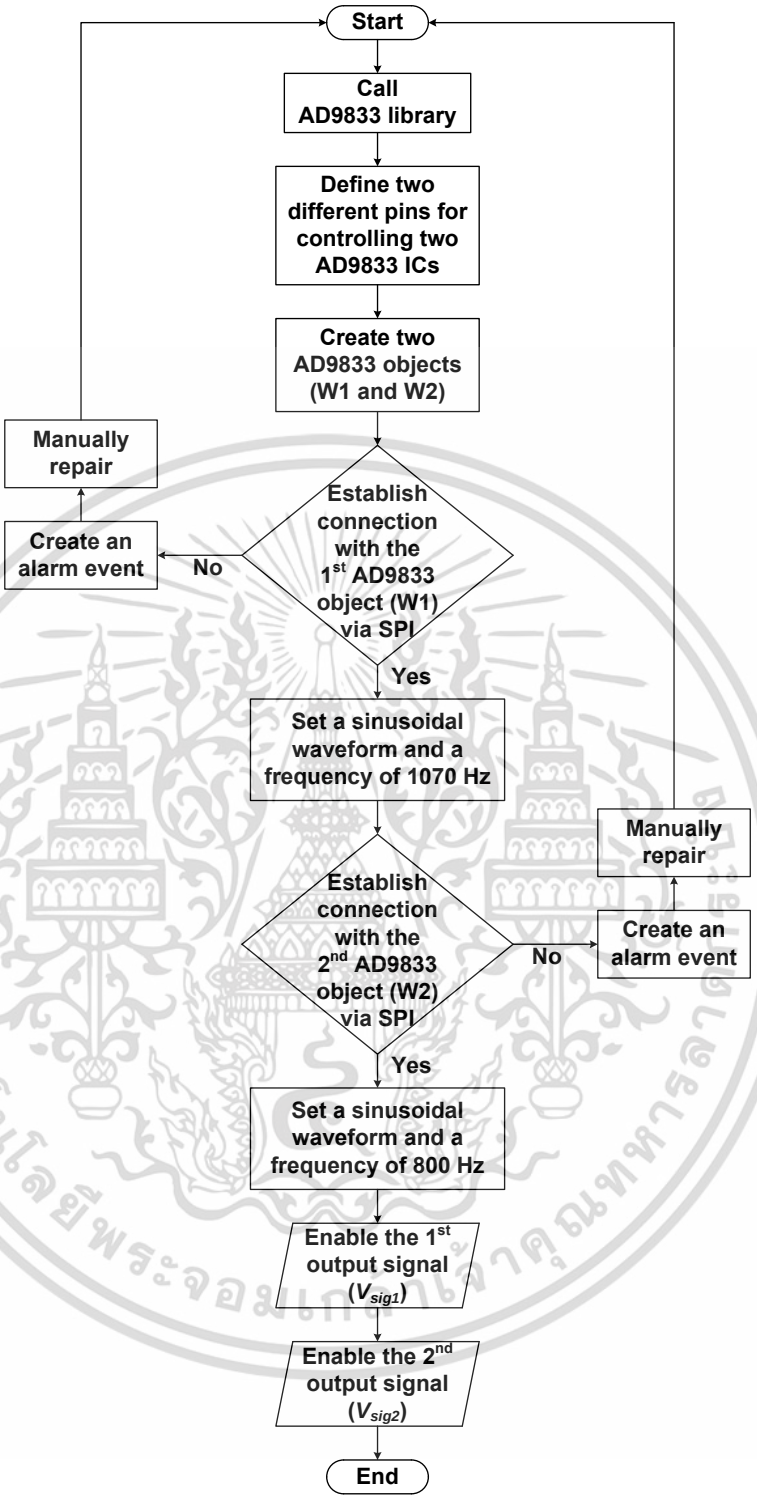

Figure 3.6 Flowchart of generating a signal.

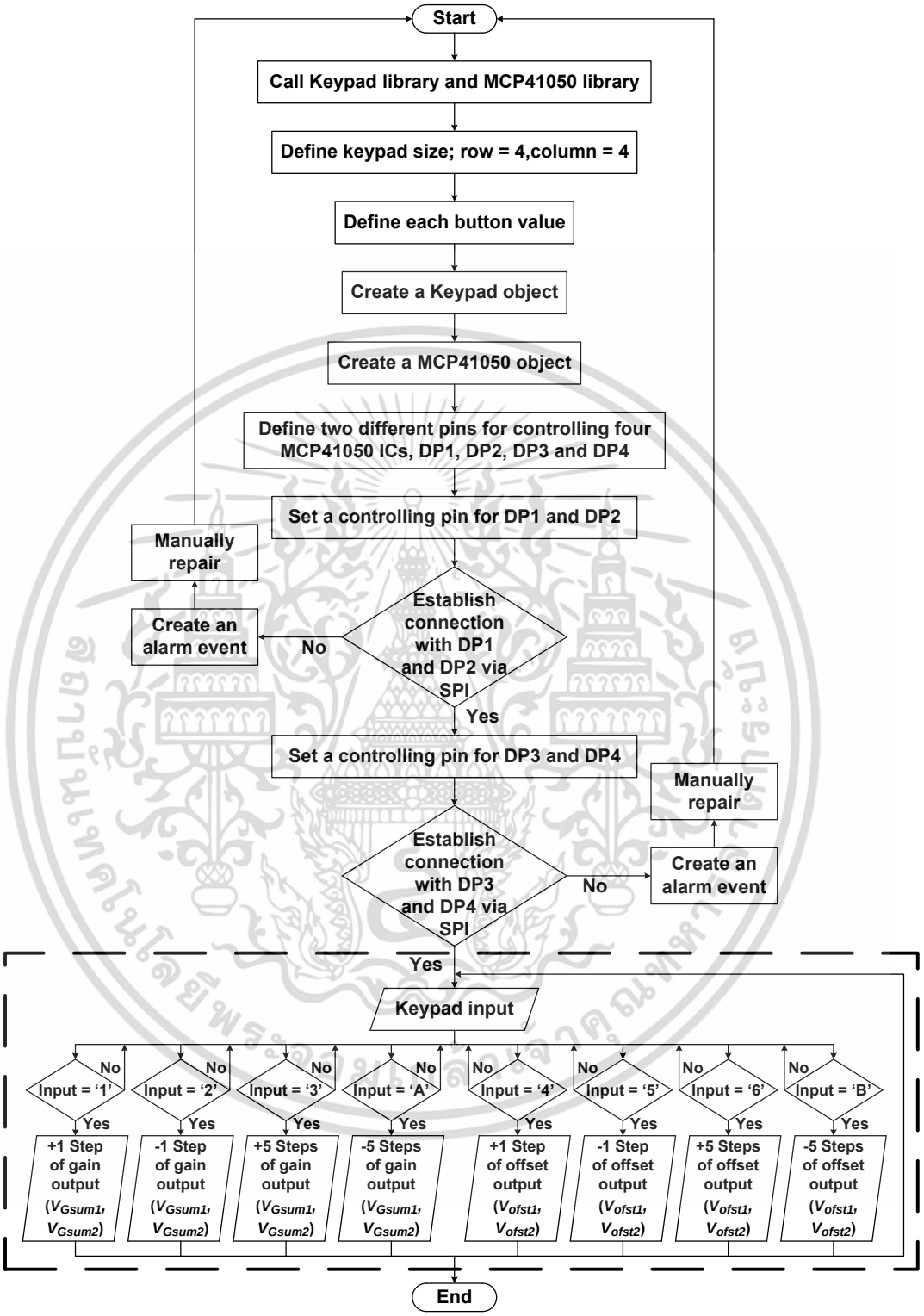

Figure 3.7 Flowchart of adjusting offset voltage and gain.

3.2.2 Reference voltage and radiated power

In a final product of a commercial pulse oximeter probe, the anode pins of red and IR LEDs are soldered together and generally wired to +5 V DC. The other two cathode pins of red and IR LEDs are left floating for the purpose of controlling. Normally, the reference voltage of 0 V DC known as the electrical ground is employed in a common pulse oximeter. The electrical ground is controlled to attach to the cathode pin of the LED that is being driven while the cathode pin of the other LED is left floating. By utilizing the constant reference voltage which is 0 V DC, each LED shines light intensity in a constant manner. To illuminate the light intensity in the sinusoidal pattern, an AC source is introduced to use as the reference voltage. In this thesis, two AC sources having different frequencies are implemented to provide two references of voltage, as depicted in Figure 3.8. Figure 3.8 is drawn from the signal generator section and the reference voltage section of Figure 3.4. One AC source is designed to fix to only one LED cathode pin. In addition, each AC source is attached to a simple buffer amplifier before connecting to the LED. The simple buffer amplifier is used to protect each AC source by blocking any unexpected effects generated by the LED and the +5 V DC source.

To calculate the power radiated by each LED, the electrical current of each LED is required. By applying Kirchhoff's current law (KCL), the electrical currents of both IR and red LEDs denoted I_{IRLED} and I_{REDLED}, shown in Figure 3.8 are mathematically expressed by Eq. (3.18) and Eq. (3.19).

$$I_{IRLED} = \frac{5V - V_{fIR} - V_{ref1}}{R_{IR2}} \tag{3.18}$$

$$I_{REDLED} = \frac{5V - V_{fRED} - V_{ref2}}{R_{RED2}} \tag{3.19}$$

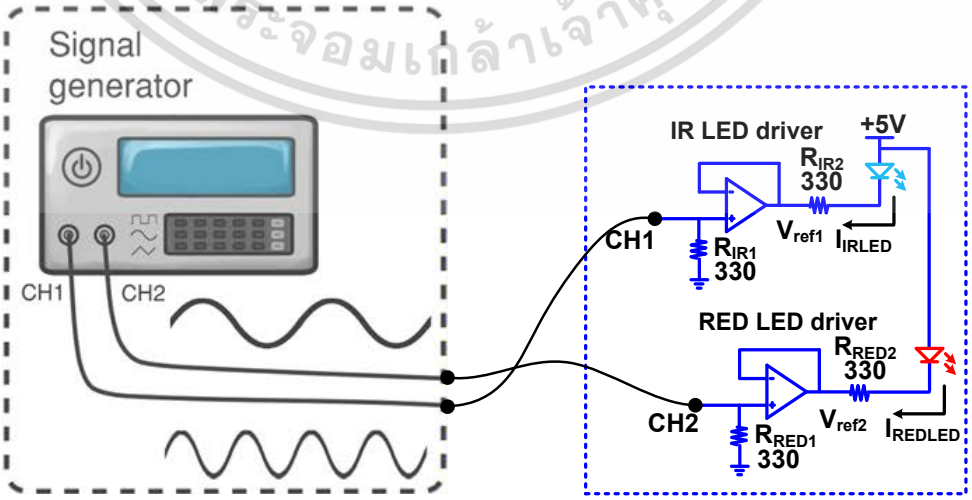

Figure 3.8 Implementation of reference voltage.

In Eq. (3.18) and Eq. (3.19), V_{fIR} and V_{fRED} are the forward voltages dropped across the IR and red LEDs. A typical IR LED has the average forward voltage of 1.8 V while a common red LED has the mean forward voltage of 1.85 V [51]. The forward voltages of both LEDs are approximated to 1.8 V because both forward voltages of IR and red LEDs are not much different. As V_{ref1} and V_{ref2} are not constant but varied in the sinusoidal pattern, each bottom voltage peak of each reference voltage is brought to calculate the current of each LED. Bearing in mind, the structures of W1, W2, DP1, DP2, DP3 and DP4 employs the electrical ground (0 V DC) as their reference voltage. As a result, V_{ref1} and V_{ref2} will never go below 0 V. At the same time, V_{ref1} and V_{ref2} are designed to always have their lowest voltage peaks at 0 V in this thesis. For the last two variables which are R_{IR2} and R_{RED2}, each defines the amount of current to flow across each LED. In this context, R_{IR2} and R_{RED2} each has the resistant value of 330 Ω. From the given information above, Eq. (3.18) and Eq. (3.19) are computed, and I_{IRLED} as well as I_{REDLED} are revealed in Eq. (3.20) and Eq. (3.21).

$$I_{IRLED} = \frac{5V - 1.8V - 0V}{330\Omega} \simeq 9.7mA \tag{3.20}$$

$$I_{REDLED} = \frac{5V - 1.8V - 0V}{330\Omega} \simeq 9.7mA \tag{3.21}$$

The resultant current of each LED, 9.7 mA, is then brought to calculate the radiated power P of each LED through Eq. (3.22).

$$P = IV \tag{3.22}$$

From Eq. (3.22), I as well as V are the current flowing across the selected LED and the voltage dropped across the selected LED. Since the forward voltages for both IR and red LEDs are equal and the resultant currents of both LEDs also equate, the radiated powers for both LEDs are thus identical. After plugging the forward voltage of 1.8 V and the resultant current of 9.7 mA into Eq. (3.22), the radiated power of each LED is roughly 17.5 mW. In this power calculation, the acquired radiated power of each LED is the maximum power dissipated by each LED. This is because the reference voltage of each LED in this calculation is the bottom voltage peak of 0 V DC.

3.2.3 Transimpedance amplifier (TIA)

A transimpedance amplifier (TIA) functions as a current-to-voltage converter. In a pulse oximeter, the transimpedance amplifier turns the current output generated by a photo-detector. Briefly, when light intensity falls upon the photo-detector, the

photo-detector converts the detected light intensity into the electrical current. To make use of the current output of the detected light intensity conveniently, the transimpedance amplifier comes into play. The transimpadance amplifier simply turns the electrical current form into the voltage form. In this thesis, the simple transimpedance amplifier based on an op-amp (see Figure 3.4) is implemented. The reason for implementing the simple transimpedance amplifier is that the desirable frequency range is located at a near-zero frequency range which fits the simple transimpedance amplifier sufficiently. Not only the transimpedance amplifier converts the electrical current form to the voltage form but also boosts the level of the voltage output. The simple transimpedance amplifier can be numerically stated by Eq. (3.23) [52] where V_{out} is the voltage output generated by converting the electrical current I_{in} of light intensity. Dividing V_{out} by I_{in}, a gain resistor is revealed.

$$-R_f \approx \frac{V_{out}}{I_{in}} \tag{3.23}$$

In this design, the gain resistor R_f is set to 10 Ω in order to furnish 10 times of the gain factor. As can be seen in Eq. (3.23), the voltage output provided by the simple transimpedance amplifier is inverted due to the negative sign. Hence, the voltage output is suggested to do the inverse of the voltage output before further processing.

3.2.4 Signal processing

A signal output produced from a transimpedance amplifier (see Figure 3.4) is sent to a computer for further processing via the same acquisition device previously used in Section 3.1. The same computer simulation program is utilized to cope with controlling the acquisition device to record the signal output. The recorded signal output is the summation of a red PPG AM signal, an IR PPG AM signal and an MA signal. The collected signal output is augmented and now in the form of voltage as a result of the current-to-voltage converter provided by the transimpedance amplifier. The recorded signal output is mathematically written in Eq. (3.24) which is based on the received signal written in Eq. (3.5). In Eq. (3.24), the recorded signal output is represented by $v_{iR\_IR\_AM}(t)$, and $v_{\phi_{R\_AM}}(t)$ as well as $v_{\phi_{IR\_AM}}(t)$ are the AM signals of red and IR PPG signals, and $v_{i_{MA}}(t)$ is the MA signal. The recorded signal output is then processed by the flow diagram in Figure 3.9 to recover the red PPG signal and the IR PPG signal. Both PPG signals are finally turned to the SpO2 value.

$$v_{iR\_IR\_AM}(t) = v_{\phi_{R\_AM}}(t) + v_{\phi_{IR\_AM}}(t) + v_{i_{MA}}(t) \tag{3.24}$$

From Figure 3.9, the received signal is firstly recorded by the computer simulation program via the acquisition device. The received signal is sampled at the

sampling rate of 5000 sample per second. Secondly, the recorded signal output is passed to two band-pass filters (BPF1 and BPF2) in order to discriminate the red PPG AM signal and the IR PPG AM signal. Each BPF is designed by an approach of Butterworth filter. The Butterworth filter is chosen in this thesis because its frequency response is maximally flat in the passband. In addition, the phase response in the passband of the Butterworth filter is more linear than other digital filters such as Chebyshev Type I / Type II and Elliptic filters. BPF1 is constructed to have the center frequency of 800 Hz and to provide 40 Hz of pass-band while BPF2 is built to filter in the range of 1050 to 1090 Hz. Each BPF is a fourth-order filter. As the MA signal is located at the near-zero frequency range, by passing the collected signal output through BPF1 and BPF2 eliminates the MA signal implicitly. Thirdly, an equivalent method of envelope detection is performed on each band-filtered output of each BPF to amplitude-demodulate the original signal back. The equivalent method of envelop detection simply performs the mathematical absolute operation on the AM signal. After the process of envelope detection, each envelope-detected signal is fed to a low-pass filter (LPF) to get rid of the carrier frequency remained in each. Each LPF is also made by the approach of Butterworth filter, and each one is a fourth-order filter having the cut-off frequency of 6 Hz. Once, the MA-free red PPG signal and the uncorrupted IR PPG signal are recovered, an algorithm of peak separation is applied on each PPG signal to separate two consecutive peaks. As one PPG signal contains many periods even each period is not exactly equal, performing the algorithm of peak separation will give two consecutive peaks severed into many sets. Eventually, the first set of two consecutive peaks of each PPG signal is plugged into Eq. (2.18) and Eq. (2.19), respectively, to calculate the SpO2 value. The SpO2 computation is iteratively run until the last set of two consecutive peaks of each PPG signal is turned to the SpO2 value. Due to many sets of two consecutive peaks, a number of SpO2 values are obtained when considering one pair of red and IR PPG signals. Therefore, all SpO2 values calculated from one pair of red and IR PPG signals are averaged in the end. Keeping in mind, all signal processing processes regarding the frequency done in the computer are converted to the angular frequency for processing. For the red PPG signal and the IR PPG signal obtained from the conventional pulse oximeter, they are also collected at the same time as the two AM signals are recorded. Each conventional PPG signal is first fed to the same LPF as previously mentioned. Then, the filtered conventional red and IR PPG signals are changed to the SpO2 value.

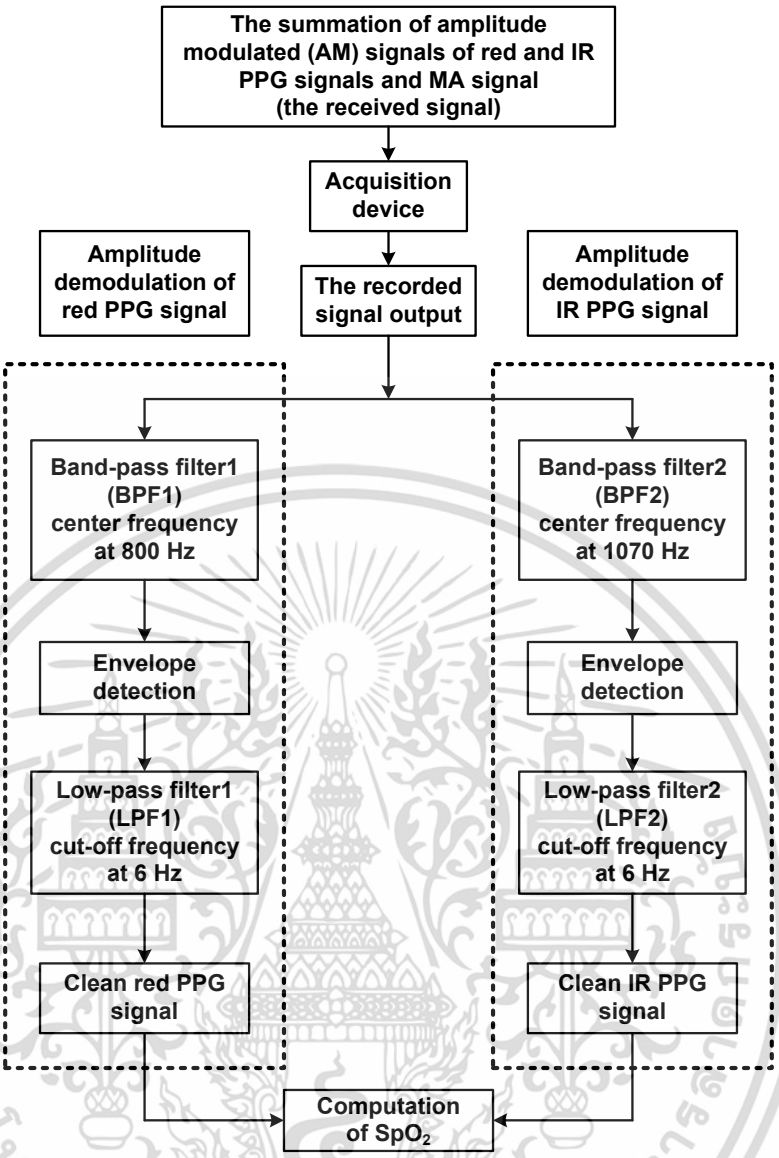

Figure 3.9 Procedures of signal processing.

3.3 Influence of light intensity

To further study the presented LEDs-emitting method, influence of light intensity on the quality of the PPG signal is focused while the MA signal is either existent or inexistent. This further study is accomplished by changing the incident light intensity i_{AC} falling upon the surface medium according to Eq. (3.4). Change of the incident light intensity i_{AC} is performed by changing the root mean square (RMS) current fed to a LED. In this thesis, three values of RMS current values which are computed from the following conditions. The first condition drives the LED by the amplitude voltage of 1 Vpp with the offset voltage of 4.5 V. Next condition, the LED is fed by the amplitude voltage of 1.5 Vpp with the offset voltage of 4.25 V. For the last condition, the LED is powered by the amplitude voltage of 2 Vpp with the offset voltage of 4 V. From the given conditions yield the RMS current values of 14.71 mA,

14.49 mA and 14.26 mA, respectively. The quality of the PPG signal is justified through a SpO2 value when the incident light intensity i_{AC} is altered.

3.4 Statistical indicators for signal evaluation

In this thesis, three statistical indicators for signal evaluation are opted. The first statistical indicator is Pearson's correlation coefficient (PCC) [53] and the second statistical indicator is mean square percentage error (MSPE) [54]. The last statistical indicator is mean absolute percentage error (MAPE) [54]. The first two statistical indicators are utilized to check the PPG morphological similarity of the PPG signals obtained from the proposed LEDs-driving technique and the conventional LEDs-shining method, respectively. For the MAPE is employed to verify the accuracy of the SpO2 value of the presented LEDs-emitting approach and the accuracy of the SpO2 value of the conventional LEDs-shining method.

3.4.1 Pearson's correlation coefficient (PCC)

The Pearson's correlation coefficient (PCC) is used to check the PPG morphological similarity in both time and frequency domains in respect of correlation in this thesis. The Pearson's correlation coefficient (PCC) is calculated by Eq. (3.25) where r_{XY} is the Pearson's correlation coefficient and X is the retrieved PPG signal and Y is the conventional PPG signal.

$$r_{XY} = \frac{\mathrm{cov}(X,Y)}{\sigma_X \sigma_Y} \tag{3.25}$$

Next, $\mathrm{cov}(X,Y)$ is the covariance of X and Y, and σ_X is the standard deviation of X as well as σ_Y is the standard deviation of Y. The level of similarity, r_{XY}, is roughly defined as follows. The value of r_{XY} in the range of 0.5 to 1 indicates high correlation (high similarity) between X and Y. For moderate correlation (average similarity), the value of r_{XY} is between 0.3 and 0.49. The last range of r_{XY} between 0 and 0.29 shows weak correlation (low similarity). The zero-value of r_{XY} suggests that the signals X and Y are not correlated. For the negative value of r_{XY} means the opposite similarity.

3.4.2 Mean square percentage error (MSPE)

The mean square percentage error (MSPE) is utilized to compare the PPG morphological similarity in the time domain in relation to error. Since the red and IR PPG AM signals as well as the conventional red IR PPG signals are sampled almost simultaneously, phase lagging between these signals is insignificant. With the insignificance of phase lagging, the mean square percentage error (MSPE) is therefore usable for checking PPG morphological similarity as well. The MSPE is computed

through Eq. (3.26) where N is the sample size and X_i is the retrieved PPG signal and Y_i is the conventional PPG signal. Broadly, the tool of MSPE holds the same properties of the mean square error (MSE). If the two considered signals have the MSE value of zero, they are cogitated to be identical [55]. Identically, the MSPE value of 0% is hence inferred that the two considered signals are also similar. In this point of view, the low value of MSPE approaching to 0% points that the signals X and Y are highly similar. By contrast, the high MSPE value implies that the signals X and Y are highly dissimilar. Besides, X and Y are normalized before computing.

$$MSPE = \frac{100}{N}\sum_{i=1}^{N}\left(\frac{X_i - Y_i}{Y_i}\right)^2 \tag{3.26}$$

3.4.3 Mean absolute percentage error (MAPE)

To measure the accuracy of the proposed strategy, the SpO2 value is employed as a criterion. The SpO2 value obtained from each moving posture of each subject is fed to mean absolute percentage error (MAPE) to quantify the amount of accuracy. The MAPE is calculated by the formula written in Eq. (3.27). In Eq. (3.27), a_{SpO2} is the actual SpO2 value is the SpO2 value measured while at rest. Also in Eq. (3.27), s_i is the measured SpO2 value while moving and N is the total number of the SpO2 values used in the MAPE calculation.

$$MAPE = \frac{100}{N}\sum_{i=1}^{N}\left|\frac{a_{SpO2} - s_i}{a_{SpO2}}\right| \tag{3.27}$$

3.5 Experiments pertaining to testing of implementation

To evaluate the implementation of the proposed LEDs-driving technique, diverse experiments to be conducted are listed as follows.

- The MA signals of common finger poses experimented by all involving participants are collected. Later, the recorded MA signal of each common posture is converted to a frequency distribution to demonstrate the overlapping frequency bands of the PPG signal and the MA signal [56].
- The designed signal generator is experimented to illustrate that two sinusoidal signals having the frequencies of 800 Hz and 1070 Hz, respectively, are generated.
- The proposed LEDs-driving technique is experimented while at rest to clearly show that two AM signals having the red and IR PPG signals as the message signals are created. In addition, the red and IR PPG frequency

components are shown that they are translated to the desirable frequency locations.

- The recovered red and IR PPG signals obtained from the proposed LEDs-driving approach are verified that their PPG morphologies are maintained and similar to the conventional LEDs-shining method. Two statistical indicators, PCC and MSPE, for checking PPG morphological similarity in are applied.
- While any finger posture is induced, the presented LEDs-emitting solution is experimented to manifest that the red and IR PPG signals are actually separated from the MA signal. Next, the red and IR PPG signals acquired from the proposed LEDs-driving strategy are turned to a SpO2 value. Later, a statistical indicator known as MAPE by employing the SpO2 value is justified.
- Change of light intensity is firstly experimented during staying at rest to check that the quality of the SpO2 value is affected. Later, change of light intensity is also experimented while motion is involved to check whether that the quality of the SpO2 value is affected. Change of light intensity is done by changing the root mean square (RMS) current fed to each LED. Three values of RMS current values, 14.71 mA, 14.49 mA and 14.26 mA are experimented.
- For a comparative study, the MA-interfered red and IR PPG signals obtained by the conventional LEDs-shining method are repaired by three well-known methods (see Chapter 2 under Section 2.5). The repaired red and IR PPG signals are converted to the SpO2 value and the obtained SpO2 value is checked its accuracy through MAPE. The MAPE of each method is compared with the MAPE of the proposed LEDs-driving technique to render the performances of the proposed LEDs-emitting approach and the three well-known methods. In the comparative study, all common postures are experimented.

The experimental results of the listed experiments will be shown and discussed in Chapter 4.

CHAPTER 4

Experimental Results and Discussion

This chapter manifests all results experimented by the list of the experiments briefly detailed in Chapter 3 under Section 3.5. For simplicity in following up all experiments, the experimental results of each experiment are sequentially illustrated according to the given list of the experiments.

4.1 Evaluation of frequency distributions of regular postures

In order to treat MA signals from regular postures produced by human movement, each posture's behavior is studied in this section. Because this thesis centers on a finger probe pulse oximeter, the regular postures are thus related to finger movements which are bending, shivering, waving, horizontal movement and vertical movement. Each given posture is analyzed in a frequency domain and the acquired frequency components of each pose are then brought to create a frequency distribution of each motion.

To generate the MA signals regarding the everyday poses for analyzing, 75 Asian participants having yellowish skin are volunteered. The involving volunteers compose of 38 males and 37 females having the age between 21 to 60 years. The overall age of male subjects is 37.21 years with the standard deviation of 13.27. For female participants, the mean age is 39.78 years with the standard deviation of 11.78. More details on the average age of each age range and the quantity of each gender of each age range are summarized in Table 4.1. Each volunteering subject is requested to do five different experiments which are relevant to the mentioned finger moves. In these experiments, every participant is asked to put the finger probe pulse oximeter mounted with a light intensity sensor, as portrayed in Figure 4.1, onto his/her left index finger. The light intensity sensor is functioned to measure any amount change of light intensity while any motion takes place. Each experiment is performed five times ten seconds each. All subjects are treated with care as well as minimal risks. All conducted experiments follow the Declaration of Helsinki. To record the MA signals performed by each involving subject, a USB-0001 portable acquisition device manufactured by National Instruments (NI) is employed through a computer simulation program. Each MA signal is sampled at the rate of 400 samples per second.

Because the light intensity sensor has a built-in amplifier, the sensed signal generated by this sensor is promptly used without requiring any extra amplifying circuits. Also, the light intensity sensor is compatible with the voltage of +5 V DC.

Table 4.1 Summary of subjects' age and gender.

Age range (years)	Amount of male participants	Mean age (years)	Standard deviation	Amount of female participants	Mean age (years)	Standard deviation
21-30	14	24.43	3.30	12	26.33	1.97
31-40	9	34.44	3.28	8	36.13	2.85
41-50	8	47.63	2.86	7	45.71	3.55
51-60	7	54.43	2.15	10	54.70	2.79
Total	**38**	37.21	13.27	**37**	39.78	11.78

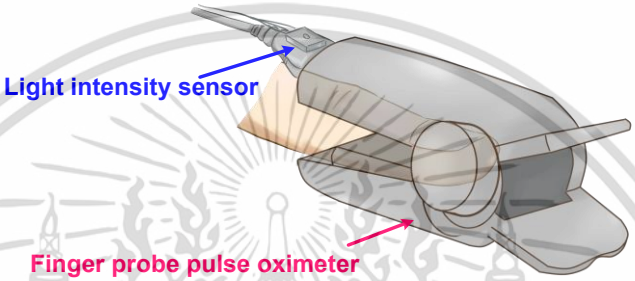

Figure 4.1 A finger probe pulse oximeter mounted with a light intensity sensor.

Once, all MA signals of all subjects are collected. The recorded MA signals are then analyzed by the same aforementioned computer simulation program. A technique of fast Fourier transform (FFT) selected as an analyzing tool is introduced to transform the entire MA signals in a time domain to the frequency domain. Lastly, some of the MA signals obtained from which both masculine and feminine subjects are randomly chosen are depicted in Figure 4.2. In Figure 4.2, the top row comprises of five sub-pictures illustrating the MA signal of each posture produced by the same male volunteer. Also in the same figure, the lower row consists of five sub-images manifesting the MA signal of each pose induced by the same female participant. The x-axis and y-axis of each sub-picture in Figure 4.2 represent time in a unit of second and amplitude in a unit of voltage, respectively. As can be observed in Figure 4.2, each MA-signal pair of each pose is not entirely similar because the movement characteristic of each person is different from person to person. Although each MA-signal pair of each posture induced by male and female volunteers does not completely look alike, each MA-signal pair of each pose bears the same frequency components. The rest MA signals of each pose for both genders also hold the same frequency components like each MA-signal pair of each posture shown in Figure 4.2.

After analyzing the total MA signals, a set of frequency distributions regarding the regular postures are demonstrated as follows. Firstly, a group of frequency distributions of each posture is illustrated in Figures 4.3-4.7. In each figure is composed

of the frequency distributions of four age ranges, which are 21-30 years, 31-40 years, 41-50 years and 51-60 years from left to right, respectively. Besides, the top trace of each figure represents the masculine frequency distributions and the down row in the same figure stands for the feminine frequency distributions. Secondly, the overall frequency distribution of each pose for the ages between 21 to 60 years is graphically summarized in Figure 4.8. In Figure 4.8, the bending posture is placed at the far left column. The second column is the illustration of the horizontal movement posture. The middle column of the figure shows the shivering posture and the fourth roll displays the vertical movement posture. For the last one (far right) is the picture of the waving posture. Similar to Figures 4.3-4.7, the upper and lower tracks are the frequency distributions of male and female in order. In each sub-picture of Figures 4.3-4.8, the MA frequency components (x-axis) are plotted against the number of occurrences (y-axis). The x-axis of the MA frequency components is shown only the first 10 Hz. This is because the MA-free PPG frequency components are located at the frequency band between 0.09 to 4 Hz [57].

According to Figures 4.3-4.7, the frequency components of each pose are found densely distributed at the low frequency between 0 to 2 Hz for all age groups of both genders. Nonetheless, the frequency distributions of the bending and shivering postures expand up to 4 Hz. For the bending pose, almost all frequencies between 0 to 4 Hz are significantly occupied for both male and female subjects of all age ranges. Nearly perfectly conforming to the bending finger movement, only the age range of 41 to 50 years of male subjects of the shivering postures has the frequency distribution exhibited differently. The frequency components for the aforementioned male age range of 41 to 50 years are principally stuck together around 0 to 2 Hz like the other three postures. From this viewpoint may briefly imply that the bending and shivering poses create more complication on the PPG signal than the postures of horizontal movement, vertical movement and waving movement. This is because the normal PPG frequency components located between 0.09 to 4 Hz are almost overlapped by the frequency components of the bending and shivering poses. For the rest postures overlaps approximately only 0 to 2 Hz of the uninterrupted PPG frequency. Figure 4.8 renders the overall frequency distribution of each posture for each sex at the age range of 21 to 60 years. The overall frequency distribution of each pose reveals that both frequency distribution shapes of male and female are in the same direction. This indicates that both genders generate the same frequency components when each posture is induced.

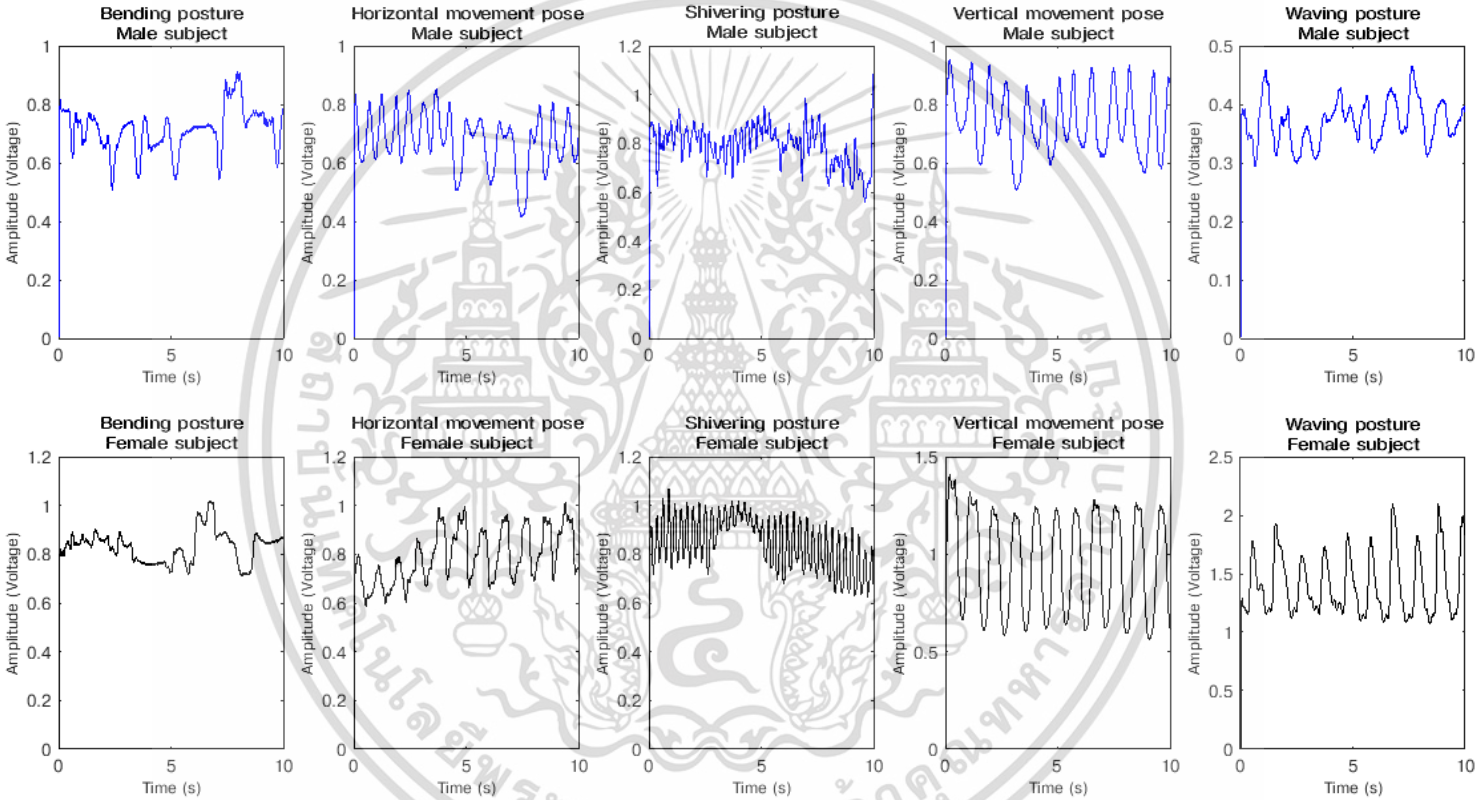

Figure 4.2 Samples of MA signals.

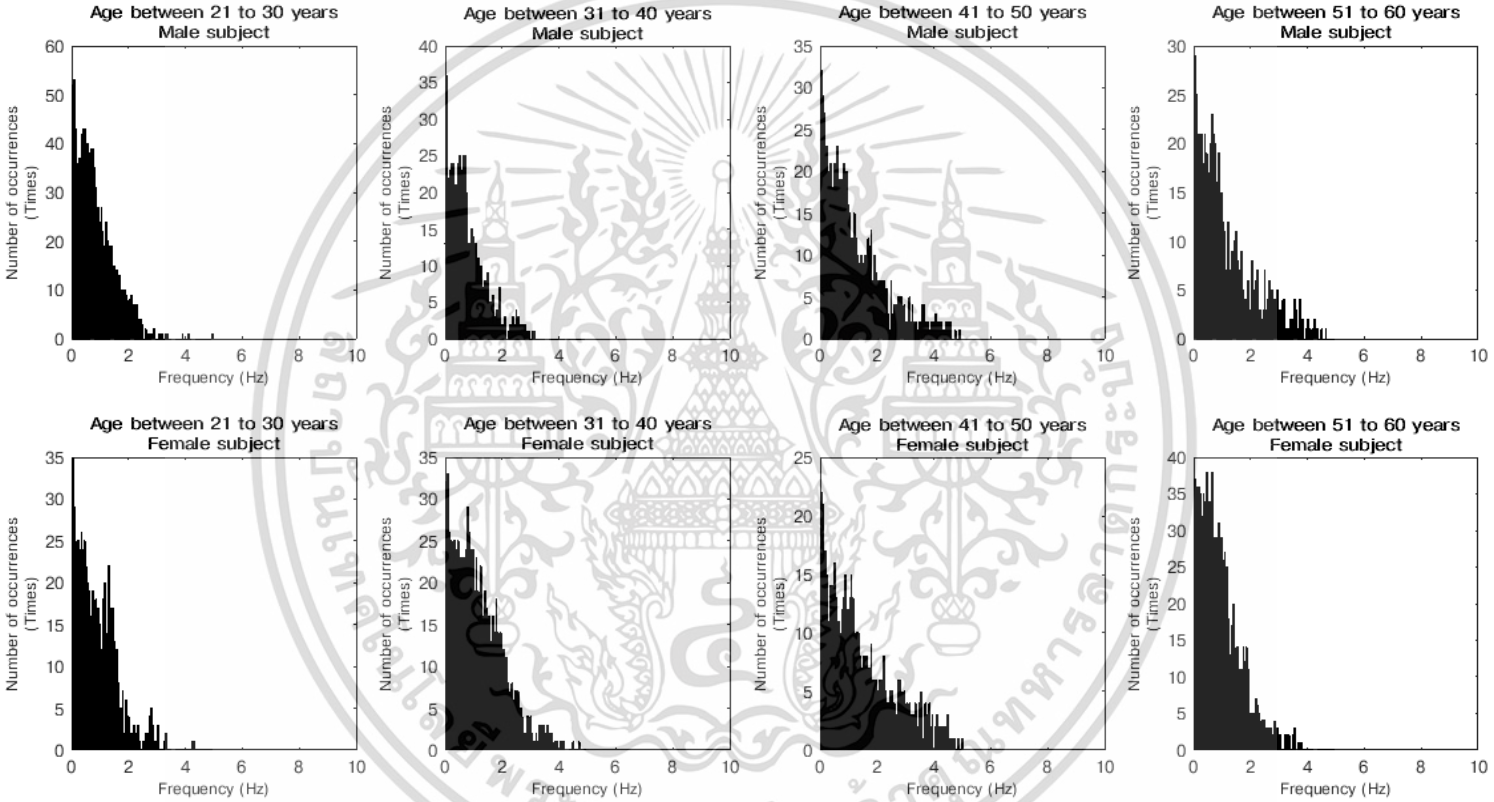

Figure 4.3 Motion noise frequency distributions of bending posture.

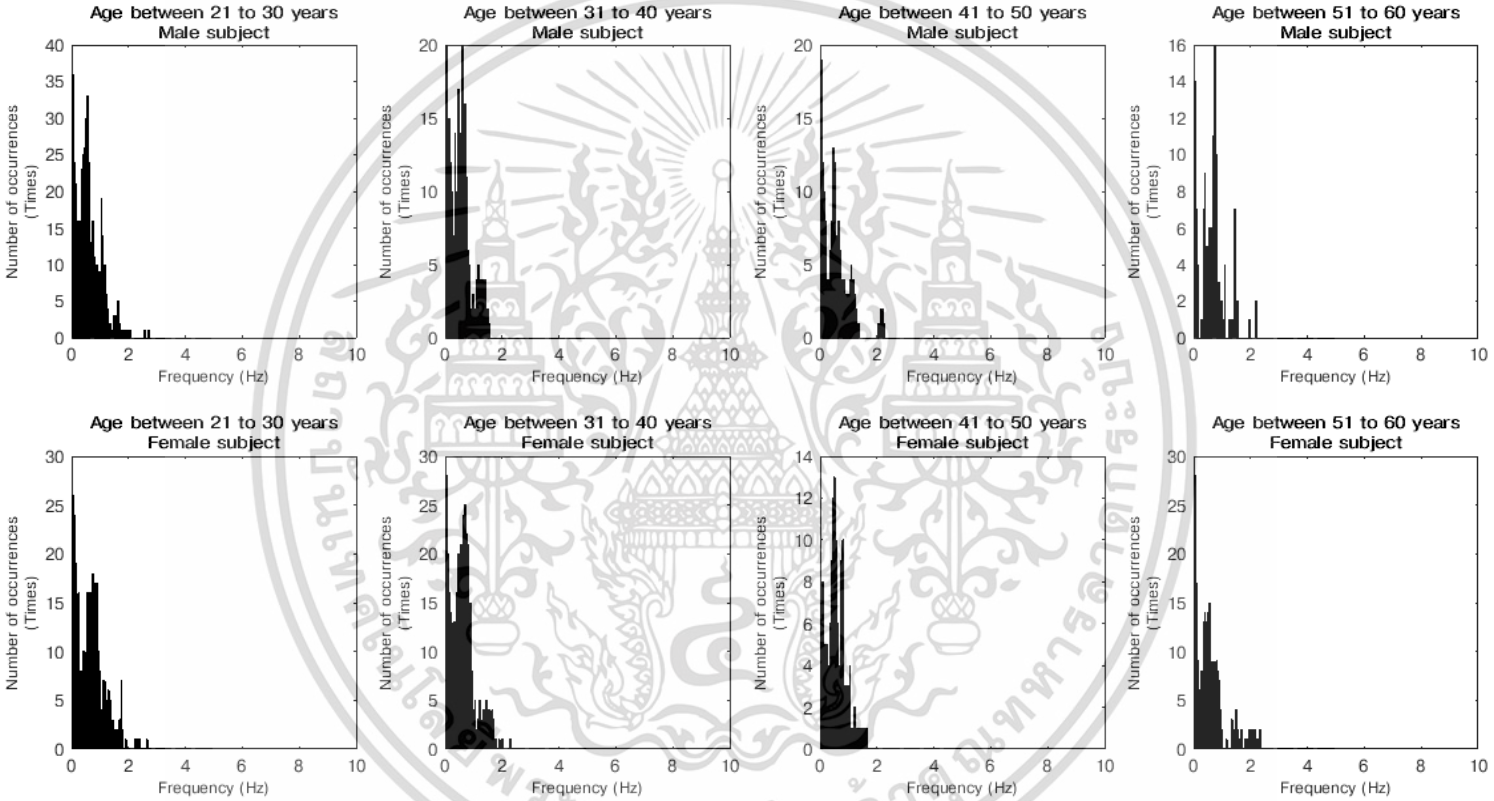

Figure 4.4 Motion noise frequency distributions of horizontal movement posture.

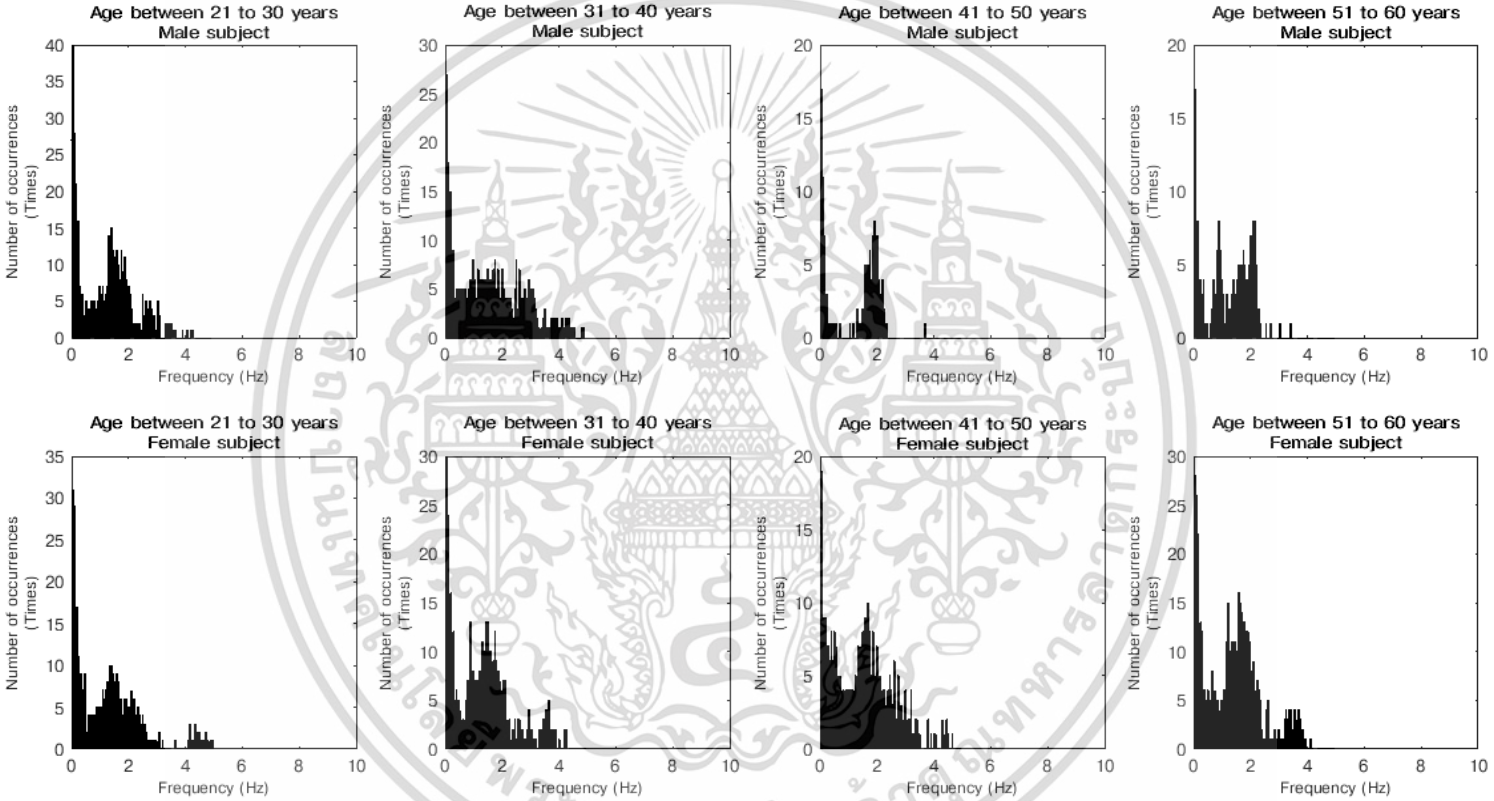

Figure 4.5 Motion noise frequency distributions of shivering posture.

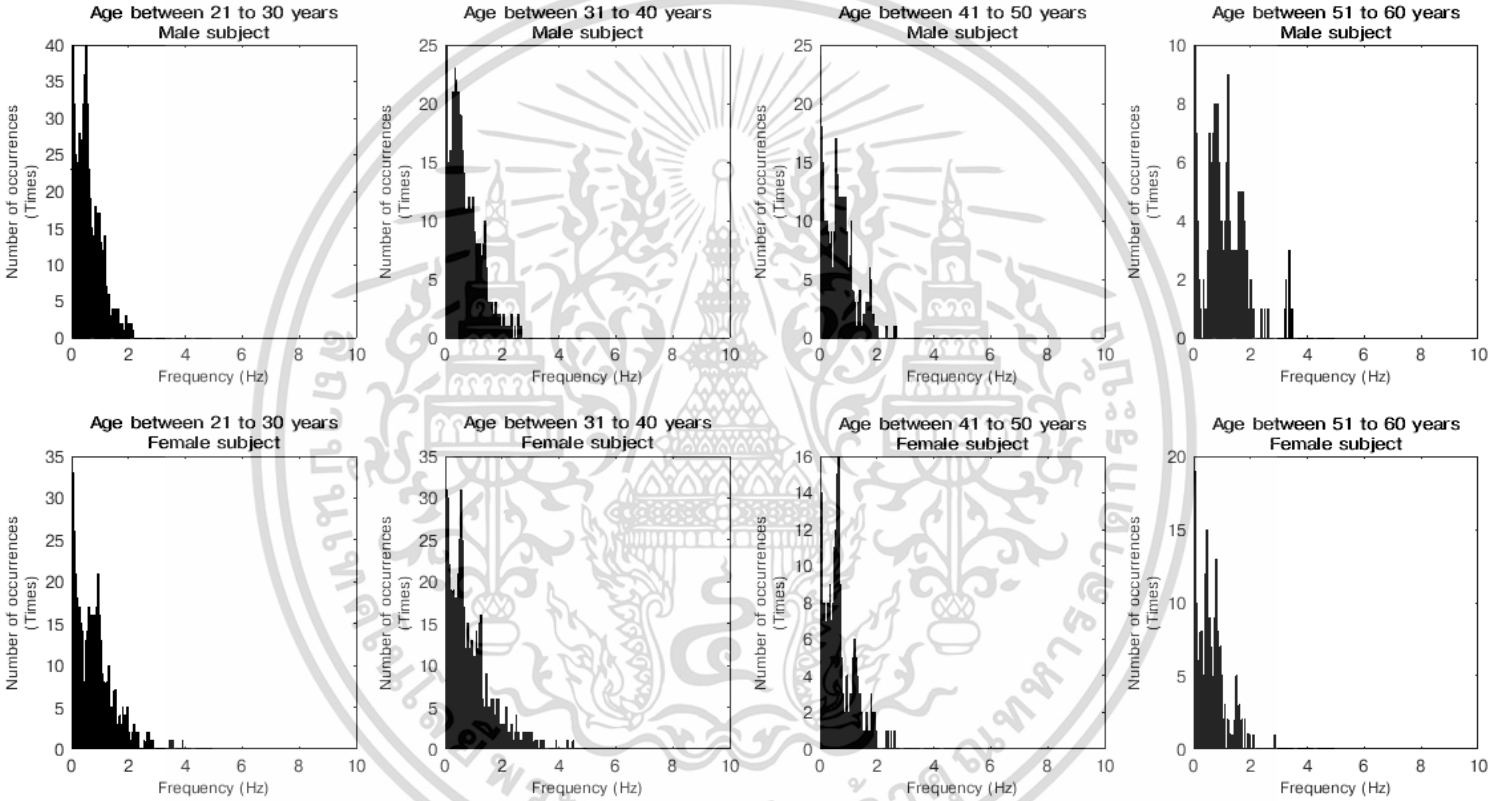

Figure 4.6 Motion noise frequency distributions of vertical movement posture.

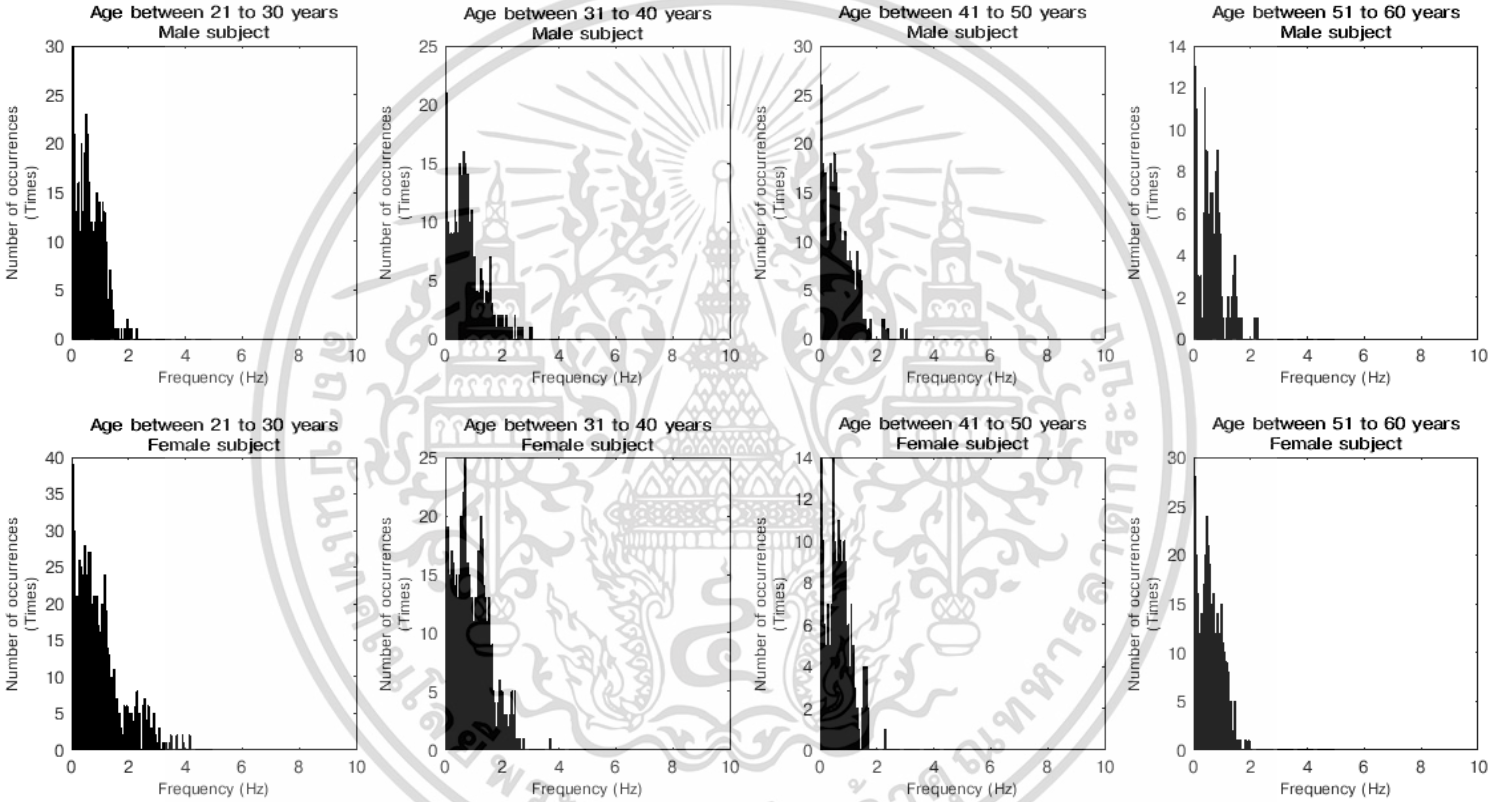

Figure 4.7 Motion noise frequency distributions of waving posture.

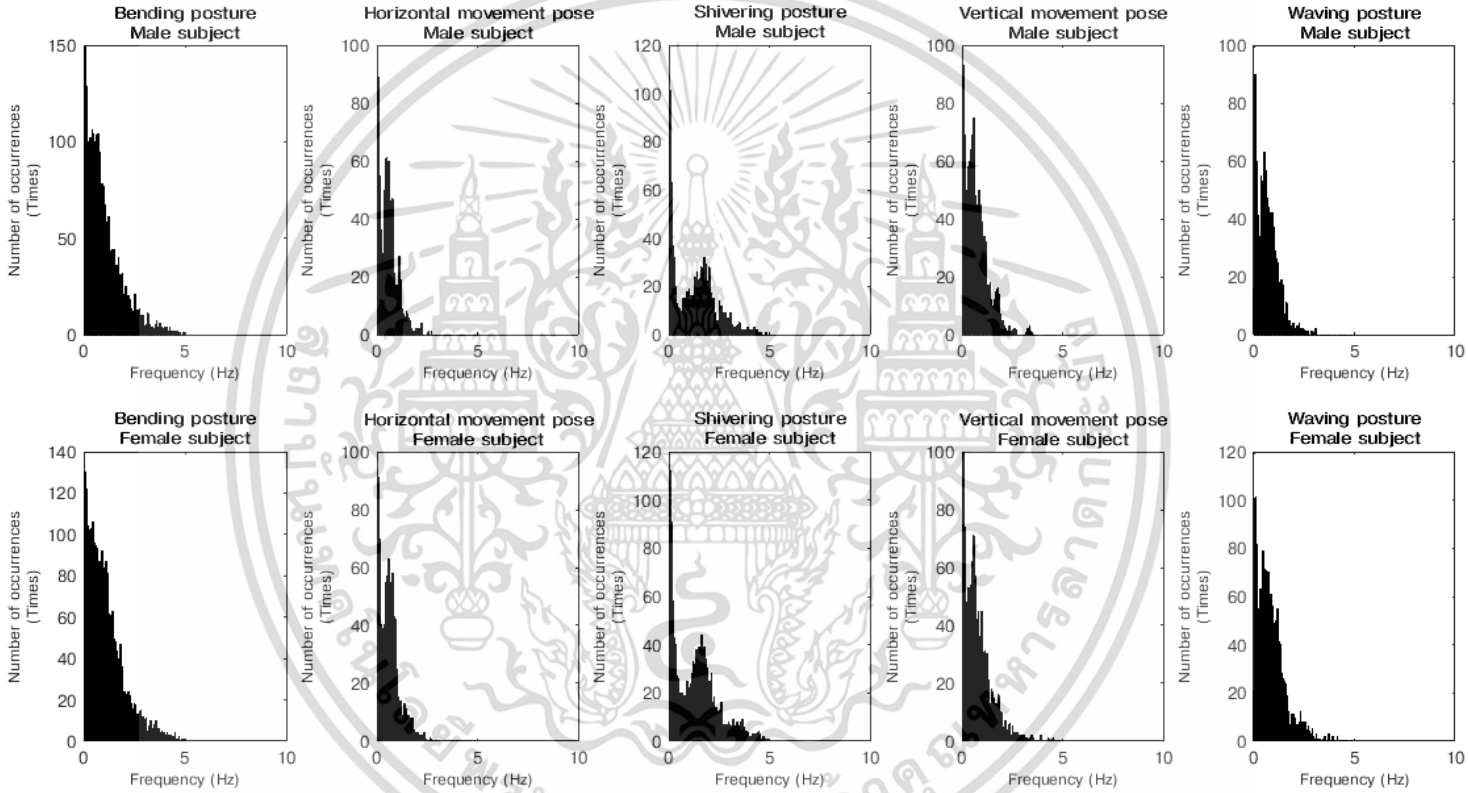

Figure 4.8 Overall frequency distributions of all postures for the age range of 21 to 60 years.

4.2 Evaluation of the proposed LEDs-emitting technique

To exhibit that the proposed LEDs-driving solution is practical, the given implementation is verified through four main experiments as follows.

The first experiment is carried out to affirm that changing DC source to AC source in LEDs-emitting actually translates the red and IR PPG frequency components to the desirable locations [57]. Also, a PPG morphological deviation of the proposed scheme from the conventional method is gauged. Next, the second experiment is conducted to illustrate that the proposed strategy potentially separates the red and IR PPG signals from the MA signal in a frequency domain. The second experiment consists of various sub-experiments to test the validity of the proposed solution [57]. The main objective of altering LEDs-driving in this thesis is expected to solve the overlapping issue of the PPG signals and the MA signal in the frequency domain. In addition, by implementing the proposed technique is anticipated in keeping all significant PPG morphologies having low distortion while any motion takes place.

The third experiment is performed to study whether the quality of a SpO2 value is impacted when the incident light intensity falling onto a subject's surface medium is changed [58]. For the last experiment is administered to compare the performances of the proposed LEDs-driving technique and other well-known methods [59]. The performance comparison employs the SpO2 value as a criterion to judge their performances.

In order to obtain the experimental results of all experiments, all 75 volunteers who participated in the previous experiments conducted in Section 4.1 are again requested to attend.

4.2.1 Evaluation of the implementation of the proposed LEDs-driving technique

4.2.1.1 Evaluation of the designed signal generator

In this implementation, the signal generator is initially configured to provide the amplitude of 1 Vpp (Voltage peak-to-peak) and the offset voltage of 0.5 V to each output channel. As each sinusoidal output is functioned as the reference voltage to each LED, the voltage fed to each LED is characterized as shown in Figure 4.9. In Figure 4.9(a), the left sub-figure is the voltage fed to the red LED over time rendering the sinusoidal signal having the frequency of 800 Hz with the offset voltage. Besides, the sub-figure on the right is zoomed to only the 800-Hz frequency spectrum of the voltage signal across the red LED even the DC component also exists. This is to show that the generated sinusoidal signal conforms to the configuration set to the signal generator. In Figure 4.9(b), the left sub-figure and the right sub-figure are illustrated in the same manner as Figure 4.9(a) but these sub-figures are stood for the frequency of 1070 Hz.

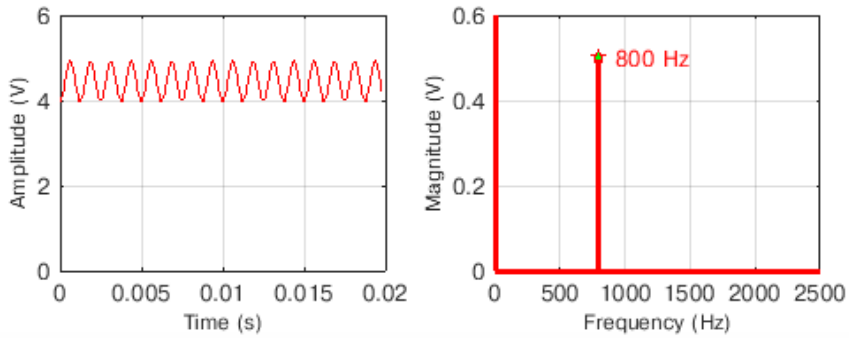

(a) Red LED.

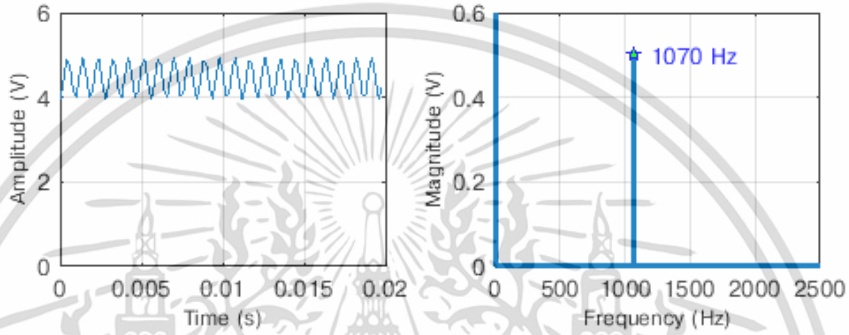

(b) IR LED.

Figure 4.9 Voltage fed to each LED.

Normally, the LED is fed by the electrical current. Hence, from Figures 4.9(a)-4.9(b), the amplitude voltages for both LEDs are turned to the electrical current in terms of root mean square (RMS). The calculated RMS current values for both LEDs are 14.71 mA.

4.2.1.2 Evaluation of translating PPG frequency components

In this experiment, each volunteer is asked to insert two pulse oximeters onto the volunteer's left hand. One pulse oximeter is put onto the volunteer's index finger. The other one is worn on the middle finger. For the index finger, the pulse oximeter implemented by the proposed LEDs-emitting technique is utilized. For the middle finger, the commercial pulse oximeter embedded with the conventional LEDs-driving method is used. The experiment is conducted by requesting each subject to place his/her left hand at rest on the provided table for 5 times, 10 seconds each. During the experiment takes place, three ambient conditions which are temperature, relative humidity (RH) and light intensity are monitored. The temperature is about 28.94 degrees Celsius with standard deviation of ±1.2, and the relative humidity is around 38.17% with standard deviation of ±2.6. For the light intensity, the value is approximately 167.88 lux with standard deviation of ±6.1. The experiment is conducted at daytime during 8am to 4pm.

To assert that the red and IR PPG signals are physically amplitude-modulated by the proposed LEDs-driving technique, some results arbitrarily picked from each age range are illustrated in Figure 4.10. Nonetheless, the rest results also characterize in the same sense like those displayed in Figure 4.10. In Figure 4.10, eight sub-figures are demonstrated in a time domain and the left column shows the male's results while the right column depicts the female's results. Also, the first row renders the masculine and feminine results selected from the age range of 21 to 30 years. Likewise, the remaining rows exhibit the male and female results chosen from the following age ranges, 31-40 years, 41-50 years and 51-60 years, respectively. Each sub-figure expresses the summation of the red PPG AM signal as well as the IR PPG AM signal as no motion is involved. As can be observed in Figure 4.10, two imaginary envelopes manifesting the PPG figure are present. The first imaginary envelope is located at the top of the summed AM signal and the other one is settled at the bottom. This indicates that both PPG signals are truly amplitude-modulated.

Each result in Figure 4.10 is transformed to a frequency domain as exhibited in Figure 4.11 to confirm that each PPG signal is amplitude-modulated to the desirable frequency of each. The FFT algorithm is responsible for time-to-frequency conversion. The layout of Figure 4.11 is organized in the identical way as Figure 4.10. As can be seen in each sub-figure of Figure 4.11, each PPG frequency components is successfully lifted to the given desirable frequency. The defined frequency for the red PPG signal is 800 Hz while the assigned frequency for the IR PPG signal is 1070 Hz.

Later, each AM signal is amplitude-demodulated to retrieve its original PPG signal. Some of the recovered red and IR PPG signals which are randomly selected from both genders are portrayed in Figure 4.12. The top two rows display two of the male results and the bottom two rows illustrate two of the female results. The left column shows the demodulated red PPG signal compared with the conventional red PPG signal for each sub-figure. For the right column, the demodulated IR PPG signal compared with the traditional IR PPG signal is manifested in each sub-figure. The remaining retrieved PPG signals from other participants also render their PPG waveforms in the same vein like those depicted in Figure 4.12. The retrieved red and IR PPG signals each is marked by the phrase, "Proposed technique," for each sub-figure. For the conventional red and IR PPG signals, each is marked by the phrase, "Conventional method," in every sub-figure. As can be noticed in Figure 4.12, the retrieved red and IR PPG signals are fairly similar to the conventional red and IR PPG signals for every sub-figures.

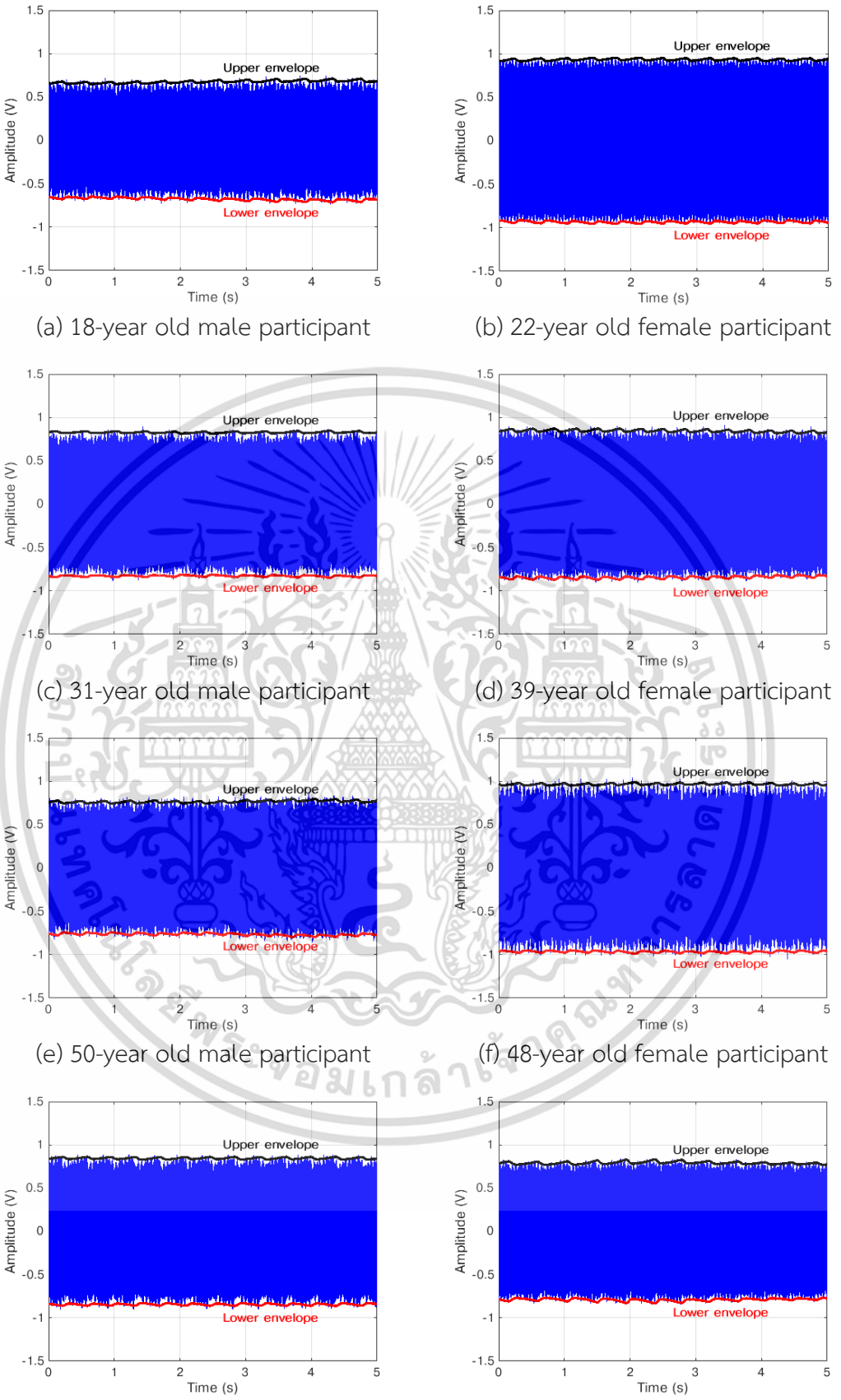

(a) 18-year old male participant (b) 22-year old female participant

(c) 31-year old male participant (d) 39-year old female participant

(e) 50-year old male participant (f) 48-year old female participant

(g) 52-year old male participant (h) 52-year old female participant

Figure 4.10 AM signals of PPG signals by the proposed LEDs-driving technique.

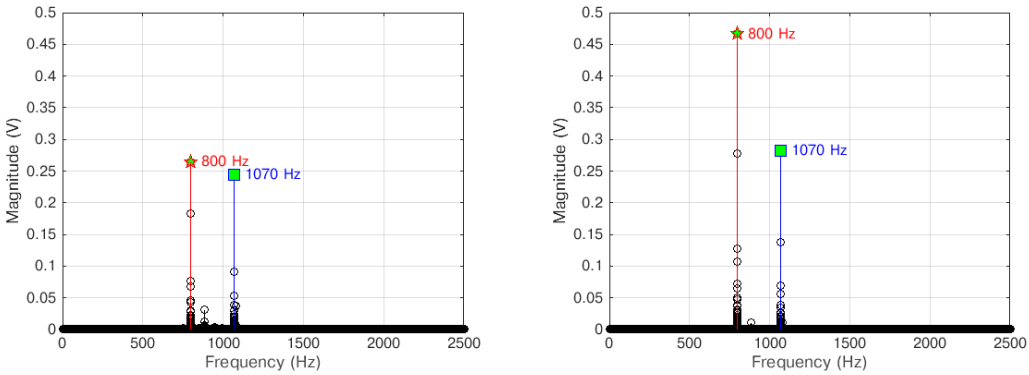

(a) 18-year old male participant (b) 22-year old female participant

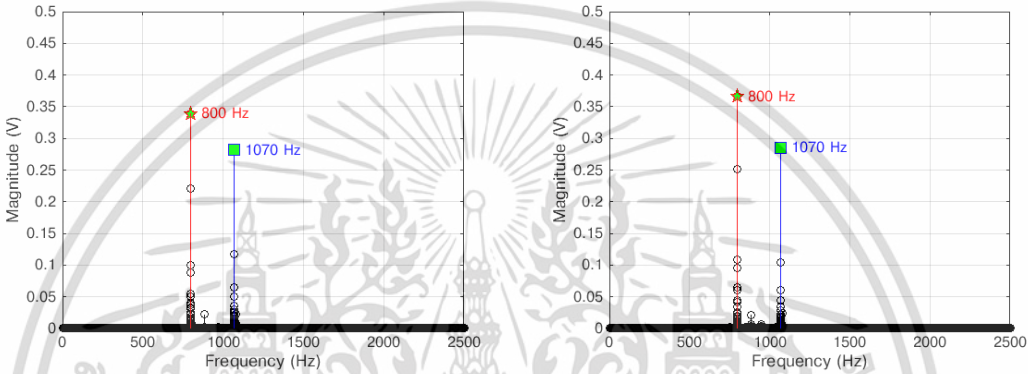

(c) 31-year old male participant (d) 39-year old female participant

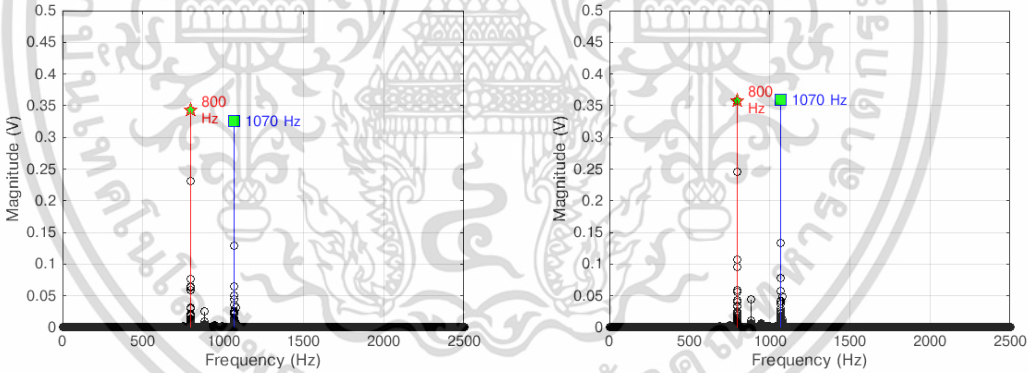

(e) 50-year old male participant (f) 48-year old female participant

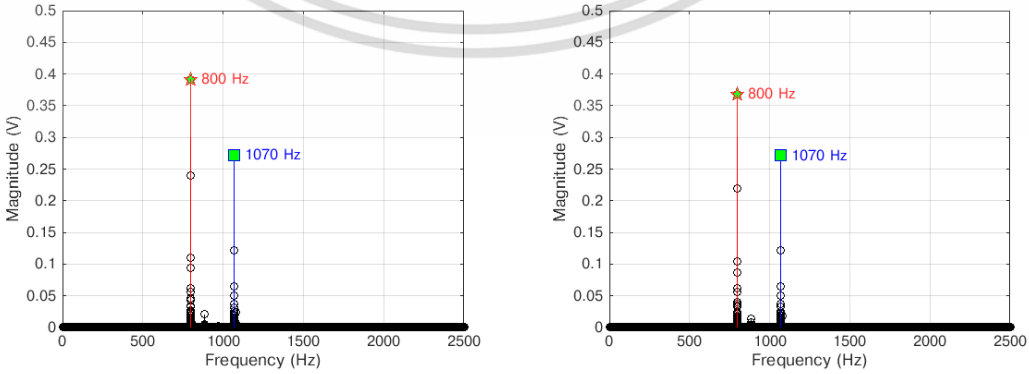

(g) 52-year old male participant (h) 52-year old female participant

Figure 4.11 Frequency spectra of AM signals.

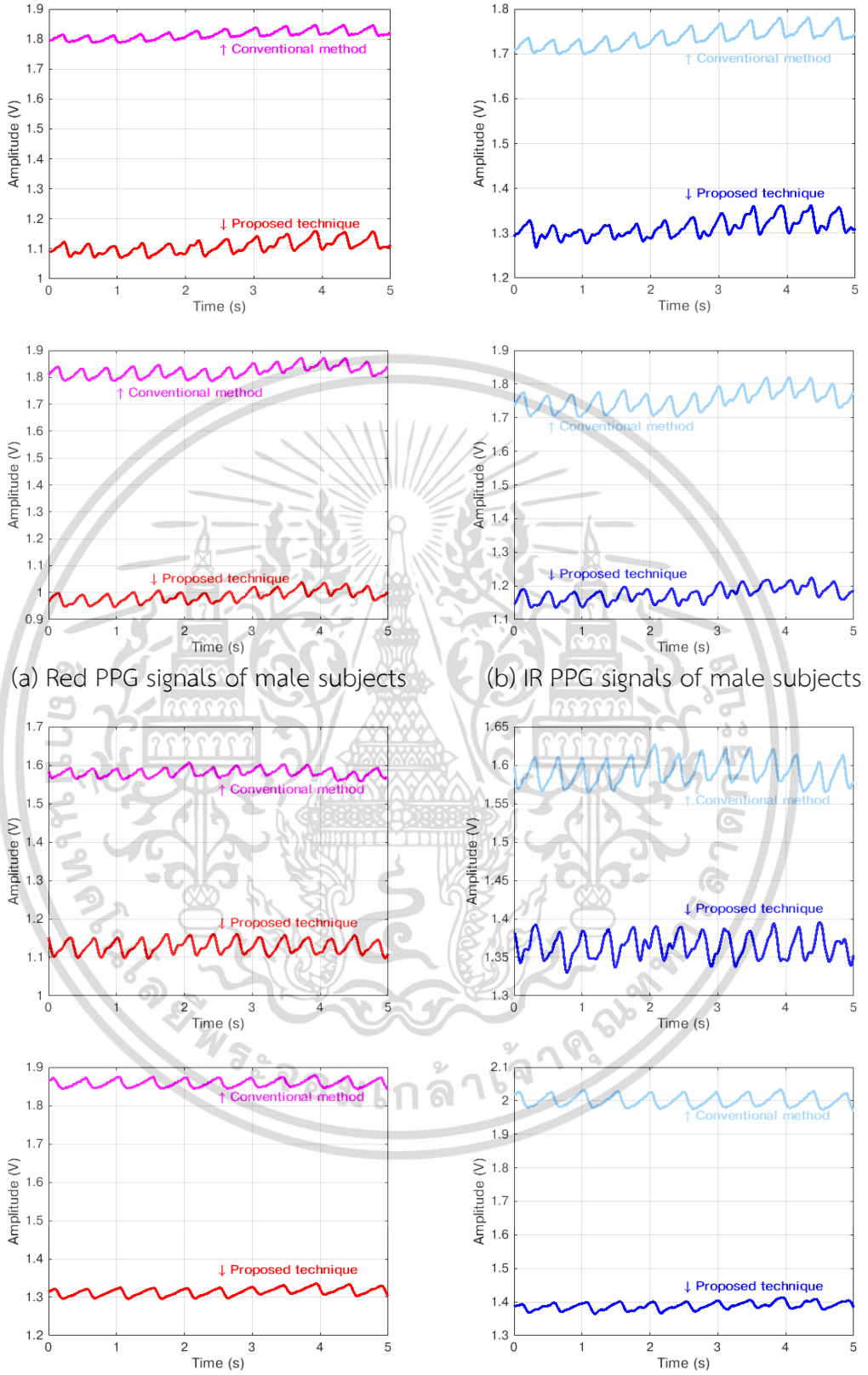

(a) Red PPG signals of male subjects (b) IR PPG signals of male subjects

(c) Red PPG signals of female subjects (d) IR PPG signals of female subjects

Figure 4.12 Retrieved PPG signals compared with conventional PPG signals.

4.2.1.3 Evaluation of PPG morphological similarity

To verify the similarity between the recovered red and IR PPG signals by the proposed LEDs-driving technique and the conventional red and IR PPG signals, two statistical tools are employed. The first statistical tool is Pearson's correlation coefficient (PCC) [54] and the second statistical tool is mean square percentage error (MSPE) [55]. The computations for PCC and MSPE are accomplished through the same aforementioned computer simulation program. For each calculation, the recovered red PPG signal is calculated with the conventional red PPG signal and the retrieved IR PPG signal is computed with the traditional IR PPG signal. As each volunteer does the resting pose for five times, the PCC result and the MSPE result each yields at least five values for each statistical tool. The results of PCC and MSPE of each volunteer are therefore averaged as well as standard-deviation-calculated and grouped in each age range and later tabularly summarized in Table 4.2. For more details of each participant is aggregated in Appendix A section under Tables A.1-A.4.

In Table 4.2, the far left column indicates the age range. The second column represents the PCC of each pair of the retrieved red PPG signal and the conventional red PPG signal. For the third column, the PCC of each pair of the recovered IR PPG signal and the traditional IR PPG signal is shown. The PPG signals used in the PCC calculation in the second and third columns are in the time domain. In the fourth and fifth columns, the PCC computation is similar to those done in the second and third columns but the utilized PPG signals is in the frequency domain. The sixth column shows the MSPE of each pair of the demodulated red PPG signal and the conventional red PPG signal. For the far right column displays the MSPE of each pair of the demodulated IR PPG signal and the conventional IR PPG signal. The PPG signals computed in the MSPE for the last two columns are in the time domain. Also in Table 4.2, the male results and the female results are top-down separated by placing the male results first and later the female results.

When considering Table 4.2, the PCC results of all age ranges for both time and frequency domains emerge in the similar direction. The overall PCC value for every age range is greater than 0.9 with low standard deviation. This indicates that the retrieved red and IR PPG signals are highly similar to the conventional red and IR PPG signals, respectively. With the MSPE results affirms that employing the proposed technique maintains all significant PPG morphologies because the overall MSPE value of each volunteer is below 1% with insignificant standard deviation. Being able to keep all significant PPG morphologies of the proposed approach implies that the retrieved PPG signals exhibit the similarity related to the conventional PPG signals. The depicted PCC results and the rendered MSPE results in Table 4.2 suggest that the presented solution can be implemented practically.

Table 4.2 Summary of PPG morphological similarity of all age ranges.

Age ranges	PCCR[1] (Time domain)	PCCIR[2] (Time domain)	PCCR[1] (Frequency domain)	PCCIR[2] (Frequency domain)	MSPER[3] (Time domain)	MSPEIR[4] (Time domain)
Male subjects						
	Average ± Standard deviation					
21-30	0.951±0.019	0.973±0.012	0.978±0.011	0.988±0.006	0.322±0.166	0.187±0.097
31-40	0.961±0.030	0.977±0.020	0.980±0.019	0.988±0.012	0.238±0.257	0.141±0.154
41-50	0.948±0.025	0.973±0.015	0.972±0.017	0.985±0.008	0.325±0.190	0.176±0.111
51-60	0.955±0.026	0.973±0.017	0.978±0.018	0.987±0.010	0.219±0.139	0.125±0.066
Female subjects						
	Average ± Standard deviation					
21-30	0.982±0.013	0.990±0.008	0.992±0.006	0.995±0.003	0.080±0.112	0.045±0.053
31-40	0.980±0.013	0.991±0.008	0.991±0.006	0.996±0.004	0.093±0.088	0.046±0.046
41-50	0.970±0.016	0.984±0.012	0.986±0.009	0.992±0.006	0.155±0.104	0.087±0.073
51-60	0.967±0.029	0.980±0.021	0.985±0.014	0.991±0.010	0.177±0.186	0.110±0.134

1 – Pearson correlation coefficients (PCC) of retrieved red PPG signals against conventional red PPG signals,

2 – Pearson correlation coefficients (PCC) of recovered IR PPG signals against conventional IR PPG signals,

3 – Mean square percentage error (MSPE) between retrieved red PPG signals and traditional red PPG signals,

4 – Mean square percentage error (MSPE) between recovered IR PPG signals and traditional IR PPG signals.

4.2.1.4 Evaluation of SpO2 reference

The retrieved red PPG signal and the recovered IR PPG signal, of each volunteer, are converted to the SpO2 value. In this SpO2 calculation, both red and IR PPG signals are collected while each subject stays at rest. Besides, the conventional red PPG signal and the traditional IR PPG signal, of each participant, are turned to the SpO2 value as well for comparison. Since each subject performs the resting posture for five times, the SpO2 values for each one are obtained at least five values for each technique. The acquired SpO2 values of each volunteer for each method are thus are averaged and standard-deviation-calculated. All SpO2 values for all age ranges of both schemes are summed up in Table 4.3. Table 4.3 is arranged as follows. The first three columns are reserved for the male results and the other three columns are held for the female results. The first and fourth columns point to the age ranges. Next, the second and third columns manifest the male SpO2 values independently calculated from the proposed technique marked as “PT” and the conventional method marked as “CM.” For the last two columns, the female SpO2 values separately computed from the PT and the CM, in order, are given. As can be noticed in Table 4.3, the acquired mean SpO2 value of the proposed technique for each age group is greater than that of employing the conventional method. Also, the averaged SpO2 values of the presented approach are superior to those of utilizing the traditional scheme for both genders.

Table 4.3 Summary SpO2 values of all age ranges while resting.

Age ranges	Male subjects		Female subjects	
	Proposed technique (PT)	Conventional method (CM)	Proposed technique (PT)	Conventional method (CM)
	Summary SpO2 values in the unit of percentage (%)			
	Average ± Standard deviation			
21-30	95.99±2.09	93.18±0.95	97.04±1.66	93.67±1.03
31-40	96.52±2.56	93.01±0.82	97.93±1.16	93.49±1.25
41-50	96.37±1.00	93.24±0.73	97.57±1.47	92.62±0.77
51-60	97.20±1.60	93.61±0.78	96.45±1.45	93.94±0.88

The SpO2 value of the proposed solution is higher the SpO2 value of the conventional method because using the presented technique provides the higher absorptions of red and IR lights. To support the statement that using the presented technique provides the higher absorptions of red and IR lights, Figure 4.12 is contemplated. After considering Figure 4.12, the red and IR PPG signals of the proposed technique are found to be lower than the red and IR PPG signals of the conventional method. This is because the leftover intensities of both lights of the proposed technique are explicitly come out lesser than the remnant intensities of both lights of the conventional scheme. With the given explanation is thus pointed out that the red and IR lights are more absorbed by the proposed technique than the conventional method. For the age group of 21 to 30 years, the mean male SpO2 value of the PT is 95.99%±2.09 while the CM is 93.18%±0.95. In the same age range, the average female SpO2 value of the PT is 97.04%±1.66 but for the CM is 93.67%±1.03. For the age range of 31 to 40 years, the male and female SpO2 values of the PT are 96.52%±2.59 and 97.93%±1.16. For the CM of the age group of 31 to 40 years, the male and female SpO2 values are 93.01%±0.82 and 93.49%±1.25. In the age range of 41 to 50 years, the male and female SpO2 values of the PT are 96.52%±2.59 and 97.93%±1.16. For the CM, the male and female SpO2 values are 93.01%±0.82 and 93.49%±1.25. For the last age range, 51 to 60 years, the male and female SpO2 values of the PT are 97.20%±1.60 and 96.45%±1.45. The male and female SpO2 values of the CM are 93.61%±0.78 and 93.94%±0.88. Each SpO2 value of each volunteer is detailed in Tables A.5-A.8 and will be used as an actual value for the error calculation in the following subsection.

4.2.2 Evaluation of separating PPG frequency components from MA frequency components

4.2.2.1 Evaluation of PPG signals during motion involvement

In Subsection 4.2.1, the proposed LEDs-emitting technique is experimented to demonstrate that the translation of the PPG frequency components is practically usable. The main experiment conducted in Subsection 4.2.1 only asks each volunteer

to place his/her left hand at rest to illustrate the shift of the PPG frequency components. To prove that the PPG frequency components are separated from the MA frequency components, each participant is requested to perform five moving sub-experiments in this subsection. These five moving sub-experiments are bending a finger, horizontal moving a finger, shivering a finger, vertical moving a finger and waving a finger. Like the experiment conducted in Subsection 3.4.1, each subject is asked to put two pulse oximeters onto the index and middle fingers, respectively, of his/her left hand. The index finger is for the pulse oximeter implemented by the proposed LEDs-emitting technique and the middle finger is for the commercial pulse oximeter having the conventional LEDs-driving method installed. Each sub-experiment is planned for each volunteer to do five times ten seconds. Besides, each participant is requested to perform each pose freely in the natural manner.

Since the red and IR PPG signals processed by the proposed technique for all subjects appear in the same way, some of the obtained PPG results are displayed. First, the results of bending a finger are portrayed in Figure 4.13. Next, the results of horizontal moving a finger are depicted in Figure 4.14. After that, the results of shivering a finger are shown in Figure 4.15. Later, the results of vertical moving a finger are manifested in Figure 4.16. Lastly, the results of waving a finger are drawn in Figure 4.17. In Figures 4.13-4.17, the left sub-figures exhibit the red and IR PPG signals provided by the proposed technique. For the right sub-figures of Figures 4.13-4.17, the red and IR PPG signals furnished by the conventional method are illustrated. From Figures 4.13-4.17, the first two rows show the male results while the other two bottom rows display the female results. All results manifested in all sub-figures in Figures 4.13-4.17 are portrayed in a time domain instead of a frequency domain. This is because the PPG frequency components plotted in the frequency domain do not reveal the distortion of the PPG waveform while any motion takes place.

Obviously, in Figures 4.13-4.17, the red and IR PPG signals provided by the proposed technique for both genders still maintain their PPG waveforms in proper shape for all moving postures. Although the red and IR PPG waveforms furnished by the proposed approach during motions are not perfect like those while resting, they are good enough to yield accurate SpO2 values. By contrast, the red and IR PPG signals obtained from the conventional method for both genders are mostly distorted from all moving poses. However, some of them are not fully disfigured. For those red and IR PPG signals acquired by the traditional method not fully misrepresented, their PPG waveforms are yet present but their baselines and amplitudes are mangled up. Overall, the red and IR PPG signals sensed by the conventional method while moving are not well enough to produce correct SpO2 values even their PPG waveforms still exist. The red and IR PPG signals acquired by both methods of each participant are converted to

the SpO2 values. Since many SpO2 values of each subject for each moving pose are generated, these calculated SpO2 values are averaged and standard-deviation-computed as well as summarized in Tables A.9-A.28. Tables A.9-A.28 are organized like Tables A.5-A.8. Tables A.9-A.12 are digested to Table 4.4 to show the SpO2 values while bending a finger for all age ranges. Next, Tables A.13-A.16 abridge to Table 4.5 to display the SpO2 values during horizontal moving a finger for all age ranges. Then, Tables A.17-A.20 are summarized into Table 4.6 to illustrate the SpO2 values while shivering a finger for all age ranges. Afterwards, Tables A.21-A.24 are summed up Table 4.7 to depict the SpO2 values during vertical moving a finger for all age ranges. Lastly, Table 4.8 concludes from Tables A.25-A.28 to demonstrate the SpO2 values while waving a finger for all age ranges. Tables 4.4-4.8 are also arranged in the same pattern as Table 4.3, and exhibit the overall SpO2 values of each age range for each pose.

With well maintaining the significant PPG morphologies, the overall SpO2 values for all moving postures of all age ranges obtained by the proposed technique emerge in the same way. Those SpO2 values are not different from the overall SpO2 values measured while resting.

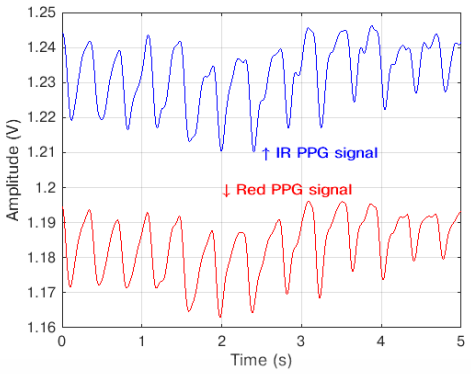

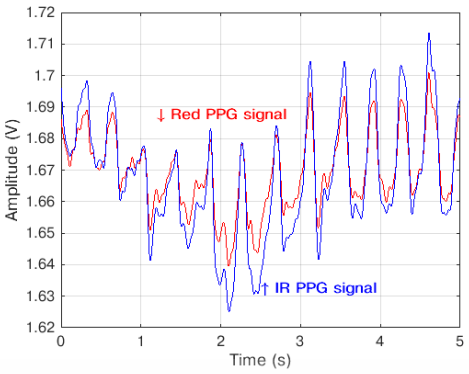

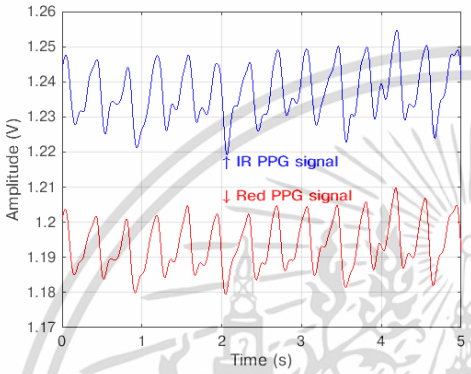

(a) Red and IR PPG signals of male subjects of the proposed technique

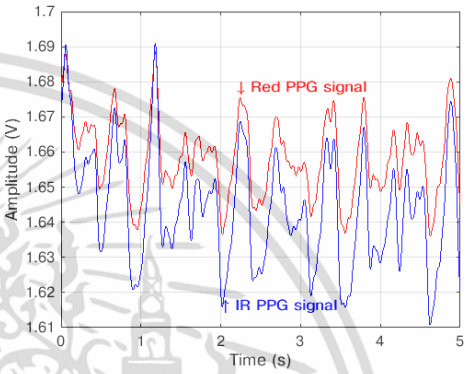

(b) Red and IR PPG signals of male subjects of the conventional method

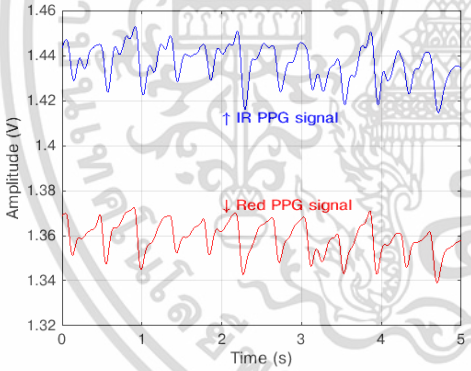

(c) Red and IR PPG signals of female subjects of the proposed technique

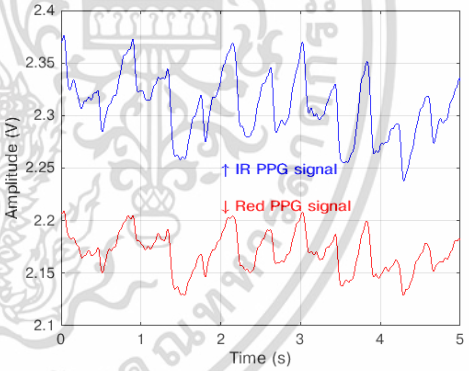

(d) Red and IR PPG signals of female subjects of the conventional method

Figure 4.13 Comparison for both techniques while bending a finger.

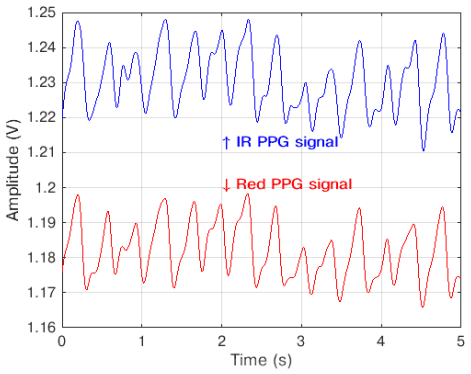

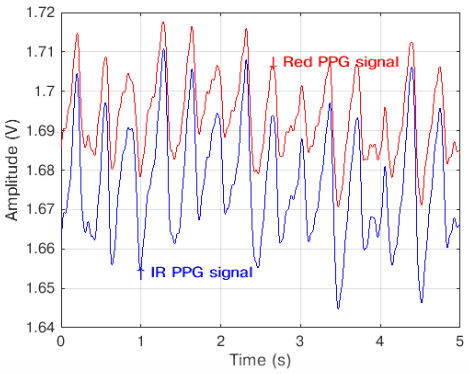

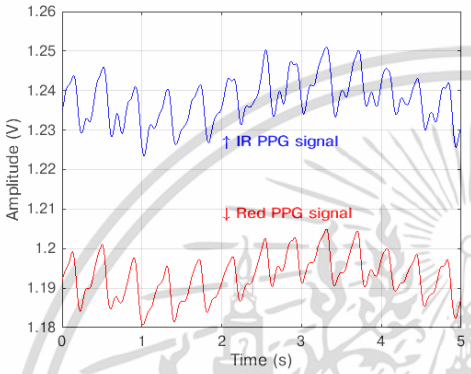

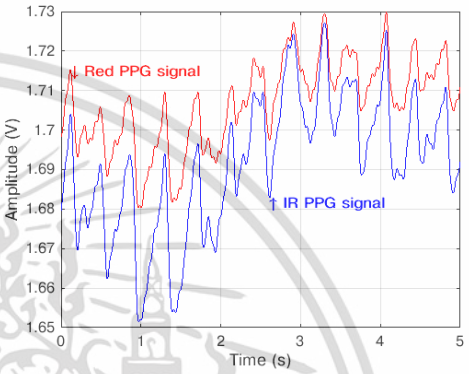

(a) Red and IR PPG signals of male subjects of the proposed technique

(b) Red and IR PPG signals of male subjects of the conventional method

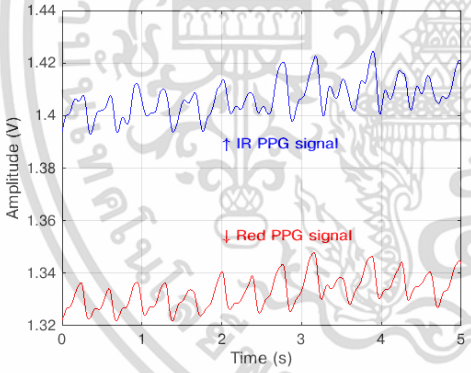

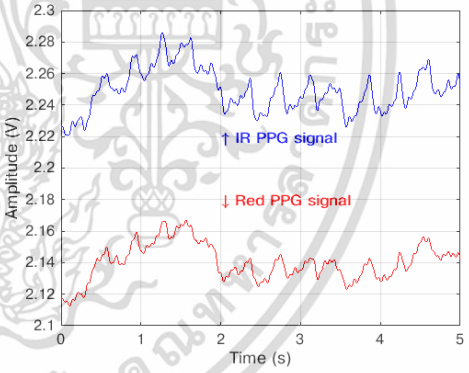

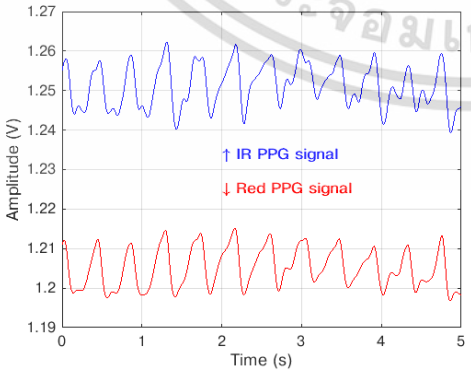

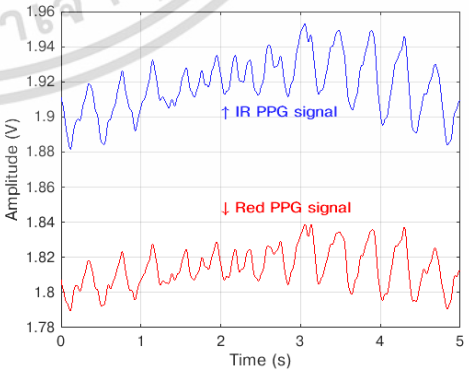

(c) Red and IR PPG signals of female subjects of the proposed technique

(d) Red and IR PPG signals of female subjects of the conventional method

Figure 4.14 Comparison for both techniques while moving a finger horizontally.

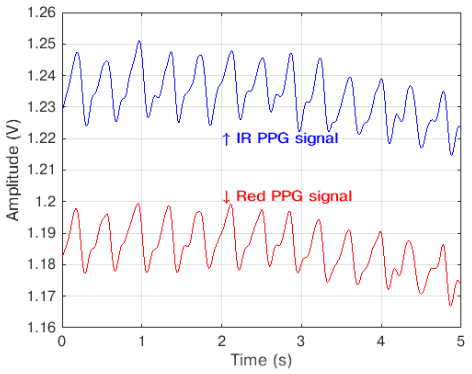

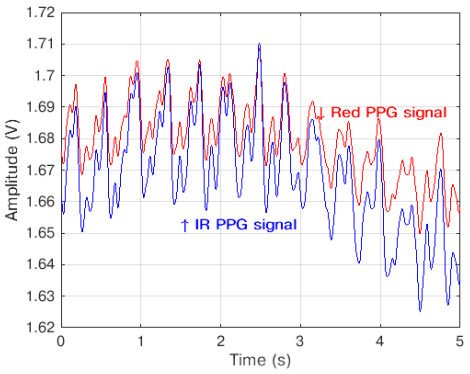

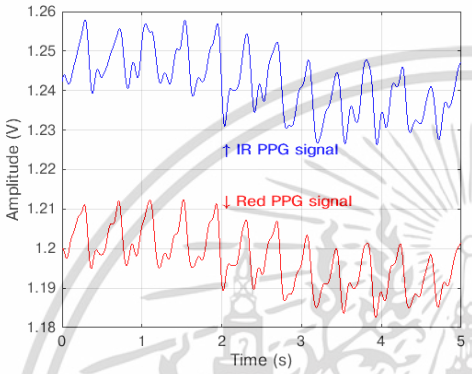

(a) Red and IR PPG signals of male subjects of the proposed technique

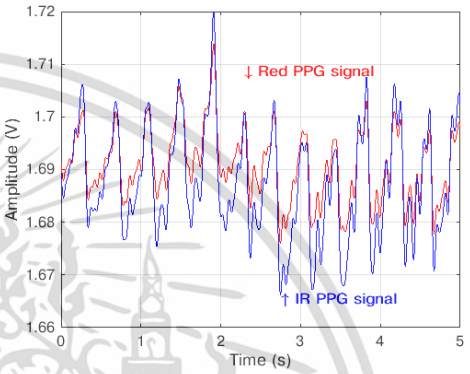

(b) Red and IR PPG signals of male subjects of the conventional method

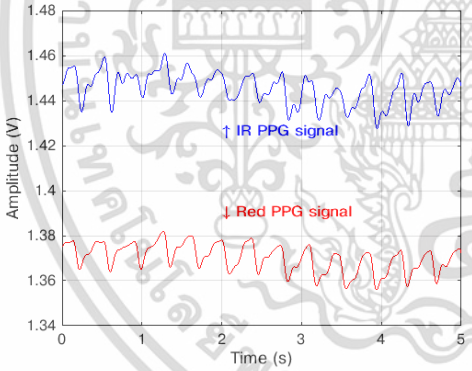

(c) Red and IR PPG signals of female subjects of the proposed technique

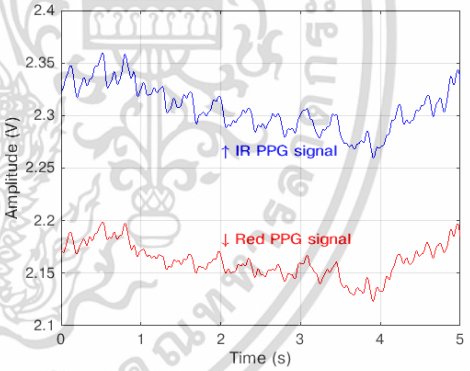

(d) Red and IR PPG signals of female subjects of the conventional method

Figure 4.15 Comparison for both techniques while shivering a finger.

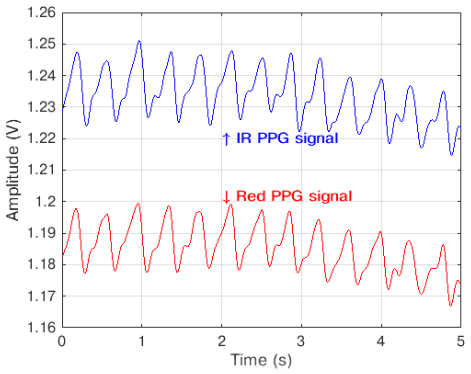

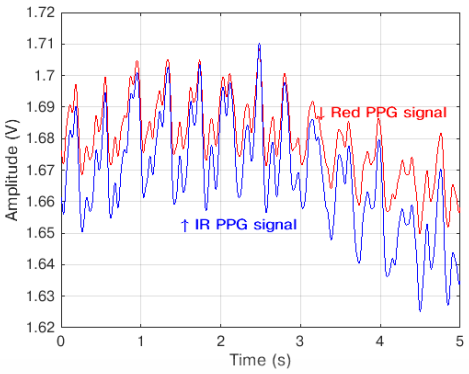

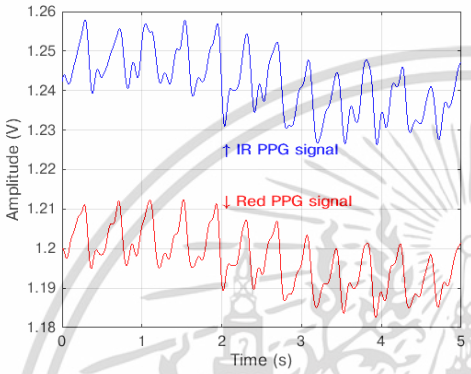

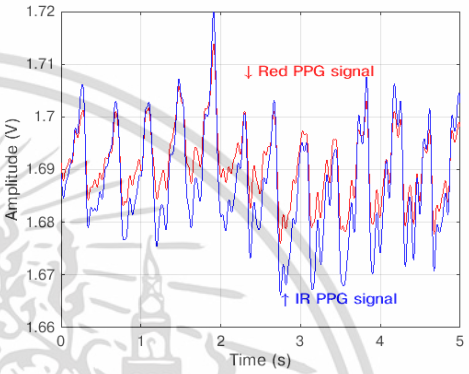

(a) Red and IR PPG signals of male subjects of the proposed technique

(b) Red and IR PPG signals of male subjects of the conventional method

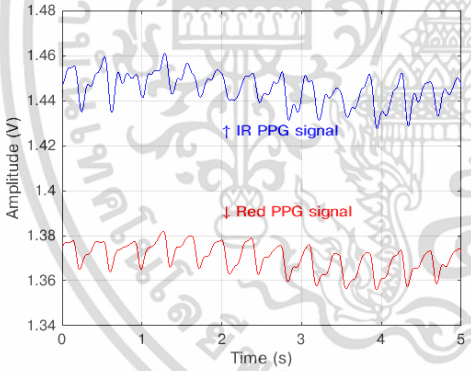

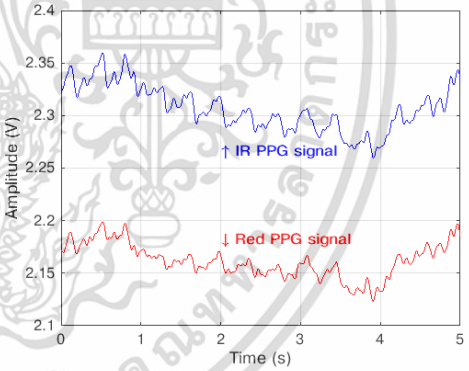

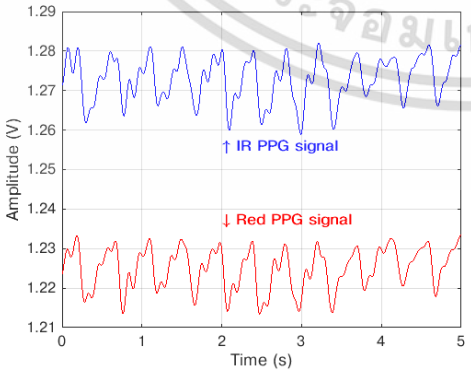

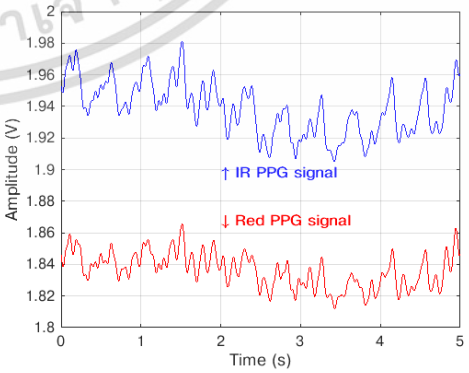

(c) Red and IR PPG signals of female subjects of the proposed technique

(d) Red and IR PPG signals of female subjects of the conventional method

Figure 4.16 Comparison for both techniques while moving a finger vertically.

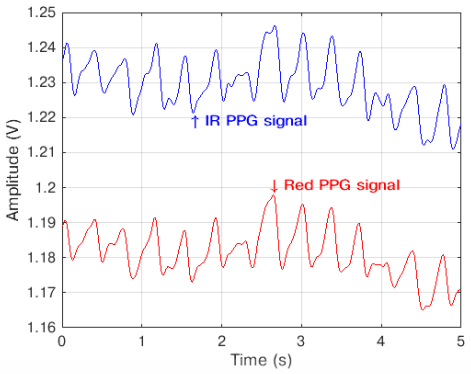

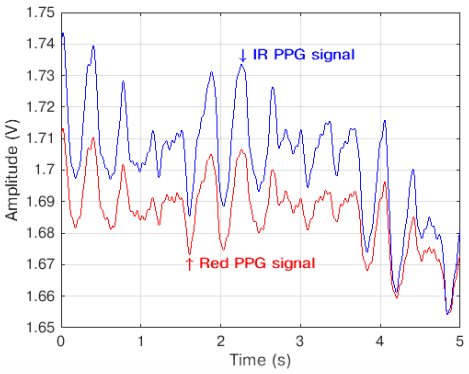

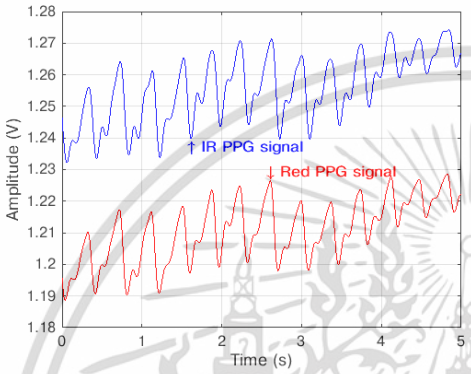

(a) Red and IR PPG signals of male subjects of the proposed technique

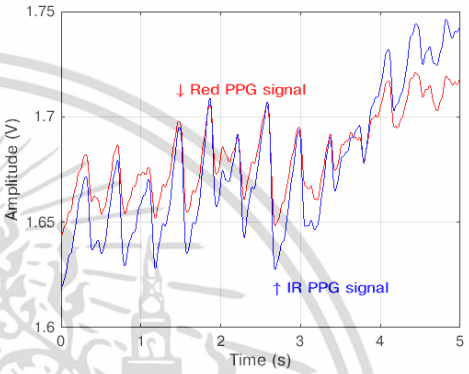

(b) Red and IR PPG signals of male subjects of the conventional method

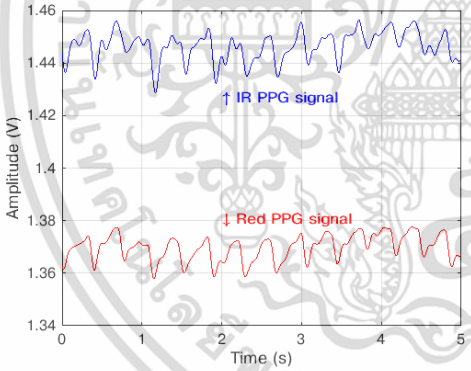

(c) Red and IR PPG signals of female subjects of the proposed technique

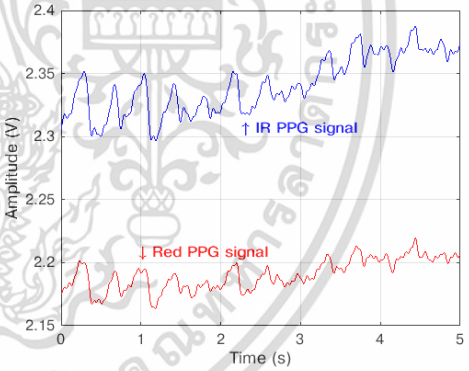

(d) Red and IR PPG signals of female subjects of the conventional method

Figure 4.17 Comparison for both techniques while waving a finger.

Table 4.4 Summary SpO2 values of all age ranges while bending.

Age ranges	Male subjects		Female subjects	
	Proposed technique (PT)	Conventional method (CM)	Proposed technique (PT)	Conventional method (CM)
	Summary SpO2 values in the unit of percentage (%)			
	Average ± Standard deviation			
21-30	96.31±1.96	90.93±2.95	96.68±1.92	88.78±4.59
31-40	96.65±2.12	88.52±4.88	98.01±1.04	83.55±8.93
41-50	96.25±2.02	89.41±2.63	97.46±1.41	89.30±3.53
51-60	97.13±1.46	89.45±2.56	96.74±1.58	85.68±7.30

Table 4.5 Summary SpO2 values of all age ranges while horizontal moving.

Age ranges	Male subjects		Female subjects	
	Proposed technique (PT)	Conventional method (CM)	Proposed technique (PT)	Conventional method (CM)
	Summary SpO2 values in the unit of percentage (%)			
	Average ± Standard deviation			
21-30	96.03±2.28	91.61±3.07	96.77±1.91	87.45±6.40
31-40	96.54±1.99	88.20±5.25	97.54±1.17	82.39±6.48
41-50	95.70±1.59	89.61±3.37	97.47±1.74	88.92±3.03
51-60	96.92±1.44	89.93±2.79	96.93±1.88	85.97±13.61

Table 4.6 Summary SpO2 values of all age ranges while shivering.

Age ranges	Male subjects		Female subjects	
	Proposed technique (PT)	Conventional method (CM)	Proposed technique (PT)	Conventional method (CM)
	Summary SpO2 values in the unit of percentage (%)			
	Average ± Standard deviation			
21-30	96.47±1.85	90.76±3.02	96.61±1.63	85.09±11.33
31-40	96.84±1.83	89.92±5.67	97.80±1.16	84.46±9.96
41-50	96.01±1.39	91.41±3.91	97.68±1.57	87.90±7.50
51-60	97.24±1.42	87.07±7.01	96.78±1.85	83.73±18.36

Table 4.7 Summary SpO2 values of all age ranges while vertical moving.

Age ranges	Male subjects		Female subjects	
	Proposed technique (PT)	Conventional method (CM)	Proposed technique (PT)	Conventional method (CM)
	Summary SpO2 values in the unit of percentage (%)			
	Average ± Standard deviation			
21-30	96.54±1.87	91.13±3.34	96.98±1.87	86.96±6.42
31-40	96.98±1.95	88.44±4.40	97.86±1.16	83.24±8.15
41-50	96.10±1.30	89.30±6.28	97.52±1.36	88.47±4.27
51-60	97.39±1.36	87.50±7.61	96.79±1.52	82.22±24.19

Table 4.8 Summary SpO2 values of all age ranges while waving.

Age ranges	Male subjects		Female subjects	
	Proposed technique (PT)	Conventional method (CM)	Proposed technique (PT)	Conventional method (CM)
	Summary SpO2 values in the unit of percentage (%)			
	Average ± Standard deviation			
21-30	96.76±1.64	90.81±2.80	96.81±1.84	87.13±10.07
31-40	97.05±1.78	89.11±4.54	97.72±1.08	90.00±7.75
41-50	96.10±1.60	87.76±6.38	97.86±1.21	88.13±3.53
51-60	97.26±1.56	90.02±2.27	96.70±1.84	85.74±12.26

4.2.2.2 Evaluation of SpO2 accuracy during motion involvement

To quantify the exactness of the proposed LEDs-emitting solution, the SpO2 value is used as a criterion. The SpO2 value acquired from each moving posture of each volunteer is plugged into the mean absolute percentage error (MAPE) (see Eq. (3.27)) to compute the amount of accuracy. In MAPE computation, the actual SpO2 value of each participant, a_{SpO2}, in this thesis uses the mean SpO2 value of each volunteer summarized in Tables A.5-A.8. For the variable s_i in Eq. (3.27) uses the measured SpO2 value of each participant while moving, shown in Tables A.9-A.28. Because one pair of red and IR PPG signals produces many SpO2 values, the measured SpO2 value of each subject is thus the mean SpO2 value of those SpO2 values. Each sub-experiment produces one averaged SpO2 value. As each sub-experiment is performed five times, the variable N in Eq. (3.27) is thus equal to five which is the total number of average SpO2 value.

Besides, the accuracy of the conventional method is also computed in the same way as the proposed technique for the performance comparison. All MAPE values for all age ranges are summed up in Tables 4.9-4.13. Tables 4.9-4.13 are arranged in the similar way as Tables 4.4-4.8. For the MAPE value of each participant is provided in Tables A.29-A.48. Since all provided data in Tables A.29-A.48 are detailed, they are therefore digested in Table 4.14 for overall consideration. Table 4.14 manifests the overall SpO2 values for each moving posture of both genders as well as the overall MAPE values for all moving poses of both sexes. The upper part of Table 4.14 illustrates the overall SpO2 values and the lower part of the same table portrays the overall MAPE values. All those provided data in Tables 4.4-4.13 are condensed into four age groups, 21-30 years, 31-40 years, 41-50 years and 51-60 years in Table 4.14.

According to Table 4.14, the SpO2 values acquired by the proposed technique for all moving postures of both genders are approximately over 96 for all age groups. However, when considering to each participant (see Tables A.9-A.28), the SpO2 values of few volunteers appear to be too low but not lesser than 91. This may be that those participants may probably have the temporary condition of poor blood perfusion

during performing finger movement. On the contrary, the SpO2 values obtained by the conventional method are roughly below 91 for all age ranges. Although the SpO2 values acquired by the traditional method are under 91, the SpO2 values of some participants for both genders are around 94 for each pose (see Tables A.9-A.28). This may be that those volunteers are asked to move their fingers in a natural manner. They may move their fingers in a way that the distorting absorption of human organs and the external light sources could not affect the red and IR PPG waveforms.

Overall, the SpO2 values of the volunteers in each age range of the proposed technique are as not different as from the volunteers' actual values for all moving postures. This is confirmed by the overall MAPE values of the volunteers in each age group for all moving poses that are lower than 1%, as depicted in Table 4.14. On the other hands, the SpO2 values of the participants in each age range of the conventional method are considerably deviated from the participants' actual values for all moving poses. This is revealed by the overall MAPE values of the participants in each age group for all moving postures that are roughly varied from 3% to 13%. Besides, when contemplating in Tables A.29-A.48, the MAPE values of the traditional method are found to show high variation.

With using the summarized MAPE values along with the summarized SpO2 values, it is can be inferred that the proposed technique is superior to the conventional method. Providing low MAPE values for all moving postures implies that the proposed technique successfully translates the red and IR PPG frequency components to the desirable frequency locations. This is because the MA frequency components no longer have any influences on the red and IR PPG frequency.

The proposed technique works well with the involved volunteers. The ability of the proposed technique on other human races along with other colors of skin cannot be concluded. Nonetheless, the proposed technique significantly shows the potentiality of solving the motion artifact issue.

Table 4.9 Summary of SpO2 percentage error of all age ranges while bending.

Age ranges	Male subjects		Female subjects	
	Proposed technique (PT)	Conventional method (CM)	Proposed technique (PT)	Conventional method (CM)
	Summary of SpO2 percentage error in the unit of percentage (%)			
	Overall (Mean) ± Standard deviation			
21-30	0.68±0.58	3.22±2.69	0.77±0.59	5.65±4.72
31-40	0.84±0.69	5.59±4.93	0.46±0.28	10.70±9.16
41-50	0.98±1.17	4.31±3.02	0.59±0.54	3.97±3.64
51-60	0.64±0.41	4.44±2.84	0.59±0.48	8.84±7.71

Table 4.10 Summary of SpO2 percentage error of all age ranges while horizontal moving.

Age ranges	Male subjects		Female subjects	
	Proposed technique (PT)	Conventional method (CM)	Proposed technique (PT)	Conventional method (CM)
	Summary of SpO2 percentage error in the unit of percentage (%)			
	Overall (Mean) ± Standard deviation			
21-30	0.76±0.64	2.92±2.59	1.08±1.01	7.03±6.51
31-40	0.98±1.05	5.31±5.70	0.98±0.87	11.85±7.22
41-50	0.84±1.01	4.53±4.85	0.75±0.78	4.06±3.05
51-60	0.71±0.60	3.93±2.81	1.35±1.17	9.46±13.96

Table 4.11 Summary of SpO2 percentage error of all age ranges while shivering.

Age ranges	Male subjects		Female subjects	
	Proposed technique (PT)	Conventional method (CM)	Proposed technique (PT)	Conventional method (CM)
	Summary of SpO2 percentage error in the unit of percentage (%)			
	Overall (Mean) ± Standard deviation			
21-30	0.82±0.70	3.17±2.86	0.90±0.65	9.23±11.92
31-40	1.20±0.65	4.36±5.72	0.94±0.92	12.71±15.98
41-50	0.61±0.65	3.24±3.75	0.71±0.62	5.60±7.37
51-60	0.77±0.46	7.24±7.14	0.86±0.59	10.95±19.37

Table 4.12 Summary of SpO2 percentage error of all age ranges while vertical moving.

Age ranges	Male subjects		Female subjects	
	Proposed technique (PT)	Conventional method (CM)	Proposed technique (PT)	Conventional method (CM)
	Summary of SpO2 percentage error in the unit of percentage (%)			
	Overall (Mean) ± Standard deviation			
21-30	0.82±0.63	3.06±3.14	0.89±0.45	7.63±6.44
31-40	1.16±0.67	5.31±4.45	0.95±0.81	10.95±9.00
41-50	0.69±0.63	5.26±6.39	0.88±0.61	5.52±6.45
51-60	0.94±0.53	6.53±7.98	1.32±0.99	12.77±25.58

Table 4.13 Summary of SpO2 percentage error of all age ranges while waving.

Age ranges	Male subjects		Female subjects	
	Proposed technique (PT)	Conventional method (CM)	Proposed technique (PT)	Conventional method (CM)
	Summary of SpO2 percentage error in the unit of percentage (%)			
	Overall (Mean) ± Standard deviation			
21-30	0.92±0.63	2.99±2.89	0.76±0.49	7.58±10.39
31-40	1.18±0.64	4.48±5.03	0.96±0.86	11.40±15.52
41-50	0.71±0.92	6.14±7.03	0.73±0.40	5.08±3.45
51-60	0.77±0.48	3.84±2.23	0.86±0.63	9.02±12.70

Table 4.14 Summary SpO2 values and SpO2 percentage error for all moving postures of all age ranges.

Age ranges	Moving postures																			
	Bending a finger				Horizontal moving a finger				Shivering a finger				Vertical moving a finger				Waving a finger			
	Proposed technique (PT)		Conventional method (CM)		Proposed technique (PT)		Conventional method (CM)		Proposed technique (PT)		Conventional method (CM)		Proposed technique (PT)		Conventional method (CM)		Proposed technique (PT)		Conventional method (CM)	
	M	F	M	F	M	F	M	F	M	F	M	F	M	F	M	F	M	F	M	F
Overview of SpO2 values in the unit of percentage (%)																				
21-30	96.31	96.68	90.93	88.78	96.03	96.77	91.61	87.45	96.47	96.61	90.76	85.09	96.54	96.98	91.13	86.96	96.76	96.81	90.81	87.13
31-40	96.65	98.01	88.52	83.55	96.54	97.54	88.20	82.39	96.84	97.80	89.92	84.46	96.98	97.86	88.44	83.24	97.05	97.72	89.11	90.00
41-50	96.25	97.46	89.41	89.30	95.70	97.47	89.61	88.92	96.01	97.68	91.41	87.90	96.10	97.52	89.30	88.47	96.10	97.86	87.76	88.13
51-60	97.13	96.74	89.45	85.68	96.92	96.93	89.93	85.97	97.24	96.78	87.07	83.73	97.39	96.79	87.50	82.22	97.26	96.70	90.02	85.74
Overall (Mean) ± Standard deviation	96.59 ±0.40	97.22 ±0.63	89.58 ±1.00	86.83 ±2.71	96.30 ±0.54	97.18 ±0.38	89.84 ±1.40	86.18 ±2.80	96.64 ±0.52	97.22 ±0.61	89.79 ±1.91	85.30 ±1.82	96.75 ±0.56	97.29 ±0.49	89.09 ±1.54	85.22 ±2.97	96.79 ±0.51	97.27 ±0.60	89.43 ±1.31	87.75 ±1.79
Overview of MAPE values in the unit of percentage (%)																				
21-30	0.68	0.77	3.22	5.65	0.76	1.08	2.92	7.03	0.82	0.90	3.17	9.23	0.82	0.89	3.06	7.63	0.92	0.76	2.99	7.58
31-40	0.84	0.46	5.59	10.70	0.98	0.98	5.31	11.85	1.20	0.94	4.36	12.71	1.16	0.95	5.31	10.95	1.18	0.96	4.48	11.40
41-50	0.98	0.59	4.31	3.97	0.84	0.75	4.53	4.06	0.61	0.71	3.24	5.60	0.69	0.88	5.26	5.52	0.71	0.73	6.14	5.08
51-60	0.64	0.59	4.44	8.84	0.71	1.35	**3.93**	9.46	0.77	0.86	7.24	10.95	0.94	1.32	6.53	12.77	0.77	0.86	3.84	9.02
Overall (Mean) ± Standard deviation	0.79± 0.16	0.60± 0.13	4.39± 0.97	7.29± 3.04	0.82± 0.12	1.04± 0.25	4.07± 1.18	8.10± 3.34	0.85± 0.25	0.85± 0.10	4.50± 1.90	9.62± 3.03	0.90± 0.20	1.01± 0.21	5.04± 1.44	9.22± 3.26	0.90± 0.21	0.83± 0.10	4.36± 1.33	8.27± 2.65

M – Male, F – Female.

4.2.3 Evaluation of influence of light intensity on the SpO2 quality

In this evaluation, change of light intensity by altering the root mean square (RMS) current fed to a LED is experimented to study the impact on the SpO2 quality. Three values of current which are 14.71 mA, 14.49 mA and 14.26 mA are selected. Each RMS current value is experimented separately. In this study, two main experiments are conducted. The first experiment requests each volunteer to stay at rest in performing the sub-experiments using the RMS current values of 14.71 mA, 14.49 mA and 14.26 mA, respectively. For the second experiment, each participant is asked to do five common postures separately by which the RMS current values of 14.71 mA, 14.49 mA and 14.26 mA, are set sequentially. Like all previous experiments, each subject is requested to do each sub-experiment in this study for five times ten seconds each. The volunteers involving the two main experiments in this study are randomly selected from the same seventy-five volunteers who participate in the prior experiments. The volunteers are chosen from all age groups. In each age range, both genders are opted about the same amount. The total number of participants is twelve.

Since the proposed LEDs-driving technique is proved that the PPG signals are not intertwined with the MA signal, the recovered PPG signals at different RMS current values are therefore not illustrated. Besides, the resultant PPG signals obtained from dissimilar amplitude values behave in the similar manner. For the sake of conciseness, only the SpO2 values at different RMS current values are considered.

4.2.3.1 Evaluation of impact of light intensity during staying at rest

All red and IR PPG signals at different RMS current values while resting obtained from the proposed LEDs-driving technique for all subjects are converted to the SpO2 values. As each SpO2 value is calculated by employing two consecutive peaks manifesting in a pair of red and IR PPG signals, many sets of two consecutive peaks are thus detected. As a result, numerous SpO2 values are generated for each subject at different RMS current values. The SpO2 values at each RMS current value of each subject are averaged and standard deviation calculated, as well as summed up in Table 4.15. Table 4.15 consists of five columns where the first column shows the subject number. The following three columns express the mean SpO2 values of each subject at the RMS current values of 14.71 mA, 14.49 mA and 14.26 mA. The last column displays the overall SpO2 value computed by averaging the SpO2 values at different RMS current values depicted in the previous three columns of each subject. The standard deviation of the overall SpO2 value is also calculated. As can be noticed in Table 4.15, all averaged SpO2 values at different RMS current values of each subject are fairly equal to the overall SpO2 value for all age ranges. This suggests that change of light intensity has no significant impact on the SpO2 quality for both sexes.

Table 4.15 Summary SpO2 values at different RMS current values while resting.

RMS current values	14.71 mA	14.49 mA	14.26 mA	Overall (Mean)
Subject no.	Average ± Standard deviation			
Age range of 21-30 years				
Female no.17	97.89±0.07	96.56±0.11	97.57±0.12	97.34±0.69
Female no.28	96.25±0.25	96.24±0.13	96.93±0.09	96.47±0.40
Male no.59	98.54±0.12	98.26±0.22	97.70±0.24	98.17±0.43
Age range of 31-40 years				
Male no.24	98.18±0.10	97.54±0.28	97.99±0.36	97.90±0.33
Male no.34	98.91±0.10	97.43±0.35	97.70±0.41	98.01±0.79
Female no.56	97.45±0.03	97.90±0.23	99.78±0.12	98.38±1.24
Age range of 41-50 years				
Male no.20	96.37±0.05	95.66±0.12	95.77±0.15	95.93±0.38
Female no.43	96.26±0.05	98.21±0.12	99.18±0.02	97.88±1.49
Male no.49	95.34±0.05	94.45±0.32	95.26±0.24	95.02±0.49
Age range of 51-60 years				
Male no.45	96.76±0.16	95.52±0.12	95.61±0.30	95.96±0.69
Female no.70	97.41±0.04	99.70±0.25	97.46±0.07	98.19±1.31
Female no.74	96.18±0.14	93.91±0.08	95.39±0.33	95.16±1.15

However, most female subjects show more SpO2 variation than the male subjects do. Additionally, the overall SpO2 value of each volunteer in each age group is moderately close to the SpO2 values of each participant obtained from different RMS current values. This points out that the age factor is not significantly influenced by altering of light intensity.

4.2.3.2 Evaluation of effect of light intensity with motion involvement

For this experiment is different from the experiment done in Sub-subsection 4.2.3.1 only that each subject is requested to do five regular postures separately instead of staying at rest. The five usual poses are as same as the five experimented postures in Subsection 4.2.2, bending a finger, horizontal moving a finger, shivering a finger, vertical moving a finger and waving a finger. Similar to Sub-subsection 4.2.3.1, the entire red and IR PPG signals of each pose of each subject are turned into the SpO2 values. The whole SpO2 values of each posture for each volunteer are administered by the same fashion as Sub-subsection 4.2.3.1, and summarized in Tables 4.16-4.20. Tables 4.16-4.20 are all organized like Table 4.15. As can be noticed in Tables 4.16-4.20, all SpO2 values at different RMS current values of each volunteer are quite alike the overall SpO2 value of each participant for all postures. From this point of view indicates that change of light intensity does not affect the SpO2 quality for all poses of all subject's age ranges significantly. When considering the SpO2 value at each RMS current value of each subject, it is found that some SpO2 values of a few

volunteers are inconsistent with the rest SpO2 values. The inconsistent SpO2 results occur because the pulse oximeter may not be worn properly.

At each RMS current value of each volunteer, the SpO2 value of each posture compared with the SpO2 value while at rest is not different significantly for over 90% of volunteers. This supports that change of light intensity has no significant influence on the SpO2 quality. For the aspects of each gender and each age range, no significant impact on the SpO2 quality is present.

Table 4.16 Summary SpO2 values at different RMS current values while bending.

RMS current values	14.71 mA	14.49 mA	14.26 mA	Overall (Mean)
Subject no.	Average ± Standard deviation			
Age range of 21-30 years				
Female no.17	97.86±0.07	98.32±0.17	98.87±0.09	98.35±0.51
Female no.28	96.44±0.29	96.30±0.15	97.01±0.29	96.58±0.38
Male no.59	98.49±0.10	98.46±0.07	98.68±0.34	98.54±0.12
Age range of 31-40 years				
Male no.24	98.47±0.09	98.82±0.13	98.70±0.09	98.66±0.18
Male no.34	99.54±0.15	97.74±0.10	98.02±0.16	98.43±0.97
Female no.56	97.66±0.19	98.95±0.24	99.97±0.05	98.86±1.16
Age range of 41-50 years				
Male no.20	95.95±0.27	95.19±0.36	94.74±0.46	95.29±0.61
Female no.43	97.13±0.10	96.60±0.00	96.40±0.00	96.71±0.38
Male no.49	95.90±0.24	93.68±0.17	95.69±0.21	95.09±1.23
Age range of 51-60 years				
Male no.45	96.42±0.11	95.17±0.17	95.95±0.12	95.85±0.63
Female no.70	97.19±0.16	99.68±0.16	97.22±0.06	98.03±1.43
Female no.74	96.34±0.21	97.14±1.68	97.02±0.61	96.83±0.43

Table 4.17 Summary SpO2 values at different RMS current values while horizontal moving.

RMS current values	14.71 mA	14.49 mA	14.26 mA	Overall (Mean)
Subject no.	Average ± Standard deviation			
Age range of 21-30 years				
Female no.17	97.98±0.12	98.32±0.17	98.87±0.09	98.39±0.45
Female no.28	95.18±0.27	96.30±0.15	97.01±0.29	96.16±0.92
Male no.59	99.30±0.10	98.46±0.07	98.68±0.34	98.81±0.44
Age range of 31-40 years				
Male no.24	98.48±0.17	98.82±0.13	98.70±0.09	98.67±0.17
Male no.34	98.94±0.12	97.74±0.10	98.02±0.16	98.23±0.63
Female no.56	98.48±0.10	98.95±0.24	99.97±0.05	99.13±0.76
Age range of 41-50 years				
Male no.20	95.46±0.08	95.14±0.08	94.95±0.40	95.18±0.26
Female no.43	97.20±0.07	96.60±0.07	96.40±0.07	96.73±0.42
Male no.49	95.54±0.08	93.68±0.17	95.69±0.21	94.97±1.12
Age range of 51-60 years				
Male no.45	96.55±0.18	95.17±0.17	95.95±0.12	95.89±0.69
Female no.70	96.78±0.30	99.68±0.16	97.22±0.06	97.89±1.56
Female no.74	92.70±0.46	97.14±1.68	97.02±0.61	95.62±2.53

Table 4.18 Summary SpO2 values at different RMS current values while shivering.

RMS current values	14.71 mA	14.49 mA	14.26 mA	Overall (Mean)
Subject no.	Average ± Standard deviation			
Age range of 21-30 years				
Female no.17	97.98±0.02	97.82±0.13	97.67±0.16	97.82±0.16
Female no.28	95.74±0.24	97.10±0.22	98.02±0.30	96.95±1.15
Male no.59	99.49±0.09	98.90±0.09	99.74±0.07	99.38±0.43
Age range of 31-40 years				
Male no.24	99.50±0.13	99.90±0.07	99.83±0.05	99.74±0.21
Male no.34	98.24±0.15	98.72±0.07	98.29±0.20	98.42±0.26
Female no.56	99.10±0.11	98.40±0.19	99.97±0.07	99.16±0.79
Age range of 41-50 years				
Male no.20	95.42±0.09	95.36±0.45	95.86±0.07	95.55±0.27
Female no.43	97.14±0.06	96.60±0.16	96.40±0.07	96.71±0.38
Male no.49	95.61±0.16	95.26±0.12	95.18±0.29	95.35±0.23
Age range of 51-60 years				
Male no.45	96.82±0.09	95.53±0.39	97.48±0.12	96.61±0.99
Female no.70	97.94±0.11	97.38±0.04	98.20±0.19	97.84±0.42
Female no.74	94.10±0.43	99.78±0.05	97.58±0.09	97.15±2.86

Table 4.19 Summary SpO2 values at different RMS current values while vertical moving.

RMS current values	14.71 mA	14.49 mA	14.26 mA	Overall (Mean)
Subject no.	Average ± Standard deviation			
Age range of 21-30 years				
Female no.17	98.16±0.09	97.82±0.07	98.30±0.12	98.09±0.25
Female no.28	95.86±0.12	97.18±0.05	98.30±0.15	97.11±1.22
Male no.59	99.36±0.09	99.10±0.15	99.89±0.18	99.45±0.40
Age range of 31-40 years				
Male no.24	99.28±0.31	99.57±0.14	99.06±0.09	99.30±0.26
Male no.34	99.46±0.21	99.09±0.07	98.42±0.09	98.99±0.53
Female no.56	98.64±0.05	97.26±0.19	99.81±0.03	98.57±1.28
Age range of 41-50 years				
Male no.20	95.74±0.21	95.11±0.18	96.02±0.19	95.62±0.47
Female no.43	97.14±0.09	96.60±0.07	96.40±0.16	96.71±0.38
Male no.49	96.06±0.11	96.26±0.16	96.62±0.21	96.31±0.28
Age range of 51-60 years				
Male no.45	96.98±0.21	96.18±0.33	97.50±0.07	96.89±0.66
Female no.70	97.19±0.35	99.86±0.14	96.76±0.48	97.94±1.68
Female no.74	93.78±0.52	99.79±0.02	97.48±0.21	97.02±3.03

Table 4.20 Summary SpO2 values at different RMS current values while waving.

RMS current values	14.71 mA	14.49 mA	14.26 mA	Overall (Mean)
Subject no.	Average ± Standard deviation			
Age range of 21-30 years				
Female no.17	98.34±0.11	98.62±0.08	99.21±0.19	98.72±0.44
Female no.28	96.06±0.21	96.84±0.07	97.69±0.26	96.86±0.82
Male no.59	99.23±0.07	99.42±0.18	99.95±0.09	99.53±0.37
Age range of 31-40 years				
Male no.24	99.37±0.19	99.86±0.14	99.27±0.08	99.50±0.32
Male no.34	98.78±0.25	98.30±0.24	98.78±0.13	98.62±0.28
Female no.56	98.51±0.10	98.31±0.07	99.85±0.07	98.89±0.84
Age range of 41-50 years				
Male no.20	95.51±0.05	95.01±0.07	94.11±0.87	94.88±0.71
Female no.43	97.19±0.02	96.60±0.12	96.40±0.07	96.73±0.41
Male no.49	95.94±0.28	95.27±0.19	94.99±0.28	95.40±0.49
Age range of 51-60 years				
Male no.45	96.66±0.17	96.46±0.08	96.87±0.11	96.66±0.21
Female no.70	97.70±0.14	97.19±0.02	98.50±0.33	97.80±0.66
Female no.74	93.97±0.22	99.85±0.09	97.94±0.06	97.25±3.00

4.2.4 Evaluation of the performances of the presented technique and other well-known methods

This subsection performs a comparative study. In this comparative study, the performances of the proposed LEDs-driving technique and the well-known methods are compared. The well-known methods which are provided in Chapter 2 under Subsections 2.5.1-2.5.3 are discrete saturation transform (DST), independent component analysis (ICA) and compression of Fourier series (CFC).

In this thesis, the method of DST employs a simple 1st-order least mean squares (LMS) algorithm with a step size of 0.01 and an initial weight coefficient of 1. For the scheme of ICA, an algorithm of fast independent component analysis (fICA) is utilized and the settings for the ICA scheme are set using the standard values. In administering the concept of CFC, the entire Fourier series coefficients are truncated. Only the first twelve Fourier series coefficients are kept. As the proper PPG-waveforms of the MA-corrupted red and IR PPG signals are not present correctly, separating the PPG cycle to perform the CFC concept is difficult and laborious. Performing the CFC is thus applied on the raw MA-contaminated red and IR PPG signals directly without parting the PPG cycles.

In comparing the performances, all recorded red and IR PPG signals involving any motions of all subjects used in Subsection 4.2.2 are first processed by the mentioned well-known schemes separately. The entire utilized red and IR PPG signals are those obtained by the conventional LEDs-emitting approach. Later, each pair of mended red and IR PPG signals is turned to the SpO2 value. All the SpO2 values computed from the MA-interfered red and IR PPG signals processed by the well-known approaches for all age ranges are summarized in Tables 4.21-4.25. For more details of each volunteer is complied in Tables A.49-A.68. Besides in Tables 4.21-4.25, the SpO2 values during any motions of the proposed LEDs-shining technique as well as the conventional LEDs-emitting method are also annexed for comparison. The SpO2 values during any motions of the proposed LEDs-shining technique and the conventional LEDs-emitting method are duplicated from Tables A.9-A.28.

Contemplating the SpO2 quality of each method shown in Tables 4.21-4.25 is done through comparing with the SpO2 value of each volunteer acquired by the conventional method for all poses. As can be noted in Tables 4.21-4.25, the method of DST obviously improves the quality of the MA-corrupted red and IR PPG signals. This is because the SpO2 values obtained by the DST method are consistently increased for all age ranges of both genders, and all postures, roughly greater than 90%. By contrast, the ICA scheme poorly performs since the calculated SpO2 values by this scheme are aggravated for all age groups of both sexes and all poses. The SpO2 values acquired by the algorithm of ICA also exhibit very high variation swinging from below

0% of SpO2 value to above 100% of SpO2 value. For the approach of CFC works well with some postures for both genders of all age ranges. This is indicated by some of the acquired SpO2 values for some postures of both genders at all age groups that are greater than 90%. Some computed SpO2 values by the CFC method are not even bettered but worsened. However, some worsened SpO2 values processed by the CFC scheme are not as worse as the SpO2 values processed by the ICA method.

Table 4.21 Comparison of SpO2 values of all age ranges while bending for the dedicated techniques.

Age ranges	Compared techniques				
	PT[1]	CM[2]	DST[3]	ICA[4]	CFC[5]
	Summary SpO2 values in the unit of percentage (%)				
	Overall (Mean) ± Standard deviation				
Male subjects					
21-30	96.31±1.96	90.93±2.95	91.66±1.50	74.11±17.74	92.16±1.94
31-40	96.65±2.12	88.52±4.88	91.17±1.27	91.80±28.15	87.64±8.93
41-50	96.25±2.02	89.41±2.63	91.65±1.10	77.93±21.79	91.67±1.10
51-60	97.13±1.46	89.45±2.56	92.08±1.40	82.57±38.92	92.09±2.55
Female subjects					
21-30	96.68±1.92	88.78±4.59	92.19±1.66	86.83±20.18	89.48±5.56
31-40	98.01±1.04	83.55±8.93	92.06±1.37	112.50±38.12	94.03±15.10
41-50	97.46±1.41	89.30±3.53	91.59±1.50	77.27±34.26	89.62±3.63
51-60	96.74±1.58	85.68±7.30	92.23±1.08	73.59±64.29	84.95±9.19

1 – PT refers to the proposed LEDs-driving technique, 2 – CM refers to the conventional LEDs-emitting method,
3 – DST stands for discrete saturation transform, 4 – ICA stands for independent component analysis,
5 – CFC stands for compression of Fourier coefficients.

Table 4.22 Comparison of SpO2 values of all age ranges while horizontal moving for the dedicated techniques.

Age ranges	Compared techniques				
	PT[1]	CM[2]	DST[3]	ICA[4]	CFC[5]
	Summary SpO2 values in the unit of percentage (%)				
	Overall (Mean) ± Standard deviation				
Male subjects					
21-30	96.03±2.28	91.61±3.07	91.42±1.36	81.44±35.54	92.60±3.07
31-40	96.54±1.99	88.20±5.25	91.15±1.35	78.22±16.81	88.40±5.82
41-50	95.70±1.59	89.61±3.37	91.43±1.46	72.36±49.88	91.28±2.25
51-60	96.92±1.44	89.93±2.79	92.31±4.09	61.40±62.64	89.38±4.09
Female subjects					
21-30	96.77±1.91	87.45±6.40	91.89±1.94	82.21±11.22	90.11±3.47
31-40	97.54±1.17	82.39±6.48	91.66±1.73	71.30±25.93	88.10±3.29
41-50	97.47±1.74	88.92±3.03	91.49±0.99	71.26±22.80	90.37±2.79
51-60	96.93±1.88	85.97±13.61	92.25±4.08	91.55±27.26	89.00±4.08

Table 4.23 Comparison of SpO2 values of all age ranges while shivering for the dedicated techniques.

Age ranges	Compared techniques				
	PT[1]	CM[2]	DST[3]	ICA[4]	CFC[5]
	Summary SpO2 values in the unit of percentage (%)				
	Overall (Mean) ± Standard deviation				
Male subjects					
21-30	96.47±1.85	90.76±3.02	91.62±1.47	78.41±14.96	93.76±1.78
31-40	96.84±1.83	89.92±5.67	91.18±1.21	67.84±32.01	92.05±3.13
41-50	96.01±1.39	91.41±3.91	91.66±1.00	86.63±43.37	93.33±1.47
51-60	97.24±1.42	87.07±7.01	92.17±1.21	80.37±15.28	92.74±2.72
Female subjects					
21-30	96.61±1.63	85.09±11.33	92.22±1.72	69.50±29.33	89.75±4.69
31-40	97.80±1.16	84.46±9.96	92.21±1.71	64.54±85.45	90.52±3.12
41-50	97.68±1.57	87.90±7.50	91.62±1.10	85.34±17.71	92.07±2.85
51-60	96.77±1.85	83.73±18.36	92.13±0.87	72.60±22.44	90.14±3.88

Table 4.24 Comparison of SpO2 values of all age ranges while vertical moving for the dedicated techniques.

Age ranges	Compared techniques				
	PT[1]	CM[2]	DST[3]	ICA[4]	CFC[5]
	Summary SpO2 values in the unit of percentage (%)				
	Overall (Mean) ± Standard deviation				
Male subjects					
21-30	96.54±1.87	91.13±3.34	91.71±1.39	83.29±40.39	93.71±2.65
31-40	96.98±1.95	88.44±4.40	91.37±1.27	79.24±18.31	89.16±4.01
41-50	96.10±1.30	89.30±6.28	91.81±1.06	67.74±30.66	91.06±6.35
51-60	97.39±1.36	87.50±	92.26±1.22	85.73±12.05	90.96±4.01
Female subjects					
21-30	96.98±1.87	86.96±6.42	92.13±1.73	85.23±30.93	87.81±5.42
31-40	97.86±1.16	83.24±8.15	91.86±1.67	84.61±20.86	89.05±4.42
41-50	97.52±1.36	88.47±4.27	91.88±1.24	53.60±61.52	89.39±4.32
51-60	96.79±1.52	82.22±24.19	92.13±1.01	66.77±28.07	89.70±4.47

Table 4.25 Comparison of SpO2 values of all age ranges while waving for the dedicated techniques.

Age ranges	Compared techniques				
	PT[1]	CM[2]	DST[3]	ICA[4]	CFC[5]
	Summary SpO2 values in the unit of percentage (%)				
	Overall (Mean) ± Standard deviation				
Male subjects					
21-30	96.76±1.64	90.81±2.80	91.97±1.43	72.25±21.76	90.99±4.86
31-40	97.05±1.78	89.11±4.54	91.32±1.23	67.52±22.58	89.75±4.41
41-50	96.10±1.60	87.76±6.38	91.83±1.02	74.49±30.03	90.77±2.57
51-60	97.26±1.56	90.02±2.27	92.29±1.31	79.58±35.89	90.94±2.73
Female subjects					
21-30	96.81±1.84	87.13±10.07	92.27±1.55	81.52±17.06	90.36±4.13
31-40	97.72±1.07	90.00±7.75	92.18±1.69	56.68±29.67	90.47±3.82
41-50	97.86±1.21	88.13±3.53	92.09±1.31	76.48±27.90	88.46±3.23
51-60	96.70±1.84	85.74±12.26	92.37±1.06	68.42±28.81	88.98±3.52

To manifest the performances of the proposed LEDs-emitting technique and the other methods, the MAPE is applied to gauge their performances. The MAPE calculations for the methods of DST, ICA and CFC are accomplished in the same manner as the MAPE computation for the conventional LEDs-shining method. In MAPE calculation, the actual SpO2 value of each subject for age ranges uses the SpO2 value obtained by the conventional LEDs-shining method while resting (see Tables A.5-A.8). The MAPE results of all techniques, the proposed LEDs-driving technique and the conventional LEDs-shining method, and the methods of DST, ICA and CFC, are summed up in Tables 4.26-4.30. In Tables 4.26-4.30, each table is tabularly separated in each age group. In addition, the MAPE values for each participant of each approaches are gathered in Tables A.69-A.88. As the MAPE values for all techniques are numerous, for considering an overview, the overall MAPE value for each age range of each posture is applied. All overall MAPE values are recapitulated in Tables 4.31-4.35. Also, the MAPE values of the proposed LEDs-driving technique including the MAPE values of the conventional LEDs-emitting method uses the MAPE values that are already written in Tables 4.30-4.49. Each posture is contemplated as follows.

For the bending posture (see Table 4.31), all overall MAPE values of the proposed LEDs-driving technique are slightly inferior to the DST method for both genders of all age groups. The entire overall MAPE values of the presented LEDs-shining strategy, for all participants, are also highly lower than the ICA algorithm but moderately lesser than the CFC scheme. The overall MAPE values of the proposed LEDs-emitting solution vary between 0.46 and 0.98 while the DST method oscillates in

the range of 1.71 to 2.04. The ICA approach extremely sways between 28.29 and 59.87 and the CFC scheme fairly swings in the gap of 2.10 to 11.89.

Next consideration is the overall MAPE values of the horizontal moving pose, depicted in Table 4.32. The whole overall MAPE values of the proposed LEDs-driving technique are as similar as the bending posture marginally lesser than the DST method for both genders of all age groups. Besides, the other two methods (ICA, CFC) are greater than the presented LEDs-emitting approach moderately to highly for all age ranges as well as all sexes. The overall MAPE values of the proposed LEDs-emitting technique rises and falls between 0.71 and 1.35 while the DST method fluctuates in the range of 1.46 to 2.27. The ICA approach very rocks between 21.85 and 59.39 and the CFC scheme somewhat seesaws in the gap of 1.92 to 5.80.

After that, the overall MAPE values of the shivering posture (see Table 4.33) are contemplated. From the contemplation, all MAPE values of the proposed LEDs-driving solution are overall lower than the entire MAPE values of the method of DST on a small scale. Likewise, the whole MAPE values of the presented LEDs-emitting scheme are lesser than all MAPE values of the approaches of ICA and CFC significantly. The overall MAPE values of the proposed LEDs-emitting solution go up and down between 0.61 and 1.20 while the DST method occurs in the range of 1.61 to 2.07. The ICA approach greatly brandishes between 25.65 and 75.85 and the CFC scheme quite alters in the interval of 1.46 to 4.82.

Later, the overall MAPE values of the vertical moving pose (see Table 4.34) are in review. Like the first three postures, the entire MAPE values of the proposed technique are better than all overall MAPE values of the schemes of DST, ICA and CFC for both genders of all age groups. The overall MAPE values of the proposed LEDs-emitting strategy occur between 0.69 and 1.32 while the DST method fluctuates in the range of 1.61 to 2.07. The ICA approach notably swings between 25.65 and 75.85 and the CFC scheme relatively moves back and forth in the interval of 1.46 to 4.82.

Lastly, the waving posture (see Table 4.35) is inspected in terms of the overall MAPE values of all age ranges for both genders. From the inspection finds that the entire overall MAPE values of the proposed LEDs-driving technique are more thoroughly than the DST method. In the same manner, all overall MAPE values of the presented LEDs-emitting method are far better than the entire overall MAPE values of the solutions of ICA and CFC. The overall MAPE values of the proposed LEDs-emitting scheme oscillate between 0.71 and 1.18 while the DST method vibrates in the range of 1.51 to 2.14. The ICA approach considerably sways between 24.38 and 52.43 and the CFC scheme relatively deviates in the interval of 3.20 to 5.60.

After the considerations of all postures, the performances of the proposed LEDs-driving technique and the methods of DST, ICA and CFC including the

conventional LEDs-shining method can be concluded coherently. The conclusion can be drawn that the performance of the proposed LEDs-emitting solution is superior to the other four approaches for all postures of all volunteers of each age range. This is because the overall MAPE values of the proposed LEDs-driving strategy are inferior to the overall MAPE values of the rest methods. In addition, only two techniques which are the proposed LEDs-driving technique and the DST approach are found to better the SpO2 quality when compared with the traditional LEDs-shining method. Nonetheless, the scheme of ICA is found that not only the SpO2 quality is not improved but also worsened when compared with the conventional LEDs-emitting method. This is because the amplitudes of the mended red and IR PPG signals are distorted from their actual amplitudes. For the CFC concept, the SpO2 quality is inharmoniously bettered as only some red and IR PPG signals are applicable to the CFC method.

Currently, the DST method is highly reliable because this method is practically implemented into the MASIMO pulse oximeters and the MASIMO pulse oximeters are sold all over the world. The MASIMO Company is one of the key leading players in the pulse oximeter industry [60]. Also, the DST method is invented by the MASIMO Company. Therefore, the performance of the DST method is utilized as a criterion to evaluate whether the performance of the proposed LEDs-driving technique is good. Since the performance of the proposed LEDs-driving technique is superior to the performance of the DST method (see Tables 4.31-4.35), this suggests that the proposed LEDs-driving technique is good. With overall low MAPE values of the proposed LEDs-driving technique points out that the presented LEDs-emitting approach manifests high potentiality of solving the MA issue. Besides, the proposed LEDs-driving method is found to be applicable for all age ranges because the results of all involving participants of each age group are in the same way.

Nevertheless, bearing in mind, the proposed LEDs-driving technique only works well with the given volunteers. This cannot be the conclusion for other human races. The experiments with other kinds of human races are advised to further investigate in order to draw a complete conclusion.

Table 4.26 Summary of SpO2 percentage error of all age ranges while bending for the dedicated techniques.

Age ranges	Compared techniques				
	PT[1]	CM[2]	DST[3]	ICA[4]	CFC[5]
	Summary of SpO2 percentage error in the unit of percentage (%)				
	Overall (Mean) ± Standard deviation				
Male subjects					
21-30	0.68±0.58	3.22±2.69	1.76±1.18	32.38±19.23	2.10±1.80
31-40	0.84±0.69	5.59±4.93	1.99±1.18	38.62±40.81	7.10±8.75
41-50	0.98±1.17	4.31±3.02	1.71±0.97	33.92±20.47	2.19±1.05
51-60	0.64±0.41	4.44±2.84	1.73±1.14	50.44±32.19	4.89±10.02
Female subjects					
21-30	0.77±0.59	5.65±4.72	1.86±1.29	28.29±17.87	5.32±5.88
31-40	0.46±0.28	10.70±9.16	1.92±0.99	59.87±33.70	11.89±18.16
41-50	0.59±0.54	3.97±3.64	1.90±1.10	55.23±46.57	4.02±2.95
51-60	0.59±0.48	8.84±7.71	2.04±0.92	42.56±62.98	9.62±9.61

1 – PT refers to the proposed LEDs-driving technique, 2 – CM refers to the conventional LEDs-emitting method,
3 – DST stands for discrete saturation transform, 4 – ICA stands for independent component analysis,
5 – CFC stands for compression of Fourier coefficients.

Table 4.27 Summary of SpO2 percentage error of all age ranges while horizontal moving for the dedicated techniques.

Age ranges	Compared techniques				
	PT[1]	CM[2]	DST[3]	ICA[4]	CFC[5]
	Summary of SpO2 percentage error in the unit of percentage (%)				
	Overall (Mean) ± Standard deviation				
Male subjects					
21-30	0.76±0.64	2.92±2.59	2.09±0.91	45.72±40.57	1.92±2.11
31-40	0.98±1.05	5.31±5.70	2.09±0.99	21.85±12.61	5.55±5.90
41-50	0.84±1.01	4.53±4.85	1.96±1.47	48.30±51.01	2.70±2.44
51-60	0.71±0.60	3.93±2.81	1.46±1.00	59.39±52.54	4.81±3.91
Female subjects					
21-30	1.08±1.01	7.03±6.51	2.26±1.26	24.37±19.45	4.29±3.85
31-40	0.98±0.87	11.85±7.22	2.27±1.37	46.62±24.71	5.80±3.65
41-50	0.75±0.78	4.06±3.05	1.66±0.99	35.13±24.32	2.82±2.24
51-60	1.35±1.17	9.46±13.96	1.84±0.02	38.09±35.57	5.45±4.07

Table 4.28 Summary of SpO2 percentage error of all age ranges while shivering for the dedicated techniques.

Age ranges	Compared techniques				
	PT[1]	CM[2]	DST[3]	ICA[4]	CFC[5]
	Summary of SpO2 percentage error in the unit of percentage (%)				
	Overall (Mean) ± Standard deviation				
Male subjects					
21-30	0.82±0.70	3.17±2.86	1.80±1.24	33.59±24.16	1.46±0.97
31-40	1.20±0.65	4.36±5.72	1.96±1.08	32.44±30.40	2.75±2.41
41-50	0.61±0.65	3.24±3.75	1.70±0.78	49.48±48.04	1.65±1.37
51-60	0.77±0.46	7.24±7.14	1.61±1.08	52.14±33.30	2.16±2.90
Female subjects					
21-30	0.90±0.65	9.23±11.92	1.82±1.39	33.46±31.40	4.82±4.92
31-40	0.94±0.92	12.71±15.98	2.07±1.13	75.85±62.89	3.45±2.88
41-50	0.71±0.62	5.60±7.37	1.84±0.75	25.65±16.82	1.94±2.30
51-60	0.86±0.59	10.95±19.37	1.92±0.86	27.42±23.73	4.26±4.01

Table 4.29 Summary of SpO2 percentage error of all age ranges while vertical moving for the dedicated techniques.

Age ranges	Compared techniques				
	PT[1]	CM[2]	DST[3]	ICA[4]	CFC[5]
	Summary of SpO2 percentage error in the unit of percentage (%)				
	Overall (Mean) ± Standard deviation				
Male subjects					
21-30	0.82±0.63	3.06±3.14	1.78±1.15	46.25±42.36	2.20±2.44
31-40	1.16±0.67	5.31±4.45	1.85±0.88	28.27±15.44	4.97±3.17
41-50	0.69±0.63	5.26±6.39	1.54±0.96	38.28±30.64	4.32±6.67
51-60	0.94±0.53	6.53±7.98	1.51±0.99	34.90±26.75	4.27±3.50
Female subjects					
21-30	0.89±0.45	7.63±6.44	1.91±1.26	34.81±35.64	6.74±5.64
31-40	0.95±0.81	10.95±9.00	2.12±1.23	38.65±21.91	4.93±4.94
41-50	0.88±0.61	5.52±6.45	1.71±0.82	58.23±55.36	4.26±4.32
51-60	1.32±0.99	12.77±25.58	1.94±0.94	31.97±28.50	4.99±4.46

Table 4.30 Summary of SpO2 percentage error of all age ranges while waving for the dedicated techniques.

Age ranges	Compared techniques				
	PT[1]	CM[2]	DST[3]	ICA[4]	CFC[5]
	Summary of SpO2 percentage error in the unit of percentage (%)				
	Overall (Mean) ± Standard deviation				
Male subjects					
21-30	0.92±0.63	2.99±2.89	1.55±0.93	30.15±22.32	3.30±4.90
31-40	1.18±0.64	4.48±5.03	1.95±0.84	38.86±29.30	4.48±4.10
41-50	0.71±0.92	6.14±7.03	1.51±1.01	31.89±29.34	3.22±2.34
51-60	0.77±0.48	3.84±2.23	1.57±0.96	40.22±30.52	3.20±2.55
Female subjects					
21-30	0.76±0.49	7.58±10.39	1.64±1.32	24.38±15.89	4.42±4.23
31-40	0.96±0.86	11.40±15.52	2.14±0.98	52.43±35.52	3.67±3.08
41-50	0.73±0.40	5.08±3.45	1.66±0.92	39.08±22.95	5.14±2.58
51-60	0.86±0.63	9.02±12.70	1.68±0.97	37.62±25.87	5.60±3.42

Table 4.31 Recapitulation of SpO2 percentage error for all age groups while bending for the dedicated techniques.

Age ranges	Compared techniques									
	PT[1]		CM[2]		DST[3]		ICA[4]		CFC[5]	
	M	F	M	F	M	F	M	F	M	F
Overview of MAPE values in the unit of percentage (%)										
21-30	0.68	0.77	3.22	5.65	1.76	1.86	32.38	28.29	2.10	5.32
31-40	0.84	0.46	5.59	10.70	1.99	1.92	38.62	59.87	7.10	11.89
41-50	0.98	0.59	4.31	3.97	1.71	1.90	33.92	55.23	2.19	4.02
51-60	0.64	0.59	4.44	8.84	1.73	2.04	50.44	42.56	4.89	9.62
Overall (Mean) ± Standard deviation	0.79± 0.16	0.60± 0.13	4.39± 0.97	7.29± 3.04	1.80± 0.13	1.93± 0.08	38.84± 8.18	46.49± 14.17	4.07± 2.40	7.71± 3.67

1 – PT refers to the proposed LEDs-driving technique, 2 – CM refers to the conventional LEDs-emitting method,
3 – DST stands for discrete saturation transform, 4 – ICA stands for independent component analysis,
5 – CFC stands for compression of Fourier coefficients,
M – Male, F – Female.

Table 4.32 Recapitulation of SpO2 percentage error for all age groups while horizontal moving for the dedicated techniques.

Age ranges	Compared techniques									
	PT[1]		CM[2]		DST[3]		ICA[4]		CFC[5]	
	M	F	M	F	M	F	M	F	M	F
Overview of MAPE values in the unit of percentage (%)										
21-30	0.76	1.08	2.51	7.03	2.09	2.26	45.72	24.37	1.92	4.29
31-40	0.98	0.98	5.31	11.85	2.09	2.27	21.85	46.62	5.55	5.80
41-50	0.84	0.75	4.53	4.06	1.96	1.66	48.30	35.13	2.70	2.82
51-60	0.71	1.35	3.93	9.46	1.46	1.84	59.39	38.09	4.81	5.45
Overall (Mean) ± Standard deviation	0.82± 0.12	1.04± 0.25	4.07± 1.18	8.10± 3.34	1.90± 0.30	2.01± 0.31	43.82± 15.80	36.05± 9.19	3.75± 1.71	4.59± 1.34

Table 4.33 Recapitulation of SpO2 percentage error for all age groups while shivering for the dedicated techniques.

Age ranges	Compared techniques									
	PT[1]		CM[2]		DST[3]		ICA[4]		CFC[5]	
	M	F	M	F	M	F	M	F	M	F
Overview of MAPE values in the unit of percentage (%)										
21-30	0.82	0.90	3.17	9.23	1.80	1.82	33.59	33.48	1.46	4.82
31-40	1.20	0.94	4.36	12.71	1.96	2.07	64.54	75.85	2.75	3.45
41-50	0.61	0.71	3.24	5.60	1.70	1.84	49.48	25.65	1.65	1.94
51-60	0.77	0.86	7.24	10.95	1.61	1.92	52.14	27.42	2.16	4.26
Overall (Mean) ± Standard deviation	0.85± 0.25	0.85± 0.10	4.50± 1.90	9.62± 3.03	1.77± 0.15	1.91± 0.11	49.94± 12.72	40.60± 23.74	2.01± 0.58	3.62± 1.25

Table 4.34 Recapitulation of SpO2 percentage error for all age groups while vertical moving for the dedicated techniques.

Age ranges	Compared techniques									
	PT[1]		CM[2]		DST[3]		ICA[4]		CFC[5]	
	M	F	M	F	M	F	M	F	M	F
Overview of MAPE values in the unit of percentage (%)										
21-30	0.82	0.89	3.06	7.63	1.78	1.91	46.25	34.81	2.20	6.74
31-40	1.16	0.95	5.31	10.95	1.85	2.12	28.27	38.65	4.97	4.93
41-50	0.69	0.88	5.26	5.52	1.54	1.71	38.28	58.23	4.32	4.26
51-60	0.94	1.32	6.53	12.77	1.51	1.94	34.90	31.97	4.27	4.99
Overall (Mean) ± Standard deviation	0.90± 0.20	1.01± 0.21	5.04± 1.44	9.22± 3.26	1.67± 0.17	1.92± 0.17	36.93± 7.48	40.92± 11.86	3.94± 1.20	5.23± 1.06

Table 4.35 Recapitulation of SpO2 percentage error for all age groups while waving for the dedicated techniques.

Age ranges	Compared techniques									
	PT[1]		CM[2]		DST[3]		ICA[4]		CFC[5]	
	M	F	M	F	M	F	M	F	M	F
Overview of MAPE values in the unit of percentage (%)										
21-30	0.92	0.76	2.99	7.58	1.55	1.64	30.15	24.38	3.30	4.42
31-40	1.18	0.96	4.48	11.40	1.95	2.14	38.86	52.43	4.48	3.67
41-50	0.71	0.73	6.14	5.08	1.51	1.66	31.89	39.08	3.22	5.14
51-60	0.77	0.86	3.84	9.02	1.57	1.68	40.22	37.62	3.20	5.60
Overall (Mean) ± Standard deviation	0.90± 0.21	0.83± 0.10	4.36± 1.33	8.27± 2.65	1.65± 0.20	1.78± 0.24	35.28± 5.00	38.38± 11.47	3.55± 0.62	4.71± 0.85

CHAPTER 5

Conclusions

A SpO2 value provided by a pulse oximeter is inherently unreliable when any motions induced by a human person take place. The SpO2 value is dependent on a pair of proper red and IR PPG signals. The red and IR PPG signals are the leftover light intensities of red and IR lights, emitted by red and IR LEDs, after being absorbed by human absorbing organs, respectively. However, both red and IR PPG signals are intrinsically contaminated by an MA signal generated by any human movement. To improve the SpO2 value, in this thesis, a novel LEDs-driving technique substituted for a conventional LEDs-emitting structure in the pulse oximeter is proposed. In developing the new LEDs-shining strategy, various contemporary methods relating to solving the MA issue as well as the MA frequency components are reviewed. From the review reveals that the reviewed methods attempt to mend the corrupted red and IR signals. The review also finds that the MA frequency components overlap with the PPG frequency components. In this proposition, each LED is driven by a carrier sinusoidal signal having a distinct frequency to separate the PPG frequency components from the MA frequency components. The separation of PPG frequency components from the MA frequency components by the proposed scheme is accomplished through a frequency translation technique using a structure of amplitude modulation (AM). As a consequence of practicing the AM concept, a traditional PPG mathematical expression is developed to satisfy the AM model, yielding the AM-based PPG mathematical statement. By utilizing the presented LEDs-driving approach prevents the PPG signals from being combined with the MA signal rather than mending the corrupted PPG signals like the review methods do. Besides, implementing the proposed LEDs-emitting technique successfully separates the PPG frequency components from the MA frequency components. With this proposed strategy, the PPG signals are not intertwined with the MA signal.

To verify that the PPG signals obtained by the presented approach maintain all significant PPG morphologies, the Pearson's correlation coefficient (PCC) and the mean square percentage error (MSPE) are applied. The PCC and MSPE results of comparing the PPG morphological similarity while at rest between the proposed technique and the conventional method are consistently in the same way. The PCC results are overall greater than 0.9 for all volunteers while the MSPE results are overall lower than 1%. With the PCC and MSPE results reveals that the PPG signals of the presented approach are highly similar to the PPG signals of the conventional method. This indicates that

the proposed technique does not distort and keeps all significant features of the PPG morphologies, and also suggests that the proposed technique is practically utilizable.

To manifest the effectiveness of the proposed technique that the PPG signals are separated from the MA signal, five common postures are experimented. These five everyday poses are a bending posture, a horizontal moving posture, a shivering posture, a vertical moving posture and a waving posture. In experimental conducting these five regular postures, the conventional method is also performed for the reason of exhibiting performance enhancement of the presented approach. The results of five moving postures emerge coherently that the red and IR PPG signals are not mingled with the MA signal because their proper PPG waveforms are yet existed. This is also ascertained by considering the SpO2 results. The SpO2 values calculated from the red and IR PPG signals of the proposed technique have very low MAPE values for all experimented postures as well as both genders. The MAPE values of the presented structure vary from 0.6% to 1.35% while the MAPE values of the conventional model are somewhat higher than the proposed technique does. The MAPE values of the traditional method are between 2.5% and 13%. From the experiments of the five common postures affirms that the proposed technique is effective and practical. In addition, the experimental results of all moving poses show that the proposed can be practiced with technique both genders for all age ranges. This suggests that age and sex do not affect the performance of the presented scheme.

As the proposed technique employs the AM structure, in this thesis, the amplitude of the generated carrier sinusoidal signal is studied by changing light intensity falling upon the absorbing medium. The light intensity is changed by adjusting the root mean square (RMS) current fed to the LED. In this study, three RMS current values (14.71 mA, 14.49 mA and 14.26 mA) are experimented to verify whether the light intensity has the influence on the SpO2 quality. Each voltage is performed for all moving postures. The results of this study disclose that change of light intensity does not show any impact on the SpO2 quality for all postures of both genders. This is because all SpO2 values at different voltages of each participant are not much different but, actually, they are fairly similar. This study points out that there is no significant influence on change of light intensity.

To evaluate that the proposed technique is competitive in the research field of resolving the MA problem in the pulse oximeter context, the performances of three well-known methods are compared. The performance comparison exposes that the presented approach is slightly superior to the DST scheme for all postures of both genders at all age ranges. Likewise, the proposed technique is significantly better than the methods of ICA and CFC. The overview MAPE values obtained by the presented strategy are roughly from 0.45% to 1.35% while the overview MAPE values provided

by the DST method are between 1.45% and 2.25%. For the approach of ICA, the overview MAPE values vary in the range of 21.00% to 76.00%. The last method, CFC, produces the overview MAPE values between 1.45% and 12.00%. With being better than all three given methods, the proposed technique can be concluded to be competitive.

Bearing in mind, the DST method is the most reliable among other well-known methods in the pulse oximeter industry these days. Since the presented strategy is superior to the DST approach, the proposed technique can be therefore implied that the presented scheme is also reliable. Having reliability of the proposed technique for the given volunteers is suggested to be further investigated with different human races to increase more reliability before implementing in a practical device.

References

[1] Lu G., Yang F., Taylor J. A. and Stein J. F. "A comparison of photoplethysmography and ECG recording to analyze heart rate variability in healthy subjects." **Journal of Medical Engineering & Technology,** vol. 33, no. 10, Nov. 2009. pp. 634-641

[2] Vandenberk T., Stans, J., Mortelmans, C., Haelst, R. V., Schelvergem V. G., Pelckmans C., Smeets C. J., Lanssens D., DeCanniere H., Storms V., Thijs I. M., Vaes B. and Vandervoort P. M. "Clinical validation of heart rate apps: mixed-methods evaluation study." **Journal or Medical Internet-Research (JMIR) mHealth and uHealth,** vol. 5, no. 8, Aug. 2017.

[3] Ye Y., Cheng Y., He W., Hou M. and Zhang Z. "Combining nonlinear adaptive–And signal decomposition for motion artifact removal in wearable photo–plethysmography." **IEEE Sensors Journal**, vol. 16, no. 19, Oct. 2016. pp. 7133-7141

[4] Karna V. R. and Kumar N. "Determination of absolute heart beat from photo–plethysmographic signals in the presence of motion artifacts." **2018 2nd International Conference on Advances in Electronics, Computers and Communications (ICAECC).** Bangalore, India, Oct., 2018.

[5] Shi P., Hu S. and Zhu Y. "A preliminary attempt to understand compatibility of photoplethysmographic pulse rate variability with electrocardiogramic heart rate variability." **Journal of Medical and Biological Engineering,** vol. 28, no. 4, Sep. 2008. pp. 173–180

[6] Rohan J. W., Yokochi C. and Lutjen-Drecoll E. **Color Atlas of Anatomy: A Photographic Study of the Human Body.** Stuttgart : Schattauer. 2011.

[7] Thompson J. C. **Netter's Concise Orthopaedic Anatomy.** Beijing : Elsevier. 2015.

[8] Wieben O. "Light absorbance in pulse oximetry." **Design of Pulse Oximeters.** New York : Taylor & Francis. 1997.

[9] Rhee S., Yang B. H. and Asada K. B. "Artifact-resistant power-efficient design of finger-ring plethysmographic sensors." **IEEE Transactions on Biomedical Engineering,** vol. 48, no. 7, July 2001. pp. 795-805

[10] Jubran A. "Pulse oximetry." **Intensive Care Medicine,** vol. 30, no. 11, July 2004. pp. 2017-2020

[11] Kline J. A., Hernandez-Nino J., Newgard C. D., Cowles D. N., Jackson R. E. and Courtney D. M. "Use of pulse oximetry to predict in-hospital complications in normotensive patients with pulmonary embolism." **The American Journal of Medicine,** vol. 115, no. 3, Aug. 2003. pp. 203-208

[12] Parameswaran G. I., Brand K. and Dolan J. “Pulse oximetry as potential screening tool for lower extremity arterial disease in asymptomatic patients with diabetes mellitus.” **Archives Internal Medicine,** vol. 165, no. 4, Feb. 2005. pp. 442-446

[13] Bakr A. F. and Habib H. S. “Combining pulse oximetry and clinical examination in screening for congenital heart disease.” **Pediatric Cardiology,** vol. 26, no. 6, Dec. 2005. pp. 832-835

[14] Masip J., Gaya M., Paez J., Betbese A., Vecilla F., Manresa R. and Ruiz P. “Pulse oximetry in the diagnosis of acute heart failure.” **Revista Espanola De Cardiologia,** vol. 65, no. 10, Oct. 2012. pp. 879-884

[15] Shah S. A., Velardo C., Gibson O. J., Rutter H., Farmer A. and Tarassenko L. “Personalized alerts for patients with COPD using pulse oximetry and symptom scores.” **2014 36th Annual International Conference of the IEEE Engineering in Medicine and Biology Society.** Chicago, USA, Nov., 2014. pp. 3164-3167

[16] Chen H. W., Weng L. C., Wang T. M. and Ng K. F. “Potential use of pulse oximetry for the diagnosis of testicular torsion.” **JAMA Pediatrics,** vol. 168, no. 6, June 2014. pp. 578-579

[17] Bargrizan M., Ashari M. A., Ahmadi M. and Ramezani J. “The use of pulse oximetry in evaluation of pulp vitality in immature permanent teeth.” **Dental Traumatology,** vol. 32, no. 1, Feb. 2016. pp. 43-47

[18] Relente A. R. and Sison G. “Characterization and adaptive filtering of motion artifacts in pulse oximetry using accelerometers.” **Proceedings of the 2nd Joint EMBS/BMES Conference.** Houston, USA, Oct., 2002. pp. 1769-1770

[19] Chan K. W. and Zhang Y. T. “Adaptive reduction of motion artifact from photoplethysmographic recordings using a variable step-size LMS filter.” **2002 IEEE Sensors.** Orlando, USA, June, 2002. pp. 1343-1346

[20] Asada H. H., Shaltis P., Reisner A., Rhee S. and Hutchinson R. C. “Mobile monitoring with wearable photoplethysmographic biosensors.” **IEEE Engineering in Medicine and Biology Magazine,** vol. 22, no. 3, May 2003. pp. 28-40

[21] Foo J. Y. A. and Wilson S. J. “A computational system to optimize noise rejection in photoplethysmography signals during motion or poor perfusion states.” **Medical & Biological Engineering & Computing,** vol. 44, no. 1, Jan. 2006. pp. 140-145

[22] Wijshoff R. W. C. G. R., Mischi M. and Aarts R. M. “Reduction of periodic motion artifacts in photoplethysmography.” **IEEE Transactions on Biomedical Engineering,** vol. 64, no. 1, Jan. 2017. pp. 196-206

[23] Jiang Y. “Two-pronged motion artifact reduction for wearable photoplethysmographic biosensors.” **IEEE Sensors Letters**, vol. 2, no. 4, Dec. 2018.

[24] Coetzee F. M. and Elghazzawi Z. “Noise-resistant pulse oximetry using a synthetic reference signal.” **IEEE Transactions on Biomedical Engineering,** vol. 47, no. 8, Aug. 2000. pp. 1018-1026

[25] Diab M. K., Kiani-Azarbayjany E. and Weber W. M. **“Signal processing apparatus.”** U.S. patent no. US008 942 777B2, Jan. 2015.

[26] Peng F., Zhang Z., Gou X., Liu H. and Wang W. “Motion artifact removal from photoplethysmographic signals by combining temporally constrained independent component analysis and adaptive filter.” **Biomedical Engineering Online,** vol. 13, no. 50, 2014.

[27] Ram R. M., Madhav K. V., Krishna E. H., Komalla N. R. and Reddy K. A. “A novel approach for motion artifact reduction in PPG signals based on AS-LMS adaptive filter.” **IEEE Transactions on Instrumentation and Measurement,** vol. 61, no. 5, May 2012. pp. 1445-1457

[28] Yousefi R., Nourani M., Ostadabbas S. and Panahi I. “A motion-tolerant adaptive algorithm for wearable photoplethysmographic biosensor.” **IEEE Journal of Biomedical and Health Informatics,** vol. 18, no. 2, Mar. 2014. pp. 670-681

[29] Luke A., Shaji S. and Menon K. A. U. “Motion artifact removal and feature extraction from PPG signals using efficient signal processing algorithms.” **2018 International Conference on Advances in Computing, Communications and Informatics (ICACCI).** Bangalore, India, Sep., 2018. pp. 624-630

[30] Ram R. M., Sivani K. and Reddy K. A. “Utilization of adaptive-coefficient estimation method for motion artifacts reduction from photoplethysmographic signals.” **2016 International Conference on Wireless Communications, Signal Processing and Networking (WiSPNET).** Chennai, India, Mar., 2016. pp. 819-822

[31] Lee J., Jung W., Kang I., Kim Y. and Lee G. “Design of filter to reject motion artifact of pulse oximetry.” **Computer Standards & Interfaces,** vol. 26, no. 3, May 2004. pp. 241-249

[32] Reddy K. A., George B. and Kumar V. J. “Use of Fourier series analysis for motion artifact reduction and data compression of photoplethysmographic signals.” **IEEE Transactions on Instrumentation and Measurement,** vol. 58, no. 5, May 2009. pp. 1706-1711

[33] Li S., Jiang S., Jiang S., Wu J., Xiong W. and Diao S. “A hybrid wavelet-based method for the peak detection of photoplethysmography signals.” **Computational Mathematical Methods in Medicine,** Nov. 2017.

[34] Hanyu S. and Xiaohui C. “Motion artifact detection and reduction in PPG signals based on statistics analysis.” **2017 29th Chinese Control and Decision Conference (CCDC).** Chongqing, China, July, 2017. pp. 3114-3119

[35] Kim B. S. and Yoo S. K. “Motion artifact reduction in photoplethysmography using independent component analysis.” **IEEE Transactions on Biomedical Engineering,** vol. 53, no. 3, Mar. 2006. pp. 566-568

[36] Chen L. Y. and Lu C. J. “An improved independent component analysis algorithm based on artificial immune system.” **International Journal of Machine Learning and Computing,** vol. 3, no. 1, Feb. 2013. pp. 93-97

[37] Gastel M. v., Stuijk S. and Haan G. d. “New principle for measuring arterial blood oxygenation, enabling motion-robust remote monitoring.” **Scientific Reports,** vol. 6, Dec. 2016.

[38] Fan F., Yan Y., Tang Y. and Zhang H. “A motion-tolerant approach for monitoring SpO2 and heart rate using photoplethysmography signal with dual frame length processing and multi-classifier fusion.” **Computer in Biology and Medicine,** vol. 91, no. 12, Dec. 2017. pp. 291-305

[39] Yan Y. S. and Zhang Y. T. “An efficient motion-resistant method for wearable pulse oximeter.” **IEEE Transactions on Information Technology in Biomedicine,** vol. 12, no. 3, May 2008. pp. 399-405

[40] Salehizadeh S. M. A., Dao D. K., Chong J. W., McManus D., Darling C., Mendelson Y. and Chon K. H. “Photoplethysmograph signal reconstruction based on a novel motion artifact detection-reduction approach. Part II: Motion and noise artifact removal.” **Annals of Biomedical Engineering,** vol. 42, no. 11, May 2014. pp. 2251-2263

[41] Fan F., Yan Y., Zhao K., Long F. and Zhang H. “Estimating SpO2 via time-efficient high resolution harmonics analysis and maximum likelihood tracking.” **IEEE Journal of Biomedical and Health Informatics,** vol. 22, no. 4, Nov. 2017. pp. 1075-1086

[42] Jang I. H., Yeom H. G. and Sim K. B. “Ring sensor and heart rate monitoring system for sensor network applications.” **Electronics Letters,** vol. 44, no. 24, Nov. 2008. pp. 1393-1394

[43] Sukor J. A., Mohktar M. S., Redmond S. J. and Lovell N. H. “Signal quality measures on pulse oximetry and blood pressure signals acquired from self-Measurement in a home environment.” **IEEE Journal of Biomedical and Health Informatics,** vol. 19, no. 1, Jan. 2015. pp. 102-108

[44] Lee H., Ko H., Jeong C. and Lee J. “Wearable photoplethysmographic sensor based on different LED light intensities.” **IEEE Sensors Journal,** vol. 17, no. 3, Feb. 2017. pp. 587-588

[45] Bonetti P. O., Pumper G. M., Higano S. T., Holmes D. R., Kuvin J. T. and Lerman A. "Noninvasive identification of patients with coronary atherosclerosis by assessment of digital reactive hyperemia." **Journal of the American College of Cardiology,** vol. 44, no. 11, Dec. 2004. pp. 2137-2141

[46] Rawlani S. and Rawlani S. **Textbook of General Anatomy.** 2nd Edition. New Delhi : JP Medical Ltd. 2013.

[47] Ziemer R. E. and Tranter W. H. **Principles of Communications.** 6th Edition. New Jersey : John Wiley & Sons. 2009.

[48] Haxha S. and Jhoja J. "Optical based noninvasive glucose monitoring sensor prototype." **IEEE Photonics Journal,** vol. 8, no. 6, Dec. 2016.

[49] Carter B. and Brown T. R. **"Handbook of Operational Amplifier Applications."** Texas Instruments, Texas, Application report, SBOA092B, Sep. 2016.

[50] Analog Devices. "**Low Cost Low Power Instrumentation Amplifier.**" Analog Devices, Massachusetts, AD620 datasheet, July 2003 [revised July 2011].

[51] Platt C. and Jansson F. **Encyclopedia of Electronic Components Volume 2: LEDs, LCDs, Audio, Thyristors, Digital Logic, and Amplification.** 1st Edition. California : Maker Media, Inc. 2014.

[52] Razavi B. "The transimpedance amplifier." **IEEE Solid-state Circuits Magazine,** vol. 11, no. 1, Feb. 2019. pp. 10-13,97

[53] Deborah P. and Rumsey J. **Statistics for Dummies.** 2nd Edition. New Jersey : Wiley. 2011.

[54] Botchkarev A. "A new typology design of performance metrics to measure errors in machine learning regression algorithms." **Interdisciplinary Journal of Information, Knowledge, and Management,** vol. 14, 2019. pp. 45-76

[55] Breakey D. and Meskell C. "Comparison of metrics for the evaluation of similarity in acoustic pressure signals." **Journal of Sound and Vibration,** vol. 332, no. 15, July 2013. pp. 3605-3609

[56] Rao M. M. and Ram R. R. "Photoplethysmography: a noninvasive tool for possible subtle energy monitoring during yogic practices." **Subtle Energies & Energy Medicine,** vol. 17, no. 2, 2006. pp. 163-179

[57] Sinchai S., Kainan P., Wardkein P. and Koseeyaporn J. "A photoplethysmographic signal isolated from an additive motion artifact by frequency translation." **IEEE Transactions of Biomedical Circuits and Systems,** vol. 12, no. 4, Aug. 2018. pp. 904-917

[58] Koseeyaporn J., Sinchai S., Tuwanut P. and Wardkein P. "Influence of light intensity on a motion artifact signal in a photoplethysmographic signal." **International Conference on Intelligent Informatics and Biomedical (ICIIBMS).** Bangkok, Thailand, Oct., 2018. pp. 8-14

[59] Koseeyaporn J., Sinchai S. and Wardkein P. “Performance of frequency translation in separating a photoplethysmographic signal from an additive motion artifact.” **2019 IEEE 4th International Conference on Computer and Communication Systems (ICCCS).** Singapore, Singapore, Feb., 2019. pp. 512-516

[60] Research and Markets. “Global pulse oximetry market 2019-2025: Masimo, Medtronic, Philips, GE Healthcare, Smith Medical, and Nihon Kohden dominates sales revenues.” **CISION PR Newswire.** [Online]. Available : https://www.prnewswire.com/news-releases/global-pulse-oximetry-market-2019-2025-masimo-medtronic-philips-ge-healthcare-smith-medical-and-nihon-kohden-dominates-sales-revenues-300796512.html. [Accessed Nov. 18, 2019].

Appendix A

Detailed Results

Table A.1 Summary of PPG morphological similarity of the age range of 21 to 30.

Male subjects						
Subj[1] no.	PCCR[2] (Time domain)	PCCIR[3] (Time domain)	PCCR[2] (Frequency domain)	PCCIR[3] (Frequency domain)	MSPER[4] (Time domain)	MSPEIR[5] (Time domain)
	Average ± Standard deviation					
08	0.972±0.012	0.986±0.004	0.990±0.005	0.996±0.001	0.131±0.037	0.054±0.014
18	0.944±0.010	0.972±0.006	0.967±0.006	0.985±0.006	0.424±0.065	0.238±0.041
36	0.982±0.014	0.989±0.004	0.993±0.005	0.996±0.002	0.093±0.049	0.071±0.029
38	0.974±0.010	0.988±0.005	0.987±0.005	0.994±0.002	0.165±0.052	0.105±0.036
40	0.934±0.017	0.967±0.009	0.966±0.016	0.982±0.006	0.521±0.197	0.306±0.107
51	0.936±0.016	0.956±0.012	0.967±0.009	0.977±0.006	0.453±0.163	0.315±0.129
57	0.961±0.014	0.980±0.004	0.982±0.013	0.991±0.005	0.203±0.043	0.127±0.022
58	0.935±0.003	0.970±0.004	0.966±0.008	0.984±0.004	0.411±0.060	0.170±0.041
59	0.970±0.017	0.985±0.004	0.985±0.011	0.991±0.005	0.128±0.055	0.085±0.046
60	0.964±0.015	0.984±0.005	0.991±0.006	0.994±0.001	0.232±0.105	0.121±0.043
61	0.936±0.013	0.958±0.006	0.976±0.006	0.985±0.003	0.291±0.189	0.182±0.094
62	0.932±0.012	0.963±0.007	0.962±0.008	0.980±0.005	0.584±0.078	0.262±0.054
63	0.942±0.020	0.964±0.011	0.981±0.010	0.986±0.007	0.347±0.151	0.239±0.093
64	0.931±0.007	0.955±0.004	0.978±0.005	0.984±0.004	0.518±0.104	0.347±0.092
Overall (Mean)	0.951±0.019	0.973±0.012	0.978±0.011	0.988±0.006	0.322±0.166	0.187±0.097
Female subjects						
Subj[1] No.	PCCR[2] (Time domain)	PCCIR[3] (Time domain)	PCCR[2] (Frequency domain)	PCCIR[3] (Frequency domain)	MSPER[4] (Time domain)	MSPEIR[5] (Time domain)
	Average ± Standard deviation					
05	0.995±0.003	0.994±0.002	0.998±0.001	0.997±0.001	0.008±0.004	0.008±0.001
06	0.992±0.009	0.997±0.002	0.997±0.002	0.999±0.001	0.019±0.016	0.007±0.005
09	0.982±0.010	0.991±0.002	0.992±0.004	0.995±0.003	0.048±0.013	0.025±0.011
11	0.984±0.012	0.994±0.002	0.992±0.004	0.997±0.001	0.058±0.035	0.026±0.013
17	0.955±0.006	0.974±0.004	0.978±0.005	0.989±0.003	0.334±0.100	0.152±0.036
27	0.993±0.012	0.994±0.001	0.997±0.003	0.997±0.001	0.005±0.002	0.018±0.006
28	0.958±0.019	0.975±0.008	0.983±0.005	0.989±0.003	0.280±0.147	0.149±0.075
29	0.989±0.013	0.988±0.014	0.995±0.006	0.995±0.009	0.008±0.009	0.012±0.006
37	0.993±0.012	0.994±0.001	0.998±0.004	0.998±0.001	0.006±0.001	0.018±0.003
41	0.983±0.014	0.991±0.007	0.991±0.008	0.995±0.005	0.046±0.030	0.026±0.022
42	0.991±0.012	0.997±0.000	0.997±0.004	0.999±0.001	0.025±0.004	0.017±0.004
52	0.975±0.024	0.987±0.010	0.990±0.009	0.994±0.005	0.128±0.099	0.080±0.068
Overall (Mean)	0.982±0.013	0.990±0.008	0.992±0.006	0.995±0.003	0.080±0.112	0.045±0.053

1 – Subject, 2 – Pearson correlation coefficients (PCC) of retrieved red PPG signals against conventional red PPG signals,

3 – Pearson correlation coefficients (PCC) of recovered IR PPG signals against conventional IR PPG signals,

4 – Mean square percentage error (MSPE) between retrieved red PPG signals and traditional red PPG signals,

5 – Mean square percentage error (MSPE) between recovered IR PPG signals and traditional IR PPG signals.

Table A.2 Summary of PPG morphological similarity of the age range of 31 to 40.

Male subjects						
Subj[1] no.	PCCR[2] (Time domain)	PCCIR[3] (Time domain)	PCCR[2] (Frequency domain)	PCCIR[3] (Frequency domain)	MSPER[4] (Time domain)	MSPEIR[5] (Time domain)
	Average ± Standard deviation					
03	0.967±0.022	0.986±0.007	0.982±0.020	0.993±0.006	0.085±0.032	0.025±0.010
12	0.982±0.007	0.992±0.002	0.991±0.004	0.996±0.003	0.092±0.048	0.061±0.027
24	0.993±0.011	0.998±0.002	0.998±0.004	0.999±0.000	0.007±0.003	0.005±0.001
34	0.946±0.038	0.959±0.035	0.965±0.024	0.974±0.018	0.396±0.372	0.304±0.277
46	0.975±0.012	0.984±0.003	0.990±0.003	0.993±0.004	0.132±0.043	0.093±0.028
47	0.990±0.014	0.996±0.002	0.997±0.005	0.999±0.001	0.017±0.005	0.017±0.005
55	0.898±0.017	0.937±0.014	0.936±0.015	0.963±0.010	0.812±0.243	0.466±0.156
67	0.955±0.022	0.976±0.013	0.984±0.009	0.993±0.004	0.233±0.165	0.123±0.057
69	0.941±0.023	0.967±0.017	0.976±0.005	0.987±0.003	0.366±0.160	0.177±0.074
Overall (Mean)	0.961±0.030	0.977±0.020	0.980±0.019	0.988±0.012	0.238±0.257	0.141±0.154
Female subjects						
Subj[1] no.	PCCR[2] (Time domain)	PCCIR[3] (Time domain)	PCCR[2] (Frequency domain)	PCCIR[3] (Frequency domain)	MSPER[4] (Time domain)	MSPEIR[5] (Time domain)
	Average ± Standard deviation					
07	0.974±0.009	0.985±0.003	0.990±0.005	0.994±0.004	0.145±0.077	0.077±0.030
15	0.993±0.013	0.999±0.001	0.998±0.004	0.999±0.000	0.007±0.003	0.003±0.002
19	0.972±0.010	0.985±0.002	0.986±0.009	0.992±0.004	0.172±0.071	0.071±0.026
32	0.954±0.017	0.975±0.006	0.981±0.009	0.988±0.002	0.250±0.135	0.135±0.044
48	0.983±0.009	0.995±0.002	0.992±0.004	0.998±0.001	0.069±0.028	0.028±0.016
54	0.992±0.012	0.998±0.001	0.997±0.004	0.999±0.000	0.016±0.012	0.012±0.003
56	0.980±0.008	0.991±0.002	0.992±0.004	0.996±0.002	0.063±0.030	0.030±0.009
73	0.990±0.011	0.997±0.002	0.996±0.004	0.999±0.001	0.020±0.008	0.008±0.003
Overall (Mean)	0.980±0.013	0.991±0.008	0.991±0.006	0.996±0.004	0.093±0.088	0.046±0.046

Table A.3 Summary of PPG morphological similarity of the age range of 41 to 50.

Male subjects						
Subj[1] no.	PCCR[2] (Time domain)	PCCIR[3] (Time domain)	PCCR[2] (Frequency domain)	PCCIR[3] (Frequency domain)	MSPER[4] (Time domain)	MSPEIR[5] (Time domain)
	Average ± Standard deviation					
16	0.930±0.035	0.975±0.008	0.956±0.034	0.985±0.007	0.416±0.147	0.139±0.020
20	0.946±0.016	0.975±0.003	0.976±0.009	0.984±0.004	0.374±0.224	0.150±0.037
30	0.912±0.005	0.950±0.003	0.945±0.009	0.971±0.007	0.639±0.088	0.393±0.032
33	0.979±0.017	0.988±0.007	0.993±0.007	0.995±0.003	0.090±0.078	0.069±0.040
35	0.957±0.015	0.979±0.007	0.977±0.012	0.990±0.006	0.271±0.152	0.151±0.079
49	0.929±0.025	0.955±0.017	0.963±0.027	0.977±0.016	0.402±0.111	0.250±0.046
66	0.984±0.017	0.992±0.004	0.994±0.008	0.996±0.003	0.047±0.013	0.042±0.007
71	0.945±0.017	0.971±0.005	0.971±0.009	0.985±0.006	0.357±0.094	0.213±0.042
Overall (Mean)	0.948±0.025	0.973±0.015	0.972±0.017	0.985±0.008	0.325±0.190	0.176±0.111
Female subjects						
Subj[1] no.	PCCR[2] (Time domain)	PCCIR[3] (Time domain)	PCCR[2] (Frequency domain)	PCCIR[3] (Frequency domain)	MSPER[4] (Time domain)	MSPEIR[5] (Time domain)
	Average ± Standard deviation					
01	0.973±0.007	0.993±0.002	0.984±0.006	0.996±0.001	0.130±0.030	0.016±0.012
10	0.947±0.008	0.966±0.007	0.976±0.004	0.984±0.003	0.334±0.075	0.218±0.077
25	0.952±0.007	0.971±0.002	0.974±0.007	0.983±0.004	0.197±0.029	0.098±0.022
43	0.994±0.012	0.999±0.000	0.998±0.004	0.999±0.000	0.007±0.005	0.004±0.004
53	0.971±0.011	0.983±0.005	0.987±0.003	0.991±0.002	0.168±0.073	0.106±0.039
68	0.983±0.011	0.992±0.001	0.994±0.005	0.997±0.001	0.066±0.010	0.046±0.009
72	0.972±0.010	0.985±0.002	0.987±0.006	0.993±0.002	0.182±0.038	0.118±0.026
Overall (Mean)	0.970±0.016	0.984±0.012	0.986±0.009	0.992±0.006	0.155±0.104	0.087±0.073

Table A.4 Summary of PPG morphological similarity of the age range of 51 to 60.

Male subjects						
Subj[1] no.	PCCR[2] (Time domain)	PCCIR[3] (Time domain)	PCCR[2] (Frequency domain)	PCCIR[3] (Frequency domain)	MSPER[4] (Time domain)	MSPEIR[5] (Time domain)
	Average ± Standard deviation					
13	0.927±0.009	0.963±0.007	0.957±0.008	0.978±0.006	0.435±0.086	0.203±0.051
22	0.972±0.025	0.980±0.020	0.993±0.005	0.996±0.001	0.071±0.054	0.052±0.047
23	0.913±0.005	0.940±0.004	0.950±0.012	0.970±0.009	0.301±0.035	0.185±0.021
44	0.989±0.010	0.995±0.004	0.996±0.004	0.998±0.001	0.029±0.013	0.029±0.012
45	0.966±0.011	0.978±0.005	0.987±0.006	0.991±0.003	0.189±0.095	0.107±0.063
50	0.956±0.017	0.972±0.011	0.981±0.011	0.988±0.008	0.266±0.150	0.158±0.074
75	0.960±0.008	0.979±0.003	0.981±0.008	0.990±0.005	0.242±0.087	0.144±0.035
Overall (Mean)	0.955±0.026	0.973±0.017	0.978±0.018	0.987±0.010	0.219±0.139	0.125±0.066
Female subjects						
Subj[1] no.	PCCR[2] (Time domain)	PCCIR[3] (Time domain)	PCCR[2] (Frequency domain)	PCCIR[3] (Frequency domain)	MSPER[4] (Time domain)	MSPEIR[5] (Time domain)
	Average ± Standard deviation					
02	0.989±0.003	0.994±0.002	0.995±0.003	0.997±0.001	0.054±0.026	0.021±0.023
04	0.994±0.004	0.997±0.002	0.998±0.001	0.999±0.001	0.019±0.010	0.004±0.001
14	0.971±0.016	0.986±0.004	0.987±0.011	0.994±0.005	0.096±0.035	0.049±0.017
21	0.970±0.009	0.990±0.001	0.987±0.006	0.996±0.001	0.170±0.049	0.046±0.017
26	0.989±0.011	0.996±0.002	0.997±0.004	0.999±0.001	0.029±0.013	0.021±0.009
31	0.916±0.007	0.937±0.005	0.959±0.010	0.972±0.006	0.483±0.094	0.385±0.073
39	0.978±0.012	0.983±0.001	0.993±0.007	0.993±0.003	0.076±0.012	0.070±0.010
65	0.992±0.010	0.997±0.001	0.997±0.004	0.999±0.000	0.018±0.012	0.008±0.003
70	0.928±0.012	0.955±0.008	0.965±0.007	0.975±0.006	0.455±0.079	0.264±0.046
74	0.939±0.007	0.966±0.003	0.976±0.003	0.984±0.003	0.368±0.046	0.232±0.023
Overall (Mean)	0.967±0.029	0.980±0.021	0.985±0.014	0.991±0.010	0.177±0.186	0.110±0.134

Table A.5 Summary SpO2 values of the age range of 21 to 30 years while resting.

Male subjects			Female subjects		
Subject no.	Proposed technique (PT)	Conventional method (CM)	Subject no.	Proposed technique (PT)	Conventional method (CM)
	SpO2 values in the unit of %			SpO2 values in the unit of %	
	Average ± Standard deviation			Average ± Standard deviation	
08	94.09±0.36	92.64±0.45	05	94.44±0.09	94.64±0.34
18	98.21±0.02	92.29±0.25	06	95.64±0.09	95.40±0.58
36	98.64±0.19	92.02±1.87	09	99.38±0.15	94.45±0.34
38	95.85±0.08	94.09±0.21	11	99.12±0.14	94.13±0.85
40	94.78±0.13	91.14±0.66	17	97.89±0.07	93.59±0.14
51	94.15±0.31	92.63±0.83	27	96.03±0.04	93.52±0.29
57	94.70±0.15	93.18±0.45	28	96.25±0.25	93.71±0.31
58	93.44±0.08	93.55±0.14	29	98.71±0.09	93.06±0.99
59	98.54±0.12	94.57±0.58	37	97.67±0.10	93.86±0.14
60	93.17±0.78	94.26±0.38	41	98.12±0.15	92.03±0.30
61	98.68±0.21	93.30±0.33	42	96.20±0.00	93.95±1.40
62	94.63±0.10	93.60±0.28	52	95.00±0.18	91.77±1.52
63	97.47±0.08	93.27±0.47	Overall (Mean)	97.04±1.66	93.67±1.03
64	97.49±0.21	93.94±1.65			
Overall (Mean)	95.99±2.09	93.18±0.95			

Table A.6 Summary SpO2 values of the age range of 31 to 40 years while resting.

Male subjects			Female subjects		
Subject no.	Proposed technique (PT)	Conventional method (CM)	Subject no.	Proposed technique (PT)	Conventional method (CM)
	SpO2 values in the unit of %			SpO2 values in the unit of %	
	Average ± Standard deviation			Average ± Standard deviation	
03	94.04±0.09	93.17±0.34	07	97.98±0.09	91.33±0.52
12	96.02±0.05	93.90±0.34	15	96.33±0.08	93.02±0.74
24	98.18±0.10	92.93±1.44	19	97.10±0.10	93.79±0.24
34	98.91±0.10	91.77±0.40	32	97.43±0.20	92.52±0.27
46	99.40±0.00	92.98±0.42	48	97.93±0.08	93.86±0.29
47	99.44±0.09	94.02±2.00	54	99.53±0.10	94.82±1.46
55	96.04±0.06	93.62±0.11	56	97.45±0.03	93.35±0.47
67	93.66±0.24	91.72±0.26	73	99.69±0.09	95.25±0.44
69	93.03±0.10	92.97±0.28	Overall (Mean)	97.93±1.16	93.49±1.25
Overall (Mean)	96.52±2.56	93.01±0.82			

Table A.7 Summary SpO2 values of the age range of 41 to 50 years while resting.

Male subjects			Female subjects		
Subject no.	Proposed technique (PT)	Conventional method (CM)	Subject no.	Proposed technique (PT)	Conventional method (CM)
	SpO2 values in the unit of %			SpO2 values in the unit of %	
	Average ± Standard deviation			Average ± Standard deviation	
16	96.06±0.35	93.13±1.08	01	99.58±0.04	92.37±0.32
20	96.37±0.05	93.67±0.33	10	98.13±0.08	91.93±0.72
30	96.06±0.02	93.27±0.22	25	95.44±0.11	93.10±0.28
33	97.16±0.11	93.23±0.17	43	96.26±0.05	91.38±1.11
35	94.86±0.09	92.73±0.27	53	97.45±0.14	92.83±0.23
49	95.34±0.05	91.83±0.54	68	99.05±0.07	93.16±0.68
66	97.74±0.15	94.13±0.56	72	97.10±0.07	93.58±0.35
71	97.38±0.08	93.94±0.40	Overall (Mean)	97.57±1.47	92.62±0.77
Overall (Mean)	96.37±1.00	93.24±0.73			

Table A.8 Summary SpO2 values of the age range of 51 to 60 years while resting.

Male subjects			Female subjects		
Subject no.	Proposed technique (PT)	Conventional method (CM)	Subject no.	Proposed technique (PT)	Conventional method (CM)
	SpO2 values in the unit of %			SpO2 values in the unit of %	
	Average ± Standard deviation			Average ± Standard deviation	
13	95.99±0.44	93.11±0.40	02	96.44±0.09	93.35±0.22
22	99.72±0.11	93.28±0.41	04	95.04±0.09	95.01±0.30
23	97.44±0.07	92.91±0.07	14	95.93±0.32	92.34±0.80
44	98.18±0.20	93.69±0.34	21	95.06±0.13	94.52±0.08
45	96.76±0.16	95.12±0.44	26	96.49±0.14	92.72±1.00
50	97.60±0.11	93.08±0.92	31	94.62±0.14	94.02±0.03
75	94.73±0.05	94.09±0.39	39	99.06±0.14	94.75±0.20
Overall (Mean)	97.20±1.60	93.61±0.78	65	98.32±0.14	94.58±0.33
			70	97.41±0.08	93.89±0.22
			74	96.18±0.14	94.24±0.10
			Overall (Mean)	96.45±1.45	93.94±0.88

Table A.9 Summary SpO2 values of the age range of 21 to 30 years while bending.

Male subjects			Female subjects		
Subject no.	Proposed technique (PT)	Conventional method (CM)	Subject no.	Proposed technique (PT)	Conventional method (CM)
	SpO2 values in the unit of %			SpO2 values in the unit of %	
	Average ± Standard deviation			Average ± Standard deviation	
08	93.82±0.24	91.68±0.21	05	93.40±0.14	90.46±0.70
18	97.84±0.08	91.74±0.14	06	94.24±0.09	86.86±1.61
36	99.34±0.14	89.79±4.98	09	98.37±0.27	90.13±1.43
38	96.30±0.08	92.70±1.37	11	99.83±0.07	91.90±1.31
40	94.54±0.10	88.45±0.87	17	97.86±0.07	92.88±0.59
51	96.10±1.16	84.73±13.84	27	95.76±0.21	92.46±0.54
57	94.78±0.21	90.81±3.36	28	96.44±0.29	92.73±1.20
58	93.72±0.18	92.08±1.92	29	97.88±0.12	82.57±5.79
59	98.49±0.10	93.72±0.52	37	95.71±0.09	88.05±2.14
60	93.69±0.44	87.04±3.86	41	98.50±0.16	84.18±9.69
61	97.43±0.29	88.95±0.47	42	97.20±0.07	79.60±4.86
62	96.07±0.49	94.22±0.97	52	94.96±0.08	93.55±0.28
63	97.86±0.08	91.40±1.68			
64	98.41±0.24	95.79±6.46	Overall (Mean)	96.68±1.92	88.78±4.59
Overall (Mean)	96.31±1.96	90.93±2.95			

Table A.10 Summary SpO2 values of the age range of 31 to 40 years while bending.

Male subjects			Female subjects		
Subject no.	Proposed technique (PT)	Conventional method (CM)	Subject no.	Proposed technique (PT)	Conventional method (CM)
	SpO2 values in the unit of %			SpO2 values in the unit of %	
	Average ± Standard deviation			Average ± Standard deviation	
03	96.00±0.14	91.61±0.77	07	98.62±0.15	79.73±3.87
12	96.93±0.14	89.23±3.21	15	97.28±0.10	81.51±2.80
24	98.47±0.09	82.32±1.68	19	96.80±0.22	92.96±1.16
34	99.54±0.15	94.15±0.67	32	96.96±0.30	84.98±4.68
46	98.16±0.29	85.93±1.64	48	97.97±0.12	91.21±1.18
47	97.80±0.14	79.97±3.92	54	99.54±0.45	84.63±1.52
55	95.87±0.08	88.61±0.85	56	97.66±0.19	64.55±30.76
67	93.93±0.10	92.61±0.39	73	99.28±0.83	88.81±4.14
69	93.15±0.23	92.21±0.52			
Overall (Mean)	96.65±2.12	88.52±4.88	Overall (Mean)	98.01±1.04	83.55±8.93

Table A.11 Summary SpO2 values of the age range of 41 to 50 years while bending.

Male subjects			Female subjects		
Subject no.	Proposed technique (PT)	Conventional method (CM)	Subject no.	Proposed technique (PT)	Conventional method (CM)
	SpO2 values in the unit of %			SpO2 values in the unit of %	
	Average ± Standard deviation			Average ± Standard deviation	
16	95.90±0.39	91.13±0.80	01	99.24±0.09	91.46±0.63
20	95.95±0.27	87.03±0.60	10	96.50±0.12	93.13±0.43
30	93.18±0.67	90.16±2.23	25	95.42±0.02	91.77±1.13
33	99.80±0.13	86.06±4.46	43	97.13±0.10	86.75±3.45
35	94.43±0.03	91.02±0.44	53	97.10±0.07	91.83±1.19
49	95.90±0.24	92.61±0.59	68	99.32±0.50	84.36±4.49
66	97.59±0.16	85.98±2.20	72	97.49±0.20	85.81±1.78
71	97.26±0.13	91.27±1.62	Overall (Mean)	97.46±1.41	89.30±3.53
Overall (Mean)	96.25±2.02	89.41±2.63			

Table A.12 Summary SpO2 values of the age range of 51 to 60 years while bending.

Male subjects			Female subjects		
Subject no.	Proposed technique (PT)	Conventional method (CM)	Subject no.	Proposed technique (PT)	Conventional method (CM)
	SpO2 values in the unit of %			SpO2 values in the unit of %	
	Average ± Standard deviation			Average ± Standard deviation	
13	96.76±0.10	92.32±0.47	02	95.40±0.14	89.25±1.84
22	98.96±0.41	91.17±0.83	04	95.28±0.11	92.21±1.19
23	96.14±0.09	90.28±0.38	14	97.25±0.20	91.27±0.67
44	98.37±0.03	85.84±2.36	21	95.71±0.23	84.24±2.19
45	96.42±0.11	91.78±0.45	26	97.14±0.13	67.55±23.43
50	98.35±0.23	87.82±2.85	31	94.68±0.13	85.00±0.02
75	94.95±0.12	86.92±3.87	39	98.97±0.11	89.59±0.59
Overall (Mean)	97.13±1.46	89.45±2.56	65	99.49±0.48	81.61±8.96
			70	97.19±0.16	91.09±3.59
			74	96.34±0.21	85.00±1.10
			Overall (Mean)	96.74±1.58	85.68±7.30

Table A.13 Summary SpO2 values of the age range of 21 to 30 years while horizontal moving.

Male subjects			Female subjects		
Subject no.	Proposed technique (PT)	Conventional method (CM)	Subject no.	Proposed technique (PT)	Conventional method (CM)
	SpO2 values in the unit of %			SpO2 values in the unit of %	
	Average ± Standard deviation			Average ± Standard deviation	
08	94.42±0.06	93.47±0.55	05	94.04±0.09	93.80±0.48
18	97.98±0.04	90.85±0.64	06	98.56±0.09	90.05±2.67
36	99.18±0.05	83.32±3.77	09	97.06±0.10	88.18±1.55
38	96.38±0.33	93.07±1.05	11	99.42±0.16	93.67±0.25
40	95.52±0.13	87.38±1.32	17	97.98±0.12	92.74±0.25
51	96.18±0.18	94.09±0.72	27	94.43±0.19	87.15±4.98
57	95.08±0.17	94.20±0.94	28	95.18±0.27	85.69±2.01
58	92.86±0.19	93.08±0.29	29	98.72±0.09	85.83±3.77
59	99.30±0.10	92.12±1.81	37	95.48±0.17	74.85±13.86
60	91.30±0.98	90.96±2.19	41	98.64±0.10	87.35±2.73
61	97.34±0.13	91.52±1.48	42	97.00±0.07	76.12±4.87
62	94.49±0.19	92.38±0.84	52	94.76±0.19	94.00±0.20
63	97.48±0.09	95.18±0.82	Overall (Mean)	96.77±1.91	87.45±6.40
64	96.95±0.22	90.91±2.17			
Overall (Mean)	96.03±2.28	91.61±3.07			

Table A.14 Summary SpO2 values of the age range of 31 to 40 years while horizontal moving.

Male subjects			Female subjects		
Subject no.	Proposed technique (PT)	Conventional method (CM)	Subject no.	Proposed technique (PT)	Conventional method (CM)
	SpO2 values in the unit of %			SpO2 values in the unit of %	
	Average ± Standard deviation			Average ± Standard deviation	
03	96.64±0.09	90.86±0.61	07	97.92±0.06	78.83±2.48
12	97.09±0.20	94.25±0.98	15	97.44±0.07	77.21±1.88
24	98.48±0.17	76.98±2.40	19	96.46±0.12	92.23±0.45
34	98.94±0.12	90.25±1.81	32	95.98±0.12	91.01±1.25
46	97.56±0.09	88.88±2.28	48	97.42±0.37	76.24±21.59
47	97.24±0.09	82.73±3.00	54	99.68±0.11	81.15±6.93
55	96.18±0.21	87.76±1.45	56	98.48±0.10	85.77±1.51
67	93.57±0.03	91.37±0.35	73	96.94±0.09	76.70±15.46
69	93.15±0.11	90.70±0.83	Overall (Mean)	97.54±1.17	82.39±6.48
Overall (Mean)	96.54±1.99	88.20±5.25			

Table A.15 Summary SpO2 values of the age range of 41 to 50 years while horizontal moving.

Male subjects			Female subjects		
Subject no.	Proposed technique (PT)	Conventional method (CM)	Subject no.	Proposed technique (PT)	Conventional method (CM)
	SpO2 values in the unit of %			SpO2 values in the unit of %	
	Average ± Standard deviation			Average ± Standard deviation	
16	95.02±0.10	91.00±0.44	01	99.72±0.11	90.87±0.40
20	95.46±0.08	88.75±0.36	10	95.77±0.14	88.31±0.99
30	93.00±0.43	91.88±1.24	25	95.06±0.07	91.75±0.37
33	96.60±0.14	90.43±0.95	43	97.20±0.07	85.26±2.86
35	94.70±0.13	91.03±1.52	53	97.29±0.21	93.00±0.23
49	95.54±0.08	92.82±0.17	68	99.54±0.07	85.56±4.50
66	98.10±0.19	81.96±13.64	72	97.72±0.20	87.69±2.63
71	97.22±0.04	88.99±1.18	Overall (Mean)	97.47±1.74	88.92±3.03
Overall (Mean)	95.70±1.59	89.61±3.37			

Table A.16 Summary SpO2 values of the age range of 51 to 60 years while horizontal moving.

Male subjects			Female subjects		
Subject no.	Proposed technique (PT)	Conventional method (CM)	Subject no.	Proposed technique (PT)	Conventional method (CM)
	SpO2 values in the unit of %			SpO2 values in the unit of %	
	Average ± Standard deviation			Average ± Standard deviation	
13	95.76±0.37	91.31±1.22	02	96.70±0.14	93.27±0.27
22	98.58±0.13	91.26±0.63	04	96.12±0.18	92.89±0.48
23	95.66±0.09	91.03±1.20	14	97.26±0.19	93.09±0.71
44	98.30±0.08	90.18±2.62	21	96.05±0.20	90.52±0.65
45	96.55±0.18	93.28±1.86	26	97.65±0.09	48.11±10.33
50	98.32±0.14	84.94±2.34	31	97.71±0.08	85.09±0.06
75	95.26±0.22	87.53±2.79	39	99.84±0.10	87.99±1.73
Overall (Mean)	96.92±1.44	89.93±2.79	65	98.52±0.09	88.46±0.68
			70	96.78±0.30	92.99±10.61
			74	92.70±0.46	87.33±2.77
			Overall (Mean)	96.93±1.88	85.97±13.61

Table A.17 Summary SpO2 values of the age range of 21 to 30 years while shivering.

Male subjects			Female subjects		
Subject no.	Proposed technique (PT)	Conventional method (CM)	Subject no.	Proposed technique (PT)	Conventional method (CM)
	SpO2 values in the unit of %			SpO2 values in the unit of %	
	Average ± Standard deviation			Average ± Standard deviation	
08	94.53±0.12	91.01±0.96	05	93.40±0.07	92.56±0.55
18	98.02±0.08	93.22±0.38	06	95.88±0.11	89.96±4.33
36	98.84±0.09	89.01±2.02	09	97.47±0.19	89.40±1.34
38	96.37±0.13	89.84±1.18	11	96.88±0.44	94.43±0.21
40	96.07±0.12	89.73±0.23	17	97.98±0.02	93.01±0.14
51	96.62±0.20	95.13±0.12	27	94.99±0.15	88.99±3.25
57	94.94±0.11	93.53±0.24	28	95.74±0.24	87.64±1.78
58	93.22±0.32	86.72±4.23	29	99.18±0.08	86.84±1.71
59	99.49±0.09	93.35±1.21	37	96.58±0.04	52.70±32.62
60	94.14±0.45	91.94±2.05	41	98.71±0.09	78.41±12.66
61	97.01±0.26	88.53±4.50	42	97.01±0.02	79.09±3.78
62	95.55±0.16	92.75±1.04	52	95.54±0.11	88.03±1.67
63	97.63±0.16	91.92±1.38			
64	98.11±0.04	84.00±6.98	Overall (Mean)	96.61±1.63	85.09±11.33
Overall (Mean)	96.47±1.85	90.76±3.02			

Table A.18 Summary SpO2 values of the age range of 31 to 40 years while shivering.

Male subjects			Female subjects		
Subject no.	Proposed technique (PT)	Conventional method (CM)	Subject no.	Proposed technique (PT)	Conventional method (CM)
	SpO2 values in the unit of %			SpO2 values in the unit of %	
	Average ± Standard deviation			Average ± Standard deviation	
03	96.24±0.09	91.82±0.74	07	98.23±0.07	85.15±3.56
12	97.19±0.24	94.48±0.44	15	97.34±0.09	63.76±61.73
24	99.50±0.13	83.02±2.48	19	96.90±0.05	88.45±1.97
34	98.24±0.15	93.91±1.04	32	96.23±0.09	92.10±0.22
46	97.86±0.06	93.89±0.30	48	97.92±0.25	96.64±0.78
47	97.88±0.14	77.87±7.12	54	99.65±0.14	81.97±5.94
55	96.40±0.29	90.99±2.41	56	99.10±0.11	88.05±5.07
67	93.90±0.20	92.26±0.66	73	97.00±0.07	79.53±3.89
69	94.35±0.09	91.07±1.16			
Overall (Mean)	96.84±1.83	89.92±5.67	Overall (Mean)	97.80±1.16	84.46±9.96

Table A.19 Summary SpO2 values of the age range of 41 to 50 years while shivering.

Male subjects			Female subjects		
Subject no.	Proposed technique (PT)	Conventional method (CM)	Subject no.	Proposed technique (PT)	Conventional method (CM)
	SpO2 values in the unit of %			SpO2 values in the unit of %	
	Average ± Standard deviation			Average ± Standard deviation	
16	95.54±0.11	91.54±1.05	01	99.48±0.11	91.33±1.07
20	95.42±0.09	89.09±4.19	10	96.27±0.27	90.98±0.07
30	94.07±0.12	94.02±0.12	25	95.42±0.17	89.83±0.67
33	97.40±0.11	91.92±0.71	43	97.14±0.06	72.14±23.73
35	94.82±0.18	95.01±0.29	53	97.78±0.15	91.48±1.49
49	95.61±0.16	93.09±0.26	68	99.67±0.09	94.46±0.73
66	98.10±0.06	85.18±4.54	72	98.03±0.05	85.11±3.57
71	97.16±0.06	84.65±4.42	Overall (Mean)	97.68±1.57	87.90±7.50
Overall (Mean)	96.01±1.39	91.41±3.91			

Table A.20 Summary SpO2 values of the age range of 51 to 60 years while shivering.

Male subjects			Female subjects		
Subject no.	Proposed technique (PT)	Conventional method (CM)	Subject no.	Proposed technique (PT)	Conventional method (CM)
	SpO2 values in the unit of %			SpO2 values in the unit of %	
	Average ± Standard deviation			Average ± Standard deviation	
13	96.50±0.18	92.35±0.19	02	96.84±0.09	91.33±0.81
22	98.80±0.07	89.68±1.35	04	94.60±0.07	93.78±0.64
23	95.90±0.10	93.72±0.19	14	97.15±0.17	92.27±0.32
44	98.80±0.14	80.26±0.81	21	96.14±0.16	91.67±0.47
45	96.82±0.09	94.01±0.35	26	97.68±0.18	32.26±54.98
50	98.43±0.14	77.16±4.69	31	94.82±0.13	85.09±0.24
75	95.45±0.18	82.28±4.97	39	99.66±0.10	88.91±0.85
Overall (Mean)	97.24±1.42	87.07±7.01	65	98.79±0.02	91.11±1.86
			70	97.94±0.11	85.08±0.91
			74	94.10±0.43	85.82±3.75
			Overall (Mean)	96.78±1.85	83.73±18.36

Table A.21 Summary SpO2 values of the age range of 21 to 30 years while vertical moving.

Male subjects			Female subjects		
Subject no.	Proposed technique (PT)	Conventional method (CM)	Subject no.	Proposed technique (PT)	Conventional method (CM)
	SpO2 values in the unit of %			SpO2 values in the unit of %	
	Average ± Standard deviation			Average ± Standard deviation	
08	94.93±0.12	91.03±0.88	05	93.40±0.07	93.52±0.61
18	97.99±0.02	92.46±0.21	06	96.48±0.18	87.21±3.60
36	99.13±0.10	87.29±2.25	09	97.37±0.10	89.77±1.49
38	96.53±0.26	91.19±6.69	11	99.90±0.11	90.24±1.84
40	95.66±0.16	88.64±1.76	17	98.16±0.09	92.91±0.32
51	96.62±0.09	94.17±0.58	27	94.96±0.18	84.64±2.49
57	94.97±0.17	93.91±1.06	28	95.86±0.12	87.87±2.36
58	93.14±0.16	93.11±0.44	29	99.11±0.07	88.64±2.31
59	99.36±0.09	95.35±0.38	37	96.67±0.08	73.99±21.53
60	94.05±0.42	92.33±0.98	41	99.01±0.09	84.11±1.63
61	97.62±0.13	86.57±2.85	42	96.96±0.05	76.21±2.75
62	95.89±0.18	94.06±0.33	52	95.86±0.11	94.42±0.27
63	98.06±0.10	91.75±1.57	Overall (Mean)	96.98±1.87	86.96±6.42
64	97.61±0.13	83.92±6.52			
Overall (Mean)	96.54±1.87	91.13±3.34			

Table A.22 Summary SpO2 values of the age range of 31 to 40 years while vertical moving.

Male subjects			Female subjects		
Subject no.	Proposed technique (PT)	Conventional method (CM)	Subject no.	Proposed technique (PT)	Conventional method (CM)
	SpO2 values in the unit of %			SpO2 values in the unit of %	
	Average ± Standard deviation			Average ± Standard deviation	
03	96.40±0.14	91.67±0.79	07	98.52±0.27	78.40±4.59
12	97.10±0.09	94.80±0.73	15	97.36±0.05	77.63±11.85
24	99.28±0.31	81.76±1.09	19	96.99±0.22	92.10±1.06
34	99.46±0.21	88.68±0.80	32	96.31±0.28	92.09±0.51
46	97.96±0.09	90.45±0.60	48	98.19±0.30	92.80±1.01
47	97.88±0.16	83.10±4.76	54	99.88±0.07	74.07±5.08
55	96.54±0.04	85.53±1.00	56	98.64±0.05	84.31±2.60
67	93.96±0.06	92.56±0.10	73	97.00±0.07	74.50±28.27
69	94.23±0.24	87.45±1.64	Overall (Mean)	97.86±1.16	83.24±8.15
Overall (Mean)	96.98±1.95	88.44±4.40			

Table A.23 Summary SpO2 values of the age range of 41 to 50 years while vertical moving.

Male subjects			Female subjects		
Subject no.	Proposed technique (PT)	Conventional method (CM)	Subject no.	Proposed technique (PT)	Conventional method (CM)
	SpO2 values in the unit of %			SpO2 values in the unit of %	
	Average ± Standard deviation			Average ± Standard deviation	
16	95.30±0.15	91.77±0.42	01	98.44±0.26	92.15±0.56
20	95.74±0.21	80.49±3.16	10	96.20±0.34	88.19±1.36
30	94.02±0.21	94.48±0.13	25	95.61±0.41	91.25±0.73
33	96.96±0.11	93.72±0.16	43	97.14±0.09	85.22±4.31
35	95.34±0.15	93.32±0.88	53	97.50±0.13	93.26±0.19
49	96.06±0.11	93.33±0.66	68	99.60±0.03	81.10±15.95
66	98.10±0.11	78.68±7.01	72	98.17±0.17	88.12±2.94
71	97.32±0.13	88.63±1.47	Overall (Mean)	97.52±1.36	88.47±4.27
Overall (Mean)	96.10±1.30	89.30±6.28			

Table A.24 Summary SpO2 values of the age range of 51 to 60 years while vertical moving.

Male subjects			Female subjects		
Subject no.	Proposed technique (PT)	Conventional method (CM)	Subject no.	Proposed technique (PT)	Conventional method (CM)
	SpO2 values in the unit of %			SpO2 values in the unit of %	
	Average ± Standard deviation			Average ± Standard deviation	
13	97.24±0.19	91.87±0.20	02	97.14±0.09	93.21±0.34
22	98.82±0.04	91.90±0.53	04	94.80±0.07	94.15±0.32
23	95.80±0.09	90.50±1.16	14	97.34±0.15	93.20±0.45
44	98.46±0.13	89.67±5.68	21	95.98±0.15	91.52±0.74
45	96.98±0.21	93.65±0.40	26	97.66±0.09	14.18±135.08
50	98.81±0.27	72.16±24.98	31	97.78±0.02	85.12±0.03
75	95.59±0.27	82.78±2.04	39	97.28±0.11	88.40±0.91
Overall (Mean)	97.39±1.36	87.50±7.61	65	98.94±0.17	88.47±0.84
			70	97.19±0.35	91.15±1.23
			74	93.78±0.52	82.79±8.31
			Overall (Mean)	96.79±1.52	82.22±24.19

Table A.25 Summary SpO2 values of the age range of 21 to 30 years while waving.

Male subjects			Female subjects		
Subject no.	Proposed technique (PT)	Conventional method (CM)	Subject no.	Proposed technique (PT)	Conventional method (CM)
	SpO2 values in the unit of %			SpO2 values in the unit of %	
	Average ± Standard deviation			Average ± Standard deviation	
08	94.54±0.18	91.62±0.76	05	92.98±0.11	91.69±0.89
18	98.11±0.07	91.81±0.37	06	94.98±0.11	91.45±0.89
36	98.73±0.14	89.28±2.03	09	97.93±0.08	88.89±1.25
38	97.08±0.11	84.97±0.55	11	98.84±0.17	93.44±1.22
40	95.67±0.16	89.32±0.30	17	98.34±0.11	94.46±0.12
51	96.25±0.09	94.91±0.36	27	95.62±0.14	90.33±0.62
57	95.39±0.31	92.78±0.71	28	96.06±0.21	89.59±2.75
58	94.34±0.41	94.02±0.31	29	98.90±0.17	86.21±7.88
59	99.23±0.07	91.90±1.81	37	96.33±0.10	57.44±32.23
60	94.86±0.18	88.43±2.26	41	98.73±0.15	86.88±1.10
61	98.09±0.21	90.91±0.80	42	97.18±0.05	81.25±1.56
62	96.24±0.22	92.18±1.41	52	95.82±0.28	93.99±0.42
63	98.11±0.23	92.68±1.14			
64	97.94±0.36	86.51±2.07	Overall (Mean)	96.81±1.84	87.13±10.07
Overall (Mean)	96.76±1.64	90.81±2.80			

Table A.26 Summary SpO2 values of the age range of 31 to 40 years while waving.

Male subjects			Female subjects		
Subject no.	Proposed technique (PT)	Conventional method (CM)	Subject no.	Proposed technique (PT)	Conventional method (CM)
	SpO2 values in the unit of %			SpO2 values in the unit of %	
	Average ± Standard deviation			Average ± Standard deviation	
03	96.12±0.11	91.67±0.88	07	98.44±0.20	82.76±2.75
12	97.41±0.10	92.77±1.02	15	97.50±0.07	104.47±71.45
24	99.37±0.19	83.94±2.00	19	96.81±0.52	92.23±0.29
34	98.78±0.25	92.43±0.28	32	96.37±0.15	90.22±1.62
46	98.14±0.11	91.33±0.28	48	97.69±0.32	94.58±0.71
47	98.12±0.11	79.60±4.99	54	99.57±0.12	78.68±4.28
55	96.58±0.06	88.11±1.19	56	98.51±0.10	88.63±1.33
67	94.23±0.15	92.37±0.47	73	96.85±0.07	88.48±5.77
69	94.72±0.20	89.80±1.86			
Overall (Mean)	97.05±1.78	89.11±4.54	Overall (Mean)	97.72±1.08	90.00±7.75

Table A.27 Summary SpO2 values of the age range of 41 to 50 years while waving.

Male subjects			Female subjects		
Subject no.	Proposed technique (PT)	Conventional method (CM)	Subject no.	Proposed technique (PT)	Conventional method (CM)
	SpO2 values in the unit of %			SpO2 values in the unit of %	
	Average ± Standard deviation			Average ± Standard deviation	
16	95.87±0.09	92.17±0.34	01	99.28±0.11	91.07±0.68
20	95.51±0.05	89.17±2.48	10	96.94±0.26	87.67±0.95
30	93.30±0.11	92.21±0.92	25	96.34±0.19	89.75±1.18
33	97.32±0.16	88.07±2.00	43	97.19±0.02	84.39±9.08
35	95.00±0.15	88.04±1.11	53	97.60±0.15	93.58±0.20
49	95.94±0.28	92.81±0.37	68	99.59±0.04	86.36±2.37
66	98.42±0.17	73.05±15.50	72	98.07±0.09	84.07±0.37
71	97.41±0.08	86.54±1.89	Overall (Mean)	97.86±1.21	88.13±3.53
Overall (Mean)	96.10±1.60	87.76±6.38			

Table A.28 Summary SpO2 values of the age range of 51 to 60 years while waving.

Male subjects			Female subjects		
Subject no.	Proposed technique (PT)	Conventional method (CM)	Subject no.	Proposed technique (PT)	Conventional method (CM)
	SpO2 values in the unit of %			SpO2 values in the unit of %	
	Average ± Standard deviation			Average ± Standard deviation	
13	95.74±0.12	92.43±0.40	02	96.48±0.11	92.74±0.54
22	98.72±0.09	91.31±0.56	04	94.44±0.09	93.32±0.71
23	96.41±0.14	88.11±1.36	14	97.14±0.07	93.49±0.38
44	98.82±0.04	88.96±1.23	21	96.00±0.14	90.34±1.85
45	96.66±0.17	93.26±0.69	26	97.63±0.07	52.62±40.98
50	99.07±0.09	88.43±3.93	31	95.18±0.92	83.14±3.16
75	95.43±0.16	87.64±1.65	39	99.54±0.10	87.52±1.44
Overall (Mean)	97.26±1.56	90.02±2.27	65	98.91±0.10	88.08±2.00
			70	97.70±0.14	92.59±0.93
			74	93.97±0.22	83.58±1.00
			Overall (Mean)	96.70±1.84	85.74±12.26

Table A.29 Summary of SpO2 percentage error of the age range of 21 to 30 years while bending.

Male subjects			Female subjects		
Subject no.	Proposed technique (PT)	Conventional method (CM)	Subject no.	Proposed technique (PT)	Conventional method (CM)
	SpO2 percentage error values in the unit of %			SpO2 percentage error values in the unit of %	
	Average			Average	
08	0.34	1.04	05	1.10	4.41
18	0.37	0.60	06	1.46	8.95
36	0.71	4.06	09	1.02	4.58
38	0.47	1.48	11	0.72	2.38
40	0.24	2.95	17	0.06	0.75
51	2.06	9.41	27	0.32	1.13
57	0.17	2.82	28	0.26	1.11
58	0.30	1.61	29	0.84	11.27
59	0.10	0.90	37	2.01	6.19
60	0.63	7.66	41	0.39	9.78
61	1.26	4.67	42	1.04	15.28
62	1.52	0.75	52	0.08	1.94
63	0.40	2.22			
64	0.94	4.97	Overall (Mean) ± Standard deviation	0.77±0.59	5.65±4.72
Overall (Mean) ± Standard deviation	0.68±0.58	3.22±2.69			

Table A.30 Summary of SpO2 percentage error of the age range of 31 to 40 years while bending.

Male subjects			Female subjects		
Subject no.	Proposed technique (PT)	Conventional method (CM)	Subject no.	Proposed technique (PT)	Conventional method (CM)
	SpO2 percentage error values in the unit of %			SpO2 percentage error values in the unit of %	
	Average			Average	
03	2.08	1.68	07	0.65	12.70
12	0.95	4.97	15	0.99	12.37
24	0.30	11.42	19	0.31	1.17
34	0.63	2.59	32	0.50	8.15
46	1.25	7.58	48	0.10	2.82
47	1.65	14.95	54	0.38	10.75
55	0.17	5.35	56	0.22	30.86
67	0.29	0.97	73	0.56	6.76
69	0.21	0.84			
Overall (Mean) ± Standard deviation	0.84±0.69	5.59±4.93	Overall (Mean) ± Standard deviation	0.46±0.28	10.70±9.16

Table A.31 Summary of SpO2 percentage error of the age range of 41 to 50 years while bending.

Male subjects			Female subjects		
Subject no.	Proposed technique (PT)	Conventional method (CM)	Subject no.	Proposed technique (PT)	Conventional method (CM)
	SpO2 percentage error values in the unit of %			SpO2 percentage error values in the unit of %	
	Average			Average	
16	0.34	2.14	01	0.34	0.98
20	0.43	7.09	10	1.65	1.31
30	3.00	3.34	25	0.02	1.64
33	2.72	7.70	43	0.90	5.07
35	0.46	1.84	53	0.36	1.07
49	0.60	0.85	68	0.44	9.44
66	0.17	8.66	72	0.40	8.30
71	0.13	2.84			
Overall (Mean) ± Standard deviation	0.98±1.17	4.31±3.02	Overall (Mean) ± Standard deviation	0.59±0.54	3.97±3.64

Table A.32 Summary of SpO2 percentage error of the age range of 51 to 60 years while bending.

Male subjects			Female subjects		
Subject no.	Proposed technique (PT)	Conventional method (CM)	Subject no.	Proposed technique (PT)	Conventional method (CM)
	SpO2 percentage error values in the unit of %			SpO2 percentage error values in the unit of %	
	Average			Average	
13	0.80	0.85	02	1.08	4.39
22	0.76	2.26	04	0.25	2.94
23	1.34	2.82	14	1.38	1.16
44	0.19	8.38	21	0.68	10.88
45	0.36	3.50	26	0.67	27.46
50	0.77	5.66	31	0.10	9.59
75	0.24	7.62	39	0.10	5.44
			65	1.19	13.71
			70	0.22	2.99
			74	0.22	9.81
Overall (Mean) ± Standard deviation	0.64±0.41	4.44±2.84	Overall (Mean) ± Standard deviation	0.59±0.48	8.84±7.71

Table A.33 Summary of SpO2 percentage error of the age range of 21 to 30 years while horizontal moving.

Male subjects			Female subjects		
Subject no.	Proposed technique (PT)	Conventional method (CM)	Subject no.	Proposed technique (PT)	Conventional method (CM)
	SpO2 percentage error values in the unit of %			SpO2 percentage error values in the unit of %	
	Average			Average	
08	0.35	0.89	05	0.42	0.88
18	0.23	1.57	06	3.05	5.60
36	0.55	9.46	09	2.33	6.63
38	0.55	1.24	11	0.31	0.49
40	0.79	4.12	17	0.13	0.90
51	2.16	1.57	27	1.67	6.80
57	0.40	1.27	28	1.11	8.55
58	0.62	0.51	29	0.08	7.77
59	0.77	2.59	37	2.24	20.25
60	2.01	2.52	41	0.53	5.08
61	1.36	2.22	42	0.83	18.99
62	0.22	1.30	52	0.25	2.43
63	0.06	2.04			
64	0.55	3.23			
Overall (Mean) ± Standard deviation	0.76±0.64	2.92±2.59	Overall (Mean) ± Standard deviation	1.08±1.01	7.03±6.51

Table A.34 Summary of SpO2 percentage error of the age range of 31 to 40 years while horizontal moving.

Male subjects			Female subjects		
Subject no.	Proposed technique (PT)	Conventional method (CM)	Subject no.	Proposed technique (PT)	Conventional method (CM)
	SpO2 percentage error values in the unit of %			SpO2 percentage error values in the unit of %	
	Average			Average	
03	2.76	2.48	07	0.07	13.68
12	1.12	0.62	15	1.15	17.00
24	0.31	17.16	19	0.66	1.67
34	0.11	1.97	32	1.49	1.63
46	1.85	4.41	48	0.51	18.77
47	2.21	12.01	54	0.15	14.41
55	0.19	6.26	56	1.06	8.13
67	0.09	0.47	73	2.76	19.48
69	0.14	2.44			
Overall (Mean) ± Standard deviation	0.98±1.05	5.31±5.70	Overall (Mean) ± Standard deviation	0.98±0.87	11.85±7.22

Table A.35 Summary of SpO2 percentage error of the age range of 41 to 50 years while horizontal moving.

Male subjects			Female subjects		
Subject no.	Proposed technique (PT)	Conventional method (CM)	Subject no.	Proposed technique (PT)	Conventional method (CM)
	SpO2 percentage error values in the unit of %			SpO2 percentage error values in the unit of %	
	Average			Average	
16	1.08	2.28	01	0.14	1.63
20	0.95	5.25	10	2.41	3.94
30	3.19	1.63	25	0.39	1.46
33	0.58	3.01	43	0.97	6.70
35	0.17	1.83	53	0.23	0.28
49	0.21	1.08	68	0.50	8.16
66	0.38	15.88	72	0.63	6.29
71	0.16	5.26			
Overall (Mean) ± Standard deviation	0.84±1.01	4.53±4.85	Overall (Mean) ± Standard deviation	0.75±0.78	4.06±3.05

Table A.36 Summary of SpO2 percentage error of the age range of 51 to 60 years while horizontal moving.

Male subjects			Female subjects		
Subject no.	Proposed technique (PT)	Conventional method (CM)	Subject no.	Proposed technique (PT)	Conventional method (CM)
	SpO2 percentage error values in the unit of %			SpO2 percentage error values in the unit of %	
	Average			Average	
13	0.33	1.93	02	0.27	0.22
22	1.15	2.17	04	1.14	2.23
23	1.82	2.02	14	1.38	0.86
44	0.11	3.74	21	1.04	4.23
45	0.23	1.93	26	1.20	48.11
50	0.74	8.75	31	3.27	9.49
75	0.57	6.98	39	0.78	7.14
			65	0.20	6.47
			70	0.64	8.54
			74	3.62	7.34
Overall (Mean) ± Standard deviation	0.71±0.60	3.93±2.81	Overall (Mean) ± Standard deviation	1.35±1.17	9.46±13.96

Table A.37 Summary of SpO2 percentage error of the age range of 21 to 30 years while shivering.

Male subjects			Female subjects		
Subject no.	Proposed technique (PT)	Conventional method (CM)	Subject no.	Proposed technique (PT)	Conventional method (CM)
	SpO2 percentage error values in the unit of %			SpO2 percentage error values in the unit of %	
	Average			Average	
08	0.47	1.75	05	1.10	2.19
18	0.20	1.00	06	0.25	5.70
36	0.20	3.30	09	1.92	5.34
38	0.54	4.52	11	2.26	0.32
40	1.37	1.55	17	0.10	0.61
51	2.63	2.69	27	1.08	4.90
57	0.24	0.38	28	0.53	6.48
58	0.31	7.30	29	0.47	6.69
59	0.97	1.29	37	1.12	43.85
60	1.05	2.46	41	0.60	14.79
61	1.69	5.11	42	0.84	15.82
62	0.97	0.99	52	0.57	4.07
63	0.19	1.52			
64	0.64	10.58	Overall (Mean) ± Standard deviation	0.90±0.65	9.23±11.92
Overall (Mean) ± Standard deviation	0.82±0.70	3.17±2.86			

Table A.38 Summary of SpO2 percentage error of the age range of 31 to 40 years while shivering.

Male subjects			Female subjects		
Subject no.	Proposed technique (PT)	Conventional method (CM)	Subject no.	Proposed technique (PT)	Conventional method (CM)
	SpO2 percentage error values in the unit of %			SpO2 percentage error values in the unit of %	
	Average			Average	
03	2.34	1.45	07	0.26	6.76
12	1.22	0.69	15	1.05	50.04
24	1.34	10.67	19	0.21	5.69
34	0.68	2.33	32	1.23	0.45
46	1.55	0.98	48	0.18	2.95
47	1.57	17.18	54	0.16	13.55
55	0.37	3.08	56	1.69	5.68
67	0.28	0.78	73	2.70	16.51
69	1.42	2.04			
Overall (Mean) ± Standard deviation	1.20±0.65	4.36±5.72	Overall (Mean) ± Standard deviation	0.94±0.92	12.71±15.98

Table A.39 Summary of SpO2 percentage error of the age range of 41 to 50 years while shivering.

Male subjects			Female subjects		
Subject no.	Proposed technique (PT)	Conventional method (CM)	Subject no.	Proposed technique (PT)	Conventional method (CM)
	SpO2 percentage error values in the unit of %			SpO2 percentage error values in the unit of %	
	Average			Average	
16	0.54	1.71	01	0.12	1.45
20	0.99	5.40	10	1.89	1.03
30	2.07	0.80	25	0.14	3.51
33	0.25	1.41	43	0.91	21.06
35	0.15	2.45	53	0.34	1.71
49	0.29	1.37	68	0.63	1.40
66	0.37	9.51	72	0.96	9.04
71	0.22	9.89			
Overall (Mean) ± Standard deviation	0.61±0.65	3.24±3.75	Overall (Mean) ± Standard deviation	0.71±0.62	5.60±7.37

Table A.40 Summary of SpO2 percentage error of the age range of 51 to 60 years while shivering.

Male subjects			Female subjects		
Subject no.	Proposed technique (PT)	Conventional method (CM)	Subject no.	Proposed technique (PT)	Conventional method (CM)
	SpO2 percentage error values in the unit of %			SpO2 percentage error values in the unit of %	
	Average			Average	
13	0.53	0.82	02	0.41	2.16
22	0.92	3.86	04	0.46	1.29
23	1.58	0.88	14	1.28	0.23
44	0.63	14.33	21	1.14	3.01
45	0.08	1.16	26	1.24	65.21
50	0.85	17.11	31	0.21	9.49
75	0.76	12.55	39	0.60	6.17
			65	0.48	3.67
			70	0.54	9.38
			74	2.16	8.94
Overall (Mean) ± Standard deviation	0.77±0.46	7.24±7.14	Overall (Mean) ± Standard deviation	0.86±0.59	10.95±19.37

Table A.41 Summary of SpO2 percentage error of the age range of 21 to 30 years while vertical moving.

Male subjects			Female subjects		
Subject no.	Proposed technique (PT)	Conventional method (CM)	Subject no.	Proposed technique (PT)	Conventional method (CM)
	SpO2 percentage error values in the unit of %			SpO2 percentage error values in the unit of %	
	Average			Average	
08	0.89	1.73	05	1.10	1.18
18	0.22	0.24	06	0.88	8.59
36	0.49	5.14	09	2.03	4.96
38	0.71	6.60	11	0.78	4.13
40	0.94	2.74	17	0.28	0.73
51	2.63	1.66	27	1.12	9.49
57	0.28	1.04	28	0.41	6.23
58	0.33	0.52	29	0.41	4.76
59	0.84	0.82	37	1.02	21.17
60	0.94	2.04	41	0.91	8.60
61	1.08	7.22	42	0.79	18.88
62	1.33	0.52	52	0.91	2.89
63	0.60	1.86			
64	0.14	10.67			
Overall (Mean) ± Standard deviation	0.82±0.63	3.06±3.14	Overall (Mean) ± Standard deviation	0.89±0.45	7.63±6.44

Table A.42 Summary of SpO2 percentage error of the age range of 31 to 40 years while vertical moving.

Male subjects			Female subjects		
Subject no.	Proposed technique (PT)	Conventional method (CM)	Subject no.	Proposed technique (PT)	Conventional method (CM)
	SpO2 percentage error values in the unit of %			SpO2 percentage error values in the unit of %	
	Average			Average	
03	2.51	1.61	07	0.56	14.15
12	1.12	0.97	15	1.07	16.55
24	1.12	12.02	19	0.20	1.81
34	0.56	3.37	32	1.15	0.54
46	1.45	2.71	48	0.32	1.23
47	1.57	11.62	54	0.35	21.88
55	0.52	8.65	56	1.22	9.69
67	0.32	0.92	73	2.70	21.78
69	1.29	5.94			
Overall (Mean) ± Standard deviation	1.16±0.67	5.31±4.45	Overall (Mean) ± Standard deviation	0.95±0.81	10.95±9.00

Table A.43 Summary of SpO2 percentage error of the age range of 41 to 50 years while vertical moving.

Male subjects			Female subjects		
Subject no.	Proposed technique (PT)	Conventional method (CM)	Subject no.	Proposed technique (PT)	Conventional method (CM)
	SpO2 percentage error values in the unit of %			SpO2 percentage error values in the unit of %	
	Average			Average	
16	0.79	1.46	01	1.14	0.50
20	0.66	14.07	10	1.96	4.07
30	2.13	1.30	25	0.39	1.99
33	0.21	0.52	43	0.91	6.74
35	0.50	1.04	53	0.11	0.47
49	0.76	1.64	68	0.56	19.04
66	0.37	16.42	72	1.10	5.83
71	0.13	5.65			
Overall (Mean) ± Standard deviation	0.69±0.63	5.26±6.39	Overall (Mean) ± Standard deviation	0.88±0.61	5.52±6.45

Table A.44 Summary of SpO2 percentage error of the age range of 51 to 60 years while vertical moving.

Male subjects			Female subjects		
Subject no.	Proposed technique (PT)	Conventional method (CM)	Subject no.	Proposed technique (PT)	Conventional method (CM)
	SpO2 percentage error values in the unit of %			SpO2 percentage error values in the unit of %	
	Average			Average	
13	1.30	1.33	02	0.73	0.31
22	0.90	1.49	04	0.25	0.91
23	1.68	2.59	14	1.48	0.94
44	0.28	4.29	21	0.96	3.18
45	0.25	1.54	26	1.21	84.71
50	1.24	22.48	31	3.35	9.46
75	0.91	12.03	39	1.80	6.70
			65	0.63	6.46
			70	0.35	2.92
			74	2.49	12.15
Overall (Mean) ± Standard deviation	0.94±0.53	6.53±7.98	Overall (Mean) ± Standard deviation	1.32±0.99	12.77±25.58

Table A.45 Summary of SpO2 percentage error of the age range of 21 to 30 years while waving.

Male subjects			Female subjects		
Subject no.	Proposed technique (PT)	Conventional method (CM)	Subject no.	Proposed technique (PT)	Conventional method (CM)
	SpO2 percentage error values in the unit of %			SpO2 percentage error values in the unit of %	
	Average			Average	
08	0.48	1.10	05	1.55	3.11
18	0.10	0.53	06	0.69	4.14
36	0.15	3.05	09	1.47	5.88
38	1.29	9.69	11	0.28	1.12
40	0.95	2.00	17	0.46	0.93
51	2.23	2.46	27	0.42	3.41
57	0.73	0.64	28	0.25	4.40
58	0.97	0.51	29	0.19	7.57
59	0.71	2.82	37	1.38	38.80
60	1.81	6.19	41	0.62	5.60
61	0.60	2.57	42	1.01	13.52
62	1.70	1.52	52	0.86	2.43
63	0.66	0.90			
64	0.47	7.91			
Overall (Mean) ± Standard deviation	0.92±0.63	2.99±2.89	Overall (Mean) ± Standard deviation	0.76±0.49	7.58±10.39

Table A.46 Summary of SpO2 percentage error of the age range of 31 to 40 years while waving.

Male subjects			Female subjects		
Subject no.	Proposed technique (PT)	Conventional method (CM)	Subject no.	Proposed technique (PT)	Conventional method (CM)
	SpO2 percentage error values in the unit of %			SpO2 percentage error values in the unit of %	
	Average			Average	
03	2.21	1.61	07	0.47	9.38
12	1.45	1.20	15	1.21	47.56
24	1.21	9.68	19	0.54	1.67
34	0.18	0.72	32	1.09	2.48
46	1.26	1.78	48	0.36	0.89
47	1.33	15.34	54	0.09	17.03
55	0.56	5.89	56	1.09	5.06
67	0.62	0.70	73	2.85	7.12
69	1.81	3.41	Overall (Mean) ± Standard deviation	0.96±0.86	11.40±15.52
Overall (Mean) ± Standard deviation	1.18±0.64	4.48±5.03			

Table A.47 Summary of SpO2 percentage error of the age range of 41 to 50 years while waving.

Male subjects			Female subjects		
Subject no.	Proposed technique (PT)	Conventional method (CM)	Subject no.	Proposed technique (PT)	Conventional method (CM)
	SpO2 percentage error values in the unit of %			SpO2 percentage error values in the unit of %	
	Average			Average	
16	0.19	1.03	01	0.30	1.41
20	0.89	4.80	10	1.21	4.64
30	2.87	1.35	25	0.94	3.60
33	0.16	5.54	43	0.96	7.65
35	0.17	5.05	53	0.16	0.81
49	0.64	1.07	68	0.55	7.30
66	0.70	22.40	72	1.00	10.16
71	0.07	7.87	Overall (Mean) ± Standard deviation	0.73±0.40	5.08±3.45
Overall (Mean) ± Standard deviation	0.71±0.92	6.14±7.03			

Table A.48 Summary of SpO2 percentage error of the age range of 51 to 60 years while waving.

Male subjects			Female subjects		
Subject no.	Proposed technique (PT)	Conventional method (CM)	Subject no.	Proposed technique (PT)	Conventional method (CM)
	SpO2 percentage error values in the unit of %			SpO2 percentage error values in the unit of %	
	Average			Average	
13	0.26	0.73	02	0.09	0.65
22	1.00	2.12	04	0.63	1.78
23	1.06	5.16	14	1.27	1.25
44	0.64	5.05	21	0.98	4.42
45	0.14	1.95	26	1.19	43.25
50	1.51	5.00	31	0.73	11.57
75	0.74	6.86	39	0.48	7.63
			65	0.60	6.87
			70	0.30	1.48
			74	2.30	11.31
Overall (Mean) ± Standard deviation	0.77±0.48	3.84±2.23	Overall (Mean) ± Standard deviation	0.86±0.63	9.02±12.70

Table A.49 Comparison of SpO2 values of the age range of 21 to 30 years while bending for the dedicated techniques.

Subject no.	Compared techniques				
	PT[1]	CM[2]	DST[3]	ICA[4]	CFC[5]
	SpO2 values in the unit of %				
	Average ± Standard deviation				
Male subjects					
08	93.82±0.24	91.68±0.21	89.02±0.15	89.16±17.57	92.06±0.36
18	97.84±0.08	91.74±0.14	89.24±0.10	83.97±8.90	91.99±0.12
36	99.34±0.14	89.79±4.98	92.83±0.10	89.25±67.48	90.78±3.00
38	96.30±0.08	92.70±1.37	91.81±0.15	87.71±10.99	93.34±1.31
40	94.54±0.10	88.45±0.87	89.75±0.12	104.91±28.70	88.37±1.10
51	96.10±1.16	84.73±13.84	92.41±0.35	53.59±63.18	91.31±2.14
57	94.78±0.21	90.81±3.36	91.34±0.10	61.60±31.68	91.31±2.94
58	93.72±0.18	92.08±1.92	90.52±0.43	76.51±10.06	94.19±0.69
59	98.49±0.10	93.72±0.52	92.96±0.12	76.02±37.23	93.80±0.47
60	93.69±0.44	87.04±3.86	92.58±0.19	40.47±42.56	88.72±1.83
61	97.43±0.29	88.95±0.47	93.05±0.10	78.60±9.81	92.20±0.63
62	96.07±0.49	94.22±0.97	91.63±0.65	72.58±25.88	94.58±1.47
63	97.86±0.08	91.40±1.68	92.19±0.10	74.83±92.70	93.76±1.94
64	98.41±0.24	95.79±6.46	93.86±0.12	48.33±106.19	93.81±8.20
Overall (Mean)	96.31±1.96	90.93±2.95	91.66±1.50	74.11±17.74	92.16±1.94
Female subjects					
05	93.40±0.14	90.46±0.70	92.83±0.10	90.82±2.85	85.34±0.37
06	94.24±0.09	86.86±1.61	96.00±0.12	91.62±1.39	85.06±0.76
09	98.37±0.27	90.13±1.43	90.95±0.15	74.35±4.18	93.12±1.96
11	99.83±0.07	91.90±1.31	91.55±0.18	77.60±64.30	92.60±3.55
17	97.86±0.07	92.88±0.59	91.25±0.19	116.39±51.98	92.59±1.51
27	95.76±0.21	92.46±0.54	91.51±0.49	95.46±45.27	93.79±0.57
28	96.44±0.29	92.73±1.20	89.79±0.12	65.08±45.83	93.43±0.83
29	97.88±0.12	82.57±5.79	92.15±0.29	62.31±15.42	89.11±2.44
37	95.71±0.09	88.05±2.14	91.93±0.32	127.48±84.34	89.73±1.99
41	98.50±0.16	84.18±9.69	92.41±0.32	64.85±12.14	90.95±8.23
42	97.20±0.07	79.60±4.86	94.55±0.49	92.29±39.79	74.68±11.75
52	94.96±0.08	93.55±0.28	91.42±0.10	83.70±5.55	93.33±0.38
Overall (Mean)	96.68±1.92	88.78±4.59	92.19±1.66	86.83±20.18	89.48±5.56

1 – PT refers to the proposed LEDs-driving technique, 2 – CM refers to the conventional LEDs-emitting method,
3 – DST stands for discrete saturation transform, 4 – ICA stands for independent component analysis,
5 – CFC stands for compression of Fourier coefficients.

Table A.50 Comparison of SpO2 values of the age range of 31 to 40 years while bending for the dedicated techniques.

Subject no.	Compared techniques				
	PT[1]	CM[2]	DST[3]	ICA[4]	CFC[5]
	SpO2 values in the unit of %				
	Average ± Standard deviation				
Male subjects					
03	96.00±0.14	91.61±0.77	89.45±0.10	83.65±0.80	85.28±0.27
12	96.93±0.14	89.23±3.21	91.04±0.24	74.01±25.02	88.96±2.92
24	98.47±0.09	82.32±1.68	92.96±0.12	117.90±65.60	65.54±15.88
34	99.54±0.15	94.15±0.67	89.88±0.15	90.13±11.99	95.40±0.29
46	98.16±0.29	85.93±1.64	92.32±0.12	74.78±18.42	87.18±0.87
47	97.80±0.14	79.97±3.92	92.70±0.18	62.23±134.33	92.06±0.63
55	95.87±0.08	88.61±0.85	91.25±0.12	84.90±10.87	87.94±1.06
67	93.93±0.10	92.61±0.39	90.05±0.10	83.57±4.51	93.17±0.15
69	93.15±0.23	92.21±0.52	90.91±0.10	154.99±177.39	93.23±1.00
Overall (Mean)	96.65±2.12	88.52±4.88	91.17±1.27	91.80±28.15	87.64±8.93
Female subjects					
07	98.62±0.15	79.73±3.87	92.02±0.26	175.18±183.23	130.44±104.69
15	97.28±0.10	81.51±2.80	93.77±0.18	68.79±8.78	82.44±2.25
19	96.80±0.22	92.96±1.16	91.34±0.18	123.20±39.25	94.14±0.94
32	96.96±0.30	84.98±4.68	89.79±0.12	118.85±73.34	86.65±4.67
48	97.97±0.12	91.21±1.18	91.25±0.19	123.78±59.02	90.12±2.59
54	99.54±0.45	84.63±1.52	93.95±0.15	101.12±24.17	88.50±1.61
56	97.66±0.19	64.55±30.76	91.81±0.15	54.07±89.48	88.83±2.79
73	99.28±0.83	88.81±4.14	92.53±0.24	134.99±147.22	91.08±3.18
Overall (Mean)	98.01±1.04	83.55±8.93	92.06±1.37	112.50±38.12	94.03±15.10

Table A.51 Comparison of SpO2 values of the age range of 41 to 50 years while bending for the dedicated techniques.

Subject no.	Compared techniques				
	PT[1]	CM[2]	DST[3]	ICA[4]	CFC[5]
	SpO2 values in the unit of %				
	Average ± Standard deviation				
Male subjects					
16	95.90±0.39	91.13±0.80	90.01±0.19	85.13±6.65	92.20±0.54
20	95.95±0.27	87.03±0.60	92.36±0.19	106.20±87.18	91.67±1.58
30	93.18±0.67	90.16±2.23	91.21±0.10	59.77±30.79	91.49±1.79
33	99.80±0.13	86.06±4.46	92.02±0.21	54.88±13.64	89.33±2.00
35	94.43±0.03	91.02±0.44	92.19±0.38	90.45±25.03	91.23±1.68
49	95.90±0.24	92.61±0.59	90.56±0.10	90.25±4.24	93.10±0.62
66	97.59±0.16	85.98±2.20	93.48±0.18	44.72±40.92	92.18±3.68
71	97.26±0.13	91.27±1.62	91.38±0.15	92.07±81.92	92.16±0.66
Overall (Mean)	96.25±2.02	89.41±2.63	91.65±1.10	77.93±21.79	91.67±1.10
Female subjects					
01	99.24±0.09	91.46±0.63	89.41±0.46	73.22±23.89	86.12±1.16
10	96.50±0.12	93.13±0.43	91.55±0.18	83.23±10.28	93.60±0.45
25	95.42±0.02	91.77±1.13	90.44±0.29	94.16±33.80	92.46±1.25
43	97.13±0.10	86.75±3.45	93.90±0.10	106.82±72.71	85.64±2.69
53	97.10±0.07	91.83±1.19	90.91±0.10	89.50±217.09	93.12±0.57
68	99.32±0.50	84.36±4.49	92.23±0.15	90.86±61.81	85.91±4.50
72	97.49±0.20	85.81±1.78	92.66±0.21	3.12±99.50	90.52±3.42
Overall (Mean)	97.46±1.41	89.30±3.53	91.59±1.50	77.27±34.26	89.62±3.63

Table A.52 Comparison of SpO2 values of the age range of 51 to 60 years while bending for the dedicated techniques.

Subject no.	Compared techniques				
	PT[1]	CM[2]	DST[3]	ICA[4]	CFC[5]
	SpO2 values in the unit of %				
	Average ± Standard deviation				
Male subjects					
13	96.76±0.10	92.32±0.47	90.74±0.10	83.90±6.59	92.52±0.23
22	98.96±0.41	91.17±0.83	90.56±0.10	81.38±14.93	93.05±0.70
23	96.14±0.09	90.28±0.38	90.56±0.10	73.71±27.78	93.02±0.55
44	98.37±0.03	85.84±2.36	93.77±0.10	112.83±91.80	86.38±28.94
45	96.42±0.11	91.78±0.45	92.96±0.12	62.04±123.49	92.69±1.53
50	98.35±0.23	87.82±2.85	93.26±0.23	20.15±43.22	93.50±1.28
75	94.95±0.12	86.92±3.87	92.66±0.10	143.99±148.99	93.51±1.49
Overall (Mean)	97.13±1.46	89.45±2.56	92.08±1.40	82.57±38.92	92.09±2.55
Female subjects					
02	95.40±0.14	89.25±1.84	91.68±0.32	86.64±3.04	85.59±1.87
04	95.28±0.11	92.21±1.19	94.33±0.18	90.00±1.82	85.33±1.21
14	97.25±0.20	91.27±0.67	91.38±0.10	83.65±4.72	92.20±0.48
21	95.71±0.23	84.24±2.19	92.28±0.18	73.86±37.17	92.37±1.72
26	97.14±0.13	67.55±23.43	93.73±0.15	145.65±95.94	60.96±61.98
31	94.68±0.13	85.00±0.02	91.12±0.11	85.00±0.00	85.00±0.01
39	98.97±0.11	89.59±0.59	91.55±0.18	-100.32±390.19	90.56±0.71
65	99.49±0.48	81.61±8.96	92.23±0.15	102.09±61.84	82.01±6.50
70	97.19±0.16	91.09±3.59	91.29±0.12	88.75±6.37	90.96±4.70
74	96.34±0.21	85.00±1.10	92.66±0.21	80.54±11.10	84.50±1.29
Overall (Mean)	96.74±1.58	85.68±7.30	92.23±1.08	73.59±64.29	84.95±9.19

Table A.53 Comparison of SpO2 values of the age range of 21 to 30 years while horizontal moving for the dedicated techniques.

Subject no.	Compared techniques				
	PT[1]	CM[2]	DST[3]	ICA[4]	CFC[5]
	SpO2 values in the unit of %				
	Average ± Standard deviation				
Male subjects					
08	94.42±0.06	93.47±0.55	89.88±0.37	85.48±14.74	92.67±0.33
18	97.98±0.04	90.85±0.64	89.58±0.44	63.44±53.10	91.41±0.97
36	99.18±0.05	83.32±3.77	93.35±0.10	120.68±50.51	84.10±1.29
38	96.38±0.33	93.07±1.05	92.06±0.10	5.93±77.44	95.34±0.40
40	95.52±0.13	87.38±1.32	89.54±0.12	51.40±36.48	88.90±0.32
51	96.18±0.18	94.09±0.72	91.89±0.12	80.05±4.85	94.33±0.64
57	95.08±0.17	94.20±0.94	91.55±0.18	92.11±33.49	95.12±0.99
58	92.86±0.19	93.08±0.29	89.79±0.12	90.29±8.79	93.47±0.55
59	99.30±0.10	92.12±1.81	92.66±0.21	36.01±151.87	92.91±2.12
60	91.30±0.98	90.96±2.19	92.70±0.35	104.80±67.99	92.25±1.08
61	97.34±0.13	91.52±1.48	90.69±0.23	80.64±3.19	93.08±0.35
62	94.49±0.19	92.38±0.84	91.55±0.18	76.49±11.56	92.84±0.90
63	97.48±0.09	95.18±0.82	91.21±0.10	103.28±63.28	93.27±0.63
64	96.95±0.22	90.91±2.17	93.43±0.12	149.51±174.60	96.70±0.49
Overall (Mean)	96.03±2.28	91.61±3.07	91.42±1.36	81.44±35.54	92.60±3.07
Female subjects					
05	94.04±0.09	93.80±0.48	92.11±0.32	89.24±2.56	85.53±0.51
06	98.56±0.09	90.05±2.67	97.03±0.12	93.01±0.68	85.12±0.43
09	97.06±0.10	88.18±1.55	90.35±0.18	73.18±6.48	92.05±1.77
11	99.42±0.16	93.67±0.25	91.38±0.15	98.90±33.82	93.67±1.06
17	97.98±0.12	92.74±0.25	90.01±0.12	88.34±5.46	92.49±0.29
27	94.43±0.19	87.15±4.98	91.85±0.41	69.10±20.57	93.56±1.04
28	95.18±0.27	85.69±2.01	90.48±0.23	76.63±25.70	88.81±3.15
29	98.72±0.09	85.83±3.77	90.86±0.19	74.82±7.83	93.49±1.23
37	95.48±0.17	74.85±13.86	92.11±0.19	61.13±25.66	85.55±5.66
41	98.64±0.10	87.35±2.73	92.41±0.18	92.48±79.73	90.48±1.70
42	97.00±0.07	76.12±4.87	93.69±0.10	84.58±61.53	87.24±1.21
52	94.76±0.19	94.00±0.20	90.44±0.12	85.16±2.26	93.34±1.13
Overall (Mean)	96.77±1.91	87.45±6.40	91.89±1.94	82.21±11.22	90.11±3.47

Table A.54 Comparison of SpO2 values of the age range of 31 to 40 years while horizontal moving for the dedicated techniques.

Subject no.	Compared techniques				
	PT[1]	CM[2]	DST[3]	ICA[4]	CFC[5]
	SpO2 values in the unit of %				
	Average ± Standard deviation				
Male subjects					
03	96.64±0.09	90.86±0.61	89.97±0.24	83.72±0.85	85.20±0.55
12	97.09±0.20	94.25±0.98	91.38±0.37	75.52±23.67	94.69±0.61
24	98.48±0.17	76.98±2.40	93.30±0.10	66.07±15.46	78.31±6.04
34	98.94±0.12	90.25±1.81	89.75±0.19	74.47±10.79	91.51±1.47
46	97.56±0.09	88.88±2.28	92.41±0.10	110.77±54.29	94.16±0.68
47	97.24±0.09	82.73±3.00	92.23±010	48.37±20.15	88.82±1.16
55	96.18±0.21	87.76±1.45	91.38±0.21	74.65±10.65	80.57±24.33
67	93.57±0.03	91.37±0.35	89.28±0.10	84.69±6.46	91.57±0.46
69	93.15±0.11	90.70±0.83	90.65±0.19	85.72±13.42	90.72±0.83
Overall (Mean)	96.54±1.99	88.20±5.25	91.15±1.35	78.22±16.81	88.40±5.82
Female subjects					
07	97.92±0.06	78.83±2.48	91.85±0.18	63.05±1.12	84.58±0.59
15	97.44±0.07	77.21±1.88	93.69±0.10	61.78±14.17	86.89±1.37
19	96.46±0.12	92.23±0.45	89.75±0.12	77.52±18.89	91.44±0.78
32	95.98±0.12	91.01±1.25	89.45±0.37	119.42±54.10	90.76±1.61
48	97.42±0.37	76.24±21.59	90.82±0.12	82.95±118.54	85.80±2.84
54	99.68±0.11	81.15±6.93	93.77±0.10	30.73±31.61	90.29±0.96
56	98.48±0.10	85.77±1.51	90.78±0.23	81.32±35.12	91.59±1.17
73	96.94±0.09	76.70±15.46	93.18±0.12	53.64±39.61	83.48±3.33
Overall (Mean)	97.54±1.17	82.39±6.48	91.66±1.73	71.30±25.93	88.10±3.29

Table A.55 Comparison of SpO2 values of the age range of 41 to 50 years while horizontal moving for the dedicated techniques.

Subject no.	Compared techniques				
	PT[1]	CM[2]	DST[3]	ICA[4]	CFC[5]
	SpO2 values in the unit of %				
	Average ± Standard deviation				
Male subjects					
16	95.02±0.10	91.00±0.44	89.88±0.15	156.64±155.31	91.90±0.35
20	95.46±0.08	88.75±0.36	90.35±0.10	83.25±9.49	92.20±0.30
30	93.00±0.43	91.88±1.24	90.35±0.10	83.67±3.10	93.45±0.37
33	96.60±0.14	90.43±0.95	92.58±0.12	89.39±32.01	90.40±0.60
35	94.70±0.13	91.03±1.52	92.23±0.21	58.37±8.85	92.90±1.58
49	95.54±0.08	92.82±0.17	90.74±0.10	86.27±3.09	93.16±0.33
66	98.10±0.19	81.96±13.64	94.20±0.10	-19.11±185.56	86.99±3.03
71	97.22±0.04	88.99±1.18	91.08±0.12	40.40±50.74	89.21±2.21
Overall (Mean)	95.70±1.59	89.61±3.37	91.43±1.46	72.36±49.88	91.28±2.25
Female subjects					
01	99.72±0.11	90.87±0.40	90.44±0.24	85.17±3.69	85.73±0.82
10	95.77±0.14	88.31±0.99	92.02±0.15	66.27±8.51	90.33±0.34
25	95.06±0.07	91.75±0.37	90.39±0.12	25.05±133.04	91.90±0.85
43	97.20±0.07	85.26±2.86	92.70±0.10	89.31±74.95	87.79±4.63
53	97.29±0.21	93.00±0.23	91.89±0.12	64.52±54.42	93.96±0.44
68	99.54±0.07	85.56±4.50	90.61±0.12	89.55±8.72	92.20±0.81
72	97.72±0.20	87.69±2.63	92.41±0.18	78.96±31.71	90.70±1.12
Overall (Mean)	97.47±1.74	88.92±3.03	91.49±0.99	71.26±22.80	90.37±2.79

Table A.56 Comparison of SpO2 values of the age range of 51 to 60 years while horizontal moving for the dedicated techniques.

Subject no.	Compared techniques				
	PT[1]	CM[2]	DST[3]	ICA[4]	CFC[5]
	SpO2 values in the unit of %				
	Average ± Standard deviation				
Male subjects					
13	95.76±0.37	91.31±1.22	90.86±0.62	84.97±8.81	91.87±0.62
22	98.58±0.13	91.26±0.63	91.04±0.91	100.90±22.45	89.00±0.91
23	95.66±0.09	91.03±1.20	91.89±1.90	29.28±81.90	92.62±1.90
44	98.30±0.08	90.18±2.62	93.60±2.54	74.63±30.23	82.58±2.54
45	96.55±0.18	93.28±1.86	92.88±1.66	142.67±138.51	94.66±1.66
50	98.32±0.14	84.94±2.34	93.30±3.27	-54.94±184.46	86.50±3.27
75	95.26±0.22	87.53±2.79	92.58±3.83	52.28±34.16	88.43±3.83
Overall (Mean)	96.92±1.44	89.93±2.79	92.31±4.09	61.40±62.64	89.38±4.09
Female subjects					
02	96.70±0.14	93.27±0.27	91.16±0.09	85.14±1.43	85.41±0.09
04	96.12±0.18	92.89±0.48	94.37±0.30	88.53±0.27	85.24±0.30
14	97.26±0.19	93.09±0.71	91.16±1.03	80.72±32.19	92.66±1.03
21	96.05±0.20	90.52±0.65	92.96±0.36	61.14±8.62	94.25±0.36
26	97.65±0.09	48.11±10.33	92.66±4.24	155.87±122.03	83.32±4.24
31	97.71±0.08	85.09±0.06	91.13±0.06	84.98±0.03	85.10±0.06
39	99.84±0.10	87.99±1.73	91.81±1.07	69.66±13.97	89.84±1.07
65	98.52±0.09	88.46±0.68	92.92±0.66	99.20±49.96	91.76±0.66
70	96.78±0.30	92.99±10.61	92.02±0.39	74.47±45.24	94.04±0.39
74	92.70±0.46	87.33±2.77	92.28±4.65	115.77±72.26	88.42±4.65
Overall (Mean)	96.93±1.88	85.97±13.61	92.25±4.08	91.55±27.26	89.00±4.08

Table A.57 Comparison of SpO2 values of the age range of 21 to 30 years while shivering for the dedicated techniques.

Subject no.	Compared techniques				
	PT[1]	CM[2]	DST[3]	ICA[4]	CFC[5]
	SpO2 values in the unit of %				
	Average ± Standard deviation				
Male subjects					
08	94.53±0.12	91.01±0.96	88.90±0.44	75.16±25.02	91.97±0.79
18	98.02±0.08	93.22±0.38	89.84±0.18	87.19±1.05	93.10±0.27
36	98.84±0.09	89.01±2.02	92.83±0.23	56.18±146.71	91.62±4.81
38	96.37±0.13	89.84±1.18	92.06±0.10	83.98±24.57	94.67±0.33
40	96.07±0.12	89.73±0.23	89.71±0.10	89.91±23.86	89.65±1.02
51	96.62±0.20	95.13±0.12	92.66±0.10	71.46±25.65	95.31±0.35
57	94.94±0.11	93.53±0.24	91.29±0.12	83.46±7.98	94.61±0.97
58	93.22±0.32	86.72±4.23	89.97±0.12	109.26±84.28	93.04±0.84
59	99.49±0.09	93.35±1.21	92.66±0.15	60.90±93.52	95.29±0.35
60	94.14±0.45	91.94±2.05	91.72±0.24	98.83±49.28	94.59±0.75
61	97.01±0.26	88.53±4.50	91.89±0.12	74.18±17.32	93.15±1.34
62	95.55±0.16	92.75±1.04	92.58±0.19	69.73±9.83	94.05±0.63
63	97.63±0.16	91.92±1.38	92.66±0.15	76.95±16.71	95.58±0.52
64	98.11±0.04	84.00±6.98	93.90±0.10	60.56±43.18	95.99±0.76
Overall (Mean)	96.47±1.85	90.76±3.02	91.62±1.47	78.41±14.96	93.76±1.78
Female subjects					
05	93.40±0.07	92.56±0.55	93.35±0.18	91.57±0.58	85.31±0.06
06	95.88±0.11	89.96±4.33	96.00±0.12	91.45±0.22	85.01±0.05
09	97.47±0.19	89.40±1.34	90.27±0.18	67.42±11.02	93.66±0.67
11	96.88±0.44	94.43±0.21	91.89±0.12	80.58±6.49	95.09±0.64
17	97.98±0.02	93.01±0.14	90.09±0.10	91.25±2.59	92.82±0.26
27	94.99±0.15	88.99±3.25	91.46±0.19	75.16±11.75	93.24±0.87
28	95.74±0.24	87.64±1.78	90.74±0.15	76.75±10.80	87.62±0.86
29	99.18±0.08	86.84±1.71	91.55±0.18	71.36±22.83	89.67±0.72
37	96.58±0.04	52.70±33.62	92.62±0.10	12.98±88.26	89.08±2.10
41	98.71±0.09	78.41±12.66	92.23±0.21	34.49±49.67	93.31±0.89
42	97.01±0.02	79.09±3.78	94.46±0.12	111.60±73.39	79.38±1.75
52	95.54±0.11	88.03±1.67	91.98±0.10	29.34±83.24	92.77±1.54
Overall (Mean)	96.61±1.63	85.09±11.33	92.22±1.72	69.50±29.33	89.75±4.69

Table A.58 Comparison of SpO2 values of the age range of 31 to 40 years while shivering for the dedicated techniques.

Subject no.	Compared techniques				
	PT[1]	CM[2]	DST[3]	ICA[4]	CFC[5]
	SpO2 values in the unit of %				
	Average ± Standard deviation				
Male subjects					
03	96.24±0.09	91.82±0.74	89.75±0.36	83.37±0.65	85.38±0.42
12	97.19±0.24	94.48±0.44	91.55±0.18	83.28±10.86	94.57±1.21
24	99.50±0.13	83.02±2.48	92.88±0.10	46.74±43.67	89.02±1.88
34	98.24±0.15	93.91±1.04	90.09±0.15	84.17±10.89	93.45±1.18
46	97.86±0.06	93.89±0.30	92.23±0.10	56.44±38.47	95.10±0.55
47	97.88±0.14	77.87±7.12	92.62±0.10	-3.90±112.05	91.13±5.23
55	96.40±0.29	90.99±2.41	91.25±0.24	66.16±17.01	94.33±1.24
67	93.90±0.20	92.26±0.66	89.84±0.10	99.19±38.87	92.96±0.22
69	94.35±0.08	91.07±1.16	90.44±0.19	95.11±15.99	92.54±0.31
Overall (Mean)	96.84±1.83	89.92±5.67	91.18±1.21	67.84±32.01	92.05±3.13
Female subjects					
07	98.23±0.07	85.15±3.56	92.75±0.24	70.30±9.38	89.77±2.04
15	97.34±0.09	63.76±61.73	94.20±0.23	90.84±97.29	86.08±4.48
19	96.90±0.05	88.45±1.97	90.95±0.34	93.42±41.48	90.07±5.07
32	96.23±0.09	92.10±0.22	89.28±0.10	85.73±6.69	86.08±12.85
48	97.92±0.25	96.64±0.78	90.78±0.10	-40.87±272.31	94.19±0.33
54	99.65±0.14	81.97±5.94	93.95±0.15	-65.57±258.15	92.15±1.82
56	99.10±0.11	88.05±5.07	92.79±0.19	73.06±33.77	93.44±0.16
73	97.00±0.07	79.53±3.89	93.00±0.12	209.43±177.97	92.36±1.95
Overall (Mean)	97.80±1.16	84.46±9.96	92.21±1.71	64.54±85.45	90.52±3.12

Table A.59 Comparison of SpO2 values of the age range of 41 to 50 years while shivering for the dedicated techniques.

Subject no.	Compared techniques				
	PT[1]	CM[2]	DST[3]	ICA[4]	CFC[5]
	SpO2 values in the unit of %				
	Average ± Standard deviation				
Male subjects					
16	95.54±0.11	91.54±1.05	90.14±0.10	85.91±9.36	92.82±0.34
20	95.42±0.09	89.09±4.19	92.62±0.38	64.72±116.34	94.40±0.79
30	94.07±0.12	94.02±0.12	91.34±0.10	76.64±17.90	94.22±0.16
33	97.40±0.11	91.92±0.71	91.72±0.12	81.76±10.05	94.15±0.28
35	94.82±0.18	95.01±0.29	91.16±0.21	189.22±249.49	93.84±0.43
49	95.61±0.16	93.09±0.26	90.95±0.15	70.82±17.78	93.87±0.28
66	98.10±0.06	85.18±4.54	93.35±0.10	45.10±133.09	89.90±3.52
71	97.16±0.06	84.65±4.42	91.98±0.10	78.88±13.55	93.40±2.85
Overall (Mean)	96.01±1.39	91.41±3.91	91.66±1.00	86.63±43.37	93.33±1.47
Female subjects					
01	99.48±0.11	91.33±1.07	90.48±0.38	85.22±0.98	85.89±0.92
10	96.27±0.27	90.98±0.70	92.23±0.15	70.89±10.97	93.56±1.28
25	95.42±0.17	89.83±0.67	91.04±0.12	102.47±38.88	91.71±0.61
43	97.14±0.06	72.14±23.73	93.56±0.10	62.23±41.94	92.31±1.07
53	97.78±0.15	91.48±1.49	90.99±0.23	111.61±56.69	93.43±0.55
68	99.67±0.09	94.46±0.73	90.82±0.12	90.82±5.66	93.49±0.33
72	98.03±0.05	85.11±3.57	92.23±0.10	74.17±3.11	94.12±0.51
Overall (Mean)	97.68±1.57	87.90±7.50	91.62±1.10	85.34±17.71	92.07±2.85

Table A.60 Comparison of SpO2 values of the age range of 51 to 60 years while shivering for the dedicated techniques.

Subject no.	Compared techniques				
	PT[1]	CM[2]	DST[3]	ICA[4]	CFC[5]
	SpO2 values in the unit of %				
	Average ± Standard deviation				
Male subjects					
13	96.50±0.18	92.35±0.19	90.65±0.12	82.25±2.60	92.67±0.36
22	98.80±0.07	89.68±1.35	90.78±0.10	99.01±38.48	92.50±0.99
23	95.90±0.10	93.72±0.19	91.89±0.12	82.22±15.14	93.88±0.20
44	98.80±0.14	80.26±0.81	93.95±0.10	64.77±103.97	86.94±6.54
45	96.82±0.09	94.01±0.35	93.00±0.29	82.01±78.24	94.72±0.38
50	98.43±0.14	77.16±4.69	92.92±0.10	95.71±111.09	93.53±3.07
75	95.45±0.18	82.28±4.97	92.02±0.10	56.58±84.53	94.92±0.61
Overall (Mean)	97.24±1.42	87.07±7.01	92.17±1.21	80.37±15.28	92.74±2.72
Female subjects					
02	96.84±0.09	91.33±0.81	91.16±0.15	84.95±0.34	84.42±1.11
04	94.60±0.07	93.78±0.64	94.12±0.10	88.47±0.48	85.04±0.20
14	97.15±0.17	92.27±0.32	91.38±0.15	87.43±23.21	92.80±0.06
21	96.14±0.16	91.67±0.47	92.53±0.12	80.86±22.78	94.01±0.30
26	97.68±0.18	32.26±54.98	92.15±0.12	20.34±53.88	89.36±1.80
31	94.82±0.13	85.09±0.24	91.24±0.07	84.87±0.19	85.28±0.14
39	99.66±0.10	88.91±0.85	91.85±0.23	83.76±12.63	91.19±0.48
65	98.79±0.02	91.11±1.86	92.06±0.18	81.52±17.35	93.88±1.43
70	97.94±0.11	85.08±0.91	92.23±0.21	68.33±8.78	93.82±1.35
74	94.10±0.43	85.82±3.75	92.62±0.41	45.44±83.82	91.57±2.26
Overall (Mean)	96.77±1.85	83.73±18.36	92.13±0.87	72.60±22.44	90.14±3.88

Table A.61 Comparison of SpO2 values of the age range of 21 to 30 years while vertical moving for the dedicated techniques.

Subject no.	Compared techniques				
	PT[1]	CM[2]	DST[3]	ICA[4]	CFC[5]
	SpO2 values in the unit of %				
	Average ± Standard deviation				
Male subjects					
08	94.93±0.12	91.03±0.88	89.88±0.55	82.36±14.12	91.98±0.60
18	97.99±0.02	92.46±0.21	89.62±0.10	88.82±3.37	92.75±0.06
36	99.13±0.10	87.29±2.25	93.18±0.12	49.76±97.15	87.89±2.60
38	96.53±0.26	91.19±6.69	92.11±0.12	47.06±53.95	94.56±1.38
40	95.66±0.16	88.64±1.76	90.27±0.44	48.23±52.26	98.56±14.66
51	96.62±0.09	94.17±0.58	92.28±0.18	49.72±62.88	94.82±0.38
57	94.97±0.17	93.91±1.06	91.81±0.34	125.74±91.95	94.73±1.25
58	93.14±0.16	93.11±0.44	90.14±0.18	87.40±2.93	93.45±0.20
59	99.36±0.09	95.35±0.38	93.05±0.18	101.17±44.11	96.02±0.23
60	94.05±0.42	92.33±0.98	91.63±0.23	76.51±17.59	94.25±0.82
61	97.62±0.13	86.57±2.85	92.41±0.18	187.82±293.43	89.42±2.66
62	95.89±0.18	94.06±0.33	90.65±0.12	72.54±11.87	94.24±0.45
63	98.06±0.10	91.75±1.57	92.79±0.19	113.19±57.00	94.22±1.06
64	97.61±0.13	83.92±6.52	94.07±0.12	35.74±128.67	95.12±2.01
Overall (Mean)	96.54±1.87	91.13±3.34	91.71±1.39	83.29±40.39	93.71±2.65
Female subjects					
05	93.40±0.07	93.52±0.61	92.79±0.12	91.07±1.84	85.15±0.15
06	96.48±0.18	87.21±3.60	96.21±0.12	91.86±0.76	84.99±0.16
09	97.37±0.10	89.77±1.49	90.74±0.10	83.22±12.72	90.99±1.87
11	99.90±0.11	90.24±1.84	91.42±0.23	163.05±134.55	89.86±1.32
17	98.16±0.09	92.91±0.32	90.09±0.10	87.97±11.30	92.65±0.34
27	94.96±0.18	84.64±2.49	92.15±0.32	31.71±142.59	92.35±0.75
28	95.86±0.12	87.87±2.36	90.78±0.10	102.57±55.22	87.92±3.24
29	99.11±0.07	88.64±2.31	91.29±0.32	63.65±33.66	92.06±0.77
37	96.67±0.08	73.99±21.53	92.41±0.10	87.51±56.65	80.13±6.45
41	99.01±0.09	84.11±1.63	92.15±0.19	79.06±3.39	86.37±1.21
42	96.96±0.05	76.21±2.75	94.50±0.12	58.84±25.88	76.66±1.51
52	95.86±0.11	94.42±0.27	91.08±0.19	82.28±2.04	94.60±0.52
Overall (Mean)	96.98±1.87	86.96±6.42	92.13±1.73	85.23±30.93	87.81±5.42

Table A.62 Comparison of SpO2 values of the age range of 31 to 40 years while vertical moving for the dedicated techniques.

Subject no.	Compared techniques				
	PT[1]	CM[2]	DST[3]	ICA[4]	CFC[5]
	SpO2 values in the unit of %				
	Average ± Standard deviation				
Male subjects					
03	96.40±0.14	91.67±0.79	90.09±0.21	84.23±1.67	85.68±0.49
12	97.10±0.09	94.80±0.73	91.72±0.12	93.24±18.94	96.02±0.55
24	99.28±0.31	81.76±1.09	93.30±0.10	62.28±2.69	84.04±1.61
34	99.46±0.21	88.68±0.80	89.75±0.12	107.07±70.22	89.03±1.41
46	97.96±0.09	90.45±0.60	92.36±0.12	80.78±4.06	88.63±0.50
47	97.88±0.16	83.10±4.76	92.53±0.19	42.52±52.32	93.14±1.57
55	96.54±0.04	85.53±1.00	91.55±0.28	76.06±34.15	85.72±1.33
67	93.96±0.06	92.56±0.10	89.79±0.12	84.82±19.61	92.73±0.30
69	94.23±0.24	87.45±1.64	91.21±0.10	82.14±38.75	87.45±2.28
Overall (Mean)	96.98±1.95	88.44±4.40	91.37±1.27	79.24±18.31	89.16±4.01
Female subjects					
07	98.52±0.27	78.40±4.59	92.41±0.41	65.02±13.23	86.84±0.78
15	97.36±0.05	77.63±11.85	93.30±0.34	52.61±19.75	86.33±3.60
19	96.99±0.22	92.10±1.06	90.18±0.24	84.13±4.68	93.16±1.40
32	96.31±0.28	92.09±0.51	89.45±0.21	108.88±54.87	92.24±0.69
48	98.19±0.30	92.80±1.01	91.08±0.32	85.21±11.62	93.97±0.89
54	99.88±0.07	74.07±5.08	93.86±0.12	79.88±83.75	81.52±3.35
56	98.64±0.05	84.31±2.60	90.99±0.18	116.62±103.80	92.04±0.51
73	97.00±0.07	74.50±28.27	93.60±0.24	84.57±53.58	86.30±4.00
Overall (Mean)	97.86±1.16	83.24±8.15	91.86±1.67	84.61±20.86	89.05±4.42

Table A.63 Comparison of SpO2 values of the age range of 41 to 50 years while vertical moving for the dedicated techniques.

Subject no.	Compared techniques				
	PT[1]	CM[2]	DST[3]	ICA[4]	CFC[5]
	SpO2 values in the unit of %				
	Average ± Standard deviation				
Male subjects					
16	95.30±0.15	91.77±0.42	90.05±0.10	87.75±12.74	92.08±0.48
20	95.74±0.21	80.49±3.16	92.28±0.18	56.20±83.24	92.44±2.77
30	94.02±0.21	94.48±0.13	91.16±0.10	83.61±3.11	94.62±0.14
33	96.96±0.11	93.72±0.16	91.72±0.12	101.48±81.53	94.16±0.29
35	95.34±0.15	93.32±0.88	92.15±0.12	80.73±4.89	94.84±0.67
49	96.06±0.11	93.33±0.66	91.21±0.10	70.23±20.88	93.92±0.40
66	98.10±0.11	78.68±7.01	93.69±0.18	1.14±62.87	75.76±29.86
71	97.32±0.13	88.63±1.47	92.19±0.28	60.81±31.53	90.69±1.90
Overall (Mean)	96.10±1.30	89.30±6.28	91.81±1.06	67.74±30.66	91.06±6.35
Female subjects					
01	98.44±0.26	92.15±0.56	90.65±0.29	85.92±1.59	85.54±0.41
10	96.20±0.34	88.19±1.36	92.75±0.12	118.12±90.66	92.45±0.40
25	95.61±0.41	91.25±0.73	90.48±0.18	-62.08±184.55	91.88±0.56
43	97.14±0.09	85.22±4.31	93.52±0.15	10.61±63.37	92.19±2.15
53	97.50±0.13	93.26±0.19	90.69±0.10	81.63±7.77	93.49±0.19
68	99.60±0.03	81.10±15.95	92.45±0.10	49.08±42.18	81.93±5.70
72	98.17±0.17	88.12±2.94	92.62±0.10	91.88±31.74	88.25±3.30
Overall (Mean)	97.52±1.36	88.47±4.27	91.88±1.24	53.60±61.52	89.39±4.32

Table A.64 Comparison of SpO2 values of the age range of 51 to 60 years while vertical moving for the dedicated techniques.

Subject no.	Compared techniques				
	PT[1]	CM[2]	DST[3]	ICA[4]	CFC[5]
	SpO2 values in the unit of %				
	Average ± Standard deviation				
Male subjects					
13	97.24±0.19	91.87±	90.95±0.15	79.22±3.44	92.27±0.34
22	98.82±0.04	91.90±	91.12±0.18	86.53±5.85	91.93±0.87
23	95.80±0.09	90.50±	90.86±0.12	70.73±22.37	90.90±1.12
44	98.46±0.13	89.67±	93.65±0.12	105.81±64.10	86.40±8.94
45	96.98±0.21	93.65±	93.13±0.18	85.93±22.21	92.58±1.09
50	98.81±0.27	72.16±	93.26±0.10	75.94±66.11	97.24±4.33
75	95.59±0.27	82.78±	92.83±0.28	95.93±117.69	85.39±2.82
Overall (Mean)	97.39±1.36	87.50±	92.26±1.22	85.73±12.05	90.96±4.01
Female subjects					
02	97.14±0.09	93.21±0.34	91.16±0.10	84.96±0.50	84.91±0.49
04	94.80±0.07	94.15±0.32	94.50±0.19	89.02±1.10	84.90±0.41
14	97.34±0.15	93.20±0.45	91.34±0.23	92.42±26.19	93.29±0.51
21	95.98±0.15	91.52±0.74	92.88±0.10	80.14±16.21	93.92±0.85
26	97.66±0.09	14.18±135.08	92.23±0.10	52.80±12.16	91.14±1.57
31	97.78±0.02	85.12±0.03	91.18±0.11	84.97±0.09	85.15±0.10
39	97.28±0.11	88.40±0.91	91.93±0.24	-2.55±130.79	90.79±0.74
65	98.94±0.17	88.47±0.84	92.32±0.12	61.78±33.16	95.26±0.49
70	97.19±0.35	91.15±1.23	91.46±0.32	58.31±38.61	93.66±1.50
74	93.78±0.52	82.79±8.31	92.32±0.12	65.85±30.61	83.97±3.68
Overall (Mean)	96.79±1.52	82.22±24.19	92.13±1.01	66.77±28.07	89.70±4.47

Table A.65 Comparison of SpO2 values of the age range of 21 to 30 years while waving for the dedicated techniques.

Subject no.	Compared techniques				
	PT[1]	CM[2]	DST[3]	ICA[4]	CFC[5]
	SpO2 values in the unit of %				
	Average ± Standard deviation				
Male subjects					
08	94.54±0.18	91.62±0.76	90.14±0.35	99.23±26.73	92.09±0.49
18	98.11±0.07	91.81±0.37	89.84±0.10	72.77±23.02	92.97±0.13
36	98.73±0.14	89.28±2.03	93.22±0.12	83.22±10.47	88.26±2.68
38	97.08±0.11	84.97±0.55	92.15±0.12	57.81±64.47	76.02±23.01
40	95.67±0.16	89.32±0.30	89.62±0.10	88.36±6.10	89.75±0.29
51	96.25±0.09	94.91±0.36	93.00±0.19	75.77±25.74	95.33±0.22
57	95.39±0.31	92.78±0.71	91.34±0.28	28.71±117.80	93.25±0.63
58	94.34±0.41	94.02±0.31	90.44±0.24	84.67±2.73	94.03±0.23
59	99.23±0.07	91.90±1.81	93.43±0.12	24.33±65.17	94.47±1.24
60	94.86±0.18	88.43±2.26	92.79±0.24	79.61±32.47	87.90±2.33
61	98.09±0.21	90.91±0.80	92.62±0.10	77.40±65.80	92.27±2.16
62	96.24±0.22	92.18±1.41	92.53±0.19	82.38±10.92	92.98±1.68
63	98.11±0.23	92.68±1.14	92.45±0.15	88.98±49.75	93.81±1.71
64	97.94±0.36	86.51±2.07	93.99±0.10	68.25±29.46	90.74±0.59
Overall (Mean)	96.76±1.64	90.81±2.80	91.97±1.43	72.25±21.76	90.99±4.86
Female subjects					
05	92.98±0.11	91.69±0.89	92.92±0.10	91.19±1.07	85.81±0.31
06	94.98±0.11	91.45±0.89	96.04±0.10	91.93±1.79	85.43±0.48
09	97.93±0.08	88.89±1.25	90.27±0.18	100.04±50.76	93.41±2.25
11	98.84±0.17	93.44±1.22	92.19±0.18	88.78±6.37	92.93±1.15
17	98.34±0.11	94.46±0.12	91.42±0.10	82.77±3.30	94.69±0.35
27	95.62±0.14	90.33±0.62	91.68±0.12	91.84±33.56	92.21±1.81
28	96.06±0.21	89.59±2.75	90.61±0.12	99.14±32.55	93.00±2.55
29	98.90±0.17	86.21±7.88	91.89±0.19	52.70±19.14	92.20±1.96
37	96.33±0.10	57.44±32.23	92.66±0.10	59.21±58.90	87.83±2.30
41	98.73±0.15	86.88±1.10	92.15±0.12	59.88±13.98	91.03±1.52
42	97.18±0.05	81.25±1.56	93.95±0.10	66.53±16.50	81.76±1.25
52	95.82±0.28	93.99±0.42	91.42±0.10	94.26±24.32	94.03±0.73
Overall (Mean)	96.81±1.84	87.13±10.07	92.27±1.55	81.52±17.06	90.36±4.13

Table A.66 Comparison of SpO2 values of the age range of 31 to 40 years while waving for the dedicated techniques.

Subject no.	Compared techniques				
	PT[1]	CM[2]	DST[3]	ICA[4]	CFC[5]
	SpO2 values in the unit of %				
	Average ± Standard deviation				
Male subjects					
03	96.12±0.11	91.67±0.88	89.84±0.18	83.86±0.58	85.17±0.16
12	97.41±0.10	92.77±1.02	91.72±0.19	68.77±10.35	95.30±0.76
24	99.37±0.19	83.94±2.00	93.52±0.10	67.05±20.84	82.55±1.88
34	98.78±0.25	92.43±0.28	90.09±0.15	78.73±9.45	93.16±0.51
46	98.14±0.11	91.33±0.28	91.51±0.12	62.81±29.25	92.37±0.36
47	98.12±0.11	79.60±4.99	92.75±0.12	99.09±107.02	86.30±0.97
55	96.58±0.06	88.11±1.19	91.08±0.19	57.57±23.78	87.60±1.88
67	94.23±0.15	92.37±0.47	90.18±0.29	17.11±166.89	92.78±0.25
69	94.72±0.20	89.80±1.86	91.21±0.10	72.65±36.50	92.51±1.11
Overall (Mean)	97.05±1.78	89.11±4.54	91.32±1.23	67.52±22.58	89.75±4.41
Female subjects					
07	98.44±0.20	82.76±2.75	92.99±0.35	65.53±14.74	88.10±0.63
15	97.50±0.07	104.47±71.45	94.12±0.35	-11.18±107.37	83.69±1.99
19	96.81±0.52	92.23±0.29	90.31±0.15	42.70±89.73	93.47±0.43
32	96.37±0.15	90.22±1.62	90.05±0.28	59.95±47.86	88.26±2.02
48	97.69±0.32	94.58±0.71	90.82±0.12	80.59±4.32	95.40±0.65
54	99.57±0.12	78.68±4.28	93.95±0.10	71.74±124.42	89.57±2.93
56	98.51±0.10	88.63±1.33	91.59±0.10	70.79±8.33	91.69±1.11
73	96.85±0.07	88.48±5.77	93.65±0.12	73.30±49.16	93.61±0.90
Overall (Mean)	97.72±1.07	90.00±7.75	92.18±1.69	56.68±29.67	90.47±3.82

Table A.67 Comparison of SpO2 values of the age range of 41 to 50 years while waving for the dedicated techniques.

Subject no.	Compared techniques				
	PT[1]	CM[2]	DST[3]	ICA[4]	CFC[5]
	SpO2 values in the unit of %				
	Average ± Standard deviation				
Male subjects					
16	95.87±0.09	92.17±0.34	90.27±0.18	81.95±4.26	92.38±0.36
20	95.51±0.05	89.17±2.48	92.11±0.12	88.29±14.49	94.74±0.25
30	93.30±0.11	92.21±0.92	90.74±0.26	84.93±7.27	91.88±1.07
33	97.32±0.16	88.07±2.00	92.32±0.12	81.40±7.76	89.67±1.37
35	95.00±0.15	88.04±1.11	92.06±0.23	50.02±56.83	87.56±2.73
49	95.94±0.28	92.81±0.37	91.46±0.24	80.03±10.80	92.80±0.77
66	98.42±0.17	73.05±15.50	93.60±0.12	14.21±65.35	87.70±4.91
71	97.41±0.09	86.54±1.89	92.06±0.18	115.06±80.81	89.47±1.62
Overall (Mean)	96.10±1.60	87.76±6.38	91.83±1.02	74.49±30.03	90.77±2.57
Female subjects					
01	99.28±0.11	91.07±0.68	90.27±0.23	83.73±2.82	85.85±0.58
10	96.94±0.26	87.67±0.95	93.05±0.10	80.88±19.07	86.92±1.06
25	96.34±0.19	89.75±1.18	90.39±0.12	30.91±105.99	91.66±1.13
43	97.19±0.02	84.39±9.08	93.77±0.10	88.94±89.43	87.24±6.90
53	97.60±0.15	93.58±0.20	92.15±0.12	60.76±52.69	94.26±0.47
68	99.59±0.04	86.36±2.37	92.49±0.10	68.37±5.92	87.49±1.20
72	98.07±0.09	84.07±0.37	92.49±0.28	121.78±79.02	85.80±5.00
Overall (Mean)	97.86±1.21	88.13±3.53	92.09±1.31	76.48±27.90	88.46±3.23

Table A.68 Comparison of SpO2 values of the age range of 51 to 60 years while waving for the dedicated techniques.

Subject no.	Compared techniques				
	PT[1]	CM[2]	DST[3]	ICA[4]	CFC[5]
	SpO2 values in the unit of %				
	Average ± Standard deviation				
Male subjects					
13	95.74±0.12	92.43±0.40	91.08±0.36	93.55±14.80	93.14±0.41
22	98.72±0.09	91.31±0.56	90.69±0.18	80.62±7.05	90.68±0.73
23	96.41±0.14	88.11±1.36	91.08±0.12	100.83±33.53	88.12±1.42
44	98.82±0.04	88.96±1.23	93.86±0.12	24.87±122.71	89.11±2.49
45	96.66±0.17	93.26±0.69	93.26±0.18	55.09±34.06	94.52±0.65
50	99.07±0.09	88.43±3.93	93.43±0.19	65.23±23.39	87.73±8.22
75	95.43±0.16	87.64±1.65	92.62±0.18	136.87±136.83	93.30±1.85
Overall (Mean)	97.26±1.56	90.02±2.27	92.29±1.31	79.58±35.89	90.94±2.73
Female subjects					
02	96.48±0.11	92.74±0.54	91.08±0.12	85.01±0.93	85.21±0.75
04	94.44±0.09	93.32±0.71	94.67±0.12	89.10±0.32	85.09±0.16
14	97.14±0.07	93.49±0.38	91.34±0.10	31.83±118.84	93.62±0.30
21	96.00±0.14	90.34±1.85	92.36±0.19	41.16±71.47	90.81±1.40
26	97.63±0.07	52.62±40.98	92.45±0.10	32.72±81.82	85.51±1.70
31	95.18±0.92	83.14±3.16	91.24±0.07	83.95±1.36	84.66±0.96
39	99.54±0.10	87.52±1.44	92.06±0.23	122.24±91.80	90.60±1.00
65	98.91±0.10	88.08±2.00	92.70±0.23	61.81±15.86	89.47±2.05
70	97.70±0.14	92.59±0.93	92.92±0.41	57.48±30.48	92.62±1.37
74	93.97±0.22	83.58±1.00	92.83±0.18	78.88±2.22	92.17±2.58
Overall (Mean)	96.70±1.84	85.74±12.26	92.37±1.06	68.42±28.81	88.98±3.52

Table A.69 Summary of SpO2 percentage error of the age range of 21 to 30 years while bending for the dedicated techniques.

Subject no.	Compared techniques				
	PT[1]	CM[2]	DST[3]	ICA[4]	CFC[5]
	SpO2 percentage error values in the unit of %				
	Average				
Male subjects					
08	0.34	1.04	3.90	14.74	0.62
18	0.37	0.60	3.31	9.20	0.33
36	0.71	4.06	0.88	45.84	2.47
38	0.47	1.48	2.43	11.90	1.05
40	0.24	2.95	1.53	20.08	3.04
51	2.06	9.41	0.28	45.05	2.03
57	0.17	2.82	1.98	35.79	2.30
58	0.30	1.61	3.24	18.21	0.91
59	0.10	0.90	1.70	31.88	0.82
60	0.63	7.66	1.79	57.07	5.88
61	1.26	4.67	0.27	15.75	1.18
62	1.52	0.75	2.10	22.46	1.21
63	0.40	2.22	1.16	65.42	1.53
64	0.94	4.97	0.09	59.89	5.99
Overall (Mean) ± Standard deviation	0.68±0.58	3.22±2.69	1.76±1.18	32.38±19.23	2.10±1.80
Female subjects					
05	1.10	4.41	1.90	4.45	9.83
06	1.46	8.95	0.63	3.96	10.83
09	1.02	4.58	3.71	21.28	1.74
11	0.72	2.38	2.75	41.19	1.99
17	0.06	0.75	2.50	36.05	1.56
27	0.32	1.13	2.15	32.26	0.46
28	0.26	1.11	4.18	30.56	0.68
29	0.84	11.27	0.98	33.04	4.24
37	2.01	6.19	2.05	68.90	4.40
41	0.39	9.78	0.41	29.53	5.91
42	1.04	15.28	0.63	29.45	20.51
52	0.08	1.94	0.38	8.79	1.70
Overall (Mean) ± Standard deviation	0.77±0.59	5.65±4.72	1.86±1.29	28.29±17.87	5.32±5.88

1 – PT refers to the proposed LEDs-driving technique, 2 – CM refers to the conventional LEDs-emitting method,
3 – DST stands for discrete saturation transform, 4 – ICA stands for independent component analysis,
5 – CFC stands for compression of Fourier coefficients.

Table A.70 Summary of SpO2 percentage error of the age range of 31 to 40 years while bending for the dedicated techniques.

Subject no.	Compared techniques				
	PT[1]	CM[2]	DST[3]	ICA[4]	CFC[5]
	SpO2 percentage error values in the unit of %				
	Average				
Male subjects					
03	2.08	1.68	3.99	10.22	8.47
12	0.95	4.97	3.05	26.25	5.25
24	0.30	11.42	0.10	49.76	29.47
34	0.63	2.59	2.06	9.81	3.95
46	1.25	7.58	0.71	19.57	6.23
47	1.65	14.95	1.40	116.24	2.08
55	0.17	5.35	2.54	10.43	6.07
67	0.29	0.97	1.82	8.89	1.58
69	0.21	0.84	2.22	96.42	0.79
Overall (Mean) ± Standard deviation	0.84±0.69	5.59±4.93	1.99±1.18	38.62±40.81	7.10±8.75
Female subjects					
07	0.65	12.70	0.76	116.45	56.23
15	0.99	12.37	0.81	26.05	11.37
19	0.31	1.17	2.62	38.94	0.82
32	0.50	8.15	2.95	62.29	6.85
48	0.10	2.82	2.78	41.93	3.99
54	0.38	10.75	0.92	21.46	6.67
56	0.22	30.86	1.66	87.82	4.85
73	0.56	6.76	2.86	83.99	4.38
Overall (Mean) ± Standard deviation	0.46±0.28	10.70±9.16	1.92±0.99	59.87±33.70	11.89±18.16

Table A.71 Summary of SpO2 percentage error of the age range of 41 to 50 years while bending for the dedicated techniques.

Subject no.	Compared techniques				
	PT[1]	CM[2]	DST[3]	ICA[4]	CFC[5]
	SpO2 percentage error values in the unit of %				
	Average				
Male subjects					
16	0.34	2.14	3.35	8.59	1.00
20	0.43	7.09	1.39	56.05	2.13
30	3.00	3.34	2.21	36.55	1.91
33	2.72	7.70	1.30	41.14	4.19
35	0.46	1.84	0.58	20.50	1.71
49	0.60	0.85	1.38	4.07	1.38
66	0.17	8.66	0.70	52.49	3.28
71	0.13	2.84	2.72	51.98	1.89
Overall (Mean) ± Standard deviation	0.98±1.17	4.31±3.02	1.71±0.97	33.92±20.47	2.19±1.05
Female subjects					
01	0.34	0.98	3.21	20.73	6.77
10	1.65	1.31	0.41	11.57	1.82
25	0.02	1.64	2.87	23.25	1.18
43	0.90	5.07	2.76	46.52	6.28
53	0.36	1.07	2.07	137.75	0.48
68	0.44	9.44	0.99	47.41	7.79
72	0.40	8.30	0.98	99.38	3.82
Overall (Mean) ± Standard deviation	0.59±0.54	3.97±3.64	1.90±1.10	55.23±46.57	4.02±2.95

Table A.72 Summary of SpO2 percentage error of the age range of 51 to 60 years while bending for the dedicated techniques.

Subject no.	Compared techniques				
	PT[1]	CM[2]	DST[3]	ICA[4]	CFC[5]
	SpO2 percentage error values in the unit of %				
	Average				
Male subjects					
13	0.80	0.85	2.55	9.92	0.64
22	0.76	2.26	2.92	13.84	0.49
23	1.34	2.82	2.52	26.50	0.54
44	0.19	8.38	0.09	67.41	27.56
45	0.36	3.50	2.26	75.71	2.55
50	0.77	5.66	0.28	78.36	1.25
75	0.24	7.62	1.52	81.34	1.17
Overall (Mean) ± Standard deviation	0.64±0.41	4.44±2.84	1.73±1.14	50.44±32.19	4.89±10.02
Female subjects					
02	1.08	4.39	1.79	7.19	8.31
04	0.25	2.94	0.72	5.28	10.19
14	1.38	1.16	1.04	9.41	0.33
21	0.68	10.88	2.37	34.16	2.27
26	0.67	27.46	1.09	87.87	34.25
31	0.10	9.59	3.08	9.60	9.59
39	0.10	5.44	3.38	205.88	4.42
65	1.19	13.71	2.48	45.04	13.29
70	0.22	2.99	2.77	6.69	3.20
74	0.22	9.81	1.68	14.54	10.34
Overall (Mean) ± Standard deviation	0.59±0.48	8.84±7.71	2.04±0.92	42.56±62.98	9.62±9.61

Table A.73 Summary of SpO2 percentage error of the age range of 21 to 30 years while horizontal moving for the dedicated techniques.

Subject no.	Compared techniques				
	PT[1]	CM[2]	DST[3]	ICA[4]	CFC[5]
	SpO2 percentage error values in the unit of %				
	Average				
Male subjects					
08	0.35	0.89	2.98	14.71	0.27
18	0.23	1.57	2.94	31.71	0.96
36	0.55	9.46	1.44	40.32	8.61
38	0.55	1.24	2.15	99.57	1.33
40	0.79	4.12	1.76	43.61	2.46
51	2.16	1.57	0.80	13.58	1.84
57	0.40	1.27	1.75	25.83	2.09
58	0.62	0.51	4.01	8.74	0.50
59	0.77	2.59	2.02	104.23	2.06
60	2.01	2.52	1.65	43.53	2.14
61	1.36	2.22	2.80	13.57	0.38
62	0.22	1.30	2.19	18.28	0.86
63	0.06	2.04	2.22	40.49	0.45
64	0.55	3.23	0.54	141.98	2.94
Overall (Mean) ± Standard deviation	0.76±0.64	2.92±2.59	2.09±0.91	45.72±40.57	1.92±2.11
Female subjects					
05	0.42	0.88	2.67	5.70	9.62
06	3.05	5.60	1.71	2.51	10.78
09	2.33	6.63	4.34	22.52	2.54
11	0.31	0.49	2.93	22.62	0.84
17	0.13	0.90	3.82	5.82	1.17
27	1.67	6.80	1.78	26.68	0.79
28	1.11	8.55	3.45	24.34	5.23
29	0.08	7.77	2.36	19.60	0.96
37	2.24	20.25	1.87	35.43	9.03
41	0.53	5.08	0.41	60.90	1.69
42	0.83	18.99	0.28	59.10	7.14
52	0.25	2.43	1.45	7.20	1.72
Overall (Mean) ± Standard deviation	1.08±1.01	7.03±6.51	2.26±1.26	24.37±19.45	4.29±3.85

Table A.74 Summary of SpO2 percentage error of the age range of 31 to 40 years while horizontal moving for the dedicated techniques.

Subject no.	Compared techniques				
	PT[1]	CM[2]	DST[3]	ICA[4]	CFC[5]
	SpO2 percentage error values in the unit of %				
	Average				
Male subjects					
03	2.76	2.48	3.44	10.15	8.55
12	1.12	0.62	2.68	19.57	0.84
24	0.31	17.16	0.40	28.91	15.73
34	0.11	1.97	2.20	18.85	1.29
46	1.85	4.41	0.62	30.10	1.27
47	2.21	12.01	1.90	48.56	5.53
55	0.19	6.26	2.40	20.27	13.94
67	0.09	0.47	2.66	7.67	0.40
69	0.14	2.44	2.50	12.60	2.42
Overall (Mean) ± Standard deviation	0.98±1.05	5.31±5.70	2.09±0.99	21.85±12.61	5.55±5.90
Female subjects					
07	0.07	13.68	0.57	30.96	7.39
15	1.15	17.00	0.72	33.58	6.60
19	0.66	1.67	4.30	17.83	2.50
32	1.49	1.63	3.32	43.97	2.32
48	0.51	18.77	3.24	95.82	8.59
54	0.15	14.41	1.10	67.59	4.77
56	1.06	8.13	2.76	34.12	1.89
73	2.76	19.48	2.18	49.12	12.36
Overall (Mean) ± Standard deviation	0.98±0.87	11.85±7.22	2.27±1.37	46.62±24.71	5.80±3.65

Table A.75 Summary of SpO2 percentage error of the age range of 41 to 50 years while horizontal moving for the dedicated techniques.

Subject no.	Compared techniques				
	PT[1]	CM[2]	DST[3]	ICA[4]	CFC[5]
	SpO2 percentage error values in the unit of %				
	Average				
Male subjects					
16	1.08	2.28	3.49	78.41	1.32
20	0.95	5.25	3.54	13.25	1.56
30	3.19	1.63	3.13	10.30	0.37
33	0.58	3.01	0.71	25.83	3.04
35	0.17	1.83	0.53	37.05	1.29
49	0.21	1.08	1.19	6.06	1.45
66	0.38	15.88	0.07	158.51	7.59
71	0.16	5.26	3.04	57.00	5.03
Overall (Mean) ± Standard deviation	0.84±1.01	4.53±4.85	1.96±1.47	48.30±51.01	2.70±2.44
Female subjects					
01	0.14	1.63	2.10	7.80	7.19
10	2.41	3.94	0.15	27.91	1.74
25	0.39	1.46	2.91	73.10	1.29
43	0.97	6.70	1.45	59.41	4.18
53	0.23	0.28	1.01	37.44	1.22
68	0.50	8.16	2.74	8.63	1.03
72	0.63	6.29	1.25	31.67	3.07
Overall (Mean) ± Standard deviation	0.75±0.78	4.06±3.05	1.66±0.99	35.13±24.32	2.82±2.24

Table A.76 Summary of SpO2 percentage error of the age range of 51 to 60 years while horizontal moving for the dedicated techniques.

Subject no.	Compared techniques				
	PT[1]	CM[2]	DST[3]	ICA[4]	CFC[5]
	SpO2 percentage error values in the unit of %				
	Average				
Male subjects					
13	0.33	1.93	2.41	11.35	1.33
22	1.15	2.17	2.41	17.79	4.60
23	1.82	2.02	1.09	68.48	1.71
44	0.11	3.74	0.13	31.41	11.86
45	0.23	1.93	2.35	77.47	1.10
50	0.74	8.75	0.24	164.79	7.07
75	0.57	6.98	1.61	44.43	6.02
Overall (Mean) ± Standard deviation	0.71±0.60	3.93±2.81	1.46±1.00	59.39±52.54	4.81±3.91
Female subjects					
02	0.27	0.22	1.83	8.79	8.51
04	1.14	2.23	1.86	6.82	10.28
14	1.38	0.86	1.85	25.89	0.98
21	1.04	4.23	1.84	35.31	0.38
26	1.20	48.11	1.87	126.75	10.14
31	3.27	9.49	1.81	9.62	9.49
39	0.78	7.14	1.81	26.48	5.18
65	0.20	6.47	1.84	41.85	2.98
70	0.64	8.54	1.83	37.42	0.36
74	3.62	7.34	1.83	61.99	6.18
Overall (Mean) ± Standard deviation	1.35±1.17	9.46±13.96	1.84±0.02	38.09±35.57	5.45±4.07

Table A.77 Summary of SpO2 percentage error of the age range of 21 to 30 years while shivering for the dedicated techniques.

Subject no.	Compared techniques				
	PT[1]	CM[2]	DST[3]	ICA[4]	CFC[5]
	SpO2 percentage error values in the unit of %				
	Average				
Male subjects					
08	0.47	1.75	4.04	21.53	0.81
18	0.20	1.00	2.66	5.53	0.87
36	0.20	3.30	0.88	96.46	3.60
38	0.54	4.52	2.15	23.49	0.61
40	1.37	1.55	1.57	21.69	1.63
51	2.63	2.69	0.03	26.08	2.90
57	0.24	0.38	2.02	10.43	1.53
58	0.31	7.30	3.83	53.72	0.72
59	0.97	1.29	2.02	57.35	0.76
60	1.05	2.46	2.69	37.28	0.69
61	1.69	5.11	1.51	20.49	0.95
62	0.97	0.99	1.10	25.50	0.66
63	0.19	1.52	0.66	17.50	2.47
64	0.64	10.58	0.05	53.26	2.19
Overall (Mean) ± Standard deviation	0.82±0.70	3.17±2.86	1.80±1.24	33.59±24.16	1.46±0.97
Female subjects					
05	1.10	2.19	1.36	3.24	9.85
06	0.25	5.70	0.63	4.14	10.89
09	1.92	5.34	4.43	28.61	0.88
11	2.26	0.32	2.38	14.40	1.02
17	0.10	0.61	3.73	3.42	0.82
27	1.08	4.90	2.20	19.63	0.62
28	0.53	6.48	3.17	18.09	6.50
29	0.47	6.69	1.62	23.32	3.64
37	1.12	43.85	1.32	86.17	5.09
41	0.60	14.79	0.23	64.75	1.39
42	0.84	15.82	0.54	44.09	15.51
52	0.57	4.07	0.23	91.63	1.65
Overall (Mean) ± Standard deviation	0.90±0.65	9.23±11.92	1.82±1.39	33.46±31.40	4.82±4.92

Table A.78 Summary of SpO2 percentage error of the age range of 31 to 40 years while shivering for the dedicated techniques.

Subject no.	Compared techniques				
	PT[1]	CM[2]	DST[3]	ICA[4]	CFC[5]
	SpO2 percentage error values in the unit of %				
	Average				
Male subjects					
03	2.34	1.45	3.67	10.52	8.36
12	1.22	0.69	2.50	11.31	1.34
24	1.34	10.67	0.06	49.71	4.21
34	0.68	2.33	1.83	8.68	1.84
46	1.55	0.98	0.80	39.30	2.28
47	1.57	17.18	1.49	104.15	3.60
55	0.37	3.08	2.54	29.34	1.34
67	0.28	0.78	2.06	25.38	1.34
69	1.42	2.04	2.73	13.55	0.46
Overall (Mean) ± Standard deviation	1.20±0.65	4.36±5.72	1.96±1.08	32.44±30.40	2.75±2.41
Female subjects					
07	0.26	6.76	1.56	23.03	1.70
15	1.05	50.04	1.27	75.59	7.47
19	0.21	5.69	3.03	31.71	4.37
32	1.23	0.45	3.50	7.73	7.60
48	0.18	2.95	3.29	143.54	0.42
54	0.16	13.55	0.92	169.15	2.81
56	1.69	5.68	0.60	27.98	0.16
73	2.70	16.51	2.36	128.05	3.04
Overall (Mean) ± Standard deviation	0.94±0.92	12.71±15.98	2.07±1.13	75.85±62.89	3.45±2.88

Table A.79 Summary of SpO2 percentage error of the age range of 41 to 50 years while shivering for the dedicated techniques.

Subject no.	Compared techniques				
	PT[1]	CM[2]	DST[3]	ICA[4]	CFC[5]
	SpO2 percentage error values in the unit of %				
	Average				
Male subjects					
16	0.54	1.71	3.21	8.83	0.41
20	0.99	5.40	1.12	90.07	0.84
30	2.07	0.80	2.08	17.83	1.02
33	0.25	1.41	1.62	12.31	0.98
35	0.15	2.45	1.69	129.98	1.20
49	0.29	1.37	0.96	22.88	2.22
66	0.37	9.51	0.84	96.76	4.73
71	0.22	9.89	2.09	17.16	1.80
Overall (Mean) ± Standard deviation	0.61±0.65	3.24±3.75	1.70±0.78	49.48±48.04	1.65±1.37
Female subjects					
01	0.12	1.45	2.05	7.75	7.02
10	1.89	1.03	0.33	22.89	1.90
25	0.14	3.51	2.22	28.47	1.50
43	0.91	21.06	2.39	50.72	1.44
53	0.34	1.71	1.98	43.28	0.67
68	0.63	1.40	2.51	5.71	0.43
72	0.96	9.04	1.43	20.73	0.62
Overall (Mean) ± Standard deviation	0.71±0.62	5.60±7.37	1.84±0.75	25.65±16.82	1.94±2.30

Table A.80 Summary of SpO2 percentage error of the age range of 51 to 60 years while shivering for the dedicated techniques.

Subject no.	Compared techniques				
	PT[1]	CM[2]	DST[3]	ICA[4]	CFC[5]
	SpO2 percentage error values in the unit of %				
	Average				
Male subjects					
13	0.53	0.82	2.64	11.66	0.47
22	0.92	3.86	2.69	25.11	1.00
23	1.58	0.88	1.09	16.15	1.04
44	0.63	14.33	0.27	83.01	8.53
45	0.08	1.16	2.22	63.06	0.52
50	0.85	17.11	0.18	80.31	2.65
75	0.76	12.55	2.20	85.63	0.92
Overall (Mean) ± Standard deviation	0.77±0.46	7.24±7.14	1.61±1.08	52.14±33.30	2.16±2.90
Female subjects					
02	0.41	2.16	2.34	8.99	9.56
04	0.46	1.29	0.94	6.88	10.50
14	1.28	0.23	1.04	20.72	0.50
21	1.14	3.01	2.10	25.63	0.54
26	1.24	65.21	0.62	78.06	3.63
31	0.21	9.49	2.96	9.73	9.29
39	0.60	6.17	3.06	16.39	3.76
65	0.48	3.67	2.66	18.78	1.03
70	0.54	9.38	1.77	27.22	0.95
74	2.16	8.94	1.72	61.83	2.84
Overall (Mean) ± Standard deviation	0.86±0.59	10.95±19.37	1.92±0.86	27.42±23.73	4.26±4.01

Table A.81 Summary of SpO2 percentage error of the age range of 21 to 30 years while vertical moving for the dedicated techniques.

Subject no.	Compared techniques				
	PT[1]	CM[2]	DST[3]	ICA[4]	CFC[5]
	SpO2 percentage error values in the unit of %				
	Average				
Male subjects					
08	0.89	1.73	2.98	13.29	0.72
18	0.22	0.24	2.89	3.88	0.50
36	0.49	5.14	1.25	52.12	4.49
38	0.71	6.60	2.11	49.98	1.31
40	0.94	2.74	0.96	47.08	9.38
51	2.63	1.66	0.38	46.33	2.36
57	0.28	1.04	1.47	49.43	1.67
58	0.33	0.52	3.65	6.57	0.18
59	0.84	0.82	1.61	28.86	1.53
60	0.94	2.04	2.78	20.16	0.61
61	1.08	7.22	0.96	164.12	4.16
62	1.33	0.52	3.15	22.50	0.69
63	0.60	1.86	0.52	39.38	1.23
64	0.14	10.67	0.14	103.87	2.03
Overall (Mean) ± Standard deviation	0.82±0.63	3.06±3.14	1.78±1.15	46.25±42.36	2.20±2.44
Female subjects					
05	1.10	1.18	1.95	3.77	10.03
06	0.88	8.59	0.85	3.71	10.91
09	2.03	4.96	3.93	12.59	3.66
11	0.78	4.13	2.88	92.71	4.54
17	0.28	0.73	3.73	10.46	1.00
27	1.12	9.49	1.46	114.89	1.24
28	0.41	6.23	3.13	36.32	6.18
29	0.41	4.76	1.90	34.47	1.07
37	1.02	21.17	1.55	47.01	14.62
41	0.91	8.60	0.14	14.09	6.15
42	0.79	18.88	0.58	37.37	18.41
52	0.91	2.89	0.75	10.34	3.09
Overall (Mean) ± Standard deviation	0.89±0.45	7.63±6.44	1.91±1.26	34.81±35.64	6.74±5.64

Table A.82 Summary of SpO2 percentage error of the age range of 31 to 40 years while vertical moving for the dedicated techniques.

Subject no.	Compared techniques				
	PT[1]	CM[2]	DST[3]	ICA[4]	CFC[5]
	SpO2 percentage error values in the unit of %				
	Average				
Male subjects					
03	2.51	1.61	3.30	9.59	8.04
12	1.12	0.97	2.32	14.60	2.25
24	1.12	12.02	0.40	32.98	9.57
34	0.56	3.37	2.20	44.80	2.99
46	1.45	2.71	0.66	13.12	4.68
47	1.57	11.62	1.59	54.77	1.73
55	0.52	8.65	2.22	34.40	8.44
67	0.32	0.92	2.10	18.49	1.10
69	1.29	5.94	1.90	31.62	5.94
Overall (Mean) ± Standard deviation	1.16±0.67	5.31±4.45	1.85±0.88	28.27±15.44	4.97±3.17
Female subjects					
07	0.56	14.15	1.18	28.81	4.91
15	1.07	16.55	0.37	43.44	7.20
19	0.20	1.81	3.85	10.30	1.19
32	1.15	0.54	3.32	31.76	0.61
48	0.32	1.23	2.97	13.20	0.69
54	0.35	21.88	1.01	70.36	14.03
56	1.22	9.69	2.53	64.56	1.41
73	2.70	21.78	1.73	46.80	9.40
Overall (Mean) ± Standard deviation	0.95±0.81	10.95±9.00	2.12±1.23	38.65±21.91	4.93±4.94

Table A.83 Summary of SpO2 percentage error of the age range of 41 to 50 years while vertical moving for the dedicated techniques.

Subject no.	Compared techniques				
	PT[1]	CM[2]	DST[3]	ICA[4]	CFC[5]
	SpO2 percentage error values in the unit of %				
	Average				
Male subjects					
16	0.79	1.46	3.30	12.24	1.13
20	0.66	14.07	1.49	53.50	2.31
30	2.13	1.30	2.26	10.36	1.45
33	0.21	0.52	1.62	57.23	0.99
35	0.50	1.04	0.63	12.94	2.27
49	0.76	1.64	0.68	23.52	2.28
66	0.37	16.42	0.47	98.79	20.72
71	0.13	5.65	1.86	37.68	3.46
Overall (Mean) ± Standard deviation	0.69±0.63	5.26±6.39	1.54±0.96	38.28±30.64	4.32±6.67
Female subjects					
01	1.14	0.50	1.86	6.98	7.40
10	1.96	4.07	0.89	54.48	0.61
25	0.39	1.99	2.82	166.68	1.31
43	0.91	6.74	2.34	88.39	2.02
53	0.11	0.47	2.30	12.06	0.72
68	0.56	19.04	0.76	50.61	12.05
72	1.10	5.83	1.02	28.42	5.69
Overall (Mean) ± Standard deviation	0.88±0.61	5.52±6.45	1.71±0.82	58.23±55.36	4.26±4.32

Table A.84 Summary of SpO2 percentage error of the age range of 51 to 60 years while vertical moving for the dedicated techniques.

Subject no.	Compared techniques				
	PT[1]	CM[2]	DST[3]	ICA[4]	CFC[5]
	SpO2 percentage error values in the unit of %				
	Average				
Male subjects					
13	1.30	1.33	2.32	14.92	0.90
22	0.90	1.49	2.32	7.26	1.45
23	1.68	2.59	2.20	23.87	2.16
44	0.28	4.29	0.10	50.43	8.99
45	0.25	1.54	2.08	19.20	2.66
50	1.24	22.48	0.19	44.46	4.47
75	0.91	12.03	1.34	84.17	9.25
Overall (Mean) ± Standard deviation	0.94±0.53	6.53±7.98	1.51±0.99	34.90±26.75	4.27±3.50
Female subjects					
02	0.73	0.31	2.34	8.98	9.04
04	0.25	0.91	0.54	6.30	10.64
14	1.48	0.94	1.09	20.05	1.03
21	0.96	3.18	1.74	17.93	0.77
26	1.21	84.71	0.53	43.06	1.95
31	3.35	9.46	3.02	9.62	9.43
39	1.80	6.70	3.06	102.69	4.18
65	0.63	6.46	2.39	43.01	0.72
70	0.35	2.92	2.63	37.90	1.20
74	2.49	12.15	2.04	30.13	10.90
Overall (Mean) ± Standard deviation	1.32±0.99	12.77±25.58	1.94±0.94	31.97±28.50	4.99±4.46

Table A.85 Summary of SpO2 percentage error of the age range of 21 to 30 years while waving for the dedicated techniques.

Subject no.	Compared techniques				
	PT[1]	CM[2]	DST[3]	ICA[4]	CFC[5]
	SpO2 percentage error values in the unit of %				
	Average				
Male subjects					
08	0.48	1.10	2.70	21.08	0.59
18	0.10	0.53	2.66	21.16	0.73
36	0.15	3.05	1.30	10.25	4.09
38	1.29	9.69	2.06	40.37	19.20
40	0.95	2.00	1.67	6.35	1.53
51	2.23	2.46	0.40	19.51	2.92
57	0.73	0.64	1.98	72.46	0.43
58	0.97	0.51	3.33	9.49	0.52
59	0.71	2.82	1.20	74.28	1.02
60	1.81	6.19	1.56	17.73	6.74
61	0.60	2.57	0.73	51.70	1.99
62	1.70	1.52	1.14	11.99	1.51
63	0.66	0.90	0.89	34.54	1.52
64	0.47	7.91	0.05	31.24	3.41
Overall (Mean) ± Standard deviation	0.92±0.63	2.99±2.89	1.55±0.93	30.15±22.32	3.30±4.90
Female subjects					
05	1.55	3.11	1.81	3.64	9.32
06	0.69	4.14	0.68	3.63	10.45
09	1.47	5.88	4.43	38.92	1.86
11	0.28	1.12	2.06	6.49	1.28
17	0.46	0.93	2.31	11.56	1.18
27	0.42	3.41	1.97	25.58	1.46
28	0.25	4.40	3.31	27.83	2.22
29	0.19	7.57	1.26	43.37	1.66
37	1.38	38.80	1.28	50.14	6.43
41	0.62	5.60	0.14	34.93	1.76
42	1.01	13.52	0.01	29.18	12.98
52	0.86	2.43	0.38	17.30	2.47
Overall (Mean) ± Standard deviation	0.76±0.49	7.58±10.39	1.64±1.32	24.38±15.89	4.42±4.23

Table A.86 Summary of SpO2 percentage error of the age range of 31 to 40 years while waving for the dedicated techniques.

Subject no.	Compared techniques				
	PT[1]	CM[2]	DST[3]	ICA[4]	CFC[5]
	SpO2 percentage error values in the unit of %				
	Average				
Male subjects					
03	2.21	1.61	3.58	9.99	8.58
12	1.45	1.20	2.32	26.76	1.49
24	1.21	9.68	0.63	27.85	11.18
34	0.18	0.72	1.83	14.21	1.52
46	1.26	1.78	1.58	32.44	0.66
47	1.33	15.34	1.36	77.24	8.21
55	0.56	5.89	2.72	38.51	6.44
67	0.62	0.70	1.68	97.65	1.15
69	1.81	3.41	1.90	25.11	1.09
Overall (Mean) ± Standard deviation	1.18±0.64	4.48±5.03	1.95±0.84	38.86±29.30	4.48±4.10
Female subjects					
07	0.47	9.38	1.82	28.24	3.54
15	1.21	47.56	1.18	112.02	10.03
19	0.54	1.67	3.71	54.47	0.49
32	1.09	2.48	2.67	41.26	4.60
48	0.36	0.89	3.24	14.14	1.64
54	0.09	17.03	0.92	99.85	5.54
56	1.09	5.06	1.89	24.17	1.78
73	2.85	7.12	1.69	45.28	1.73
Overall (Mean) ± Standard deviation	0.96±0.86	11.40±15.52	2.14±0.98	52.43±35.52	3.67±3.08

Table A.87 Summary of SpO2 percentage error of the age range of 41 to 50 years while waving for the dedicated techniques.

Subject no.	Compared techniques				
	PT[1]	CM[2]	DST[3]	ICA[4]	CFC[5]
	SpO2 percentage error values in the unit of %				
	Average				
Male subjects					
16	0.19	1.03	3.07	12.00	0.81
20	0.89	4.80	1.67	13.83	1.15
30	2.87	1.35	2.72	10.86	1.60
33	0.16	5.54	0.98	12.70	3.83
35	0.17	5.05	0.72	55.53	5.57
49	0.64	1.07	0.40	12.85	1.19
66	0.70	22.40	0.56	89.48	6.84
71	0.07	7.87	1.99	47.88	4.76
Overall (Mean) ± Standard deviation	0.71±0.92	6.14±7.03	1.51±1.01	31.89±29.34	3.22±2.34
Female subjects					
01	0.30	1.41	2.28	9.36	7.06
10	1.21	4.64	1.22	20.82	5.44
25	0.94	3.60	2.91	66.80	1.70
43	0.96	7.65	2.62	70.36	5.82
53	0.16	0.81	0.73	35.31	1.55
68	0.55	7.30	0.72	26.61	6.09
72	1.00	10.16	1.16	44.30	8.30
Overall (Mean) ± Standard deviation	0.73±0.40	5.08±3.45	1.66±0.92	39.08±22.95	5.14±2.58

Table A.88 Summary of SpO2 percentage error of the age range of 51 to 60 years while waving for the dedicated techniques.

Subject no.	Compared techniques				
	PT[1]	CM[2]	DST[3]	ICA[4]	CFC[5]
	SpO2 percentage error values in the unit of %				
	Average				
Male subjects					
13	0.26	0.73	2.18	10.35	0.30
22	1.00	2.12	2.78	13.58	2.79
23	1.06	5.16	1.97	20.61	5.15
44	0.64	5.05	0.18	87.01	4.89
45	0.14	1.95	1.95	42.09	0.74
50	1.51	5.00	0.38	31.25	7.06
75	0.74	6.86	1.57	76.69	1.48
Overall (Mean) ± Standard deviation	0.77±0.48	3.84±2.23	1.57±0.96	40.22±30.52	3.20±2.55
Female subjects					
02	0.09	0.65	2.43	8.93	8.72
04	0.63	1.78	0.35	6.22	10.45
14	1.27	1.25	1.09	66.76	1.38
21	0.98	4.42	2.28	56.45	3.92
26	1.19	43.25	0.30	69.32	7.78
31	0.73	11.57	2.96	10.71	9.95
39	0.48	7.63	2.83	66.03	4.38
65	0.60	6.87	1.98	34.65	5.40
70	0.30	1.48	1.04	40.78	1.51
74	2.30	11.31	1.50	16.31	2.50
Overall (Mean) ± Standard deviation	0.86±0.63	9.02±12.70	1.68±0.97	37.62±25.87	5.60±3.42

Appendix B

Related Publications

A Photoplethysmographic Signal Isolated From an Additive Motion Artifact by Frequency Translation

Sakkarin Sinchai, Pattana Kainan, Paramote Wardkein, *Member, IEEE*, and Jeerasuda Koseeyaporn

***Abstract*—Acquiring a precise percentage of oxygen saturation (SpO2) from a finger-probe pulse oximeter is dependent on both artifact-free red and infrared photoplethysmoghaphic (PPG) signals. Nonetheless, in real-life situations, these PPG signals are corrupted by a motion artifact (MA) signal that is generated from either finger or hand movement. To resolve this MA interference, the cause of the adulteration of PPG signals by the MA signal is examined. The MA signal is found to behave like an additive noise. Additionally, the frequency responses of the MA and PPG signals show that these signals are in the same frequency band. Hence, instead of direct current, a sinusoidal wave alternating current is proposed to drive an LED source in order to shift the PPG frequency band away from the MA frequency band. Experimentally, a commercial finger-probe pulse oximeter is employed. To determine the performance of the presented scheme, the resulting PPG signals are compared with those from employing the old-fashioned LED-driving method. In addition, the accuracy is verified by computing the SpO2 value. The results reveal that the proposed approach successfully retains the fundamental morphologies of the PPG structures when motion occurs. Moreover, the calculated SpO2 values from the proposed technique provide an average error of approximately 1.4%, whereas the conventional method yields a mean error approximately 4.2%.**

***Index Terms*—Amplitude modulation, Motion artifact (MA), optical biosensor, photoplethysmography (PPG), pulse oximeter.**

I. Introduction

SINCE the pulse oximeter was invented, invasive methods have no longer been the first option to measure oxygen saturation in human blood. The invasive techniques are required only when the percentage of oxygen saturation (SpO2) is fairly low and the pulse oximeter cannot obtain measurements. The SpO2 value provided by the pulse oximeter can be used in assessing or screening some symptoms such as pulmonary embolism [1], hypoxemia[2], lower extremity arterial disease [3], congenital heart disease[4], acute heart failure [5], and chronic obstructive pulmonary disease [6]. Apart from assessing the symptoms, the pulse oximeter can be potentially utilized in evaluating testicular torsion [7] and pulp vitality [8] as well. Today, the pulse oximeter is not only used in medical fields but also applied in the sport, fitness and even aerospace fields. The conventional non-invasive pulse oximeter operates by emitting two light wavelengths, namely, red and infrared (IR), through a human body (forehead, earlobe and finger). By illuminating these two light sources, two photoplethysmographic (PPG) signals are generated, with the red source markedly absorbed by deoxyhemoglobin (Hb) and the IR source largely absorbed by oxyhemoglobin (HbO2). Employing a ratio of the Hb PPG signal to the HbO2 PPG signal allows the acquisition of SpO2. Intrinsically, SpO2 provides an exact percentage of oxygen saturation only when subject being measured stays still. However, in practice, movement during measuring always transpires due to various factors, such as unconsciousness, shivering, and neurological disease. When any movement occurs, an unwanted signal is formed. The unwanted signal from movement, which is known a motion artifact (MA) signal, disturbs the PPG signal, which results in an incorrect SpO2 value. Consequently, a patient may not be diagnosed accurately or cured in a suitable time. Therefore, many research efforts have dedicated to improve the PPG signal corrupted by the MA signal to obtain a precise SpO2 percentage. Principally, solutions toward eliminating MA are categorized into two groups: 1) generating a reference signal to remove MA [9]–[19] and 2) designing a decomposing MA approach without using a reference signal [20]–[31].

In the former group, a reference signal is fed to an adaptive filter to cancel a MA signal added to a PPG signal. The reference signal is obtained by either using additional hardware, namely, an accelerometer sensor [9], [12], [13], an optoelectronic sensor [10], an optical sensor [11], a motion relative sensor [13] or a light source [14] or synthesizing the reference signal from both the acquired red and IR PPG signals [15]–[19]. Using extra hardware [9]–[14] is probably the simplest method, but the reference signal sensed from those sensors must be highly correlated with the PPG signals. Otherwise, the recovered PPG signals are even more aggravated. By contrast, the synthetic approaches excellently produce a reference signal correlated with either the MA signal or the PPG signals because these techniques select a biological signal from a human body, such as heart rate, blood volume or modified PPG signals, that corresponds to the MA or PPG signal to be synthesized. Consequently, the PPG signals retrieved in [15]–[19] are superior to the PPG signals recovered by systems employing auxiliary hardware [9]–[14]. Nevertheless, MA still exists in the PPG signals.

In the latter group, various signal processing techniques are performed to alleviate an MA signal overlapping with the PPG

Manuscript received January 4, 2018; revised March 9, 2018; accepted April 14, 2018. Date of publication May 15, 2018; date of current version August 15, 2018. This paper was recommended by Associate Editor E. Y. Lam. *(Corresponding author: Sakkarin Sinchai.)*

The authors are with the Department of Telecommunications Engineering, Faculty of Engineering, King Mongkut's Institute of Technology Ladkrabang, Bangkok 10520, Thailand (e-mail: 58601019@kmitl.ac.th; 60601155@kmitl.ac.th; pramote@telecom.kmitl.ac.th; jeerasuda@telecom.kmitl.ac.th).

Color versions of one or more of the figures in this paper are available online at http://ieeexplore.ieee.org.

Digital Object Identifier 10.1109/TBCAS.2018.2829708

signals as follows. The concept of the multi-rate filter bank is introduced to seek the frequency band of the MA [20]. Additionally, MA suppression in a frequency domain is accomplished on a cycle-by-cycle basis of Fourier series analysis [21]. Naturally, the PPG and MA signals are contemplated independent of each other. Bearing this in mind, a linear combination of PPG and MA signals is formed to distinguish the PPG and MA signals [22]–[24]. In the same sense of independenct signals, a technique of singular value decomposition is iteratively performed to discriminate the MA signal from the PPG signal [25]. Also, an estimation of signal parameters via rotational invariance techniques is applied to discern high resolution harmonics of the PPG signal from the MA signal [26]. In [27], a minimum correlation approach is used as a cost function to differentiate the PPG and MA signals. Instead of processing in a real number domain, the method of [28] encodes the MA-induced PPG signal to a complex number domain. Statistical analysis and phase filtering are then applied to remove the MA signal. Among the state-of-the-art ideas is the use of a 3rd-order polynomial model to fit the MA signal [29]. Most works have contributed to improve the MA-polluted PPG signals but not for [30]. This approach devises a simple thresholding algorithm based on a correct PPG morphological waveform to select only the best shape of the PPG waveform. Aside from those mentioned signal processing schemes, a differential amplifier with common-mode rejection is designed to cancel the MA signal [31].

Based on the literature review, these approaches endeavor to recover exact PPG signals maintaining all morphological figures from the MA-appended PPG signals. Nonetheless, recovering the exact PPG signal is not simple. Moreover, some techniques may work well only under a specific condition.

Although physical motion is inevitable, in this work, intensity modulation based on a simple amplitude modulation technique is proposed to solve the problem of additive MA signals. With the proposed approach, the frequency band of the PPG signals is shifted away from the frequency band of the MA signals. Because of this shifting, the PPG signals are free from the effect of the additive MA signals.

II. Severing PPG Signals from MA Signals

The widely used pulse oximeter depends on an appropriate waveform of red and IR PPG signals to estimate the SpO2 value. Usually, the red and IR PPG signals are measured from a fingertip, an earlobe or a forehead, where these signals are deformed easily by any movement. Nevertheless, the fingertip is the most concerning because a finger probe is more likely to be interfered with unintentionally and is more ubiquitously used than other probes. Although other factors, such as low profusion, temperature and random noise, have the ability to distort the PPG signals as well, these factors may not affect the PPG signals as severely as MA.

A. PPG Model

Forming a mathematical model is helpful in applying mathematical techniques to remove MA. In this work, a PPG signal is acquired from a fingertip. To represent the PPG signal with a mathematical equation, the intensity of light arriving at a photodetector after being absorbed by various absorbing substances inside the fingertip is employed. However, the absorbing mathematical expression derived from the fingertip is not limited to only the fingertip. Other parts of a human body, forehead or earlobe, are also applicable to the mathematical function drawn from the fingertip because of absorbing in the same manner as the fingertip.

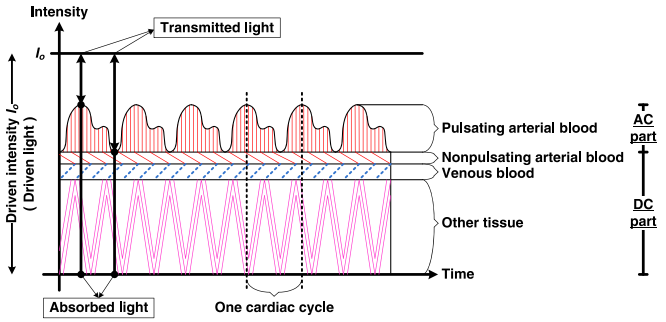

Fig. 1. General PPG waveform.

Modeling the mathematical form of the PPG signal is accomplished using Beer-Lambert's law [32]. The law simply mentions that light passing through a medium containing only one absorbing substance or multiple absorbing substances is attenuated. Later, the absorbing substance was called as an absorber. By nature, when emitted light penetrates the medium, the emitted light is split into two parts. One part is absorbed, whereas the other part is transmitted through the medium. The transmitted light is the light intensity remaining after absorption. The relationship of the light intensity absorption described by the Beer-Lambert's law is chiefly expressed by (1).

$$i = i_o e^{-\sum_{k=1}^{N} \varepsilon_k(\lambda) c_k d_k} \tag{1}$$

From (1), the transmitted light having the transmitted intensity, i, is the multiplication between the emitted light denoted as i_o, and an exponential decay value, $e^{-\sum_{k=1}^{N} \varepsilon_k(\lambda) c_k d_k}$. The emitted light is the incident light with an intensity, i_o, falling upon the medium's surface. The exponent of the exponential decay value is the negative summation of N absorbing characteristic values of N absorbers. The absorbing characteristic value of each absorber is the multiplication of three absorbing parameters which are $\varepsilon_k(\lambda)$, c_k and d_k. The first parameter, $\varepsilon_k(\lambda)$, is the extinction coefficient, ε_k, of a specific wavelength λ of the kth-absorber. Next, c_k is the concentration of the kth-absorber. Lastly, d_k is the optical path length of the kth-absorber.

Since the mathematical statement in (1) is a broad absorbing model of Beer-Lambert's law, (1) is revised to represent the absorbing feature in the human body. For convenience in modeling, a general PPG waveform of transmitted light refered in [32] is considered, and the general PPG waveform is drawn in Fig. 1. As can be noticed in Fig. 1, the emitted light having the intensity, i_o, is mainly absorbed by other tissue, venous blood, nonpulsating arterial blood and pulsating arterial blood. These four media are categorized into two parts according to their absorbing characteristics. The first three media, their

absorbing characteristics, rarely change over time so these media are grouped as a static part. On the other hand, the absorbing characteristic of the last medium is varied over time due to the nature of systole and diastole, and classified as a dynamic part. After being absorbed by both parts, the leftover intensity of the emitted light is sensed by the photo-detector which produces the resulting intensity in terms of electrical current. For the absorption in the static part, the photo-detector gives a direct current (DC) signal while the photo-detector delivers an alternating current (AC) signal for absorbing in the dynamic part. With this grouping, (1) is rewritten as (2).

$$i = i_o[DC_{\text{part}} + AC_{\text{part}}] \tag{2}$$

To express both DC_{part} and AC_{part} in terms of exponential decay values, DC_{part} is considered to be one homogeneous DC absorber. Similarly, AC_{part} is contemplated as one homogeneous AC absorber. (2) is reformed to (3).

$$i = i_o \left[\underbrace{e^{-\varepsilon_{\text{ts}}(\lambda) c_{\text{ts}} d_{\text{ts}}}}_{\text{DC}_{\text{absorber}}} + \underbrace{e^{-\varepsilon_{\text{dav}}(\lambda) c_{\text{dav}} d_{\text{dav}}}}_{\text{AC}_{\text{absorber}}} \right] \tag{3}$$

In fact, the optical path length (d_{dav}) of AC_{absorber} changes over time. Hence, the optical path length (d_{dav}) in (3) is suitably stated in a function of time and (3) is written in (4).

$$i(t) = i_o \left[\underbrace{e^{-\varepsilon_{\text{ts}}(\lambda) c_{\text{ts}} d_{\text{ts}}}}_{\text{DC}_{\text{absorber}}} + \underbrace{e^{-\varepsilon_{\text{dav}}(\lambda) c_{\text{dav}} d_{\text{dav}}(t)}}_{\text{AC}_{\text{absorber}}} \right] \tag{4}$$

From (4), $\varepsilon_{\text{ts}}(\lambda)$, c_{ts} and d_{ts} are represented as the absorbing properties of the DC absorber. Next, $\varepsilon_{\text{dav}}(\lambda)$, c_{dav} and $d_{\text{dav}}(t)$ denote the absorbing properties of the AC absorber.

Measuring oxygen saturation using the pulse oximeter relies on the light absorption of Hb and HbO2 inside the pulsating arterial blood (AC_{absorber}). The pulse oximeter uses red and IR light to measure the amount of light absorbed by Hb and HbO2 because the red light is highly absorbed by Hb but not by HbO2, whereas the IR light is highly absorbed by HbO2 but not by Hb. Consequently, (4) is modified to afford (5), where $\varepsilon_{\text{dav}}(\lambda)c_{\text{dav}}$ is superseded by the summation of the absorption parameters of Hb and HbO2, which are $\varepsilon_{\text{Hb}}(\lambda)c_{\text{Hb}}$ and $\varepsilon_{\text{HbO}}(\lambda)c_{\text{HbO}}$. In addition, Hb and HbO2 absorb light inside the pulsating arterial blood; thus, the optical path lengths of Hb and HbO2 are $d_{\text{dav}}(t)$.

$$i_{\text{cPPG}}(t) = i_o[e^{-\varepsilon_{\text{ts}}(\lambda) c_{\text{ts}} d_{\text{ts}}} + e^{-[\varepsilon_{\text{Hb}}(\lambda) c_{\text{Hb}} + \varepsilon_{\text{HbO}}(\lambda) c_{\text{HbO}}] d_{\text{dav}}(t)}] \tag{5}$$

After being absorbed by Hb and HbO2, the remaining light intensity in (5) is considered as a mathematical model of the PPG signal. As the derivation of the acquired mathematical model does not involve MA, (5) therefore represents the clean PPG signal and is denoted $i_{\text{cPPG}}(t)$.

B. Occurrence and Interference of MA

In the event of finger motion, a mechanical force is introduced to a finger probe of a pulse oximeter, and this force is prone to corrupt the PPG signals. However, the PPG signals are collected in the form of the amount of remaining light intensity from the transmitted or reflected light that falls upon a photo-detector in the pulse oximeter. The photo-detector is a transducer converting the quantity of light into the level of current. However, the mechanical force occurring due to motion is not light, and thus, the mechanical force is not sensed by the photo-detector. Although finger movement generates mechanical force, this force may not affect the PPG signals directly. In fact, when a finger shifts, the marring of the PPG signals is caused by external light sources penetrating through the pulse oximeter where the external light sources are mainly ambient light and natural light. For the problem of the external light interference, there are many articles [33]–[44] proposed the approaches to overcome this problem.

Even though a plastic finger-shaped cover is put onto a finger to prevent interference from the external light sources, the interfering light still passes through the pulse oximeter. Above all, bringing a plastic cover to exclude the unwanted light may not be convenient for use with a patient because the cover needs to enclose an entire finger. Covering the entire finger not only makes a patient feel uncomfortable but also creates heat as well as moisture, which leads to a musty and damp environment and generates poor PPG signals.

To confirm that the external light from ambient light sources interferes with the PPG waveforms during motion, fingers at rest and making a waving motion are tested under bright and dark conditions.

Under the bright conditions, the test is set in a room at noon biased by the fluorescent light and the light from the natural sources entering through the room's windows. On the other hand, under the dark conditions, the experiment is done at the same room at night, which is dark and not influenced by any light sources.

The experiment is set up by inserting an index finger-like log into a transmittance finger-type pulse oximeter and binding the pulse oximeter onto the real index finger with masking tape. In the experiment, the index finger is kept at rest or waved under the conditions described above, and the results of light absorption are collected and illustrated in the forms of voltage level in Fig. 2. By contemplating the results from the motionless finger, it is found that both voltage levels under bright and dark conditions [see Fig. 2(A1)–(B1)] are constant. These resulting constant voltage levels seem to only elevate the DC part of the PPG signals but not to cause any deformity to PPG waveforms. Nonetheless, when analyzing the results from the waving finger, the voltage level under the bright conditions consistently changes relative to the waving motion, as depicted in Fig. 2(A2). With this changing characteristic, the PPG waveforms are obviously disfigured by external light. By contrast, the voltage level for the waving finger in the dark is unchanged because of the lack of interference from external light, as manifested in Fig. 2(B2). In addition, the equal constant voltage levels from both motionless and waving finger in the dark condition strengthen the reason that external light affects the PPG signals. Factually, the photo-detector creates an electrical signal even there is no light due to the non-ideal material [45]. The electrical signal generated in the dark, called the dark current, mainly depends on the input voltage fed to the photo-detector. In this experiment, a

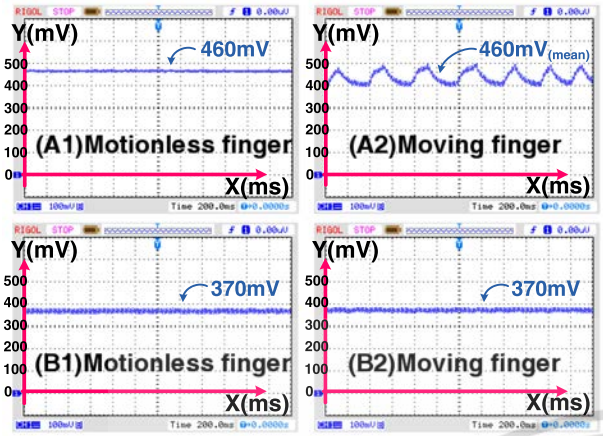

Fig. 2. Photo-detector output signals in case of motionlessness and in motion fingers under (a) bright and (b) dark conditions. Y-axis in each subfigure is the signal amplitude in millivoltage (mV) and X-axis is time in millisecond (ms).

constant voltage of 5.0 V is fed to the photo-detector. With the given property of the photo-detector, the voltage levels in the dark illustrated in Fig. 2(B1)–(B2) are deterministic and easily eliminated, and considered no impact on the pulse oximeter. Hence, the results obtained from the waving finger show explicitly that the external light sources have the impact on the pulse oximeter. As can be observed in Fig. 2(A2), the voltage level of the external light after subtracting the voltage level of the dark current swings from 0 V to 90 mV. For the PPG signals, the voltage levels are in a range of 1 μV to 100 mV [46]. It is seen that the determined external light voltage is in the same magnitude of the general PPG signals. When these signals are summed together, the PPG waveform is completely disfigured. Thus, the external light interference is considered to have high impact on the PPG signals measured by the pulse oximeter.

According to this altering behavior, the light distortion of motion is considered to be an additive noise. To conveniently analyze and eliminate the motion additive noise, a mathematical model of a received signal from the photo-detector is expressed as (6).

$$i_r(t) = i_{\mathrm{MA}}(t) + i_{\mathrm{cPPG}}(t) \tag{6}$$

In (6), $i_r(t)$ is the received PPG signal, which is the summation of $i_{\mathrm{MA}}(t)$, an MA signal, and $i_{\mathrm{cPPG}}(t)$, a clean PPG signal. To analyze the received PPG signal, (6) is further examined in a frequency domain in the next subsection.

C. Analysis of the Combined Clean PPG and MA Signals

For simplicity, a fast Fourier transform (FFT) is chosen to analyze the received PPG signal which is the aggregate of a clean PPG signal and an MA signal. In analyzing how the two signals are overlapped, some possible MA signals and an artifact-free PPG signal are required. The possible MA signals are sampled using the same procedure experimented in the earlier subtopic. The pose for MA signals is acquired from bending, waving, shivering, horizontal moving, and vertical shifting an index finger. On the other hand, the motionless PPG signal is collected

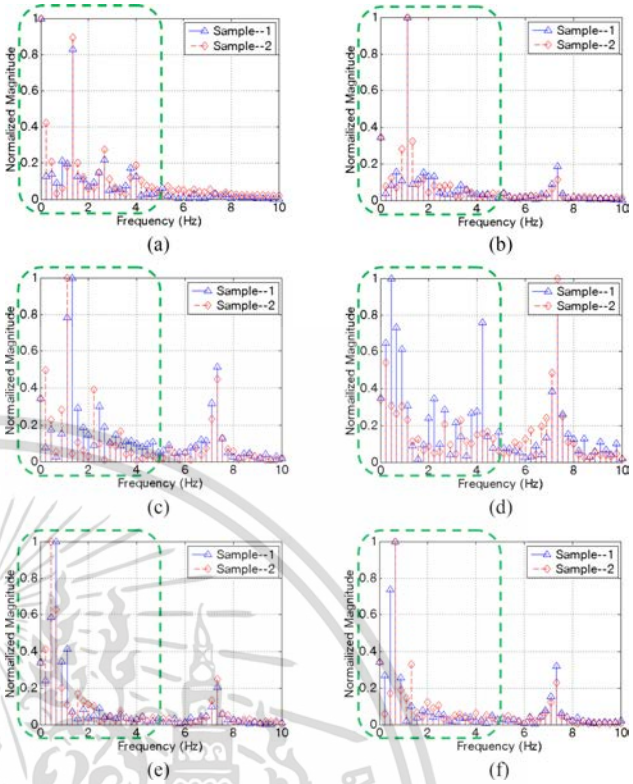

Fig. 3. Frequency components of motionless PPG signal and MA signals. (a) Motionless posture. (b) Bending posture. (c) Waving posture. (d) Shivering posture. (e) Horizontal motion. (f) Vertical shifting.

by utilizing a real index finger while staying still. Each posture, including staying still pose, is performed 2 times, 10 seconds each. After all samples (12 samples) are obtained, the FFT is applied on each sample through MATLAB in order to express frequency components of each pose as delineated in Fig. 3.

The frequency range of the uncorrupted PPG signal is generally between 0.09 Hz and 4 Hz, which is denoted by the dashed box in Fig. 3(a). Undoubtedly, the frequency range of MA signals also lies in the same range as the uncontaminated PPG signal, as can be seen in the dashed boxes in Fig. 3(b)–(f). Indeed, the MA signals are added to the normal PPG signal as revealed in (6). Some of MA signals, however, contain frequency components higher than 4 Hz, as shown in Fig. 3(b)–(f), that can also worsen the clean PPG signal.

D. Proposed PPG Frequency Band Shifting Solution

In a commercial pulse oximeter, red and IR light emitting diodes (LEDs) are used as light sources to generate red and IR PPG signals. To obtain both red and IR PPG signals, the red and IR LEDs are alternately emitted as diagrammed in Fig. 4. In LED driving, a direct current (DC) source is fed to each LED.

With feeding DC to drive the LEDs, both the generated red and IR light intensities are considered constant. Therefore, both the acquired red and IR PPG signals would be characterized by (5). As an MA signal is always and unavoidably involved, (6) represents the obtained red and IR PPG signals. However, by alternately emitting the LEDs, the red and IR PPG signals

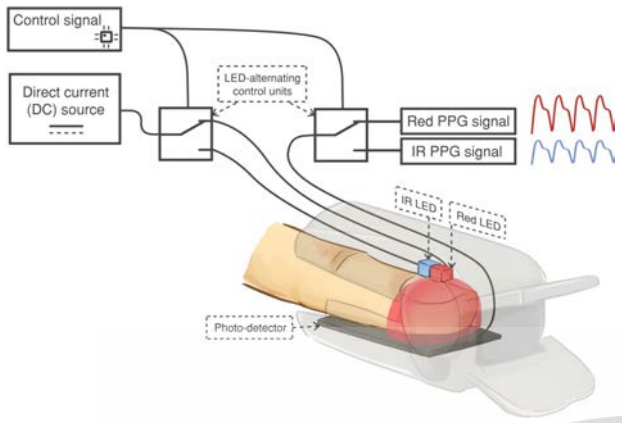

Fig. 4. Diagram of the acquisition of a PPG signal using a commercial pulse oximeter.

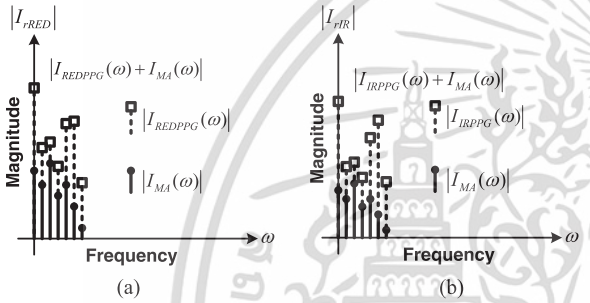

Fig. 5. Frequency spectra of mixing the clean PPG and MA signals. (a) Frequency spectra of (9), MA+ REDPPG. (b) Frequency spectra of (10) , MA+ IRPPG.

are detected alternately, providing two separate signals in (7) and (8).

$$i_{\mathrm{rRED}}(t) = i_{\mathrm{MA}}(t) + i_{\mathrm{REDPPG}}(t) \tag{7}$$

$$i_{\mathrm{rIR}}(t) = i_{\mathrm{MA}}(t) + i_{\mathrm{IRPPG}}(t) \tag{8}$$

In the previous subsection, the frequency of the PPG signals and the frequency of the MA signals are shown to be in the same band. Therefore, (7) and (8) would certainly illustrate the overlapping of the PPG and MA signals in a frequency domain. Then, (7) and (8) are subjected to a Fourier transformation, providing (9) and (10), respectively. By finding the absolute values of (9) and (10), the frequency spectra of (9) and (10) are obtained, as depicted in Fig. 5.

$$I_{\mathrm{rRED}}(\omega) = I_{\mathrm{MA}}(\omega) + I_{\mathrm{REDPPG}}(\omega) \tag{9}$$

$$I_{\mathrm{rIR}}(\omega) = I_{\mathrm{MA}}(\omega) + I_{\mathrm{IRPPG}}(\omega) \tag{10}$$

Because they are in the same frequency range as the MA signals, the clean red and IR PPG signals are thus shifted to higher frequency. Because both the red and IR PPG frequency bands move, the MA signals have no effect on the red and IR PPG signals. To shift the red and IR PPG frequency bands, two sinusoidal waves with different frequencies are proposed to drive both the red and IR LEDs. Using the proposed LED driving method generates two double sideband with carrier (DSB-WC) amplitude modulation (AM) signals with both the red and IR PPG signals as the information signals. To explain how the red and IR PPG signals are collected, the PPG model in (5) is restructured to conform with the model of the DSB-WC AM signal. For convenience, the model of the DSB-WC AM signal is shorten to AM for the rest of this paper.

To satisfy the AM technique, (5) needs to conform to the DSB-WC AM form [47] expressed in (11).

$$\phi_{\mathrm{AM}}(t) = A_c[1 + k_a m(t)] \cos(\omega_c t)\ ,\ \omega_c{=}2\pi f_c \tag{11}$$

In (11), $\phi_{\mathrm{AM}}(t)$ is the AM signal, $m(t)$ is the message signal, $cos(\omega_c t)$ is the sinusoidal carrier signal, and A_c is the amplitude of the sinusoidal carrier signal. In addition, k_a is the AM sensitivity, and f_c and ω_c are the carrier frequencies in Hertz and radians, respectively.

In practice, the value of $e^{-\varepsilon_{\mathrm{ts}}(\lambda)c_{\mathrm{ts}}d_{\mathrm{ts}}}$ in (5) rarely varies over time. Therefore, the value of $e^{-\varepsilon_{\mathrm{ts}}(\lambda)c_{\mathrm{ts}}d_{\mathrm{ts}}}$ in (5) is determined to be constant and defined as A_{ts}. Then, A_{ts} is replaced in (5), which is rearranged to provide (12) by applying the distributive property.

$$i_{\mathrm{cPPG}}(t) = i_o A_{\mathrm{ts}}[1 + A_{\mathrm{ts}}^{-1} e^{-([\varepsilon_{\mathrm{Hb}}(\lambda)c_{\mathrm{Hb}} + \varepsilon_{\mathrm{HbO}}(\lambda)c_{\mathrm{HbO}}]d_{\mathrm{dav}}(t))}] \tag{12}$$

From (12), $e^{-([\varepsilon_{\mathrm{Hb}}(\lambda)c_{\mathrm{Hb}} + \varepsilon_{\mathrm{HbO}}(\lambda)c_{\mathrm{HbO}}]d_{\mathrm{dav}}(t))}$ is information of interest, which is considered the message signal, $m(t)$. In addition, A_{ts}^{-1} is the AM sensitivity, k_a. With the given message signal and the provided AM sensitivity, (12) is rewritten as (13).

$$\begin{aligned} i_{\mathrm{cPPG}}(t) &= i_o A_{\mathrm{ts}}[1 + k_a m(t)]\ , \\ k_a m(t) &= A_{\mathrm{ts}}^{-1} e^{-([\varepsilon_{\mathrm{Hb}}(\lambda)c_{\mathrm{Hb}} + \varepsilon_{\mathrm{HbO}}(\lambda)c_{\mathrm{HbO}}]d_{\mathrm{dav}}(t))} \end{aligned} \tag{13}$$

To make (13) comply with (11), the sinusoidal carrier signal must be present in (13). In this work, an alternating current (AC) source is proposed to supersede the DC source in the commercial pulse oximeter. The DC source generating the incident light with the intensity value, i_o, represented in (13) is replaced by the AC source having a frequency of f_c Hz, $i_{\mathrm{AC}}cos(2\pi f_c t)$. After supplanting, the intensity value, i_o, in (13) becomes a sinusoidal intensity wave with a frequency of f_c Hz, $i_{\mathrm{AC}}cos(2\pi f_c t)$. Therefore, (13) is restated as (14) and $i_{\mathrm{AC}}cos(2\pi f_c t)$ is manifested in the angular frequency instead.

$$\phi_{\mathrm{AM\_cPPG}}(t) = i_{\mathrm{AC}}cos(\omega_c t)A_{ts}[1 + k_a m(t)]\ ,\ \omega_c = 2\pi f_c \tag{14}$$

In this proposed technique, two AC sources with frequencies of f_{c1} Hz and f_{c2} Hz are used to illuminate both the red and IR LEDs instead of the DC source. Additional, if there are multiple carrier signals, as in this work, the gap between the frequencies f_{c1} and f_{c2} must be wide enough to prevent overlap between the frequencies of the message signals.

As the proposed scheme drives both LEDs concurrently, the LED-alternating control units are removed, and two bandpass filters (BPFs) are added instead. In this way, the modulated clean red and IR PPG signals, including the MA signals, are detected at the same time on the photo-detector. Nonetheless, using the projected method completely shifts the frequency components of the pure red and IR PPG signals to a high frequency. On the other hand, the frequency components of the artifact-free red and IR PPG signals do not exist at a low frequency. Because of that

shift achieved by the proposed technique, the signal received by the photo-detector is modeled as (15).

$$i_{\mathrm{rR\_IR\_AM}}(t) = i_{\mathrm{MA}}(t) + i_{\mathrm{REDPPG}}(t) + i_{\mathrm{IRPPG}}(t) \quad (15)$$

For consistency, $i_{\mathrm{REDPPG}}(t)$ and $i_{\mathrm{IRPPG}}(t)$ in (15) are replaced by $\phi_{R\_AM}(t)$ and $\phi_{IR\_AM}(t)$, respectively, because these terms are now the AM signals. Thus, (15) is modified to afford (16), where i_R and i_{IR} are the intensities of the red and IR LEDs, respectively.

$$\begin{aligned} i_{\mathrm{rR\_IR\_AM}}(t) &= i_{\mathrm{MA}}(t) + \phi_{R\_AM}(t) + \phi_{IR\_AM}(t)\,, \\ \phi_{R\_AM}(t) &= i_R A_{\mathrm{Rts}}[cos(\omega_{c1}t) \\ &\quad + k_{\mathrm{Ra}} m_R(t) cos(\omega_{c1}t)], \\ \phi_{IR\_AM}(t) &= i_{\mathrm{IR}} A_{\mathrm{IRts}}[cos(\omega_{c2}t) \\ &\quad + k_{\mathrm{IRa}} m_{\mathrm{IR}}(t) cos(\omega_{c2}t)] \end{aligned} \quad (16)$$

As (16) is in a time domain, the shift in the uncorrupted red and IR PPG signals is not explicitly seen. Then, (16) is Fourier transformed into a frequency domain expressed in (17) to show the frequency spectra of the shifted pure red and IR PPG signals and the MA signal.

$$\begin{aligned} I_{\mathrm{rR\_IR\_AM}}(\omega) &= \underbrace{I_{\mathrm{MA}}(\omega)}_{\mathrm{FSB1}} \\ &+ \underbrace{\frac{i_R A_{\mathrm{Rts}}}{2}[\delta(\omega-\omega_{c1}) + \delta(\omega+\omega_{c1})]}_{\mathrm{FSB2}} \\ &+ \underbrace{\frac{i_R A_{Rts} k_{\mathrm{Ra}}}{2}[M_R(\omega-\omega_{c1}) + M_R(\omega+\omega_{c1})]}_{\mathrm{FSB3}} \\ &+ \underbrace{\frac{i_{\mathrm{IR}} A_{\mathrm{IRts}}}{2}[\delta(\omega-\omega_{c2}) + \delta(\omega+\omega_{c2})]}_{\mathrm{FSB4}} \\ &+ \underbrace{\frac{i_{\mathrm{IR}} A_{\mathrm{IRts}} k_{\mathrm{IRa}}}{2}[M_{\mathrm{IR}}(\omega-\omega_{c2}) + M_{\mathrm{IR}}(\omega+\omega_{c2})]}_{\mathrm{FSB5}} \end{aligned} \quad (17)$$

From (17), the $FSB1$ term is the Fourier transform of the MA signal, $i_{\mathrm{MA}}(t)$. Next, the $FSB2$ term is altered from the red LED carrier signal, $i_R A_{\mathrm{Rts}} cos(\omega_{c1}t)$, and the $FSB4$ term is changed from the IR LED carrier signal, $i_{\mathrm{IR}} A_{\mathrm{IRts}} cos(\omega_{c2}t)$. Lastly, the $FSB3$ and $FSB5$ terms are converted from the shifted red and IR PPG signals, which are $i_R A_{\mathrm{Rts}} k_{\mathrm{Ra}} m_R(t) cos(\omega_{c1}t)$ and $i_{\mathrm{IR}} A_{\mathrm{IRts}} k_{\mathrm{IRa}} m_{\mathrm{IR}}(t) cos(\omega_{c2}t)$, respectively. Next, the frequency spectra are obtained by calculating the absolute value of (17) and are displayed in Fig. 6. As shown in Fig. 6, the frequency ranges of the faultless red and IR PPG signals (the dashed box on the right) are obviously shifted. Conversely, Fig. 6 also reveals that the frequency band of the MA signal (the dotted box on the left) is located at the same frequency band. As demonstrated by Fig. 6, the unperturbed red and IR PPG signals are no longer interfered with by the MA signal.

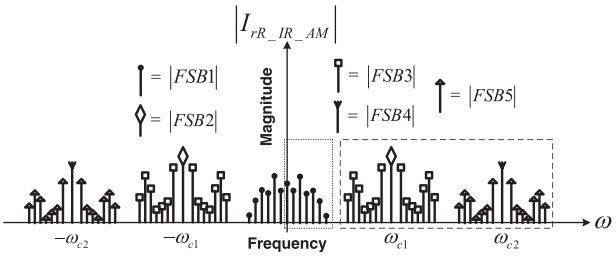

Fig. 6. Shifted frequency spectra of the pure red and IR PPG signals.

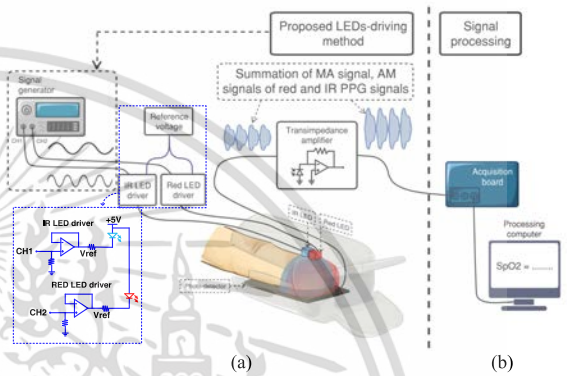

Fig. 7. Implementation block diagram. (a) Proposed LEDs-driving technique. (b) Signal processing.

III. Implementation of the Proposed Technique

To implement the proposed technique, this work is divided into two parts. These two parts, which are drawn as the block diagram shown in Fig. 7, are a) the proposed LED-driving technique and b) signal processing. The former part, which is the main contribution of this work, shifts the frequency spectra of the red and IR PPG signals away from the frequency spectra of the MA signal. Although this first component is the major contribution, the latter part is required to recover both the red and IR PPG signals and to estimate the SpO2 value.

A. Proposed LEDs-Driving Technique

In this implementation, both built-in red LED and IR LED driving circuits of a commercial transmittance finger-probe pulse oximeter are replaced by the proposed LED-driving technique depicted in the dotted box in Fig. 7. The proposed LED-driving scheme induces the red LED and IR LED simultaneously using sinusoidal waves with different frequencies, also known as an AC. By contrast, the built-in driving circuits generate DC to alternate between emitting the red LED and IR LED at a high frequency [48]. In practice, the anode pins of the red and IR LEDs embedded inside the commercial transmittance finger-probe from the maker are soldered to each other for connecting a DC source. The cathode pins are left floating for the traditional driving purpose. To make use of the present LED-driving technique, two designed LED drivers are separately connected to each cathode pin of the red and IR LEDs, respectively. The employed LED-driving circuits are simple buffer amplifiers, as equivalently sketched at the left-corner of Fig. 7. Besides, both

anode pins are attached to a 5 VDC source. By plugging each cathode pin to the different LED drivers instead of to the ground, thus, the reference voltage of each LED is independent to each other and freely varied by the fed sinusoidal signal.

To induce both LEDs to emit using sinusoidal signals at high frequencies, a signal generator is employed to generate two sinusoidal waves with amplitudes of 1.5 Vpp (Vpeak-to-peak). Furthermore, the frequency gap between both generated sinusoidal waves is roughly set to 480 Hz to circumvent the overlapping of the message signals. To generate red light, the red LED is driven at a frequency of 1070 Hz, f_{c1}. Similarly, the IR LED is radiated at a frequency of 1550 Hz, f_{c2}, to produce IR light. After these sinusoidal waves are formed, the voltage offsets of -0.15 V and 0.95 V are then added to these two signals, respectively, before driving the LEDs.

By illuminating these LEDs onto a fingertip with the produced sinusoidal waves, the remaining light absorbance of each light (red and IR lights) becomes the amplitude of the light intensity modulated signals.

Due to the amplitude of light intensity modulated red and IR PPG signals, including the MA signal, contacting the photodetector concurrently, these three signals are summed and transformed into a current. Nonetheless, the current of the summed signal is fairly low. To enhance the quality of the summed signal, a transimpedance amplifier is introduced to amplify the current level of the summed signal. The transimpedance amplifier not only augments the current level but also converts the current level into the form of the voltage level simultaneously. As a result of converting of the transimpedance amplifier, the summed signal is now represented in the form the voltage level, which is convenient to collect. After passing through the transimpedance amplifier, (16) is revised as a voltage function, which is written in (18).

$$v_{i_{\mathrm{rR\_IR\_AM}}}(t) = v_{i_{\mathrm{MA}}}(t) + v_{\phi_{R\_AM}}(t) + v_{\phi_{IR\_AM}}(t) \quad (18)$$

Additionally, the transimpedance amplifier in this work is designed to provide 10 times the gain. After boosting, this augmented summed signal is further processed in a computer.

B. Signal Processing

In this part, MATLAB is employed to handle the augmented summed signal. The augmented summed signal is processed by transferring it to a computer and then sampling 16000 samples per second for 10 seconds through an NI DAQPad-6014 acquisition card manufactured by National Instruments. To extract the clean red and IR PPG signals, the transferred signal is processed according to the processing procedures in Fig. 8 as follows. Firstly, only the AM signals of the red and IR PPG signals are classified since the MA signal no longer causes interference. To distinguish these two AM signals, two BPFs are first designed using the 2nd-order Butterworth technique, in which the center frequencies are 1070 Hz (BP1) and 1550 Hz (BP2). Next, the received summed signal, represented by (18), is initially fed to BP1 and BP2 to classify these signals. The obtained output from BP1 is the AM signal of the red PPG signal, whereas the acquired output from BP2 is the AM signal of the IR PPG signal. These two AM signals are then subjected to an equivalent envelope-detection method to demodulate the red and IR PPG signals. The equivalent envelope-detection method simply finds the absolute values of those two AM signals. Later, the AM signals of the red and IR PPG signals are demodulated, and the red and IR PPG signals are obtained. However, the demodulated red and IR PPG signals still contain high frequency components. To eliminate these high frequency components, two lowpass filters denoted LPF1 and LPF2 are established using the 2nd-order Butterworth scheme with a cut-off frequency of 10 Hz. Finally, the demodulated red and IR PPG signals are filtered by LPF1 and LPF2, respectively, and recovered to provide the clean red and IR PPG signals.

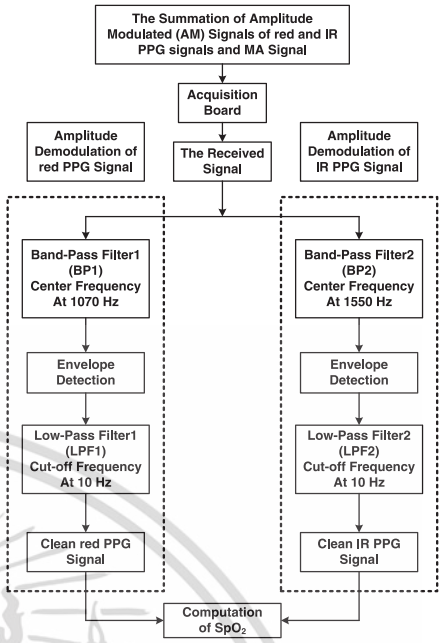

Fig. 8. Signal processing procedures.

According to the previous processing, the appropriate PPG signals are now artifact free. Consequently, the correct value of SpO2 can be calculated by applying the following relationship.

$$SpO2 = 110 - 25 \times R\,,\; R = \frac{\frac{V_{\mathrm{ppR}}}{V_{\mathrm{DCR}}}}{\frac{V_{\mathrm{ppIR}}}{V_{\mathrm{DCIR}}}} \quad (19)$$

In (19), V_{ppR} and V_{DCR} are the peak-to-peak value and the DC component of the red PPG signal, respectively. Similarly, V_{ppIR} and V_{DCIR} expressed in (19) are the peak-to-peak value and the DC component of the IR PPG signal, respectively. Normally, to apply (19), both the red and IR PPG signals are separated beat-by-beat to obtain V_{ppR} and V_{ppIR} for each beat in order to compute SpO2 precisely.

IV. Experimental Results

A. Rest Posture

In this experiment, ten healthy volunteer subjects are tested. The subjects consist of five men and five women. The male's average age is 23.20 years old with a standard deviation of ± 5.12

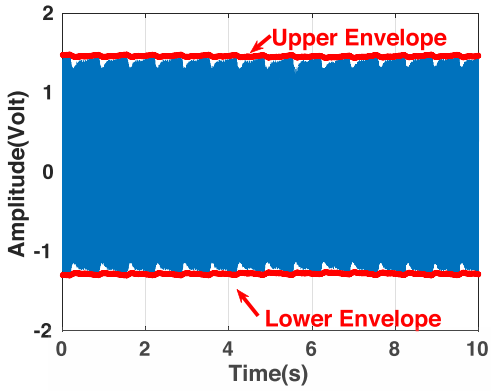

Fig. 9. Summed AM signals.

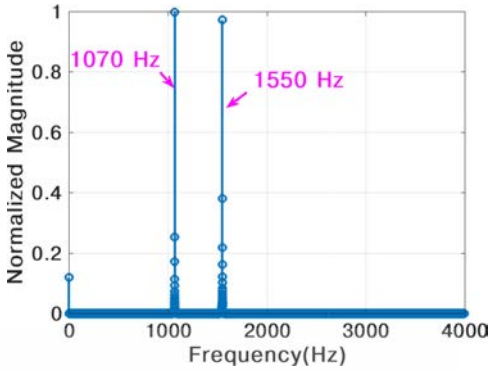

Fig. 10. AM frequency spectra.

while the female's mean age is 22.80 years old with a standard deviation of ± 2.17. All subjects are Asian and their skin is yellowish. Each subject is asked to put a finger-probe pulse oximeter in which the LEDs are driven by the proposed technique on the index finger of his/her left hand. Additionally, on the same hand, a commercial transmittance finger-probe pulse oximeter using traditional LEDs-emitting is inserted on each subject's middle finger for the purpose of PPG waveform comparison. To validate the proposed technique, two experiments, namely, (1) affirming the practicality of the LED-driving strategy using a sinusoidal signal yielding an AM signal and (2) producing different MAs to interfere with the PPG signals, are conducted. The procedures for these two experiments are designed to have minimal risk and performed in keeping with the Declaration of Helsinki. Both experiments are carried out during the daytime in a room where some natural light penetrates through a window. The room is also lit by five fluorescent tubes. Given the room conditions, the ambient light while the experiments take place is 630 Lux.

For the confirmation experiment, each subject is asked to keep the left hand still for 5 times, 10 seconds each, to demonstrate the AM signal created by the proposed technique. Instantly, the red and IR lights pass through the index finger of each subject, and two AM signals of clean red and IR PPG signals are formed. Since the left hand of each subject stays at rest, no MA signal is involved. As a result, only two AM signals of clean red and IR PPG signals contact the photo-detector. With summing property of the photo-detector circuit, the photo-detector output signal is the summation of two AM signals in the time domain, as exhibited in Fig. 9. The result shown in Fig. 9 is collected from one of the subjects. The rest subjects' results also manifest in the same manner as Fig. 9. To show that the combined AM signals comprise two PPG signals modulated by two given sinusoidal carrier waves, the merged AM signals are then analyzed in the frequency domain. Thus, a Fourier transform is applied to the integrated AM signals. With the transform of the summed AM signals, the frequency spectra of the transformed AM signals are obtained and presented in Fig. 10. In accordance with the design, Fig. 10 shows the frequency spectra of the sinusoidal carrier waves, along with the frequency spectra of the PPG signals.

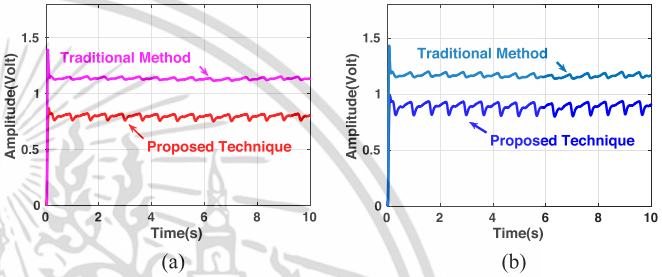

Fig. 11. PPG morphology comparison. (a) Red PPG signals. (b) IR PPG signals.

To utilize these AM signals, an amplitude demodulation is performed as described in the implementation section. After the amplitude demodulation, the clean red and IR PPG signals are recovered and depicted in Fig. 11(a) and (b). In Fig. 11(a) and (b), the red and IR PPG signals from a commercial pulse oximeter are plotted together with the recovered PPG signals for comparison.

Notably, the morphological shapes of the recovered clean red and IR PPG signals are similar to those of the red and IR PPG signals measured by the commercial pulse oximeter. The similarity of the retrieved PPG signals compared to the PPG signals collected from the commercial pulse oximeter is computed by employing Pearson correlation coefficient and normalized Euclidean distance. In calculation, the obtained clean red and IR PPG signals are computed separately. The recovered red PPG signals are merely calculated with the red PPG signals acquired from the conventional pulse oximeter for each subject. Likewise, the retrieved IR PPG signals and the IR PPG signals collected from the traditional method are computed in the same manner. The similar levels of each subject are summarized in terms of average values of each subject in Table I. According to Table I, the recovered red and IR PPG signals display high degree of similarity because their Pearson correlation coefficients are higher than 0.5 [49]. In addition, the normalized Euclidean distance values of the recovered red and IR PPG signals are strongly low and close to zero. With low normalized Euclidean distance values, the recovered red and IR PPG signals are strengthened to have high level of similarity.

However, the amplitudes of the PPG signals from the proposed technique differ from those of the PPG signals from the

TABLE I
LEVEL OF SIMILARITY

Subject No.	PCCR[1]	PCCIR[2]	NEDR[3]	NEDIR[4]
	Mean±Standard deviation			
No.1 (Male)	0.86±0.1	0.86±0.1	0.0021±0.0	0.0014±0.0
No.2 (Male)	0.93±0.0	0.93±0.0	0.0019±0.0	0.0015±0.0
No.3 (Female)	0.83±0.1	0.85±0.1	0.0033±0.0	0.0024±0.0
No.4 (Male)	0.95±0.0	0.95±0.0	0.0024±0.0	0.0017±0.0
No.5 (Male)	0.74±0.3	0.95±0.0	0.0033±0.0	0.0022±0.0
No.6 (Female)	0.93±0.2	0.95±0.0	0.0021±0.0	0.0018±0.0
No.7 (Male)	0.77±0.1	0.70±0.2	0.0025±0.0	0.0021±0.0
No.8 (Female)	0.95±0.0	0.96±0.0	0.0023±0.0	0.0023±0.0
No.9 (Female)	0.88±0.1	0.94±0.1	0.0027±0.0	0.0022±0.0
No.10 (Female)	0.88±0.1	0.87±0.1	0.0029±0.0	0.0020±0.0

1–Pearson correlation coefficients of recovered red PPG signals,
2–Pearson correlation coefficients of retrieved IR PPG signals,
3–Normalized Euclidean distance values of recovered red PPG signals,
4–Normalized Euclidean distance values of retrieved IR PPG signals.

TABLE II
SPO2 VALUES AT THE RESTING CONDITION

Subject No.	SpO2 (Proposed technique)	SpO2 (Conventional method)
	Mean±Standard deviation	
No.1 (Male)	95.69±0.36	93.40±1.09
No.2 (Male)	95.54±0.41	93.30±0.78
No.3 (Female)	95.80±0.58	94.72±0.75
No.4 (Male)	95.83±0.73	93.65±1.88
No.5 (Male)	93.78±1.52	93.34±1.14
No.6 (Female)	95.91±0.86	94.49±0.73
No.7 (Male)	94.45±0.29	92.01±0.73
No.8 (Female)	96.83±0.15	95.28±0.21
No.9 (Female)	95.56±0.28	92.65±2.20
No.10 (Female)	96.28±0.22	94.39±0.65

commercial pulse oximeter due to different LED-driving-circuit designs. Both amplitudes of the PPG signals from the proposed approach are lower than those of the PPG signals from the commercial pulse oximeter. From this viewpoint, the results of the proposed technique imply that the light intensity absorption of the proposed method may be greater than that of the conventional one (see Eq. (5)). To strengthen the given implication, the level of SpO2 is verified. Hence, the SpO2 values of each subject obtained from the presented LEDs-driving and the SpO2 values acquired from the commercial pulse oximeter are calculated and depicted in Table II. The resulting SpO2 values are calculated period-by-period and the results in Table II are the mean SpO2 values of each subject from the proposed and conventional techniques. As can be observed in Table II, the overall SpO2 values of the presented LEDs-driving are higher than those SpO2 values of the commercial pulse oximeter. This indicates that using the proposed technique provide more light intensity absorption than that of employing the traditional pulse oximeter. In addition, the SpO2 values of both male and female subjects of the presented design are are not much different. These resulting SpO2 values suggest that the proposed technique is applicable for both genders.

B. Motion Postures

To illustrate that the PPG signals are no longer in the frequency band of MA, all subjects from the previous experiment

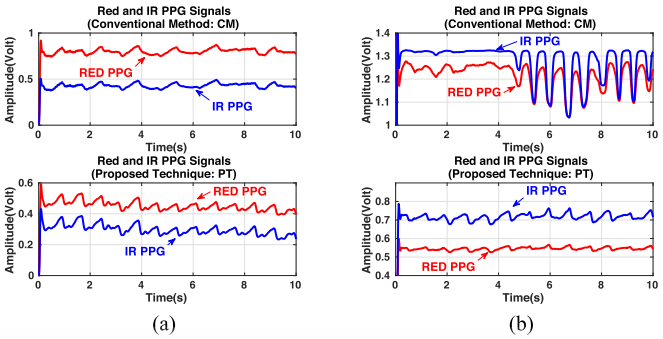

Fig. 12. Finger bending results. (a) Male subject. (b) Female subject.

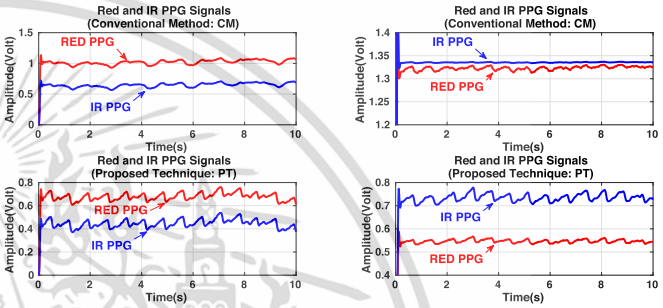

Fig. 13. Finger waving results. (a) Male subject. (b) Female subject.

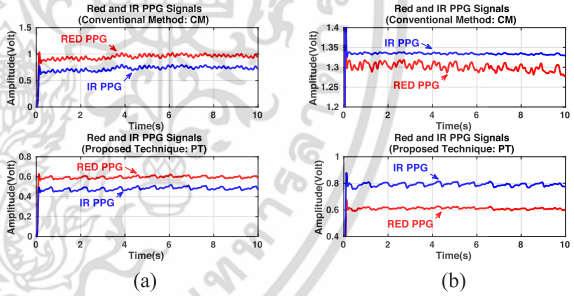

Fig. 14. Finger shivering results. (a) Male subject. (b) Female subject.

are asked to perform five types of daily motion. These five motions are bending a finger, waving a finger, making a finger shiver, moving a finger vertically and moving a finger horizontally. To compare the performance between the proposed LED-driving pulse oximeter and the commercial one, two fingers of the subjects' left hand are used. In this experiment, the index finger is inserted into the proposed LED-driving pulse oximeter, whereas the middle finger is put on the commercial pulse oximeter. During the performance of each type of motion, the subjects are asked to naturally move the index and middle fingers simultaneously. Moreover, to analyze the performance, each motion of the fingers is performed for 5 times, 10 seconds each. Some processed results of each motion are rendered to show the capability of the proposed scheme, as manifested in the time domain in Figs. 12–16. The displayed results are from one male subject and one female subject for all motions. In each resulting performance figure, the first subplot is the red and IR

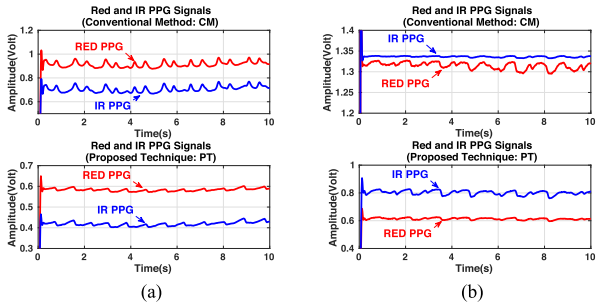

Fig. 15. Vertical finger move results. (a) Male subject. (b) Female subject.

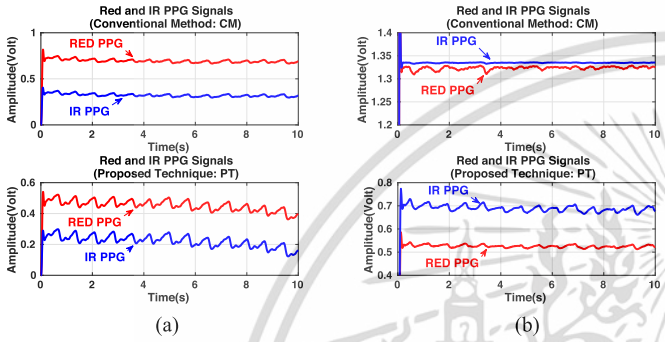

Fig. 16. Horizontal finger move results. (a) Male subject. (b) Female subject.

PPG signals measured using the traditional pulse oximeter, and the next trace is the red and IR PPG signals acquired by the proposed LED-driving pulse oximeter.

To calculate the value of SpO2, the appearance of the proper PPG waveform in each beat is required, as the computation of SpO2 is based on the peak-to-peak value in each cycle of the PPG signal according to (19). Clearly, isolating the PPG frequency band from MA frequency band using the presented approach is effective, as shown by the results expressed in the second subplots of Figs. 12–16. The recovered red and IR PPG signals are uncorrupted by all kinds of the MA signals. By contrast, each PPG signal measured from the commercial pulse oximeter is affected by the ambient light from finger movement. When combining PPG signals and MA signals of the commercial pulse oximeter together, the peak-to-peak value in each beat of the PPG waveform does not appear correctly. As a result, the SpO2 values of the MA-interfered PPG signals of each pose are definitely miscalculated.

Nevertheless, the acquired calculated SpO2 values of each pose from the proposed and conventional techniques are numerous, as the calculation of SpO2 is carried out beat-by-beat. Therefore, all SpO2 values computed cycle-by-cycle of each posture from both approaches are averaged and standard deviation calculated for the purpose of convenience, as summarized in Table III.

By contemplating Table III, it is obvious that the overall SpO2 values of the proposed approach are greater than 94 percentage of oxygen saturation for all motions. On the other hand, the SpO2 values of the conventional method are lesser than 89 for all most motions. From this standpoint, it is indicated that the red and IR PPG signals from the presented technique are well MA-resistant to the influence of external light. By contrast, the red and IR PPG signals from the traditional scheme are rather MA-absorbed than MA-resistant. With the reason of well MA-resistance, the proposed technique is therefore superior to the conventional one.

From the results expressed in Table III, bending a finger, waving a finger, shivering a finger and vertical moving a finger are highly interfered by the external light. The SpO2 values from the mentioned motions acquired by the traditional scheme of each subject are various and mostly below 90 percentage of oxygen saturation.

For horizontal moving a finger, the SpO2 values of the conventional method are averaged greater than 90, and not much different with those values of the presented technique. This points out that the external light has low impact on the red and IR PPG signals in case of horizontal moving a finger for both methods.

In SpO2 computation, the peak-to-peak values in each period of the red and IR PPG signals are automatically detected using a function of findpeaks in MATLAB. Since the red and IR PPG signals measured by the conventional method do not clearly present the peak and trough, the peak-to-peak values are rarely detected. Therefore, only few samples of the SpO2 values of the conventional method are generated. This explains why the SpO2 values obtained by the conventional method of each subject, shown in Table III, are not much fluctuated. On the contrary, the red and IR PPG signals obtained by the proposed technique do explicitly display the peak and trough. Thus, many samples of the SpO2 values of the proposed technique are generated. Still, the SpO2 values obtained by the presented scheme of each subject are less varied. This suggests that the proposed method resists the MA-interference caused by the external light.

C. Error Computation

After all SpO2 values are computed, evaluating the accuracy of these SpO2 values is necessary. To achieve this, a mean absolute percentage error (MAPE) is used as expressed in (20).

$$MAPE = \frac{100}{N}\sum_{i=1}^{N}\left|\frac{de - m_i}{de}\right| \tag{20}$$

From (20), de is a desired SpO2 value. Generally, the desired SpO2 value is computed from the red and IR PPG signals in which no motion is involved. In this work, the desired SpO2 value of each subject uses the averaged SpO2 value according to Table II. For the error computation of the proposed technique, the mean SpO2 value of each subject obtained from the presented method is selected to be the desired SpO2 value. The error computation of the conventional approach is also calculated in the same way as the proposed scheme. In addition, m_i is the SpO2 value calculated from the red and IR PPG signals while motion is occurring. N is the total number of calculated mean SpO2 values of each pose. Since each posture is experimented for 5 times, five computed averaged SpO2 values are generated. Hence, N is set to five for each pose.

By applying (20), the MAPEs of each pose are computed and rendered in Table IV. Noticeably, the proposed technique is superior to the traditional method, as the presented strategy provides lower overall MAPEs than the conventional approach

TABLE III
SUMMARY OF SPO2 VALUES

Subject No.	BF[1] PT[6]	BF[1] CM[7]	WF[2] PT[6]	WF[2] CM[7]	SF[3] PT[6]	SF[3] CM[7]	VF[4] PT[6]	VF[4] CM[7]	HF[5] PT[6]	HF[5] CM[7]
	Mean ±Standard deviation									
No.1 (Male)	95.24 ±0.27	87.80 ±0.53	95.41 ±0.07	90.88 ±0.27	96.14 ±0.32	91.76 ±0.07	94.54 ±0.40	88.93 ±0.73	96.44 ±0.89	92.96 ±1.62
No.2 (Male)	92.92 ±0.37	88.77 ±0.42	96.01 ±0.26	91.04 ±0.14	95.70 ±0.17	92.25 ±0.27	95.06 ±0.12	92.27 ±0.52	95.41 ±0.08	93.11 ±0.34
No.3 (Female)	91.57 ±1.86	84.24 ±1.95	94.44 ±0.49	80.59 ±4.08	92.04 ±1.00	83.83 ±4.46	94.18 ±1.18	82.97 ±1.29	96.85 ±0.18	95.35 ±0.22
No.4 (Male)	96.81 ±0.29	90.90 ±0.70	94.00 ±0.68	89.35 ±0.62	90.54 ±0.35	84.65 ±0.97	94.99 ±0.15	88.32 ±0.12	95.95 ±0.20	92.80 ±0.39
No.5 (Male)	95.62 ±1.35	84.79 ±1.19	95.53 ±0.19	88.28 ±0.81	95.44 ±0.16	86.89 ±0.18	93.70 ±0.52	81.62 ±5.50	95.83 ±0.11	93.91 ±0.08
No.6 (Female)	95.63 ±0.17	89.13 ±1.03	96.55 ±0.13	93.27 ±0.45	91.94 ±0.40	87.32 ±0.41	96.30 ±0.27	90.16 ±0.85	94.87 ±1.02	95.07 ±0.05
No.7 (Male)	92.47 ±0.26	88.16 ±0.90	94.71 ±0.10	91.09 ±0.18	94.99 ±0.09	89.85 ±0.44	95.08 ±0.13	90.29 ±1.01	95.62 ±0.16	88.88 ±2.06
No.8 (Female)	94.12 ±0.52	91.55 ±1.10	97.11 ±1.13	85.77 ±0.10	94.04 ±0.68	91.62 ±1.02	96.15 ±0.21	89.91 ±0.57	97.59 ±0.12	94.19 ±0.72
No.9 (Female)	93.10 ±0.27	86.36 ±2.31	95.85 ±0.25	89.87 ±1.43	91.78 ±0.17	85.65 ±1.36	96.24 ±0.12	89.57 ±0.17	96.01 ±0.08	93.97 ±1.20
No.10 (Female)	97.59 ±1.76	92.54 ±0.71	95.09 ±0.08	92.94 ±0.09	96.66 ±0.23	93.00 ±0.36	95.34 ±0.15	92.01 ±0.45	94.83 ±0.29	93.44 ±0.06

1–Bending a finger, 2–Waving a finger, 3–Making a finger shiver,
4–Vertical movement of a finger, 5–Horizontal movement of a finger,
6–Proposed technique and 7–Conventional method.

TABLE IV
PERCENTAGE ERROR OF EACH POSE

Subject No.	BF[1] PT[6]	BF[1] CM[7]	WF[2] PT[6]	WF[2] CM[7]	SF[3] PT[6]	SF[3] CM[7]	VF[4] PT[6]	VF[4] CM[7]	HF[5] PT[6]	HF[5] CM[7]
No.1 (Male)	0.30	4.96	0.29	2.70	0.47	1.76	1.20	4.79	0.79	1.42
No.2 (Male)	2.27	3.93	0.50	2.42	0.17	1.12	0.51	1.10	0.14	0.37
No.3 (Female)	4.42	9.27	2.46	14.91	3.93	11.50	1.69	12.40	1.10	0.66
No.4 (Male)	0.88	2.35	1.91	4.59	5.52	9.61	0.87	5.69	0.20	0.91
No.5 (Male)	1.52	7.59	1.87	5.42	1.77	6.91	0.48	12.56	2.19	0.61
No.6 (Female)	0.25	4.74	0.67	1.29	4.14	7.59	0.43	4.59	1.08	0.62
No.7 (Male)	1.66	3.57	0.28	1.00	0.57	2.35	0.67	1.87	1.23	3.40
No.8 (Female)	2.13	3.24	0.29	9.99	2.88	3.84	0.70	5.64	0.79	1.15
No.9 (Female)	2.01	5.94	0.35	3.00	3.96	7.56	0.71	3.33	0.47	1.46
No.10 (Female)	1.19	1.36	1.24	1.53	0.39	1.48	0.98	2.52	1.51	1.01
Overall mean error ±Standard deviation (Male and female)	1.66 ±1.20	4.70 ±2.39	0.99 ±0.82	4.69 ±4.47	2.38 ±1.95	5.00 ±3.73	0.82 ±0.39	5.45 ±4.01	0.95 ±0.62	1.16 ±0.86
Overall mean error ±Standard deviation (Male)	1.33 ±0.76	4.48 ±1.97	0.97 ±0.84	3.23 ±1.77	1.70 ±2.22	4.35 ±3.72	0.75 ±0.30	5.20 ±4.54	0.91 ±0.84	1.34 ±1.22
Overall mean error ±Standard deviation (Female)	2.00 ±1.55	4.91 ±2.98	1.00 ±0.90	6.14 ±6.05	3.06 ±1.57	6.39 ±3.86	0.90 ±0.48	5.70 ±3.93	0.99 ±0.39	0.98 ±0.35

for all finger movements. However, for the horizontal movement of a finger, the ambient light does not vary much. As a result, the ambient light slightly affects the measured PPG signals of both techniques, which explains why the MAPE of the conventional method is not much different from the MAPE of the proposed technique for this posture. Nevertheless, the MAPE of the proposed technique is still better.

In addition, the male and female MAPEs of each posture indicate that female subjects are more sensitive to MA-interference than male subjects. This is because female MAPEs are higher than male MAPEs for all kinds of motions. Nevertheless, both male and female MAPEs are quite low. It suggests that the proposed technique is applicable to use with both genders. However, the experiments are conducted with the subjects having yellowish skin at their fingertips, and the presented method works well with yellowish skin. The capability of the proposed technique on other colors of skin cannot be concluded. This issue is further investigated in the future work.

V. PERFORMANCE ANALYSIS

Due to the fact that an ideal bandpass filter which is a brick wall as illustrated in Fig. 17(a) is not possibly constructed. Practically, a non-ideal bandpass filter shaped like a symmetrical trapezoid as portrayed in Fig. 17(b) is applicable to be implemented. Because of the non-ideal bandpass filter, the lower and upper transition bands as depicted in Fig. 17(b) are added to both sides of the ideal bandpass filter. Subsequently, having these transition bands causes the undesired frequencies to be

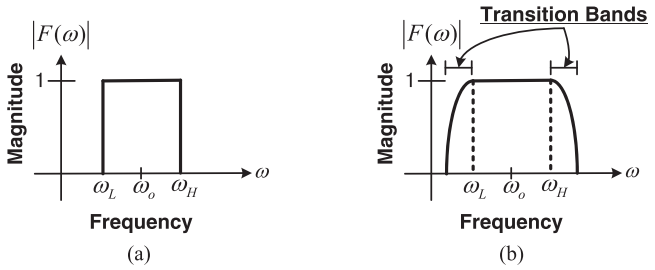

Fig. 17. Comparison of bandpass filters. (a) Ideal filter. (b) Practical filter.

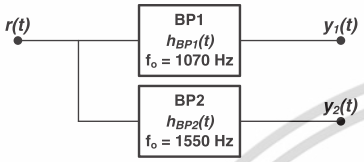

Fig. 18. Signal distinguishing.

filtered out and conjoined with the desired frequencies at the same time. With this problem, the erroneous amplitude of any given filtered signal is apparently noticed. In this work, the received signal as expressed in (18) is analyzed. However, for convenience in error analyzing, both sides of (18) are altered to be the simple function as written in (21).

$$r(t) = r_1(t) + r_2(t) + r_3(t) \tag{21}$$

From (21), on the left side, $r(t)$ is the aggregate of two AM signals and MA signal. Next, on the right side, $r_1(t)$ and $r_2(t)$ are amplitude-modulated by the carrier frequencies of 1070 Hz and 1550 Hz, respectively, and $r_3(t)$ is the MA signal located at lower frequency band. Nevertheless, only $r_1(t)$ and $r_2(t)$ are interested. Therefore, to distinguish $r_1(t)$ and $r_2(t)$, two bandpass filters are utilized as illustrated in Fig. 18. These two bandpass filters, marked as BP1 and BP2 in Fig. 18, are second order filters designed by employing Butterworth technique whose center frequencies are at 1070 Hz and 1550 Hz with 20 Hz bandwidth. Naturally, by passing any signal through any given filter, the produced output is the convolution of the input signal and the transfer function of the given filter. Similarly, feeding $r(t)$ from (21) through both bandpass filters (see Fig. 18) yields the outputs, $y_1(t)$ and $y_2(t)$ which are expressed in the mathematical convolution relations in (22) and (23).

$$y_1(t) = [r_1(t) + r_2(t) + r_3(t)] * h_{\mathrm{BP1}}(t) \tag{22}$$

$$y_2(t) = [r_1(t) + r_2(t) + r_3(t)] * h_{\mathrm{BP2}}(t) \tag{23}$$

To analyze the filtered frequency components of $y_1(t)$ and $y_2(t)$, (22) and (23) are transformed into a frequency domain. Hence, a Fourier transformation are taken on (22) and (23) giving rise to (24) and (25).

$$Y_1(\omega) = [\underbrace{R_1(\omega)}_{1} + \underbrace{R_2(\omega)}_{2} + \underbrace{R_3(\omega)}_{3}] \times H_{BP1}(\omega) \tag{24}$$

$$Y_2(\omega) = [\underbrace{R_1(\omega)}_{1} + \underbrace{R_2(\omega)}_{2} + \underbrace{R_3(\omega)}_{3}] \times H_{BP2}(\omega) \tag{25}$$

Since the unwanted third terms of (24) and (25) are at lower frequency bands and in the stopbands of BP1 and BP2, these third terms are neglected. In reality, with the non-ideality of bandpass filter, the undesired terms in (24) and (25) are not completely eliminated causing error in the outputs, $y_1(t)$ and $y_2(t)$. As a result, for (24), the desired first term is only affected by the second term and (24) is recast as (26). In the same way, for (25), the desired second term is merely influenced by the first term and (25) is revised as (27). Also, (26) and (27) are recast using a distributive property.

$$Y_1(\omega) = \underbrace{R_1(\omega)H_{\mathrm{BP1}}(\omega)}_{1} + \underbrace{R_2(\omega)H_{\mathrm{BP1}}(\omega)}_{2} \tag{26}$$

$$Y_2(\omega) = \underbrace{R_1(\omega)H_{\mathrm{BP2}}(\omega)}_{1} + \underbrace{R_2(\omega)H_{\mathrm{BP2}}(\omega)}_{2} \tag{27}$$

To measure how much the unwanted terms in (26) and (27) have the influence on the desired terms, the SNR is used as a criterion. In order to calculate the SNR value, the averaged power of each term in (26) and (27) is required. As each term of (26) and (27) is not consisted only one frequency component, power spectral density (PSD) is brought to represent each term of (26) and (27). Also, to acquire each mean power of each PSD term of (26) and (27), Parseval's theorem is performed on each term producing (28) and (29).

$$P_{Y1} = \frac{1}{2\pi}\left[\underbrace{\int_{\omega_{1L}}^{\omega_{1H}} S_{R1}(\omega)|H_{\mathrm{BP1}}(\omega)|^2 d\omega}_{\text{Passband:P1}} + \underbrace{\int_{\omega_{2L}}^{\omega_{2H}} S_{R2}(\omega)|H_{\mathrm{BP1}}(\omega)|^2 d\omega}_{\text{Transitionband:T1}}\right] \tag{28}$$

$$P_{Y2} = \frac{1}{2\pi}\left[\underbrace{\int_{\omega_{1L}}^{\omega_{1H}} S_{R1}(\omega)|H_{\mathrm{BP2}}(\omega)|^2 d\omega}_{\text{Transitionband:T2}} + \underbrace{\int_{\omega_{2L}}^{\omega_{2H}} S_{R2}(\omega)|H_{BP2}(\omega)|^2 d\omega}_{\text{Passband:P2}}\right] \tag{29}$$

In (28), the term, P_1, is the interested power term (Passband) as well as the term, T_1, is the uninterested power term (Transition band). While, for (29), the term, P_2, is the desired power term (Passband) and the term, T_2, is the undesired power term (Transition band). It is noted that $S_{R1}(\omega)$ and $S_{R2}(\omega)$ of the AM modulating PPG signals are not easily determined. For the sake of convenience in the analysis of the effect generated by the transition bands of BP1 and BP2, thus, the terms, $S_{R1}(\omega)$ and $S_{R2}(\omega)$, are assumed to be the PSD of white noise which is $N_0/2$.

TABLE V
MEAN POWER AND SNR VALUES

	Filters	
	BP1	BP2
Mean desired power of passband(Watt).	0.84	0.84
Mean undesired power of transition band(Watt).	2.80×10^{-7}	1.09×10^{-7}
$\mathrm{SNR}_{(dB)}$	64.79	68.87

By taking a logarithm of each ratio of the wanted terms and the unwanted terms from (28) and (29), two SNR expressions are obtained as written by (30) and (31). Since $S_{R1}(\omega)$ and $S_{R2}(\omega)$ equal to $N_0/2$, then these terms are canceled out and disappeared in (30) and (31).

$$SNR_{\mathrm{BP1(dB)}} = 10\log\left[\frac{\int_{\omega_{1L}}^{\omega_{1H}} |H_{\mathrm{BP1}}(\omega)|^2 d\omega}{\int_{\omega_{2L}}^{\omega_{2H}} |H_{\mathrm{BP1}}(\omega)|^2 d\omega}\right] \tag{30}$$

$$SNR_{\mathrm{BP2(dB)}} = 10\log\left[\frac{\int_{\omega_{2L}}^{\omega_{2H}} |H_{\mathrm{BP2}}(\omega)|^2 d\omega}{\int_{\omega_{1L}}^{\omega_{1H}} |H_{\mathrm{BP2}}(\omega)|^2 d\omega}\right] \tag{31}$$

As can be seen in (30), the impact of the undesirable term, T_1, on the desirable term, P_1, is depended on the averaged power in the transition band of BP1. In the same direction for (31), the mean power in the transition band of BP2 defines the amount of the influence of the uninterested term, T_2, on the interested term, P_2.

In this study, the averaged power values of the transition bands of BP1 and BP2 are very low compared to the passbands' mean power values as recapitulated in Table V. Obviously, the calculated SNR values of BP1 and BP2 in Table V suggest that the undesired terms, T_1 and T_2, insignificantly affect the required terms, P_1 and P_2, and can be ignored. Thereupon, the filtered outputs, $y_1(t)$ and $y_2(t)$, in (22) and (23) are approximated as (32) and (33).

$$y_1(t) \approx r_1(t) \tag{32}$$

$$y_2(t) \approx r_2(t) \tag{33}$$

VI. CONCLUSION

In this work, a new LED-driving technique applied to a pulse oximeter is proposed. By employing the proposed LED-emission method, the PPG frequency band is shifted away from the MA frequency band. With this presented solution, the PPG signals are no longer disrupted. To characterize its efficacy, the proposed scheme, as well as a conventional LED-driving method set up in a commercial oximeter, is used to test five common finger movements. In addition, SpO2 is computed from the resulting PPG signals to demonstrate the accuracy of the presented approach as well as the traditional method. In the SpO2 calculation, the clean SpO2 value computed from the MA-free PPG signals is used as a reference to the exactness of the proposed technique and the old-fashioned scheme. According to the calculated SpO2 results, the presented approach still has some error up to 2.4%, even though the recovered PPG waveforms seem to be perfectly intact. In contrast, the common method provides computed SpO2 results with an error oscillating between approximately 1% and 5.5% because of the deformation of the PPG waveforms. Although the proposed technique is still unable to thoroughly eliminate the interference of MA, the presented method is superior to the traditional approach. Also, a performance analysis is performed to manifest the error generated by the proposed design. The error is found to have an insignificant impact on the retrieved PPG waveforms. It is noted that most related researches focus on improving the contaminated PPG signals whereas the proposed technique presents a method to prevent the pure PPG signals not to be interfered by the MA signals. With the difference in the schemes, the proposed technique thus is compared with the conventional pulse oximeter only.

REFERENCES

[1] J. A. Kline *et al.*, "Use of pulse oximetry to predict in-hospital complications in normotensive patients with pulmonary embolism," *Amer. J. Med.*, vol. 115, no. 3, pp. 203–208, 2003.
[2] A. Jubran, "Pulse oximetry," *Intensive Care Med.*, vol. 30, no. 11, pp. 2017–2020, 2004.
[3] G. I. Parameswaran, K. Brand, and J. Dolan, "Pulse oximetry as a potential screening tool for lower extremity arterial disease in asymptomatic patients with diabetes mellitus," *Archives Internal Med.*, vol. 165, no. 4, pp. 442–446, 2005.
[4] A. Bakr and H. Habib, "Combining pulse oximetry and clinical examination in screening for congenital heart disease," *Pediatr Cardiol*, vol. 26, no. 6, pp. 832–835, 2005.
[5] J. Masip *et al.*, "Pulse oximetry in the diagnosis of acute heart failue," *Revista Espa de Cardiol.*, vol. 65, no. 10, pp. 879–884, 2012.
[6] S. A. Shah, C. Velardo, O. J. Gibson, H. Rutter, A. Farmer, and L. Tarassenko, "Personalized alerts for patients with copd using pulse oximetry and symptom scores," in *Proc. Conf. IEEE Eng. Med. Biol. Soc.*, Chicago, USA, 2014, pp. 3164–3167.
[7] H.-W. Chen, L.-C. Weng, T.-M. Wang, and K.-F. Ng, "Potential use of pulse oximetry for the diagnosis of testicular torsion," *JAMA Pediatr*, vol. 168, no. 6, pp. 578–579, 2014.
[8] M. Bargrizan, M. A. Ashari, M. Ahmadi, and R. Jamileh, "The use of pulse oximetry in evaluation of pulp vitality in immature permanent teeth," *Dent Traumatol*, vol. 165, no. 4, pp. 43–47, 2016.
[9] A. R. Relente and L. G. Sison, "Characterization and adaptive filtering of motion artifacts in pulse oximetry using accelerometers," in *Proc. 2nd Joint EMBS/BMES Conf.*, Houston, USA, 2002, pp. 1769–1770.
[10] K.-W. Chan and Y.-T. Zhang, "Adaptive reduction of motion artifact from photoplethysmographic recordings using a variable step-size lms filter," in *Proc. IEEE Sens.*, Orlando, USA, 2002, pp. 1343–1346.
[11] H. H. Asada, P. Shaltis, A. Reisner, S. Rhee, and H. R. C., "Mobile monitoring with wearable photoplethysmographic biosensors," *IEEE Eng. Med. Biol. Mag.*, vol. 22, no. 3, pp. 28–40, May 2003.
[12] J. Y. A. Foo and S. J. Wilson, "A computational system to optimize noise rejection in photoplethysmography signals during motion or poor perfusion states," *Med. Biol. Eng. Comput.*, vol. 44, no. 1, pp. 140–145, 2006.
[13] R. W. C. G. R. Wijshoff, M. Mischi, and R. M. Aarts, "Reduction of periodic motion artifacts in photoplethysmography," *IEEE Trans. Biomed. Eng.*, vol. 64, no. 1, pp. 196–207, Jan. 2017.
[14] C.-Y. Wang and K.-T. Tang, "Active noise cancellation of motion artifacts in pulse oximetry using isobestic wavelength light source," in *Proc. IEEE Int. Symp. Circuits Syst.*, Rio de Janeiro, Brazil, 2011, pp. 1029–1032.
[15] F. M. Coetzee and Z. Elghazzawi, "Noise-resistant pulse oximetry using a synthetic reference signal," *IEEE Trans. Biomed. Eng.*, vol. 47, no. 8, pp. 1018–1026, Aug. 2000.
[16] F. Peng, Z. Zhang, X. Gou, H. Liu, and W. Wang, "Motion artifact removal from photoplethysmographic signals by combining temporally constrained independent component analysis and adaptive filter," *Biomed. Eng. Online*, vol. 13, no. 50, pp. 1–14, 2014, [Online]. Available: http://dx.doi.org/10.1186/1475-925X-13-50

[17] J. M. Goldman, M. T. Petterson, R. J. Kopotic, and S. J. Barker, "Masimo signal extraction pulse oximetry," *J. Clin. Monit. Comput.*, vol. 16, no. 7, pp. 475–483, 2000.
[18] M. R. Ram, K. V. Madhav, E. H. Krishna, N. R. Komalla, and K. A. Reddy, "A novel approach for motion artifact reduction in ppg signals based on as-lms adaptive filter," *IEEE Trans. Instrum Meas.*, vol. 61, no. 6, pp. 1445–1457, May 2012.
[19] R. Yousefi, M. Nourani, S. Ostadabbas, and I. Panahi, "A motion-tolerant adaptive algorithm for wearable photoplethysmographic biosensors," *IEEE J. Biomed. Health Inform*, vol. 18, no. 2, pp. 670–681, Mar. 2014.
[20] J. Lee, W. Jung, I. Kang, Y. Kim, and G. Lee, "Design of filter to reject motion artifact of pulse oximetry," *Comput. Stand Interfaces*, vol. 26, no. 3, pp. 241–249, 2004.
[21] K. A. Reddy, B. George, and V. J. Kumar, "Use of fourier series analysis for motion artifact reduction and data compression of photoplethysmographic signals," *IEEE Trans. Instrum. Meas.*, vol. 58, no. 5, pp. 1706–1711, May 2009.
[22] B. S. Kim and S. K. Yoo, "Motion artifact reduction in photoplethysmography using independent component analysis," *IEEE Trans Biomed. Eng.*, vol. 53, no. 3, pp. 566–568, Mar. 2006.
[23] F. Fan, Y. Yan, Y. Tang, and H. Zhang, "A motion-tolerant approach for monitoring SpO2 and heart rate using photoplethysmography signal with dual frame length processing and multi-classifier fusion," *Comput. Biol. Med.*, vol. 91, no. 12, pp. 291–305, 2017.
[24] M. v. Gastel, S. Stuijk, and G. d. Haan, "New principle for measuring arterial blood oxygenation, enabling motion-robust remote monitoring," *Sci. Rep.*, vol. 6, pp. 1–16, 2016. [Online]. Available: http://dx.doi.org/10.1038/srep38609
[25] S. M. Salehizadeh *et al.*, "Photoplethysmograph signal reconstruction based on a novel motion artifact detection-reduction approach. Part II: Motion and noise artifact removal," *Ann. Biomed. Eng.*, vol. 42, no. 11, pp. 2251–2263, 2014.
[26] F. Fan, Y. Yan, K. Zhao, F. Long, and H. Zhang, "Estimating SpO2 via time-efficient high resolution harmonics analysis and maximum likelihood tracking," *IEEE J. Biomed. Health Inform*, 2017, [Online]. Available: http://dx.doi.org/10.1109/JBHI.2017.2769699
[27] Y.-S. Yan and Y.-T. Zhang, "An efficient motion-resistant method for wearable pulse oximeter," *IEEE Trans. Inf. Technol. Biomed.*, vol. 12, no. 3, pp. 399–405, May 2008.
[28] M. K. Diab, "Systems and methods for determining blood oxygen saturation values using complex number encoding," U.S. Patent US008 948 835B2, 2015.
[29] I.-H. Jang, H.-G. Yeom, and K.-B. Sim, "Ring sensor and heart rate monitoring system for sensor network applications," *Electron. Lett.*, vol. 44, no. 24, pp. 1393–1394, 2008.
[30] J. A. Sukor, M. S. Mohktar, S. J. Redmond, and N. H. Lovell, "Signal quality measures on pulse oximetry and blood pressure signals acquired from self-measurement in a home environment," *IEEE J. Biomed. Health Inform*, vol. 19, no. 1, pp. 102–108, Jan. 2015.
[31] H. Lee, H. Ko, C. Jeong, and J. Lee, "Wearable photoplethysmographic sensor based on different led light intensities," *IEEE Sensors J*, vol. 17, no. 3, pp. 587–588, Feb. 2017.
[32] O. Wieben, *Light Absorbance in Pulse Oximetry*. New York, NY, USA: Taylor & Francis, 1997, pp. 40–55.
[33] A. J. Dillon, J. A. Secunda, and T. Johnson, "Partially rigid-partially flexible electro-optical sensor for fingertip transillumination," U.S. Patent US005 891 021A, 1999.
[34] A. Dettling, A. Martin, and K. Aronow, "Method for ambient light subtraction in a photoplethysmographic measurement instrument," U.S. Patent US005 954 644A, 1999.
[35] S. A. Mascaro and H. H. Asada, "Photoplethysmograph fingernail sensor for measuring finger forces without heptic obstruction," *IEEE Trans. Robot. Autom.*, vol. 17, no. 5, pp. 698–708, Oct. 2001.
[36] C. E. Schulz, E. E. Mason, and A. A. Ali, "Shielded optical probe and method," U.S. Patent US006 580 086B1, 2003.
[37] K. T. Lau, S. Baldwin, R. L. Shepherd, P. H. Dietz, W. S. Yerzunis, and D. Diamond, "Novel fused-leds devices as optical sensors for colorimetric analysis," *Talanta*, vol. 63, no. 1, pp. 167–173, 2004.
[38] A. E. Colvin *et al.*, "System and method for attenuating the effect of ambient light on an optical sensor," U.S. Patent US007 227 156B2, 2007.
[39] E. Petersen, W. Shea, and B. B. Chew, "Oximeter ambient light cancellation," U.S. Patent US007 400 919B2, 2008.
[40] S. B. Lynch and S. P. Hotelling, "Ambient light interference reduction for optical input devices," U.S. Patent US20 100 001 978A1, 2010.
[41] M.-Z. Poh, D. J. McDuff, and R. W. Picard, "Non-contact, automated cardiac pulse measurements using video imaging and blind source separation," *Opt. Express*, vol. 18, no. 10, pp. 10 762–10 774, 2010.
[42] P. H. Mahowald, "Ambient light sensor with reduced sensitivity to noise from infrared sources," U.S. Patent US008 076 628B2, 2011.
[43] S. Haxha and J. Jhoja, "Optical based noninvasive glucose monitoring sensor prototype," *IEEE Photon. J.*, vol. 8, no. 6, pp. 1–12, Dec. 2016, [Online]. Available: http://doi.org/10.1109/JPHOT.2016.2616491
[44] J. Wang, Z. Wen, B. Yang, and X. Yang, "Optical carbon dioxide sensor based on fluorescent capillary array," *Results Phys.*, vol. 7, pp. 323–326, 2017.
[45] R. A. Yotter and D. M. Wilson, "A review of photodetectors for sensing light-emitting reporters in biological systems," *IEEE Sensors J.*, vol. 3, no. 3, pp. 288–303, Jun. 2003.
[46] J. H. Nagel, *Biopotential Amplifiers*. Boca Raton, FL, USA: CRC Press, 2000, ch. 70.
[47] H. Taub and D. L. Schilling, *Principles of Communication Systems*. New Delhi, India: McGraw-Hill, 2011, pp. 153–162.
[48] S. Rhee, B.-H. Yang, and K.-B. Asada, "Artifact-resistant power-efficient design of finger-ring plethysmographic sensors," *IEEE Trans. Biomed. Eng.*, vol. 48, no. 7, pp. 795–805, Jul. 2001.
[49] P. Deborah and J. Rumsey, *Statistics for Dummies*. Hoboken, NJ, USA: Wiley, 2011, p. 284.

Sakkarin Sinchai received the B.E. and M.E. degrees in telecommunications engineering from King Mongkut's Institute of Technology Ladkrabang, Bangkok, Thailand, in 2008 and 2015, respectively, where he is currently working toward the D.E. degree in the area of electrical engineering. His current research interests include signal processing, control system, and instrumentation and measurement.

Pattana Kainan received the B.E and M.E. degrees in telecommunications engineering from King Mongkut's Institute of Technology Ladkrabang, Bangkok, Thailand, in 2014 and 2016, respectively, where he is currently working toward the D.E. degree in the area of electrical engineering. His current research interests include analog circuits, communication circuit, biomedical instrumentation, and biomedical signal processing.

Paramote Wardkein received the M.E. and D.E. degrees in electrical engineering from King Mongkut's Institute of Technology Ladkrabang (KMITL), Bangkok, Thailand, in 1990 and 1997, respectively. He is currently an Associate Professor with the Department of Telecommunications Engineering, Faculty of Engineering, KMITL. His current research interests include analog/digital communications, circuit design, system analysis, queuing theory, and signal processing.

Jeerasuda Koseeyaporn received the M.S. and Ph.D. degrees in electrical engineering from Vanderbilt University, Nashville, TN, USA, in 1999 and 2003, respectively. She is currently an Associate Professor with the Department of Telecommunications Engineering, Faculty of Engineering, King Mongkut's Institute of Technology Ladkrabang, Bangkok, Thailand. Her current research interests include analog circuits in telecommunication systems, and digital signal processing.

ICIIBMS 2018, Track3: Bioinformatics, Medical Imaging, and Neuroscience, Bangkok, Thailand

Influence of Light Intensity on a Motion Artifact Signal in a Photoplethysmographic Signal

Jeerasuda Koseeyaporn*, Sakkarin Sinchai*‡, Panwit Tuwanut† and Paramote Wardkein*
*Department of Telecommunications Engineering, Faculty of Engineering,
†Faculty of Information Technology,
King Mongkut's Institute of Technology Ladkrabang (KMITL), Bangkok, Thailand, 10520
jeerasuda.ko@kmitl.ac.th, ‡58601019@kmitl.ac.th, panwit@it.kmitl.ac.th, pramote@telecom.kmitl.ac.th

***Abstract*—A photoplethygraphic (PPG) signal acquired from a commercial pulse oximeter is habitually disfigured by a motion artifact (MA) signal while any motion takes place. Inherently, the MA signal can either be additive or multiplicative. By having the MA signal intertwined with the PPG signal, the estimate of the oxygen saturation (SpO2) value is unreliable. The computation of SpO2 value is based on proper red and infrared (IR) PPG signals measured by the pulse oximeter. Generally, the frequency components of the red and IR PPG signals as well as the MA signal are in the same range. To overwhelm this problem, the frequency components of the red and IR PPG signals are severed from the frequency band of the MA signal. To implement the separation, a legacy source of driving red and IR LEDs in the pulse oximeter is replaced by two alternating current sources having different frequencies. With this solution, the additive MA signal is no longer involved but the multiplicative MA signal is yet not concluded. In this work, change in light intensity fed to both red and IR LEDs is studied whether the changed light intensity has any impact on the multiplicative MA signal. According to the study, it is found that change in light intensity does not affect the multiplicative MA signal. The multiplicative MA signal still exists since the overall calculated SpO2 values have some error up to 1%. Besides, change in light intensity does not improve the quality of the estimated SpO2 values while resting.**

I. Introduction

With affordable cost of a bio-optical instrument, obtaining a photoplethysmographic (PPG) signal is by far easier. The PPG signal is the leftover light intensity after passing through absorbing media of a human body. These days, usage of the PPG signal is seen in various aspects but the obvious one is the approximation of oxygen saturation (SpO2) in human's blood [1]. The estimate of SpO2 uses the components of red and infrared (IR) PPG signals in the computational process. The red and IR PPG signals are the remaining red and IR light intensities after being absorbed by the human body. Both red and IR PPG signals are gauged by a pulse oximeter.

Even though the PPG signal is effortlessly acquired but the clean PPG signal is somewhat arduous. Often, the PPG signal is plagued by mostly motion artifact (MA) signals while the human body moves. By utilizing the MA-interfered PPG signal gives rise to low quality of any biological indicators deriving from the PPG components for instance SpO2, heart rate (HR) and blood pressure (BP). In this context, improving the SpO2 quality is focused. Nonetheless, quality enhancing involves increasing the accuracy of the PPG signal. Hence, not only the SpO2 quality is enriched but also the quality of HR and BP is by-product elevated unquestioningly.

Basically, when any motion takes place, the identical occurring moving artifact noise is also absorbed by both red and IR lights at almost the same time. With this cause, the MA signals mingled within both red and IR PPG signals are considered to be similar.

As a consequence of the waveform distortion produced by the MA signal, plenty of solutions has been released to better the smirched PPG signal. Most methods employ an adaptive filtering algorithm to cancel the MA signal from the MA-ridden PPG signal. To retrieve the pure PPG signal using the adaptive filtering technique, a reference signal significantly plays a vital role. This is because feeding a poor reference signal to the adaptive filter solely makes the recovered PPG signal even worse. The reference signal can be extracted or synthesized from diverse sources for example motion feature tracing sensors [2]–[5] or human biological signals [6]–[8].

In [9], the MA signals residing in red and IR PPG signals are assumed to be mathematical factors of red and IR contaminated PPG signals. By applying the mathematical factoring concept, the ratio of red and IR corrupted PPG signals are performed to cancel out the selfsame MA-components yielding the clean quasi-PPG signal. The clean quasi-PPG signal is the resultant of the ratio of red and IR pure PPG signals. The magnitude of the clean quasi-PPG signal may either be too big or too small. Therefore, the clean quasi-PPG signal needs properly scaling before further processing. Otherwise, the clean quasi-PPG signal cannot be used.

To avoid red and IR PPG signals being combined with the MA signal, the idea of shifting PPG frequency components away from MA frequency components is reported in [10]. Instead of driving red and IR light emitting diodes (LEDs) in a traditional manner, each light is driven by feeding a sinusoidal signal at a specific frequency for each. As a result of changing LEDs-driving method, red and IR PPG signals seem not to be interfered with the MA signal. However, a small amount of error still emerges.

According to the narrative reviews, it is indicated that all works perform well to some extent because the MA signal has yet existed. Nonetheless, the method of [10] appears to be a

978-1-5386-7516-8/18/$31.00 ©2018 IEEE

promising solution to make the PPG signal to be free from the MA signal.

The aim of this scheme is to study whether the technique of [10] is more resistant to the MA signal if the amount of driven light intensity is altered. Besides, the by-product of this investigation is to render the influence of light intensity on the MA signal. Although the work of [11] shows that changing light intensity has an impact on the PPG signal, this mentioned work does not utter the impact on the MA signal.

II. Model of Light Absorption

A. General form of light absorption

Light absorption refers to the absorption of light intensity, and is approximated by employing the model of Beer-Lambert [12]. The Beer-Lambert's law states that any light passing through an absorbing medium is absorbed. In the absorption, light intensity is debilitated in a form of an exponential decay function expressed by (1), where $i(\lambda)$ is the leftover light intensity at a specific wavelength, λ. The remainder of light intensity is the product of the incident light intensity, i_o, falling upon the surface of the medium and the exponential decay function, $e^{-\varepsilon(\lambda)cd}$. In the exponential decay function consists of three absorbing parameters as follows. Initially, $\varepsilon(\lambda)$ is the absorptivity, ε, of a specific wavelength λ of the medium. Later, c is the concentration of the medium as well as d is the optical path length of the medium.

$$i(\lambda) = i_o e^{-\varepsilon(\lambda)cd} \quad (1)$$

For multiple media, the Beer-Lambert's law is also applicable. After light intensity is absorbed by the first absorbing medium, the leftover light intensity is the light intensity input for the second absorbing medium. This absorbing process goes on until passing through the last medium, and returns the complete remainder of light intensity. The complete remnant light intensity is called the transmitted light intensity which is written as the mathematical statement by (2). In fact, the transmitted light intensity is varied over time due to the optical path length, d_k, of each medium tends to change over time.

$$i(\lambda, t) = i_o e^{-\sum_{k=1}^{M} \varepsilon_k(\lambda) c_k d_k(t)} \quad (2)$$

Thus, the transmitted light intensity is then manifested as a function of a specific wavelength and time, $i(\lambda, t)$. In addition, the exponent of the exponential factor is the negative sum of M absorbing feature values of M media. The first absorbing feature parameter is the absorptivity, ε_k, of a specific wavelength λ of the k^{th}-medium. The second absorbing feature parameter is the concentration, c_k, of the k^{th}-medium. The last absorbing feature parameter is the optical path length, d_k, of the k^{th}-medium, but d_k is stated in a function of time, $d_k(t)$, because of oscillating over time.

B. Light absorption of PPG model

For a pulse oximeter, a PPG signal is measured from a fingertip, a wrist, an earlobe or a forehead of a human subject. Ordinarily, the PPG signal is the leftover light intensity after being absorbed by human's absorbing media such as pulsating arterial blood, non-pulsating arterial blood, venous blood and so forth. Having absorbed by the human's absorbing media, the resultant PPG signal can be approximately portrayed by Fig. 1 [12].

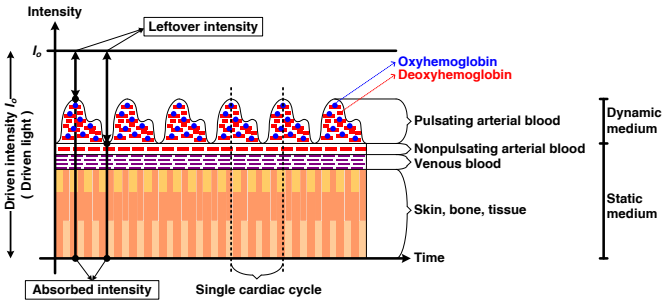

Fig. 1. Normal PPG signal.

As can be noticed in Fig. 1, the resultant PPG signal consists of two chief media, dynamic medium and static medium. Based on two main media, a mathematical statement of the PPG signal is modeled by modifying (2) leading to (3). From (3), $i_{PPG}(\lambda, t)$ is the PPG signal which is the resultant of the absorption of human's absorbing media. The human's absorbing media are divided into two separate absorbing parts which are $Static_{part}$ and $Dynamic_{part}$.

$$i_{PPG}(\lambda, t) = i_o[Static_{part} + Dynamic_{part}] \quad (3)$$

In this work, studying the efficiency of [10] is focused. By virtue of this motive, the further improvement of (3) is in line with [10]. According to [10], the static medium refers to any media whose their optical path length values seldom alter over time. For this context, the sub-media, skin, bone, tissue, venous blood and non-pulsating arterial blood, are considered the static medium due to their optical path length values rarely change. On the other hand, the dynamic medium points to any media whose their optical path length values constantly vary over time. By complying with the dynamic medium characteristic, the pulsating arterial blood is contemplated the dynamic medium. Thence, (3) is converted back in the form of the exponential decaying functions as written in (4). In (4), ε_{sm}, c_{sm} and d_{sm} stand for the absorbing characteristics of the static medium while ε_{dm}, c_{dm} and $d_{dm}(t)$ are the absorbing properties of the dynamic medium.

$$i_{PPG}(\lambda, t) = i_o[\underbrace{e^{-\varepsilon_{sm}(\lambda)c_{sm}d_{sm}}}_{\text{Static medium}} + \underbrace{e^{-\varepsilon_{dm}(\lambda)c_{dm}d_{dm}(t)}}_{\text{Dynamic medium}}] \quad (4)$$

Since the pulse oximeter centers on the amount of SpO2 in the pulsating arterial blood, the absorption by red and IR lights of oxyhemoglobin (HbO2) and deoxyhemoglobin (Hb) is measured. With this aspect, the dynamic medium in (4) is slightly adjusted as recast in (5) where the absorbing parameters of

Hb and HbO2 which are $\varepsilon_{Hb}(\lambda)c_{Hb}$ and $\varepsilon_{HbO2}(\lambda)c_{HbO2}$.

$$i_{cPPG}(\lambda,t) = i_o[\underbrace{e^{-\varepsilon_{sm}(\lambda)c_{sm}d_{sm}}}_{\text{Static medium}} + \underbrace{e^{-[\varepsilon_{Hb}(\lambda)c_{Hb}+\varepsilon_{HbO2}(\lambda)c_{HbO2}]d_{dm}(t)}}_{\text{Dynamic medium}}] \quad (5)$$

Additionally, the absorption of Hb and HbO2 takes place inside the dynamic medium resulting their optical path length values to be the identical value denoted as $d_{dm}(t)$. Lastly, the mathematical model of the PPG signal in (5) is the expression of the clean PPG signal because the model is derived under no motion. Hence, $i_{PPG}(\lambda,t)$ is replaced by $i_{cPPG}(\lambda,t)$.

C. PPG model involving motion

An MA signal is generated when a human subject causes any motion to a pulse oximeter. The MA signal exhibits an additive characteristic, as rendered in [10]. With this behavior, the MA signal is supplemented to a clean PPG signal in an additive manner. Under the motion conditions, the leftover light intensity received at a photo-detector is the summation of the MA signal and the clean PPG signal as written in (6). The received leftover light intensity is denoted as $i_r(\lambda,t)$.

$$i_r(\lambda,t) = i_{MA}(t) + i_{cPPG}(\lambda,t) \quad (6)$$

In reality, the MA signal depends on the human subject's movement. Given that, the MA signal is subject to change over time, and thus stated in a function of time, $i_{MA}(t)$.

III. Shifting PPG signals away from MA signals

Generally, a clean PPG signal approximately comprises of frequency components from 0.09 Hz to 4 Hz [13]. However, an MA signal also has its frequency components in the same range as the pure PPG signal. Being in the same frequency interval causes both signals to overlap. To stymie the overlapping issue, the PPG frequency components are shifted away from the MA frequency elements.

For a convenient reason in explanation, (5) is re-expressed in the form of summation of sinusoidal signals. In general, a Fourier series expansion is employed to represent any periodic signals but is inapplicable to the PPG signal. By nature, the PPG signal exhibits a quasi-periodicity. To form the PPG signal in sum of sinusoidal signals, a method of additive synthesis [14] is applied. The additive synthesis technique is mostly utilized to form an almost periodic signal or a quasi-periodic signal by the sinusoidal summing expression of (7).

$$s(t) = \sum_{k=1}^{M} A_k(t)\cos(\theta_k(t)) \quad (7)$$

In (7), $A_k(t)$ is a time-varying amplitude for each frequency component, and $\theta_k(t)$ is a frequency-scaling time-varying function, and *M* is the amount of frequency components.

By revising the mathematical model of (5), the static medium is defined a constant value, denoted as A_{dc}, while the dynamic medium is substituted by (7) with slight alteration. From the revision, (5) is updated to (8) where $A_k(\lambda,t)$ is the time-varying amplitude based on a specific wavelength λ. In addition, $\theta_k(t)$ is the frequency-scaling time-varying function of the PPG frequency components.

$$i_{cPPG}(\lambda,t) = i_o[A_{dc} + \sum_{k=1}^{M} A_k(\lambda,t)\cos(\theta_k(t))] \quad (8)$$

To move the PPG frequency components away from the MA frequency band, a classic LED-driving source, constant intensity, is supplanted by a sinusoidal LED-emitting source, varying intensity. As a result of LED-discharging adjustment, the intensity i_o in (8) is replaced by $i_{ac}cos(2\pi f_c t)$ which is a sinusoidal alternating source containing a frequency of f_c Hz with intensity i_{ac}. Practically, the frequency is implemented in an angular frequency so $i_{ac}cos(2\pi f_c t)$ is rewritten as $i_{ac}cos(\omega_c t)$ where ω_c equals to $2\pi f_c$, and (8) is developed to (9).

$$i_{cPPG}(\lambda,t) = i_{ac}\cos(\omega_c t)[A_{dc} + \sum_{k=1}^{M} A_k(\lambda,t)\cos(\theta_k(t))] \quad (9)$$

Under the improvement of LED-shining technique, the shifting procedure is further carried on. Firstly, the term $i_{ac}cos(\omega_c t)$ in (9) is distributed into the parenthesis forming $i_{ac}A_k(\lambda,t)cos(\omega_c t)cos(\theta_k(t))$. Later, the trigonometric product-to-sum formula stated in (10) is applied to the mentioned term, $i_{ac}A_k(\lambda,t)cos(\omega_c t)cos(\theta_k(t))$.

$$\cos(u)\cos(v) = \frac{1}{2}[\cos(u-v)+\cos(u+v)] \quad (10)$$

With this modification, (9) is rearranged to (11). Furthermore, $i_{cPPG}(\lambda,t)$ is altered to $i_{sfPPG}(\lambda,t)$ to indicate that the clean PPG signal is shifted.

$$\begin{aligned} i_{sfPPG}(\lambda,t) = {} & i_{ac}A_{dc}\cos(\omega_c t) \\ & + \sum_{k=1}^{M} \frac{i_{ac}A_k(\lambda,t)}{2}\cos(\omega_c t - \theta_k(t)) \\ & + \sum_{k=1}^{M} \frac{i_{ac}A_k(\lambda,t)}{2}\cos(\omega_c t + \theta_k(t)) \end{aligned} \quad (11)$$

Lastly, $i_{cPPG}(\lambda,t)$ in (6) is superseded by $i_{sfPPG}(\lambda,t)$ in (11) giving rise to the realistic received PPG signal shown in (12).

$$\begin{aligned} i_r(\lambda,t) = {} & i_{MA}(t) \\ & + i_{ac}A_{dc}\cos(\omega_c t) \\ & + \sum_{k=1}^{M} \frac{i_{ac}A_k(\lambda,t)}{2}\cos(\omega_c t - \theta_k(t)) \\ & + \sum_{k=1}^{M} \frac{i_{ac}A_k(\lambda,t)}{2}\cos(\omega_c t + \theta_k(t)) \end{aligned} \quad (12)$$

As can be observed in (12), the first term is the MA signal which still stays at lower frequency according to the nature of MA. However, the last three terms displays the characteristic of double-sideband with carrier (DSB-WC) known as a

broadcasting amplitude modulation (AM) [15] by which the second term is a carrier signal. The third and the fourth terms are the lower and the upper sidebands of the information signal modulated by the AM. For this reason, the PPG signal is shifted to higher frequency by the AM whose the carrier frequency is ω_c. As a consequence of utilizing the AM, the PPG frequency components, $\theta_k(t)$, are stored on the lower and upper sidebands of the carrier frequency, ω_c.

IV. Experimental Setup

A. Device preparation

For this work, a commercial finger-probe transmittance pulse oximeter is used. Normally, the commercial pulse oximeter drives red and IR LEDs alternately. When the red LED is on, the IR LED is off. On the other hand, the IR LED is on while the red LED is off. In traditional LEDs emission, each LED is emitted by employing a direct current (DC) source. To shift the PPG frequency components, both red and IR LEDs are driven by two sinusoidal waves having different frequencies at the same time. By changing the method of LEDs-driving, the original direct current LEDs-driving system is replaced by the new LEDs-illuminating technique of two alternating current (AC) sources as illustrated in Fig. 2.

In Fig. 2, the classic LEDs-driving system consisting of a DC source and two LEDs-switching units, framed by the dashed boundary, is removed. After removing the old system, an improved system composing of two AC sources and two band pass filters (BPFs) is inserted instead.

To set up the experiment, two signal generators are brought to emit the red and IR LEDs. Both red and IR LEDs are beamed out by two sinusoidal signals having frequencies of 1.07 kHz and 1.55 kHz, respectively. In addition, the DC offset of positive 4.5 V is extra added to the red and IR LEDs in the LEDs-radiating process.

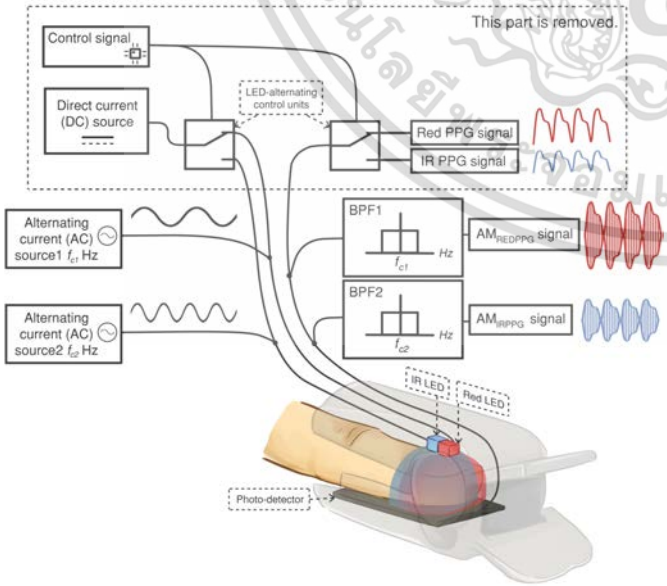

Fig. 2. Modification of LEDs-driving system.

In reality, the resultant leftover light intensity detected by a photo-detector is fairly low. In order to make use of the detected leftover light intensity signal, a common transimpedance amplifying (TIA) circuit is designed to enhance the detected leftover light intensity signal by 10 times.

B. Procedures of experiment

The experimental procedures are explained as follows. In this work, four healthy volunteers, two males and two females, are enrolled to participate the experiments. The mean age of male subjects is 19.5 years old, and the averaged age of female is 23.0 years old. All volunteered participants are Asian and their skin is yellowish. These volunteers are requested to do five experiments comprising of one pose of finger resting and another four postures of finger movement which are bending, shivering, waving and vertical movement. To do the given experiments, a commercial finger-probe transmittance pulse oximeter is put on a left index finger of each volunteer while experimenting. Besides, the participated subjects are informed to do all posture experiments in a natural style not to intentionally induce. Each pose experiment is performed for three times ten seconds each at different levels of light intensity. The levels of light intensity are quantified by the amplitude voltage levels being fed to the red and IR LEDs which affect the term $i_{ac}cos(\omega_c t)$ in (9). For all posing experiments, three different amplitude voltage levels which are 1 Vpp(Vpeak-to-peak), 1.5 Vpp and 2 Vpp, respectively, are employed.

During the experiments, each resulting signal from each posture is recorded and evaluated by a MATLAB program through an NI DAQPad-6014 acquisition card manufactured by National Instruments. Recording of each resulting signal is sampled at 16000 times per second. After the recording of each resulting signal is finished, the recorded signal is further processed by the following steps as diagrammed in Fig. 3. Each resulting signal is the summation of red and IR PPG AM signals.

C. SpO2 estimation

Before the SpO2 approximation, the red and IR PPG signals are extracted from the recorded signal. The extracting steps are processed from top to down of Fig. 3. At first, the recorded signal is fed to two band pass filters having center frequencies of 1.07 kHz and 1.55 kHz to distinguish the red and IR PPG AM signals. These band pass filters are created using a method of Butterworth. Both band pass filters have passband of 20 Hz, the order of these filters is two. Once each AM signal is separated, each AM signal is demodulated by a similar envelop detector. In MATLAB, the similar envelop detector of AM demodulation is done by finding the absolute value of the AM signal. By finding the absolute value of each AM signal, the message of interest of each AM signal is demodulated. Nevertheless, the message of interest of each AM signal still contains a high frequency of the carrier frequency. Then, each demodulated signal is passed through a low pass filter having a

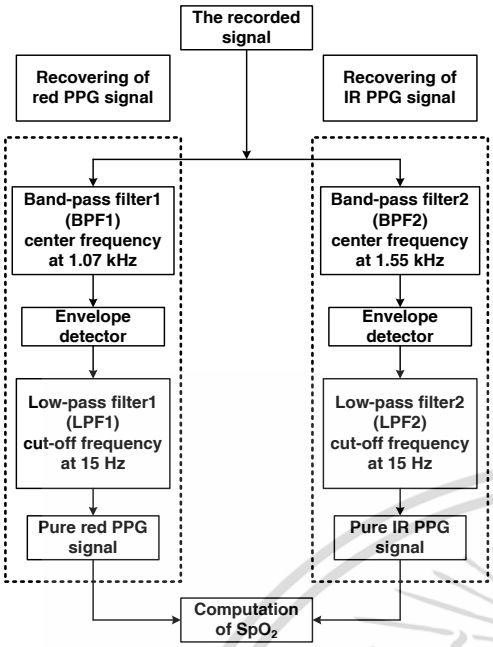

Fig. 3. Processing steps.

cut-off frequency of 15 Hz. The low pass filter is also made up by the technique of Butterworth with the order of two. After low filtering, the pure red and IR PPG signals are acquired. In the end, the SpO2 value is approximated from these clean red and IR PPG signals by (13).

$$SpO2 \quad = 110 - 25 \times R \ , \ R = \frac{V_{ppR}/V_{DCR}}{V_{ppIR}/V_{DCIR}} \qquad (13)$$

From (13), V_{ppR} is the peak-to-peak value of the red PPG signal and V_{DCR} is the DC component of the red PPG signal. Likewise, V_{ppIR} is the peak-to-peak value of the IR PPG signal and V_{DCIR} is the DC component of the IR PPG signal. Commonly, each PPG signal is severed cycle-by-cycle in order to estimate the SpO2 value by (13) more accurately.

V. Experimental Results

A. No motion interference

Changing the light intensities of red and IR LEDs results the leftover light intensity fallen upon a photo-detector to either increase or decrease as illustrated in Fig. 4. As can be observed in Figs. 4(A1), 4(B1) and 4(C1), the remaining light intensity (peak-to-peak value) of summed red and IR PPG amplitude-modulated (AM) signals tends to rise. This is due to the fed light intensity is raised between 1 Vpp and 2 Vpp. The remnant light intensities displayed in Fig. 4 are in a unit of voltage as a result of the transimpedance amplifying circuit. The circuit turns the electrical current level of the light intensity dropping on the photo-detector to the voltage level. The results portrayed in Fig. 4 are belonged to one of the volunteers while finger resting. For the rest subjects, their results also exhibit as same as the drawn results in Fig. 4. Besides, Figs. 4(A2), 4(B2) and 4(C2) show that the red and IR PPG AM signals are shifted to the frequencies of 1.07 kHz and 1.55 kHz according to (11), respectively.

To find out whether the SpO2 values are affected, all recorded results during finger resting at each voltage level are further processed according to the procedures in Fig. 3. After completing the processing steps, the demodulated red and IR PPG signals are obtained, as manifested in Fig. 5. Clearly, the red and IR PPG signals of a male subject in Figs. 5(A1), 5(B1) and 5(C1) are only different in their amplitudes but their waveform is still same. Likewise, for a female subject, the female subject's red and IR PPG signals in Figs. 5(A2), 5(B2) and 5(C2) also show the same manner as the male subject. Nonetheless, only two recovered red and IR PPG signals, (one male and one female), are shown as the rest retrieved red and IR PPG signals render the same pattern.

As the computation of SpO2 is done beat-by-beat using (13), thus, the number of the acquired estimated SpO2 values of each subject at different voltage levels is numerous. For this reason, the approximated SpO2 values of each subject at different voltage levels are averaged and summarized in Table I. Also, the standard deviation of each voltage level of SpO2 values is computed. Obviously, changing the light intensities of red and IR LEDs according to the given voltage levels does not enhance the quality of SpO2 values. As can be observed in Table I, the overall SpO2 value of each subject has low standard deviation. This can infer that there is no significant change in the SpO2 values acquired by different conditions. It is also implied that the amount of oxygen in blood already fully absorbs and can no longer absorb thus the change in light intensity has no effect. The overall SpO2 value is the averaged SpO2 value calculated by averaging the mean SpO2 values obtained from LEDs-driving at 1.0 Vpp, 1.5 Vpp and 2.0 Vpp.

B. Motion involvement

By processing in the same fashion as the finger resting condition, the red and IR PPG signals of each motion posture are retrieved as illustrated in Fig. 6. The red and IR PPG signals shown in Fig. 6 are recovered from finger shivering posture of the same old two volunteers (one male and one female). Distinctly, the female PPG waveform is likely to be corrupted by the MA signal for all voltage levels fed to red and IR LEDs (see Figs. 6(A2), 6(B2) and 6(C2)). By contrary, the male PPG waveform is more resistant to the MA signal than that of the female PPG waveform at all voltage levels (see Figs. 6(A1), 6(B1) and 6(C1)). Although the female PPG waveform inclines to be interfered partially, the female PPG waveform is still in a good shape to estimate the SpO2 values.

The finger shivering pose is chosen because this posture is regularly generated by an unconscious patient. Nevertheless,

TABLE I. SpO2 Values of Finger Resting Posture

Driven voltage: Subject no.	SpO2 (1.0 Vpp)	SpO2 (1.5 Vpp)	SpO2 (2.0 Vpp)	SpO2 (Overall)
	Mean±Standard deviation			
No.1 (Male)	96.3±0.27	96.3±0.51	96.0±0.25	96.2±0.19
No.2 (Male)	94.8±0.88	95.2±0.17	96.1±0.18	95.4±0.66
No.3 (Female)	95.9±0.19	95.9±0.10	96.3±0.12	96.0±0.24
No.4 (Female)	97.2±0.41	97.4±0.08	96.6±0.16	97.1±0.45

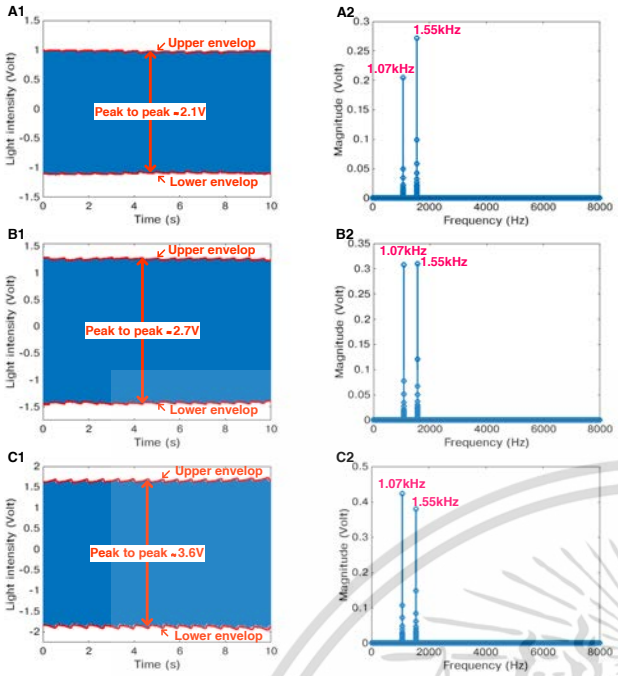

Fig. 4. Leftover light intensity of summation of red and IR PPG AM signals, and its frequency spectrum. (A1) Result of red and IR LEDs driven by 1.0 Vpp. (A2) Frequency spectra of A1. (B1) Result of red and IR LEDs driven by 1.5 Vpp. (B2) Frequency spectra of B1. (C1) Result of red and IR LEDs driven by 2.0 Vpp. (C2) Frequency spectra of C1.

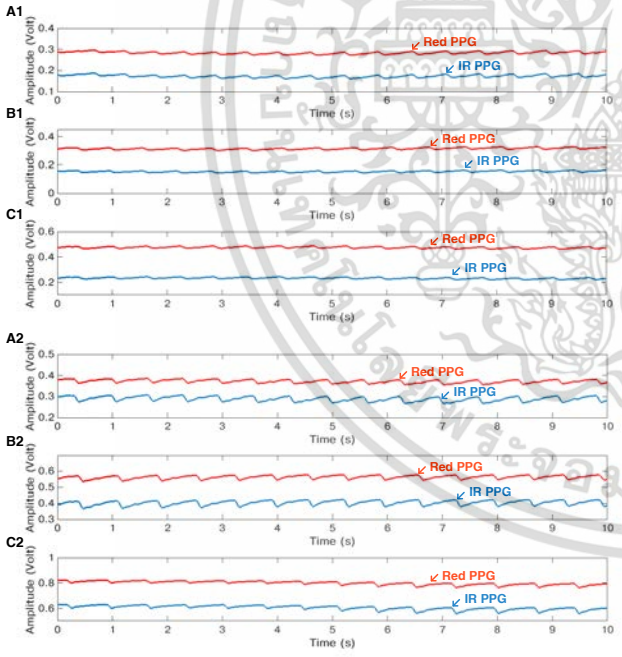

Fig. 5. Recovered red and IR PPG signals from finger resting condition. (A1) and (A2) are the results of male and female subjects by LEDs-emitting at 1.0 Vpp. (B1) and (B2) are the results of male and female subjects by LEDs-emitting at 1.5 Vpp. (C1) and (C2) are the results of male and female subjects by LEDs-emitting at 2.0 Vpp.

the red and IR PPG signals of other finger poses are also resistant to the finger moving interference like the results plotted in Fig. 6.

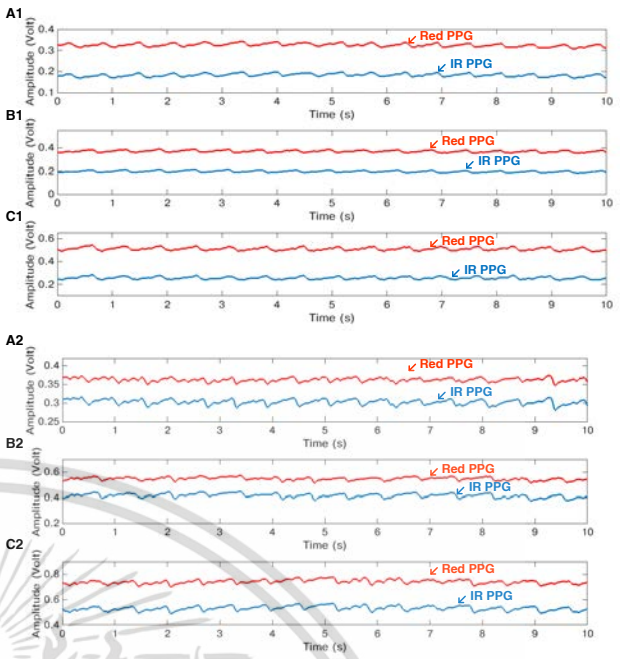

Fig. 6. Recovered red and IR PPG signals from finger shivering condition. (A1) and (A2) are the results of male and female subjects by LEDs-driving at 1.0 Vpp. (B1) and (B2) are the results of male and female subjects by LEDs-driving at 1.5 Vpp. (C1) and (C2) are the results of male and female subjects by LEDs-driving at 2.0 Vpp.

After acquiring the red and IR PPG signals of each pose, the SpO2 values for all mentioned kinds of finger movement are computed. The calculated SpO2 values for finger bending, finger shivering, finger waving and vertical movement of a finger are summed up in Tables II, III, IV and V. As can be noticed in Tables II, III, IV and V, the SpO2 values of finger movement mostly approach to the SpO2 value of 95% for all driven voltage levels. The overall SpO2 values shown in Tables II, III, IV and V are computed by employing the same method administered in Table I.

C. Discussion

With approaching to 95% of the SpO2 values during finger motion can be concluded that changing light intensity by the given voltage levels does not improve the SpO2 quality. This is because the overall SpO2 of finger resting for all driven voltage levels is around 96% which is roughly higher than the SpO2 values while motion up to 1%. Change in light intensity seems to solely either increase or decrease the leftover light intensity after absorption, and does not alleviate the amount of the MA signal. For this reason, altering light intensity is deduced to have no influence on the MA signal in the red and IR PPG signals. Even though the MA signal is severed by (12) in the first place but the mentioned MA signal shown in (12) is an additive kind. From this viewpoint, the existing MA signal in both red and IR PPG signals is considered a multiplicative MA signal which will later be investigated.

Although there is no significant change in light intensity with the participated healthy teenage volunteers, this finding

TABLE II. SPO2 VALUES OF FINGER BENDING POSTURE

Driven voltage: Subject no.	SpO2 (1.0 Vpp)	SpO2 (1.5 Vpp)	SpO2 (2.0 Vpp)	SpO2 (Overall)
	Mean±Standard deviation			
No.1 (Male)	96.2±0.59	95.5±0.62	94.0±0.42	95.4±1.36
No.2 (Male)	95.7±0.25	95.2±0.61	96.8±0.52	95.2±0.46
No.3 (Female)	94.7±0.89	95.6±0.63	95.9±0.23	95.4±0.66
No.4 (Female)	94.6±0.83	95.2±0.73	95.6±1.64	95.1±0.53

TABLE III. SPO2 VALUES OF FINGER SHIVERING POSTURE

Driven voltage: Subject no.	SpO2 (1.0 Vpp)	SpO2 (1.5 Vpp)	SpO2 (2.0 Vpp)	SpO2 (Overall)
	Mean±Standard deviation			
No.1 (Male)	96.5±0.81	95.2±0.23	95.7±0.47	95.8±0.65
No.2 (Male)	94.7±1.11	94.9±0.43	94.7±0.66	94.8±0.18
No.3 (Female)	93.2±0.08	94.8±1.28	94.9±0.26	94.3±0.96
No.4 (Female)	96.5±1.28	94.4±1.22	95.7±0.40	95.5±1.02

TABLE IV. SPO2 VALUES OF FINGER WAVING POSTURE

Driven voltage: Subject no.	SpO2 (1.0 Vpp)	SpO2 (1.5 Vpp)	SpO2 (2.0 Vpp)	SpO2 (Overall)
	Mean±Standard deviation			
No.1 (Male)	96.8±1.27	95.9±0.51	95.9±0.21	96.2±0.51
No.2 (Male)	95.2±0.88	95.2±0.41	95.9±0.29	95.4±0.40
No.3 (Female)	96.3±0.26	93.9±0.81	96.5±0.30	95.6±1.46
No.4 (Female)	95.7±1.75	96.2±0.43	94.7±1.04	95.5±0.75

TABLE V. SPO2 VALUES OF VERTICAL FINGER MOVEMENT POSTURE

Driven voltage: Subject no.	SpO2 (1.0 Vpp)	SpO2 (1.5 Vpp)	SpO2 (2.0 Vpp)	SpO2 (Overall)
	Mean±Standard deviation			
No.1 (Male)	96.1±0.30	95.1±0.22	95.5±0.06	95.6±0.47
No.2 (Male)	94.9±0.42	95.1±0.07	95.3±0.39	95.1±0.15
No.3 (Female)	96.6±0.37	96.6±0.27	96.2±0.43	96.5±0.25
No.4 (Female)	94.0±2.92	96.1±0.10	95.9±0.29	95.4±1.18

may manifest significant alteration with poor health volunteers and senile people. The issue in poor health volunteers and senile people will be further studied for drawing the complete and consistent conclusion.

Driving red and IR LEDs with higher voltage level than the experimented voltage levels can harm the volunteers' skin around their fingertips due to the heat emitted from both LEDs. In addtion, with high voltage level fed to the red and IR LEDs makes the volunteered participants feel uncomfortable. This is the reason why this work uses the voltage levels from 1.0 Vpp to 2.0 Vpp.

VI. CONCLUSION

In this paper, the influence of changing light intensity on the MA signal in the red and IR PPG signals is studied. To operate this study, the legacy red-and-IR LEDs-driving method in a commercial pulse oximeter is changed to the technique of feeding two different sinusoidal signals to red and IR LEDs. By superseding the legacy LEDs-driving method with the mentioned technique, the additive MA signal is no longer concerned but the multiplicative MA signal still exists. This study alters the light intensity by changing the voltage level fed to the red and IR LEDs to verify whether the multiplicative MA signal is affected. In order to verify, the calculation of SpO2 value is used as a criterion. The employed voltage levels are 1.0 Vpp, 1.5 Vpp and 2.0 Vpp, respectively. Additionally, the DC offset of positive 4.5 V is added to the operated voltage levels. The study consists of two main experiments which are change in light intensity during finger resting and finger movement. According to the study, it is found that change in light intensity does not enhance the quality of the red and IR PPG signals. This is because the overall computed SpO2 values from all driven voltage levels are indifferent. Similarly, for finger movement, change in light intensity fails to eliminate the multiplicative MA signal as some error up to 1% is still shown in the calculated SpO2 values. From this viewpoint, it can be concluded that change in light intensity does not have any influence on the multiplicative MA signal. With the existence of the multiplicative MA signal, the elimination of the multiplicative MA signal will be further investigated in the future work.

REFERENCES

[1] A. Jubran, "Pulse oximetry," *Critical Care*, vol. 9, no. 272, 2015, available at: http://dx.doi.org/10.1186/s13054-015-0984-8.

[2] S. Ardalan, M. Siavash, and S. Jaafari, "Motion noise cancelation in heartbeat sensing using accelerometer and adaptive filter," *IEEE Embedded Syst. Lett.*, vol. 7, no. 4, pp. 101–104, 2015.

[3] Y. Ye, Y. Cheng, W. He, M. Hou, and Z. Zhang, "Combining nonlinear adaptive filtering and signal decomposition for motion artifact removal in wearable photoplethysmography," *IEEE Sensors J.*, vol. 16, no. 19, pp. 7133–7141, 2016.

[4] R. W. C. G. R. Wijshoff, M. Mischi, and R. M. Aarts, "Reduction of periodic motion artifacts in photoplethysmography," *IEEE Trans. Biomed. Eng.*, vol. 64, no. 1, pp. 196–207, 2017.

[5] D. Yang, Y. Cheng, J. Zhu, D. Xue, G. Abt, H. Ye, and Y. Peng, "A novel adaptive spectrum noise cancellation approach for enhancing heartbeat rate monitoring in a wearable device," *IEEE Access*, vol. 6, pp. 8364–8375, 2018, available at: http://dx.doi.org/10.1109/ACCESS.2018.2805223.

[6] F. Peng, Z. Zhang, X. Gou, H. Liu, and W. Wang, "Motion artifact removal from photoplethysmographic signals by combining temporally constrained independent component analysis and adaptive filter," *Biomed. Eng. Online*, vol. 13, no. 50, pp. 1–14, 2014, available at: http://dx.doi.org/10.1186/1475-925X-13-50.

[7] M. R. Ram, K. Sivani, and K. A. Reddy, "Utilization of adaptive-coefficient estimation method for motion artifacts reduction from photoplethysmographic signals," in *Int. Conf. on Wireless Commun., Signal Process. and Network. (WiSPNET)*, Chennai, India, 2016, pp. 818–822.

[8] K. T. Tanweer, S. R. Hasan, and A. M. Kamboh, "Motion artifact reduction from ppg signals during intense exercise using filtered x-lms," in *IEEE Int. Sympo. on Circuits and Syst.*, Baltimore, USA, 2017.

[9] J. A. C. Patterson and G.-Z. Yang, "Ratiometric artifact reduction in low power reflective photoplethysmography," *IEEE. Trans. Biomed. Circuits Syst.*, vol. 5, no. 4, pp. 330–338, 2011.

[10] S. Sinchai, P. Kainan, P. Wardkein, and J. Koseeyaporn, "A photoplethysmographic signal isolated from an additive motion artifact by frequency translation," *IEEE. Trans. Biomed. Circuits Syst.*, vol. 12, no. 4, pp. 904–917, 2018.

[11] R. Shriram, M. Sundhararajan, and N. Daimiwal, "Effect of change in intensity of infrared led on a photoplethysmogram," in *Int. Conf. on Commun. and Signal Process.*, Melmaruvathur, India, 2014, pp. 1064–1067.

[12] O. Wieben, *Light Absorbance in Pulse Oximetry*. New York, USA: Taylor & Francis, 1997, pp. 40–55.

[13] M. M. Rao and R. R. Ram, "Photoplethysmography: a noninvasive tool for possible subtle energy monitoring during yogic practices," *Subtle Energies & Energy Medicine*, vol. 17, no. 2, pp. 163–179, 2006.

[14] J. O. Smith III, *Spectral Modeling Synthesis*. USA: W3K Publising, 2011, pp. 361–375.

[15] R. E. Ziemer and W. H. Tranter, *Principles of Communications*. New Jersey, USA: John Wiley & Sons, 2009, pp. 115–120.

2019 IEEE 4th International Conference on Computer and Communication Systems

Performance of Frequency Translation in Separating a Photoplethysmographic Signal from an Additive Motion Artifact

Jeerasuda Koseeyaporn, Sakkarin Sinchai and Paramote Wardkein
Department of Telecommunications Engineering, Faculty of Engineering
King Mongkut's Institute of Technology Ladkrabang (KMITL)
Bangkok, Thailand, 10520
e-mail: jeerasuda.ko@kmitl.ac.th, 58601019@kmitl.ac.th, pramote@telecom.kmitl.ac.th

***Abstract*—Obtaining red and infrared (IR) photoplethysmographic (PPG) signals by a general method in a commercial pulse oximeter is overlapped with an additive motion artifact (MA) signal routinely. When the red and IR PPG signals are combined with the MA signal, a percentage of oxygen saturation (SpO2) is unreliable. To prevent the overlapping problem, a technique of frequency translation is introduced to shift the PPG frequency components away from the MA frequency components. The introduced approach remodels an LED-driving system by substituting an alternating current (AC) source for a traditional direct current (DC) source in the commercial pulse oximeter. To assess the performance, the SpO2 values computed from the red and IR PPG signals acquired by the presented solution are evaluated when four natural poses of motion occur. Besides, the well-known methods are used to calculate the SpO2 values from the red and IR PPG signals sensed by the conventional LED-emitting system during motion for the efficient comparison. The well-known methods are discrete saturation transform (DST), fast independent component analysis (fICA) and compression of Fourier coefficients (CFC). The resulting SpO2 values show that the technique of frequency translation provides overall mean error lower than the selected schemes for all postures. The overall mean error of the introduced technique is 1.1% while the approaches of DST, fICA and CFC yield the overall mean errors by 2.9%, 15.4% and 8.4%, respectively.**

Keywords-photoplethysmographic (PPG) signal; frequency translation; amplitude modulation (AM); motion artifact (MA)

I. INTRODUCTION

To obtain an accurate PPG signal, a subject must stay still. In practice, the subject is not at rest all the time and usually moves. With this reason, motion frequently involves while measuring the PPG signal, and distorts the PPG waveform of the PPG signal. Later, any motion is called as a motion artifact (MA) signal throughout this paper. When the PPG signal is corrupted by the MA signal, consequently, the contaminated PPG signal may not be proper to be used or further analyzed.

In literature, various approaches have endeavored to get rid of the MA signal from the polluted PPG signal to retrieve the clean PPG signal. The most common implementing technique is an adaptive filtering algorithm. It is noted that the PPG signal will be used as the clean PPG signal in this paper. By employing the adaptive filtering algorithm, a reference signal is utilized to cancel out the MA signal. To yield good cancellation, the reference signal must be highly correlated to the MA signal. If not, the output PPG signal becomes even more worsen. Chiefly, the reference signal is synthesized from either human biological signals [1][2] or extra motion sensor signals [3]. Among the adaptive approaches, a method of discrete saturation transform (DST) [1] is most reliable as this method provides good efficiency and is commercially used. Aside from the adaptive model, some mathematical tools like independent component analysis (ICA) [4-6], compression of Fourier coefficients (CFC) [7] or wavelet [8] also effectively distinguish the PPG signal and the MA signal. In eliminating the MA signal of these mentioned schemes [1-8], the MA signal is considered to be an additive noise being in the same frequency band of the PPG signal. With assuming to be the additive noise of the MA signal, a technique of frequency translation [9] is applied to isolate the PPG signal from the MA signal. Using the approach of frequency translation, the additive MA signal is not entangled in the PPG signal. Still, some error exists in the PPG signal because the acquired overall SpO2 value is slightly deviated from the actual value of SpO2. Nevertheless, the deviation of the obtained overall SpO2 value is fairly low, and can be neglected. The strategy of frequency translation renders the potential in well-maintaining the artifact-free PPG signal even the MA signal is induced.

In this work, the performance of the frequency translation solution is assessed by comparing with the performances of the well-known methods under different moving poses. The selection criteria of the well-known methods are based on good efficiency, simple implementation and no requirement of extra sensors. The selected schemes for comparing are discrete saturation transform (DST), fast independent component analysis (fICA) and compression of Fourier coefficients (CFC). In comparison, the mean absolute percentage error (MAPE) is chosen as an indicator to manifest the performances of the frequency translation technique and the selected schemes. The MAPE measures the error magnitude deviated from the resting SpO2 value.

The structure of this paper is as follows. The technique of frequency translation applied in a traditional pulse oximeter is described in section II. In section III, the experiments and results are drawn. The performance comparison is furnished in section IV. Section V is dedicated to the conclusion.

978-1-7281-1322-7/19/$31.00 ©2019 IEEE

II. TECHNIQUE OF FREQUENCY TRANSLATION

A. *Inherent PPG Signal*

In SpO2 calculation of a pulse oximeter, a pair of red and infrared (IR) PPG signals is employed. The red PPG signal is the remaining red light intensity after being absorbed by most deoxyhemoglobin (Hb), dull red blood carrying no oxygen. For another one, IR light intensity is best sucked up by oxyhemoglobin (HbO2), bright red blood having oxygen ridden. The leftover IR light intensity is the IR PPG signal. To express each PPG signal in a mathematical model, an approximated light intensity absorption of Beer-Lambert's law [10][11] is utilized. Practically, the light intensity absorption in a human body varies over time due to the expansion and contraction of a human heart. With the expansion and contraction causes an optical path length of Beer-Lambert's law to fluctuate. The approximated light intensity absorption is then expressed in a function of time by (1) where $i(\lambda,t)$ is the remnant of light intensity after absorption of human's absorbing media.

$$i(\lambda,t) = i_o e^{-\sum_{k=1}^{N} \varepsilon_k(\lambda) c_k d_k(t)} \tag{1}$$

Next, i_o is the incident light intensity dropping onto the surface of the medium as well as $e^{-\sum_{k=1}^{N} \varepsilon_k(\lambda) c_k d_k(t)}$ is an exponential decaying function. The exponential decaying function is the negative sum of N absorbing media. Each absorbing medium is formed by the product of three absorbing factors. These absorbing factors are $\varepsilon_k(\lambda)$, c_k and $d_k(t)$ Firstly, $\varepsilon_k(\lambda)$ is the absorptivity, ε_k, of a specific wavelength λ of the k^{th} medium. Secondly, c_k is the concentration of the k^{th} medium. Lastly, $d_k(t)$ is the optical path length of the k^{th} medium.

Nonetheless, the mathematical model of light intensity absorption in (1) is a general absorbing expression for any medium having ability to absorb. For the light intensity absorption in a human tissue, the absorbance model in (1) needs to be adjusted to comply with the pulse oximeter manner. The original absorption of Beer-Lambert's in (1) is decomposed into the sum of a static medium and a dynamic medium as graphically depicted in Fig. 1. To distinguish the static and the dynamic media, an optical path length criterion is justified. According to the given decomposition, the mathematical statement in (1) is ameliorated and written in (2) where $i_{cPPG}(\lambda,t)$ is contemplated as a clean PPG signal.

$$i_{cPPG}(\lambda,t) = i_o[\underbrace{e^{-\varepsilon_{sm}(\lambda)c_{sm}d_{sm}}}_{\text{Static medium}} + \overbrace{e^{-[\varepsilon_{Hb}(\lambda)c_{Hb}+\varepsilon_{HbO}(\lambda)c_{HbO}]d_{dm}(t)}}^{\text{Dynamic medium}}] \tag{2}$$

For the static medium refers to all absorbing media whose optical path length values rarely alter over time. These absorbing media are skin, bone, tissue, venous blood and non-pulsating arterial blood. For simplicity, these absorbing media conglomerate into the static medium having $\varepsilon_{sm}(\lambda)$, c_{sm} and d_{sm} to be absorbing attributes shown in the first term of (2). Because the optical path length of the static medium seldom displays any variation over time, a function of time for d_{sm} is no longer needed.

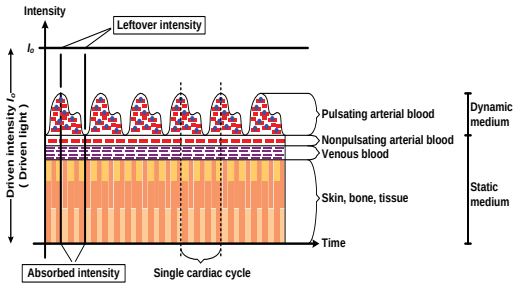

Figure 1. Inherent clean PPG waveform.

On the contrary, the dynamic medium indicates all absorbing media whose optical path length values vary over time. With this reason, the optical path length of the dynamic medium is manifested by the function of time. Mainly, only pulsating arterial blood medium is considered to be the dynamic medium. In the pulse oximeter, the red and IR lights are principally absorbed by Hb and HbO2, respectively. Therefore, the second term of (2) merely exhibits the absorbing parameters of Hb and HbO2 which are $\varepsilon_{Hb}(\lambda)c_{Hb}$ and $\varepsilon_{HbO}(\lambda)c_{HbO}$, respectively. In addition, both Hb and HbO2 absorb light inside the same dynamic medium resulting their optical path length values to be the similar value denoted as $d_{dm}(t)$.

In the incident that the pulse oximeter is involved with any motions, the MA signal is generated and annexed to the clean PPG signal in an additive manner [9]. The clean PPG signal stated in (2) is thus impaired, and becomes (3) where $n(t)$ is the MA term varying over time.

$$i_{rPPG}(\lambda,t) = i_{cPPG}(\lambda,t) + n(t) \tag{3}$$

In (3), $i_{rPPG}(\lambda,t)$ is the inherent PPG signal, which is the aggregate of the clean PPG signal, $i_{cPPG}(\lambda,t)$, and the MA signal, $n(t)$.

B. *PPG Signal Shifting*

Since the MA signal and the clean PPG signal are low frequency, they are certainly overlapping in frequency band. A method of frequency translation based on an amplitude modulation with large carrier (AM) is used to avoid intertwining of these two signals. With the usage of the AM model, the frequency band of the PPG signal is then shifted away from the MA signal's frequency band and (2) is developed to (4).

$$i_{cPPG}(\lambda,t) = \overbrace{i_a \cos(2\pi f_c t)}^{\text{AC source}}[\overbrace{e^{-\varepsilon_{sm}(\lambda)c_{sm}d_{sm}}}^{\text{Static medium}} + \overbrace{e^{-[\varepsilon_{Hb}(\lambda)c_{Hb}+\varepsilon_{HbO}(\lambda)c_{HbO}]d_{dm}(t)}}^{\text{Dynamic medium}}] \tag{4}$$

By changing i_o to $i_a \cos(2\lambda f_c t)$, a sinusoidal LED-driving source which furnishes oscillating light intensity is

substituted for an old-fashion LED-emitting source which beams out constant light intensity. The sinusoidal LED-driving source known as an alternating current (AC) source while the old-fashion LED-emitting source simply is a direct current (DC) source.

The sinusoidal LED-driving source generates an incident sinusoidal light intensity wave in the range of $\pm i_a$ varying by a carrier frequency of f_c Hz, as shown in (4). To simplify (4), the value of the static term, static medium, rarely changes so this term is denoted a constant variable, A_s. On the other hand, the value of the dynamic term referring to the dynamic medium oscillates over time and is contemplated as the absorption message of interest. Hence, the dynamic term is defined by $m(\lambda,t)$ as a function of time. After simplifying, (4) is restated giving rise to (5).

$$i_{cPPG}(\lambda,t) = \overbrace{i_a \cos(2\pi f_c t)}^{AC\ source}[\ \overbrace{A_s}^{Static\ medium} + \overbrace{m(\lambda,t)}^{Dynamic\ medium}\ ] \quad (5)$$

To reveal the amplitude modulation with large carrier (AM) [12], (5) is rearranged as (6) where $1/A_s$ is the modulating sensitivity, k_a.

$$i_{cPPG}(\lambda,t) = i_a \cos(2\pi f_c t) A_s[1 + k_a m(\lambda,t)] \quad (6)$$

By replacing (6) into (3), the inherent PPG signal is re-expressed as (7).

$$i_{rPPG}(\lambda,t) = i_a \cos(2\pi f_c t) A_s[1 + k_a m(\lambda,t)] + n(t) \quad (7)$$

Since the PPG signal is shifted to the carrier frequency, f_c, according to (6), the appended MA signal, $n(t)$, in (7) no longer interferes the clean PPG signal.

III. Experiments and Results

A. Instrument Setup

To implement the technique of frequency translation, a commercial finger-probe pulse oximeter is utilized. However, the built-in conventional LED-emitting system of the commercial pulse oximeter is supplanted by the sinusoidal LED-driving system as illustrated in Fig. 2. Commonly, the commercial pulse oximeter drives red and IR LED alternately at a frequency of 1 kHz. For this work, the commercial pulse oximeter is modified to emit both LEDs at the same time. The red and IR LEDs are driven by a signal generator at the frequencies of 1.07 kHz and 1.55 kHz, respectively. Each LED is powered by 1.5 Vpp (peak-to-peak voltage) along with 4.5 V offset voltage from the signal generator. In addition, a simple transimpedance amplifier (TIA) is designed to provide 10 times of gain before further processing because the output level sensed by the photo-detector is fairly low.

B. Signal Processing

The signal processing part is handled by a computer simulation program. Once the output signal of the photo-detector is amplified, the augmented signal is transferred to a computer via an NI DAQPad-6014 acquisition card manufactured by National Instruments. The augmented signal is sampled 16000 times per second. After sampling the amplified signal, processing is processed as follows.

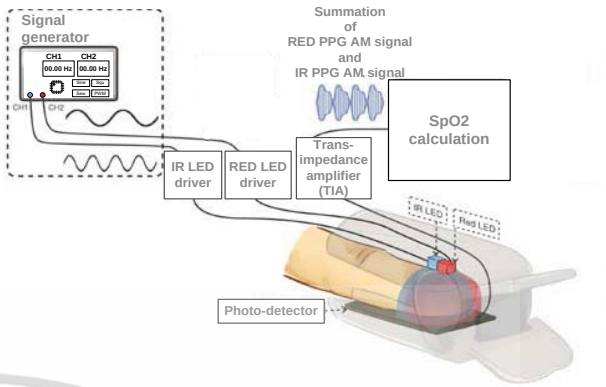

Figure 2. A sinusoidal LED-driving diagram.

Initially, the recorded signal is fed to two bandpass filters to segregate the red PPG AM signal and the IR PPG AM signal. Both bandpass filters are designed by a Butterworth algorithm to have filter order of 2 with 20 Hz passband and center frequencies of 1.07 kHz and 1.55 kHz, respectively. Secondly, each segregated AM signal is demodulated to recover the message of interest by a method of envelope detection. Next, each demodulated signal is passed to a lowpass filter to remove the carrier component of the carrier sinusoidal signal in order to retrieve the original message of interest. Each lowpass filter is also designed by the Butterworth algorithm to provide filter order of 2 along with 6 Hz cut-off frequency. Lastly, the recovered red and IR PPG signals are subject to compute the value of SpO2 by the calibration curve formula [11], as written in (8).

$$SpO2 = 110 - (25 \times R)\ ,\ R = \frac{V_{ppR}/V_{DCR}}{V_{ppIR}/V_{DCIR}} \quad (8)$$

The SpO2 calculation relies on V_{ppR}, V_{DCR}, V_{ppIR} and V_{DCIR}. The value of V_{ppR} is the peak-to-peak value of the red PPG signal and the value of V_{DCR} is the DC component of the red PPG signal. Similarly, the value of V_{ppIR} is the peak-to-peak value of the IR PPG signal and the value of V_{DCIR} is the DC component of the IR PPG signal. Typically, each PPG signal is parted period-by-period to approximate the value of SpO2 according to (8) more correctly.

C. Experimental Details and Results

In this work, a series of experiments is conducted to measure the SpO2 value while finger resting, finger bending, finger shivering, finger waving and vertical finger moving, respectively. Four volunteers are participated in this series of experiments. These four participants consist of two men and two women which are yellowish complexion Asian and their average age is 21.67 with a standard deviation of ±0.47. All volunteers are treated with minimum risk during each experiment is taken place. In the series of experiments, each participant is asked to put two pulse oximeters on the left hand at the same time while each experiment is performed. The modified pulse oximeter is inserted on an index finger and the original commercial pulse oximeter is drawn on a

middle finger. Each experiment is tested for three times ten seconds each. After finishing all experiments, 60 sets of samples are collected. Each set consists of two pairs of red and IR PPG signals. The first pair is acquired by the technique of frequency translation and the second pair is obtained by the conventional method.

In SpO2 computation, each pair is searched for a starting and stopping location of each single cardiac cycle to determine the peak-to-peak value and the DC component according to (8). Due to one recorded signal has many cardiac cycles, the calculated SpO2 values for all poses are numerous. The SpO2 values of each pose are thus averaged and standard deviation calculated, and summarized in Tables I and II.

Table I exhibits the SpO2 values of the technique of frequency translation and the conventional method during resting. As can be seen, the overall SpO2 value of the technique of the frequency translation is slightly higher than the overall SpO2 value of the conventional method by roughly 3%. This is due to the LED-driving circuit of each scheme is designed differently thus the light absorption is different. With 3% higher of the approach of frequency translation indicates that the light absorption of the technique of frequency translation is more efficient than the conventional method.

Table II renders the SpO2 values when moving postures are produced. In Table II, the SpO2 values of the technique of frequency translation are displayed along with the SpO2 values of the approaches of discrete saturation transform (DST), fast independent component analysis (fICA) and compression of Fourier coefficients (CFC). As can be noticed, each SpO2 value of each subject acquired from the technique of frequency translation for all moving poses is close to his/her resting SpO2 value. For DST, each SpO2 value of each subject is improved from the conventional method fairly well for all moving postures. Nevertheless, each SpO2 value of each subject is still lower than his/her resting SpO2 value obtained from the conventional method. In the same manner for fICA and CFC, each SpO2 value of each subject is also mended but only for some poses. For some poses, fICA and CFC fail to improve the quality of the SpO2 value but aggravate instead. In addition, the SpO2 values of all subjects for moving poses of fICA and CFC are overall inferior to the techniques of frequency translation and DST, respectively.

TABLE I. SPO2 VALUES OF FINGER RESTING POSTURE

Methods: / **Subject no.**	**FT_1**	**CM_2**
	Mean ± Standard deviation	
1. Male	97.2 ± 0.4	92.7 ± 1.1
2. Male	96.1 ± 0.8	94.9 ± 3.3
3. Female	97.0 ± 0.1	93.9 ± 0.4
4. Female	94.6 ± 0.1	91.3 ± 1.5
1-Frequency translation, 2-Conventional method.		

IV. PERFORMANCE COMPARISON

To compare the performance of the technique of frequency translation with the selected methods, a mean absolute percentage error (MAPE) is employed and expressed by (9).

$$MAPE = \frac{100}{N}\sum_{i=1}^{N}\left|\frac{de - m_i}{de}\right| \quad (9)$$

In (9), *de* is the mean SpO2 value while at rest of each subject which is depicted in Table I. For the MAPE calculation of the frequency translation, *de* is the mean SpO2 value while resting of each subject acquired by the technique of frequency translation. Likewise, the value of *de* for the approaches of DST, fICA and CFC uses the average SpO2 value while no motion case is obtained from the conventional method. Next, m_i is the average SpO2 value of each posture per one experiment for each subject, and N is the amount of experiments of each pose.

By utilizing (9), the MAPEs of each pose for all mentioned techniques including the conventional method are calculated and summarized in Table III. Clearly, the MAPE results reveal that the technique of frequency translation is better than the methods of DST, fICA, CFC and the traditional scheme. The overall MAPE values of the technique of frequency translation are lower than the overall MAPE values of the compared methods for all postures. This is because the technique of frequency translation well separates the red and IR PPG signals from the MA signal. By contrast, the approaches of DST, fICA and CFC mend the MA-overlapped red and IR PPG signals. Naturally, correcting the MA-interfered red and IR PPG signals is not as good as isolating the red and IR PPG signals from the MA signal.

V. CONCLUSION

This work evaluates the performance of the frequency translation technique of frequency translation while motion is involved. This assessment uses the value of MAPE as an indicator to quantify the performance. The MAPE value is calculated by employing the value of SpO2 as a parameter. In addition, the performance of the frequency translation strategy is strengthened by comparing with the performances of the approaches of DST, fICA, CFC and the conventional method. The resulting MAPE values indicate that performance of the technique of frequency translation is good, and superior to the performances of the schemes of DST, fICA, CFC and the conventional method. The overall MAPE value of the frequency translation technique is approximately 1.1% whereas the overall MAPE values of DST, fICA, CFC and the conventional method are 2.9%, 15.4%, 8.4% and 42.0%, respectively, for all poses. With this performance evaluation, the technique of frequency translation is concluded to be comparable to the schemes of DST, fICA and CFC.

TABLE II. SPO2 VALUES OF EACH POSE

Methods:	**FT_1**	**CM_2**	**DST_3**	**$fICA_4$**	**CFC_5**	**FT_1**	**CM_2**	**DST_3**	**$fICA_4$**	**CFC_5**
	Mean ± Standard deviation									
Subject no.	**Finger bending posture**					**Finger shivering posture**				
1. Male	96.9±0.2	84.6±7.3	89.8±0.1	73.2±11.6	85.3±0.1	96.6±2.5	96.1±1.6	93.8±0.6	82.8±3.8	85.0±0.1
2. Male	96.4±0.6	63.6±3.5	89.9±0.3	67.2±4.9	85.1±0.2	95.3±0.1	63.4±1.9	90.6±0.2	75.3±3.5	84.9±0.1
3. Female	93.7±0.2	88.8±7.2	92.4±0.2	81.2±6.5	86.0±0.4	95.3±0.6	88.4±5.2	92.2±0.2	78.1±6.0	86.7±1.5
4. Female	95.0±0.3	38.0±9.5	89.9±0.1	85.0±0.0	85.2±0.3	93.8±0.6	-21.5±4.2	89.0±0.1	83.3±2.9	85.1±0.2
Subject no.	**Finger waving posture**					**Vertical finger movement posture**				
1. Male	95.7±0.1	94.3±0.9	89.6±0.1	82.6±4.1	85.0±0.5	95.3±0.1	68.3±1.4	90.6±0.3	82.4±4.5	85.0±0.2
2. Male	96.5±0.2	69.8±3.5	90.4±0.2	83.0±3.5	85.1±0.1	95.4±0.1	66.8±4.6	89.9±0.1	76.0±11.0	84.9±0.3
3. Female	97.1±0.1	70.9±3.7	92.5±0.1	67.4±15.7	86.0±0.7	96.1±0.4	82.2±2.1	91.8±0.3	82.6±4.1	87.1±0.4
4. Female	95.1±0.2	-26.3±13.9	89.0±0.0	77.9±7.1	85.0±0.2	95.5±0.3	-46.4±1.9	88.8±0.0	82.6±4.1	85.0±0.1
3–Discrete saturation transform, 4–Fast independent component analysis, 5–Compression of Fourier coefficients.										

TABLE III. PERCENTAGE ERROR COMPARISON OF EACH POSE

Methods:	**FT_1**	**CM_2**	**DST_3**	**$fICA_4$**	**CFC_5**	**FT_1**	**CM_2**	**DST_3**	**$fICA_4$**	**CFC_5**
	Mean									
Subject no.	**Finger bending posture**					**Finger shivering posture**				
1. Male	0.30	8.70	3.13	21.01	7.97	2.16	3.65	1.19	10.66	8.26
2. Male	0.56	32.95	5.23	29.19	10.37	0.84	33.19	4.50	20.67	10.58
3. Female	3.40	5.44	1.60	13.50	8.40	1.75	5.82	1.85	16.80	7.68
4. Female	0.45	58.35	1.50	6.90	6.66	0.83	123.57	2.56	8.73	6.77
Overall mean error ± Standard deviation	**1.18** ±1.49	**26.36** ±24.61	**2.87** ±1.74	**17.65** ±9.61	**8.35** ±1.54	**1.40** ±0.67	**41.56** ±56.30	**2.53** ±1.43	**14.22** ±5.51	**8.32** ±1.63
Subject no.	**Finger waving posture**					**Vertical finger movement posture**				
1. Male	1.56	1.77	3.38	10.85	8.25	1.98	26.30	2.27	11.08	8.35
2. Male	0.46	26.43	4.71	12.56	10.28	0.78	29.58	5.23	19.89	10.49
3. Female	0.13	24.50	1.46	28.23	8.44	0.95	12.51	2.24	11.99	7.24
4. Female	0.52	128.78	2.52	14.66	6.89	0.94	150.86	2.74	9.49	6.90
Overall mean error ± Standard deviation	**0.67** ±0.62	**45.37** ±56.72	**3.02** ±1.37	**16.58** ±7.92	**8.47** ±1.39	**1.16** ±0.55	**58.81** ±64.46	**3.12** ±1.43	**13.11** ±4.63	**8.25** ±1.62

REFERENCES

[1] M. K. Diab, E. Kiani-Azarbayjany, and W. M. Weber, "Signal processing apparatus," U.S. Patent US008 942 777B2, Jan. 2015.

[2] M. Raghu Ram, K. Sivani, and K. Ashoka Reddy, "Utilization of adaptive-coefficient estimation method for motion artifacts reduction from photoplethysmographic signals," Int. Conf. Wireless Communications, Signal Processing and Networking (WiSPNET), Chennai, India, Mar. 2016, pp. 819-822.

[3] R. W. C. G. R. Wijshoff, M. Mischi, and R. M. Aarts, "Reduction of periodic motion artifacts in photoplethysmography," IEEE Trans. Biomed. Eng., vol. 64, no. 1, Jan. 2017, pp. 196–207.

[4] T. Jensen et al., "Independent component analysis applied to pulse oximetry in the estimation of the arterial oxygen saturation (S_pO_2) – a comparative study," Annual Int. Conf. of the IEEE Engineering in Medicine and Biology Society (EMBS), Minneapolis, USA, Sep. 2009, pp. 4039–4044.

[5] M. Raghuram, K. Sivani, and K. Ashoka Reddy, "Reduction of motion artifacts from pulse oximeter's PPG signals using MSICA," Int. Conf. Control, Instrumentation, Communication and Computational Technologies (ICCICCT), Kumaracoil, India, Dec. 2016, pp. 491-494.

[6] F. Fan, Y. Yan, Y. Tang, and H. Zhang, "A motion-tolerant approach for monitoring SpO2 and heart rate using photoplethysmography signal with dual frame length processing and multi-classifier fusion," Computers in Biology and Medicine, vol. 91, no. 12, Dec. 2017, pp. 291-305.

[7] K. A. Reddy, B. George, and V. J. Kumar, "Use of Fourier series analysis for motion artifact reduction and data compression of photoplethysmographic signals," IEEE Trans. Instrum. Meas., vol. 58, no. 5, May 2009, pp. 1706–1711.

[8] S. Li, S. Jiang, S. Jiang, J. Wu, W. Xiong and S. Diao, "A hybrid wavelet-based method for the peak detection of photoplethysmography signals," Compututational Mathematical Methods in Medicine, Nov. 2017. [Online]. Available: https://dx.doi.org/10.1155/2017/9468503.

[9] S. Sinchai, P. Kainan, P. Wardkein, and J. Koseeyaporn, "A photoplethysmographic signal isolated from an additive motion artifact by frequency translation," IEEE Trans. Biomed. Circuits Syst., vol. 12, no. 4, Aug. 2018, pp.904–917.

[10] Y. Khan et al., "A flexible organic reflectance oximeter array," Proc. National Academy of Sciences of the United States of America (PNAS)., vol. 115, no. 47, Nov. 2018, pp. E11015–E11024.

[11] S. M. Salehizadeh et al., "Photoplethysmograph signal reconstruction based on a novel motion artifact detection-reduction approach. Part II: Motion and noise artifact removal," Annals of Biomedical Engineering, vol. 42, no. 11, Nov. 2014, pp. 2251-2263.

[12] J. W. Leis, Communication Systems Principles Using MATLAB. New Jersey, USA: John Wiley & Sons, 2018, pp. 155–179.

Author Biography

Given name:	Mr. Ananta
Family name:	Sinchai
Former given name:	Mr. Sakkarin
Family name:	Sinchai
Date of birth:	December 25th, 1985
Contact address:	242/86, Moo. 17, Soi Karnjanapisek 0015, Karnjanapisek Rd, Salathammasop, Thawi-watthana, Bangkok, 10170
Education background:	- Bachelor of Telecommunications Engineering, King Mongkut's Institute of Technology Ladkrabang, (KMITL), 2008 - Master of Telecommunications Engineering, King Mongkut's Institute of Technology Ladkrabang, (KMITL), 2015
Research of interest:	- Statistical signal processing - Biomedical signal processing - Biomedical circuits and systems - Signals and systems - Programming regarding machine and microcontroller - Instrumentation and measurement